

INFORMATION TO USERS

This manuscript has been reproduced from the microfilm master. UMI films the text directly from the original or copy submitted. Thus, some thesis and dissertation copies are in typewriter face, while others may be from any type of computer printer.

The quality of this reproduction is dependent upon the quality of the copy submitted. Broken or indistinct print, colored or poor quality illustrations and photographs, print bleedthrough, substandard margins, and improper alignment can adversely affect reproduction.

In the unlikely event that the author did not send UMI a complete manuscript and there are missing pages, these will be noted. Also, if unauthorized copyright material had to be removed, a note will indicate the deletion.

Oversize materials (e.g., maps, drawings, charts) are reproduced by sectioning the original, beginning at the upper left-hand corner and continuing from left to right in equal sections with small overlaps. Each original is also photographed in one exposure and is included in reduced form at the back of the book.

Photographs included in the original manuscript have been reproduced xerographically in this copy. Higher quality 6" x 9" black and white photographic prints are available for any photographs or illustrations appearing in this copy for an additional charge. Contact UMI directly to order.



University Microfilms International
A Bell & Howell Information Company
300 North Zeeb Road, Ann Arbor, MI 48106-1346 USA
313/761-4700 800/521-0600

Order Number 9409267

Binary separations by pressure swing adsorption processes

Fatehi, Ashraf Husein Ismail, Ph.D.

King Fahd University of Petroleum and Minerals (Saudi Arabia), 1992

U·M·I
300 N. Zeeb Rd.
Ann Arbor, MI 48106

Binary Separations by Pressure Swing
Adsorption Processes

BY

Ashraf Husein Ismail Fatehi

A Dissertation Presented to the
FACULTY OF THE COLLEGE OF GRADUATE STUDIES
KING FAHD UNIVERSITY OF PETROLEUM & MINERALS
DHAHMAN, SAUDI ARABIA

In Partial Fulfillment of the
Requirements for the Degree of

DOCTOR OF PHILOSOPHY

In

CHEMICAL ENGINEERING

July 1992

KING FAHD UNIVERSITY OF PETROLEUM & MINERALS

DHAHRAN, SAUDI ARABIA

This dissertation, written by

ASHRAF HUSEIN ISMAIL FATEHI

under the direction of his Dissertation Advisor, and approved by his Dissertation Committee, has been presented to and accepted by the Dean, College of Graduate Studies, in partial fulfillment for the requirements for the degree of

DOCTOR OF PHILOSOPHY IN CHEMICAL ENGINEERING

Dissertation Committee

Kevin F. Loughlin

Chairman (Dr. Kevin F. Loughlin)

Mirza Mominul Hassan

Member (Dr. Mirza M. Hassan)

Abdulla A. Shaikh

Member (Dr. Abdulla A. Shaikh)

Ghassan A. Owaimreen

Member (Dr. Ghassan A. Owaimreen)

Mazen A. Shalabi

Dr. Mazen A. Shalabi
Department Chairman

Ala H. Al-Rabeh

Dr. Ala H. Al-Rabeh
Dean College of Graduate Studies

Date : 5-7-92



Dedicated to

My parents, Ismail and Khadija

and

my wife, Rashida

ACKNOWLEDGEMENTS

Acknowledgement is due to all those who made this work possible. Firstly I appreciate the material and financial support from King Fahd University of Petroleum & Minerals.

I like to express my most sincere thanks to Dr. Kevin F. Loughlin, my dissertation committee chairman, and Dr. Mirza M. Hassan, my dissertation committee member, for extending all possible help, guidance and assistance during the entire course of this work. Thanks are also due to Dr. Abdulla A. Shaikh and Dr. Ghassan A. Oweimreen for their suggestions and comments as dissertation committee members.

I also like to thank all personnel in the workshop and laboratories for extending their fullest co-operation and assistance for my experimental work.

I also like to extend my thanks to the chairman, faculty, staff and graduate students of the chemical engineering department for their co-operation at all times.

Finally, I like to express my gratitude to my parents, my wife Rashida, my daughter Gulrez and other members of my family whose prayers, patience and sacrifice helped me achieve this goal.

CONTENTS

	Page
LIST OF TABLES	... ix
LIST OF FIGURES	... xi
ARABIC ABSTRACT	... xvii
ABSTRACT	... xix
 1 INTRODUCTION	 ... 1
1.1 Introduction	... 1
1.2 A brief overview of modelling Pressure Swing Adsorption Separation Processes	... 3
1.3 Cyclic Separation Processes	... 6
1.4 Outline of the Present Study	... 8
References	... 11
 2 ADSORPTIVE DIFFUSION OF BINARY MIXTURES IN MICROPOROUS CRYSTALS	 ... 16
2.1 Introduction	... 17
2.2 Literature Review	... 18
2.3 Mathematical Model for Adsorption in a Crystal	... 21
2.4 Results and Discussion	... 29
2.5 Conclusions	... 32
References	... 33

3 THEORETICAL STUDY OF NONLINEAR ISOTHERMAL PACKED BED ADSORBERS: COMPARISON OF PECLET AND CELL NUMBERS	... 40
3.1 Introduction	... 40
3.2 Mathematical Model	... 45
3.3 Results and Discussion	... 48
3.4 Conclusions	... 52
References	... 53
 4. EQUILIBRIUM AND KINETICS OF SORPTION OF NITROGEN AND METHANE ON ZEOLITE 4A AND CARBON MOLECULAR SIEVES	 ... 71
4.1 Introduction	... 71
4.2 Equilibrium and Kinetic Parameters for Zeolite 4A	... 72
4.3 Experimental Techniques for Sorption and Equilibrium Data	... 72
4.3.1 Volumetric Method	... 73
4.3.2 Gravimetric Method	... 74
4.3.3 Chromatographic Method	... 74
4.4 Equilibrium Results for Carbon Molecular Sieves	... 75
4.5 Kinetic Results for Carbon Molecular Sieves	... 76
4.6 Conclusions	... 86
References	... 88

5	PSA SEPARATION OF METHANE - NITROGEN MIXTURE ON CARBON MOLECULAR SIEVES	... 113
5.1	Introduction	... 113
5.2	Literature Review	... 114
5.3	Theoretical Modelling and Simulation	... 115
5.4	Apparatus	... 124
5.5	Procedure	... 125
5.6	Results and Discussion	... 126
5.7	Conclusions and Recommendations	... 137
	References	... 138
6	PSA SEPARATION OF METHANE - NITROGEN MIXTURE ON ZEOLITE 4A	... 171
6.1	Introduction	... 171
6.2	Literature review	... 171
6.3	Theoretical Modelling and Simulation	... 172
6.4	Apparatus	... 174
6.4.1	Two Column PSA unit	... 174
6.4.2	Description of Single Column PSA unit	... 175
6.5	Procedure	... 176
6.5.1	Two Column Unit	... 176
6.5.2	Single Column Unit	... 177
6.6	Results and Discussion	... 177

6.7 Conclusions	... 190
References	... 192
7 CONCLUSIONS AND RECOMMENDATIONS	... 217
7.1 Conclusions	... 217
7.2 Recommendations for Further Study	... 220
NOMENCLATURE	... 222
APPENDICES	
A.1 Raw Data	
A.1.1 Raw Data for Two Column PSA Experiments with Carbon Molecular Sieves	... 227
A.1.2 Raw Data for Two Column PSA Experiments with 4A Zeolite	... 248
A.1.3 Raw Data for Single Column PSA Experiments with 4A Zeolite	... 269
A.1.4 Raw Data for Sorption Experiments with CMS	... 306
A.2 Specification of Equipment	... 335
A.3 Dimensionless Form of Collocation Equations	... 339
Vita	

LIST OF TABLES

Table	Page
2.1 Parameters used in the computations	... 34
3.1 Transport Models describing Mass Transfer in Packed Catalytic Reactors and Adsorbers	... 58
3.2 Parameters used in the computations	... 59
4.1 Activation Energy E, Preexponential Factor D*, Crystal diameter and Diffusional Time Constant at 300 K of Nitrogen and Methane in 4A zeolite	... 90
4.2 Summary of the Henry Constant Measurements for the Sorption of Nitrogen and Methane on CMS	... 91
4.3 Summary of the Rate Data Measurements for the Sorption of Nitrogen and Methane on CMS	... 92
4.4 Comparison of Equilibrium and Kinetic Parameters Reported in the Literature with Results of this Study on CMS	... 93
4.5 Diffusion Time Constant of Methane and Nitrogen in Carbon Molecular Sieves based on Long Time Solution of the Barrier Resistance Model	... 94
5.1 Experimental Conditions and Parameters used in the simulation for two column PSA Unit	... 140
5.2 Summary of two column experiments with Molecular Sieve Carbon	... 141
6.1 Experimental Conditions and Parameters used in the simulation for two column and single column PSA Unit	... 193
6.2 Summary of two column experiments with Zeolite 4A	... 194
6.3 Summary of single column experiments with Zeolite 4A	... 197
6.4 Simulated exit concentration for a single column experiment as a function of Ω factor of nitrogen and methane.	... 202

6.5	Simulated exit concentration for a single column experiment as a function of Ω factor of nitrogen and methane.	...	203
6.6	Simulated exit concentration in a single column experiment as a function of Henry law constants and Ω factor of nitrogen and methane	...	204
6.7	Experimental and simulated exit concentration in a single column unit along with sum of squares (Cycle time 60 sec)	...	205
6.8	Experimental and simulated exit concentration in a two column unit along with sum of squares (Cycle time 60 sec)	...	206

LIST OF FIGURES

Figure	Page
1.1 Packed Adsorbent Column loaded with Pellets of Zeolite 5A Crystals.	... 12
1.2 Linear Driving Force Approximation Factor as a Function of Dimensionless Half Cycle Time as reported by (A) Nakao & Suzuki(2) and (B) Raghavan et al.(3)	... 13
1.3 Schematic Isotherm showing Pressure Swing, Thermal Swing and Combined Pressure-Temperature Swing Operation for an Adsorption Process	... 14
1.4 Program Flow Chart for a Typical Simulation of a PSA process(9)	... 15
2.1 Plot of Normalized Uptake Ratio with Dimensionless Time on CMS. Constant Diffusivity Case (Parameter is Biot No. of O ₂ , $D_{O_2}/D_{N_2} = 31.82$)	... 35
2.2 Plot of Normalized Uptake Ratio with Dimensionless Time on CMS. Constant Diffusivity Case (Parameter is Biot No. of O ₂ , $D_{O_2}/D_{N_2} = 62.5$)	... 36
2.3 Plot of Normalized Uptake Ratio with Dimensionless Time on CMS. Variable diffusivity Case (Parameter is Pressure (atm) / Biot No. of O ₂ , $D_{O_2}/D_{N_2} = 31.82$)	... 37
2.4 Plot of Normalized Uptake Ratio with Dimensionless Time on CMS. Variable Diffusivity & Feed concentration case. (Parameter is Pressure(atm)/ N ₂ Mole Fraction)	... 38
2.5 Plot of Dimensionless Temperature with Dimensionless Time on zeolite 4A. Constant Diffusivity Case (Parameter is Diffusion to Thermal Time Constant)	... 39
3.1 Breakthrough Curves - Oxygen on Carbon Molecular Sieves	... 60
3.2A Adsorption of Methane on 5A Zeolite - Equilibrium Model	... 61
3.2B Desorption of Methane on 5A Zeolite - Equilibrium Model	... 62

3.3	Sorption of Ethylene on 5A Zeolite - Equilibrium Model	...	63
3.4A	Adsorption of Oxygen on Carbon Molecular Sieves - Non Equilibrium Model	...	64
3.4B	Adsorption of Oxygen on Carbon Molecular Sieves - Non Equilibrium Model	...	65
3.4C	Desorption of Oxygen on Carbon Molecular Sieves - Non Equilibrium Model	...	66
3.5A	Adsorption of Ethylene on 4A Zeolite - Non Equilibrium Model	...	67
3.5B	Desorption of Ethylene on 4A Zeolite - Non Equilibrium Model	...	68
3.6	Plot of Peclet No. vs. No. of Cells for Methane on 5A Zeolite - Equilibrium Model	...	69
3.7	Plot of Peclet no. vs. No. of Cells for Oxygen on Carbon Molecular Sieves - Non Equilibrium Model	...	70
4.1	Temperature Dependence of Henry constants for Sorption of Nitrogen in 4A zeolite	...	95
4.2	Temperature Dependence of Henry constants for Sorption of Methane in 4A zeolite	...	96
4.3	Plot of Cumulative and Relative Volumes vs. Pore Radius for the CMS sample used in this study	...	97
4.4	Vant Hoff Plot of the Henry Constants K_p vs. $1/T$ for Nitrogen and Methane Sorption on CMS.	...	98
4.5	Equilibrium Isotherm of Nitrogen on CMS at 25°C	...	99
4.6	Equilibrium Isotherm of Methane on CMS at 25°C	...	100
4.7	Comparison of volumetric uptake rates with standard solution of Fick's Law for diffusion in spheres for Nitrogen at 25 and 80 °C on 2.33 mm pellets	...	101
4.8	Comparison of volumetric uptake rates with standard solution of Fick's Law for diffusion in spheres for Methane at 25 °C on 2.33 mm pellets	...	102

4.9	Experimental uptake curves for Nitrogen on CMS reported in the literature. 3 mm pellet at 303K;30-60 mesh at 303 K;30-60 mesh at 273 K;Reproduced from Ph. D Thesis of Hassan(23)	...	103
4.10	Comparison of volumetric uptake curves of Nitrogen on 2.33 mm pellets with standard solution assuming both macropore - micropore diffusional resistances.	...	104
4.11	Semilogarithmic plot of volumetric uptake rate of methane on 2.33 mm pellets on CMS at 25 °C	...	105
4.12	Semilogarithmic plot of volumetric uptake rate of nitrogen on 2.33 mm pellets on CMS at 323, 352 and 420 °K	...	106
4.13	Semilogarithmic plot of volumetric uptake rate of methane on 2.33 mm pellets on CMS at 323, 351.4, 400 and 420 °K	...	107
4.14	Semilogarithmic plot of volumetric uptake rate of methane on 2.33 mm pellets on CMS at 323, 351.4, 400 and 420 °K showing both regions of the curve	...	108
4.15	Semilogarithmic plot of rate values k_s versus $1/T$ for volumetric and chromatographic data	...	109
4.16	Comparison of activation energy obtained in this work and reported literature value for diffusional activation energy with van der Waals diameter for diffusion in 4A and 5A zeolites and 5A molecular sieve {Data abstracted from Ruthven, D., Principles of Adsorption and Adsorption Processes, pg.148, John Wiley & Sons, New York(1985)}	...	110
4.17	Correlation of activation energy for this work and activation energy for micropore diffusion reported in the literature with isotheric heat of adsorption {Data abstracted from Chihara, K. et al, AIChE Journal, 24, 243(1978)}	...	111
4.2	Temperature Dependence of Diffusional Time Constant of Methane in Carbon Molecular Sieve	...	112
5.1	Schematic Diagram of the Two Column PSA Experimental Unit	...	144
5.2	Schematic Diagram of the Steps involved in PSA Cycle	...	145
5.3	Feed Flow during the course of a 540 sec Cycle	...	146

5.4	Product and Purge Flow during the course of a 540 sec Cycle	...	147
5.5	Typical output from an Integrator of a Gas Chromatograph	...	148
5.6	Methane concentration during the course of a 100 sec. cycle (Run 26)	...	149
5.7	Methane concentration during the course of a 600 sec. cycle (Run 25)	...	150
5.8	Exit Experimental and Simulated Product Concentration 2 sec. prior to the end of the Adsorption step as a function of the No. of cycles (Runs 1-6). Parameter is cycle time	...	151
5.9	Exit Experimental and Simulated Product Concentration 2 sec. prior to the end of the Adsorption step as a function of the No. of cycles (Runs 7-12). Parameter is cycle time	...	152
5.10	Exit Experimental and Simulated Product Concentration 2 sec. prior to the end of the Adsorption step as a function of the No. of cycles (Runs 13-18). Parameter is cycle time	...	153
5.11	Exit Experimental and Simulated Product Concentration 2 sec. prior to the end of the Adsorption Step as a function of the No. of cycles (Runs 19-24). Parameter is cycle time	...	154
5.12	Exit Experimental and Simulated Product and Purge Concentration 2 sec. prior to the end of the Sorption step as a function of No. of Cycles (Run 25)	...	155
5.13	Exit Experimental and Simulated Product Concentration 2 sec. prior to the end of the Adsorption step as a function of the No. of cycles (Runs 26-30). Parameter is cycle time	...	156
5.14	Exit Experimental and Simulated Purge Concentration 2 sec. prior to the end of the Adsorption Step as a function of the No. of cycles (Runs 26-30). Parameter is cycle time	...	157
5.15	Exit Experimental and Simulated Product and Purge Concentration at Cyclic Steady State (Runs 1-30)	...	158
5.16	Theoretical Exit Methane Concentration as a function of Cycle Time with Φ Factor for Methane/Nitrogen as parameter	...	159

5.17	Plot of Methane and Nitrogen Factor (Φ) as a function of Dimensionless Half Cycle Time	...	160
5.18	Plot of Equivalent Methane and Nitrogen ($15*\Phi$) factor with LDF factor of Suzuki et al(18) and Raghavan et al(11) as a function of Dimensionless Half Cycle Time	...	161
5.19	Exit Methane Concentration as a function of L/v_{II} with Cycle Time as a parameter	...	162
5.20	Methane Concentration in Gas Phase along the Column with No. of Cycles as a parameter	...	163
5.21	Methane Concentration in Gas Phase at specific points in the Column as a function of No. of Cycles	...	164
5.22	Methane Concentration in Solid Phase along the Column with No. of Cycles as a parameter	...	165
5.23	Methane Concentration in Solid Phase at specific points in the Column as a function of No. of Cycles	...	166
5.24	Nitrogen Concentration in Solid Phase along the Column with No. of Cycles as a parameter	...	167
5.25	Nitrogen Concentration in Solid Phase at specific points in the Column as a function of No. of Cycles	...	168
5.26	Normalised Velocity Profile along the Column with No. of Cycles as a parameter	...	169
5.27	Normalised Velocity Profile at specific points in the Column as a function of No. of Cycles	...	170
6.1	Schematic Diagram of the Single Column PSA Experimental Unit	...	207
6.2	Plot of exit concentration vs. Ω factor for nitrogen. Parameter is Ω ratio of methane to nitrogen. Two sets of curves for different values of equilibrium constants	...	208
6.3	Plot of deviation between experimental and simulated exit concentration vs. Ω factor for nitrogen	...	209

6.4	Plot of experimental and simulated exit concentration vs. No. of Cycles on the single column (Run 4)	...	210
6.5	Plot of Gas Phase methane Concentration Profile at the end of adsorption step vs.dimensionless distance in a single column(Run 4)	...	211
6.6	Plot of Solid phase Methane Concentration profile at the end of adsorption step vs.dimensionless distance in a single column(Run 4)	...	212
6.7	Plot of Solid phase Nitrogen Concentration profile at the end of adsorption step vs.dimensionless distance in a single column(Run 4)	...	213
6.8	Plot of Gas phase Methane concentration profile at the end of adsorption step vs. No. of cycles in a single column(Run 4)	...	214
6.9	Plot of Solid phase Methane concentration profile at the end of adsorption step vs. No. of cycles in a single column(Run 4)	...	215
6.10	Plot of Gas phase Methane concentration profile at the end of adsorption step vs. No. of cycles in a single column(Run 4)	...	216

خلاصة الرسالة

إسم الطالب : أشرف حسين إسماعيل فتيحي
عنوان الدراسة : الفصل الثنائي بواسطة عمليات إمتزاز الضغط المتراجع
التخصص : الهندسة الكيميائية
تاريخ الشهادة : يوليو ١٩٩٢م

تنشر في هذه الدراسة أبحاث نظرية وتجريبية عن إمتزاز وإنتشار وفصل المخلوط الثنائية الغازية النقية في الممتزات : زيولايت 4A والغربال الجزيئي الكربوني (CMS) .
طور نموذج رياضي لامتزاز وانتشار مخلوط ثنائي من النيتروجين والأكسجين في زيولايت 4A وفي الغربال الجزيئي الكربوني أخذاً في الاعتبار تغير الإنتشارية وخط التحارر غير الخطي والإمتزاز متغير الحرارة والمقاومة الغشائية لانتقال المادة والحرارة . وضعت نتائج النموذج على شكل نسبة أخذ معايرة مقابل الزمن اللابيدي (τ) . تنتقل نسبة الأخذ المعايرة من منطقة تحكم الإنتشار إلى منطقة تحكم الإيزان عندما تتغير τ من صفر إلى ∞ . في منطقة تحكم الإنتشار ، وجد أن نسبة الأخذ تتناقص بزيادة معامل بيوت (Biot) ، غير متأثرة بانضغاط في حالة ثبوت الانتشارية ، ولكن تعتمد إعتداداً كبيراً على الضغط والتركيب في حالة الإنتشارية المتغيرة .

طورت نماذج لمنحنيات الإمتزاز والمج لمازان التشتت المحوري ونموذج الخلية في حالتي الإيزان وعدم الإيزان لأنظمة بخط تحاور لاخطي من نوع لانغمور (Langmuir) . وقد درست الأنظمة النموذجية التالية :
أختير الإيثيلين - هليوم والميثان - هليوم على زيولايت 5A في حالة الإيزان وأختير الإيثيلين - هليوم على زيولايت 4A والأكسجين - هليوم على CMS في حالة عدم الإيزان . وقد أخذت الزمن المطلوب ليتغير التركيز اللابيدي من ٩٩.٠ إلى ٠.١ ر. كمعيار لمقارنة رقم بكلييه (Peclet) لنموذج التشتت المحوري بالعدد من الخلايا (N) لنموذج الخلية . وحسب قيمة هذا الزمن لكل الأنظمة باستخدام النموذجين وبقيم مختلفة من المقدار λ .
وجد أن نسبة معامل بكلييه (Peclet) تتغير من ٢ عندما تكون λ منخفضة إلى 1 عندما تكون قيمة λ مرتفعة ($\lambda = ٨٥$) . وذلك في حالتي الإيزان وعدم الإيزان خلال عملية الإمتزاز ، أما عند المج فيمكن إعتبار هذه النسبة مساوية ٢ دائماً .

أخذت قياسات الإمتزاز والإنتشار للميثان والنيتروجين على الغربال الجزيئي الكربوني (CMS) في جهاز حجمي وذلك لتحديد القيم التوازنية والحركية لإستخدامها في النموذج الرياضي لتجارب إمتزاز الضغط المتراجع . لم تكن النتائج متفقة مع البيانات الكروتوجرافية للنيتروجين على الغربال الجزيئي الكربوني . يمكن أن تفسر النتائج بافتراض وجود مقاومة حاجزة بالإضافة إلى المقاومة الإنتشارية . أشار التحليل إلى وجود توافق بين المقاومة كما حسبت بالطرق الكروماتوجرافية وبين ٩٠٪ من منحنى الأخذ كما حسب من التجارب الحجمية . وهذا يمثل المقاومة الحاجزة أما المقاومة الإنتشارية فلا يمكن إيجادها إلا من الجهاز الحجمي

وبعد مرور زمن طويل . وجد أن طاقة التنشيط اللازمة للتغلب على المقاومة الحازمة هي ١٣٩٧ كيلو كالوري للمول الواحد من الميثان و ٨١١ كيلو كالوري للمول من النيتروجين . أما طاقة التنشيط اللازمة للتغلب على المقاومة الإنتشارية فيمكن إيجادها للميثان فقط وهي تساوي ١٢٥٦ كيلو كالوري . هذه القيم أكبر بكثير من القيم المنشورة في الأبحاث السابقة مما يشير إلى وجود فتحة سمية أصغر قليلاً من ٤ أنجستروم لهذه العينة . استخدم نوعان من المخاليط الغازية في الدراسة التجريبية الهادفة إلى رفع نسبة الميثان في الخلوط ، أحدهما يحتوي على نسبة ٤٠٪ نيتروجين والآخر يحتوي على ٨٪ وهي مشابهة للغازات الصناعية الموجودة في المملكة العربية السعودية . وقد أجريت الدراسة على وحدة ضغط متراجع ذات عمودين ومزودة بالغربال الجزيئي الكربوني وزيلوليت 4A ، كما أجريت على وحدة ذات عمود واحد مزودة بالزيلوليت 4A . لم ترتفع نسبة الميثان عند استخدام الوحدة ذات العمودين والزيلوليت 4A ، ولكن عند استخدام الغربال الكربوني كانت نسبة الميثان في الناتج تتراوح بين ٤٨ - ٧٥٪ حسب زمن الدورة وذلك عندما تكون النسبة $\frac{L}{V} = ٦٩$. أما في الوحدة ذات العمود الواحد والمزودة بزيلوليت 4A فقد كانت نسبة الميثان ٨٤٪ وباستخدام الهيليوم كمطهر وبجعل مدة المج مساوية لثلاثة أمثال مدة الإمتزاز .

طور نموذجاً حركياً ذا قوة دافعة خطية لامتناهات الضغط المتراجع وبخط تحارر لا تقموري ثنائي وحل عددياً بطريقة التنظيم المتعامد وذلك للتنبؤ بنتائج التجارب لكل من الوحدة ذات العمودين والوحدة ذات العمود الواحد . بالنسبة للزيلوليت 4A فلا يمكن التنبؤ بالنتيجة باستخدام القيم المنشورة في الأبحاث السابقة . وقد حصل توافق بين النتائج النظرية والتجريبية عند استخدام ٣٣٪ و ٢٠٪ من القيمة النظرية لكل من الميثان والنيتروجين على التوالي . وهذا يشير إلى أن القيمة $\frac{D}{r_c^2}$ المستخدمة هي أعلى من تلك المنشورة .

وللحصول على فصل أفضل فقد أجريت دراسات نظرية لتحديد القيم المناسبة للقيمة $\frac{D}{r_c^2}$.

بالنسبة للغربال الجزيئي الكربوني ، فقد لوحظ من الدراسات وجود إختلاف كلي في عامل سرعة التغير واتجاهاته وذلك عند استخدام نموذج القوة الدافعة الخطية وهو انعكاس لوجود المقاومة الحازمة .

درجة الدكتوراه في الفلسفة
جامعة الملك فهد للبترول والمعادن
الظهران ، المملكة العربية السعودية

يوليو ١٩٩٢

DISSERTATION ABSTRACT

Name of the Student : ASHRAF HUSEIN ISMAIL FATEHI
Title of Study : BINARY SEPARATIONS BY PRESSURE
SWING ADSORPTION PROCESSES
Major Field : CHEMICAL ENGINEERING
Date of Degree : July 1992

Theoretical and experimental investigations are reported for the sorption, diffusion and separation of pure and binary mixtures of gases in microporous adsorbents - 4A zeolite and carbon molecular sieve (CMS).

A mathematical model is developed for the sorption and diffusion of binary mixtures of N_2 and O_2 in 4A zeolite and CMS accounting for variable intracrystalline diffusivity, non-linear isotherm, non isothermal adsorption and film resistance to heat and mass transfer. The model results are expressed as a normalized uptake ratio versus dimensionless time (τ): the uptake ratio moves from a diffusion to an equilibrium control regime as τ moves from 0 to ∞ . In the diffusion control regime the uptake ratio was found to decrease with Biot number independent of pressure for the constant diffusivity case, but is highly dependent on both pressure and composition for the variable diffusivity case.

Theoretical adsorption and desorption curves are modelled for axial dispersion and cell model adsorbents, for equilibrium and non-equilibrium systems having non linear Langmuir type of isotherms. As representative systems ethylene-helium and methane-helium on 5A zeolite are selected for the equilibrium systems and ethylene-helium on 4A zeolite and oxygen-helium on CMS for the non-equilibrium systems. The time to change the dimensionless exit concentration level between 0.99 and 0.01 ($\tau_{0.99-0.01}$) is chosen as the criterion to find a correspondence between the Peclet number in the axial dispersion model and N , the number of cells in the cell model. Computations were performed to estimate $\tau_{0.99-0.01}$ for all the systems by both models for various values of the non-linearity parameter λ . For both the equilibrium and the non equilibrium processes the ratio of Peclet number changes from a value of 2 at low λ to unity when λ is high ($\lambda = 0.85$) during adsorption. However, this ratio can be taken as 2 during desorption.

Uptake measurements of sorption and diffusion of methane and nitrogen on the CMS sample are performed on a volumetric apparatus to determine the kinetic and equilibrium parameters for use in the mathematical modelling of the pressure swing adsorption (PSA) experiments. The results, explained by a diffusion mechanism hypothesis, are inconsistent with available chromatographic data for nitrogen on the CMS sample (methane is too slow to measure). The results can be explained by a presence of a barrier resistance along with the diffusion mechanism. The analysis of the results show consistency with the resistance measured by chromatographic method and

90% of the uptake curve from the volumetric experiments. This represents the barrier resistance, while the diffusional resistance can only be obtained from the volumetric apparatus at large times. The activation energies for overcoming the barrier resistance are found to be 13.97 and 8.11 kcal/mole for methane and nitrogen respectively. The activation energies for the diffusional resistance can be measured only for methane and is found to be 12.56 kcal/mole. These are much greater than values reported in the literature indicating a pore opening somewhat less than 4 Å for this sample

Experimental study for enriching methane in two model feed mixtures (40% and 8% nitrogen in methane), similar to important industrial gas streams in Saudi Arabia, is done on a two column PSA unit using CMS and 4A zeolite and on a single column PSA unit using 4A zeolite. Exit high pressure product or vacuum are used as purge gas in the 2 column unit while methane or helium or vacuum are used as purge in the single column unit respectively. No significant enrichment is obtained in the two column unit with 4A zeolite but exit mole fraction from 48% up to 75% methane is obtained with CMS depending on the cycle time for a high L/v ratio of 69. In single column unit with 4A zeolite exit methane mole fraction reached up to 84% with helium as purge and a desorption period thrice the adsorption step.

A linear driving force (LDF) kinetic PSA model with binary Langmuir isotherm, is solved by orthogonal collocation method to predict the results of two column and single column experiments. For 4A zeolite it is not possible to predict a priori the outlet concentrations using available literature data. Using 33% and 20% of the theoretical Ω values for CH_4 and N_2 respectively, a reasonable fit is obtained. This suggests that the D_c/r_c^2 values used for both sorbates is higher than the reported literature values. Theoretical studies are performed to establish desirable D_c/r_c^2 for these sorbates in order to achieve better separation. This could possibly be done by tailoring the pore size distribution.

The studies involving the CMS indicate that a totally different rate factor and trend is observed in LDF approximation. This difference is a reflection of the barrier resistance mechanism.

DOCTOR OF PHILOSOPHY DEGREE
KING FAHD UNIVERSITY OF PETROLEUM & MINERALS
Dhahran, Saudi Arabia
July 1992

CHAPTER 1

INTRODUCTION

1.1 Introduction

Separation processes represent the bulk of downstream operations in most chemical and pharmaceutical industries since products obtained through reactions or synthesis are either contaminated or form bulk mixtures with the reactants. The refinement processes which follow are relatively simple for heterogeneous vis a vis the homogeneous mixtures, but are usually energy intensive. Economy is the key factor in selection of such a process. Ongoing research and development, however, does improve and alter the economic viability of a process, thereby making it more competitive or attractive. Gas separation processes are among those witnessing significant innovations. Separation at ambient temperatures, by preferential adsorption of certain components from mixtures is gaining ground over the established energy intensive processes like liquefaction and cryogenic distillation. Better understanding and efficient operation of adsorptive separation processes will lead to wider applications.

Gas separation processes are either used for purification purposes, the aim of which is to remove or reduce an undesirable component from a stream without recovery, or bulk separation in which the feed is divided into two (or more) fractions of different compositions where both the fractions contain recoverable

products. Earlier applications were mainly used for purification, such as removal of hydrogen sulfide, mercaptans and moisture from gas streams. Bulk separations are more recent developments. The process scheme used in this separation differs due to obvious reasons, but the underlying general principles of design and operation remain similar. Initial applications were separation of linear paraffins from branched and cyclic isomers and recovery of aromatic hydrocarbons.

An economical process requires an adsorbent with high selectivity, large capacity and long life. Selectivity usually depends on steric properties adsorption kinetics and or adsorption equilibrium. The steric property allows only limited specific constituents of the mixture to penetrate the adsorbent. This is usually the case when the size of the constituent molecules differs largely. Kinetic selectivity is the ratio of diffusive resistances of the adsorbing species. Selectivity in adsorption equilibrium can be defined analogous to that in distillation as follows

$$\alpha_{AB} = \frac{q_A / C_A}{q_B / C_B} \quad (1.1)$$

where q and C refer to the concentrations in the adsorbed and fluid phases respectively. α_{AB} is dependent on the adsorbent used. The separation characteristics, whether equilibrium or kinetic, are dependent on the gases to be separated and the adsorbent used. Hence, a gas mixture can be separated in different

ways depending on the adsorbent used. As an example, a nitrogen oxygen mixture separated on 5A zeolite results in oxygen as the product due to a higher equilibrium adsorption of nitrogen while the same mixture separated on CMS results in nitrogen as the product due to faster diffusion of oxygen. The former is an equilibrium separation while the latter is a kinetic separation. Processes based on equilibrium separation are widespread in applications.

1.2 A brief overview of modelling Pressure Swing Adsorption (PSA) Separation Processes

A detailed view of a typical adsorption column is shown in Fig. 1.1. The pellet, which form the packed bed, consists of microporous crystals bound together. The macropore between the crystals is also shown. In any sorption process there are two phases, the fluid phase consisting of the adsorbates and the solid phase consisting of porous adsorbent. The adsorbates have to penetrate the film, macropores and micropores before sorption occurs on the surface of the adsorbent crystal and same holds for desorption. These resistances coupled with sorption affinity are specific characteristics of the component and adsorbent under consideration. The differences in these characteristics between various gas solid pair form the basis of adsorptive separation processes. The principle underlying any adsorptive separation is the appropriate exploitation of these characteristics.

The first step in development of an industrial process is to obtain the adsorption kinetics and adsorption equilibrium parameters for the system. This is culled either from a literature search or experimentally determined. The latter is often preferred as each production batch of the adsorbent has a property variation to the extent of 5 to 10 percent even with good quality control.

Industrial processes are normally scaled either based on results from a pilot plant data or from a simulation study of the process using an appropriate model. The two main approaches to simulation of PSA processes are the rigorous and the simplified model. A rigorous model considers the individual rate processes governing the micropore, macropore and film resistance for the pellet along with the axial dispersion model for flow through the packed bed. Solution of such a model involves extensive computations and is quite expensive. An alternate and widely used method is the simplified model obtained by replacing the mass balance equations within the particle by a simplified approximate expression relating the overall uptake rate and the bulk flow concentration:

$$\frac{\partial \bar{q}}{\partial t} = f((q^* - \bar{q}))$$

These are referred to as driving force approximations, since the rate is expressed as a function of overall driving force. In most applications, the significant resistance is the micropore diffusion for which f is a function of the parti-

cle diffusion time constant D/r^2 . The first and the most popular approximation derived by Gluckauf (1) was linear and is referred to as the Linear Driving Force (LDF) approximation:

$$\frac{\partial \bar{q}}{\partial t} = \frac{15D}{r^2} (q^* - \bar{q})$$

For cyclic operations this is valid for Dt/r^2 values > 0.1 . The factor of 15 is valid for a spherical particle. This approximation derived for a step change boundary condition was extended for cyclic boundary conditions by Nakao and Suzuki(2) and further studied for a PSA process by Raghavan et al(3). Both studies involved comparing the solution obtained by both the rigorous and LDF model. A variable LDF factor Ω was used for the cyclic process instead of the constant 15 derived by Gluckauf. The results, as shown in Fig. 1.2, indicated that Ω is a function of dimensionless half cycle time, $Dt_{1,2}/r^2$ and is also consistent with Gluckauf's result. This approach reduces the complexity associated with modelling within the particle. For flow through the bed two typical models are the axial dispersed flow or mixed cells in series, the former being more realistic in formulation while the latter is easier to solve mathematically.

This gives a brief overview underlining the modelling of a binary gas separation process using PSA separation technique. Elaborate explanations of these principles and techniques are found in the literature (4,5).

1.3 Cyclic Separation Processes :

Large scale adsorption processes are in operation either as cyclic batch systems in which the adsorbent bed is alternately saturated and regenerated in a cyclic manner or as continuous flow systems which are normally counter current contactors between the feed and the adsorbent. Cyclic batch systems are preferred where the separation factor is high and mass transfer resistance is low due to their low capital cost.

All cyclic separation processes undergo alternate loading and regeneration phases but differ on the method of regeneration as follows:

- 1.) Thermal swing : The bed is regenerated by raising the temperature usually by passing a preheated gas. The effect of temperature is indicated in Fig. 1.3. Although being the oldest and the most completely developed method, this is a relatively slow process and is used mainly for purification purposes.
- 2.) Pressure swing : A widely used method of regeneration because of the simplicity and ease of operation. The total pressure of the system is reduced thereby reducing the solid phase concentration as indicated in Fig. 1.3. This method is quite flexible in terms of process modification but modelling this process is quite difficult and complex.
- 3.) Purge gas stripping: Regeneration of the bed is done by purging the column with a nonadsorbing carrier gas at essentially constant temperature and pressure. This method is applied in chromatographic separations.

- 4.) Displacement desorption : Adsorbed material is displaced by another species in the adsorbent.

Each of these methods have their own merits. Much used industrially is the pressure swing method which is widely applied and had its beginning when Skarstrom developed the "Heatless drier" for air drying which was a two bed PSA system(6). Although use of PSA systems have increased rapidly, theoretical studies have been limited. Most studies till recently were based on equilibrium selectivity. Kinetic separation, a process more complex to model, is now being studied for oxygen-nitrogen separation on carbon molecular sieves. The rate process is either lumped (7) or solved for each resistance (8). A typical PSA simulation flowchart, being developed by the BOC group, and titled Dynamic Adsorption Process Simulator (DAPS) is shown in Fig 1.4 (9) indicating the organization of the various parameters such as rate processes, equilibrium isotherms, cycle sequencing, and energy equations in order to obtain purity, yield and material balance. This is being developed with the broad aim of creating a general purpose type of computer model and physical property databases for PSA process and research engineers to develop, design and optimize their PSA process. Mathematical model of a PSA process consists of numerous differential equations, normally stiff in character, which consumes a lot of CPU time. A paradox of a rigorous model PSA simulation is that it takes less time experimentally to run a few hundred cycles than to simulate the same. The way to go about this is to go for fast and easy solutions based on lumped parameter mod-

els, although non reliable at times. Although simulation of PSA is plagued with these problems, it is an important avenue to the understanding of the PSA processes

1.4 Outline of the present study:

The present study is towards adsorptive separation of binary gas mixtures. The first part consists of fundamental studies related to binary gas separations, while the latter part consists of studies related to PSA experiments and simulation using model binary gas mixtures of 8% and 40% nitrogen in methane. These mixtures are representatives of natural gas (SAUDI ARAMCO) and industrial (SAUDI METHANOL) gas streams in the Kingdom of Saudi Arabia. A major use of the gas stream containing 40% nitrogen in methane is for heating purposes but prior to this it is essential to increase the methane concentration to 80%, generally referred to as "pipeline quality". Two methods of enriching such streams in methane is either an energy intensive liquefaction process or a capital intensive PSA process involving kinetic separation. The former is in use while the latter is yet to be studied and used on commercial scale.

In the following chapter, the dynamic behaviour of an adsorbent crystal and pellet separating a binary gas mixture under realistic conditions is studied theoretically. A mathematical model is developed for the sorption and diffusion by considering the nonlinearity of the adsorption isotherm and concentration

dependence of diffusivity. Uptake rates are studied as a function of pressure and Biot number under cases of constant and varying diffusivities. In case of pellet where both micropore and macropore diffusion resistances co-exist, this is studied only to a limited extent.

In chapter 3 the adsorption column dynamics is studied using the quasicon-
tinuum axial dispersed plug flow model and discrete cell approach model. Adsorption and desorption curves are generated for equilibrium and non equilibrium systems having Langmuir type of isotherm. Ethylene-helium and methane helium on zeolite 5A represent the equilibrium case while ethylene-helium on 4A zeolite and oxygen-helium on carbon molecular sieve represent non-equilibrium case. The breakthrough curves are analysed for a correlation between the Peclet number and number of cells in the two models respectively.

In chapter 4 theoretical and experimental studies of sorption of methane and nitrogen on carbon molecular sieves and zeolite 4A are reported in order to obtain the adsorption equilibrium and kinetic parameters. The experimental studies are performed using volumetric and gravimetric techniques and results are compared with the literature and in particular the results obtained from the chromatographic study of Zahur(10). These parameters are needed in the simulation of PSA process separating the binary mixture on the above mentioned adsorbents.

Chapter 5 onward forms the latter part of the dissertation where PSA as a adsorptive separation process is studied experimentally and numerically. In chapter 5, PSA separation of two model methane-nitrogen mixtures on carbon molecular sieve using two columns is studied experimentally. Also a simulation of the entire process is done using a suitable model and results are compared with the experimental data.

In chapter 6 the above model mixtures are separated by PSA process on zeolite 4A using either two columns or a single column. The advantage of using a single column is the flexibility of using unsymmetric sequencing of PSA operation. Simulation is done for both cases using a suitable model and results are compared with the experimental data.

References

- (1) Glueckauf, E., Trans. Faraday Soc., 51, 1540 (1955).
- (2) Nakao, S. I., Suzuki, M., J. Chem. Engg. Japan 16, 114, (1983).
- (3) Raghavan, N. S., Hassan, M. M., Ruthven, D. M., Chem. Engg. Sci., 41, 2787, (1986).
- (4) Yang, R. T., Gas Separation by Adsorption Processes, Butterworths, 1987.
- (5) Ruthven, D. M., Principles of Adsorption and Adsorption Processes, John Wiley, New York, 1984.
- (6) Skarstrom, C. W., Recent Development in Separation Science, Vol 2, 95, CRC Press, Cleveland, Ohio (1972). ACS Symp. Series, 223, 195 (1983).
- (7) Shendalman, L. H., Mitchell, J. E., AIChE Symp. Ser. 69, No. 134, 25, (1973).
- (8) Hassan, M. M., Raghvan, N. S., Ruthven, D. M., Chem. Engg. Sci., 42, 2037, (1987).
- (9) Doong, S. J., LaCava, A.I., Simulation of Pressure Swing Processes, Adsorption News, Vol 2, No.1, February 1991.
- (10) Zahur, M., M. S. Thesis, KFUPM (1991).

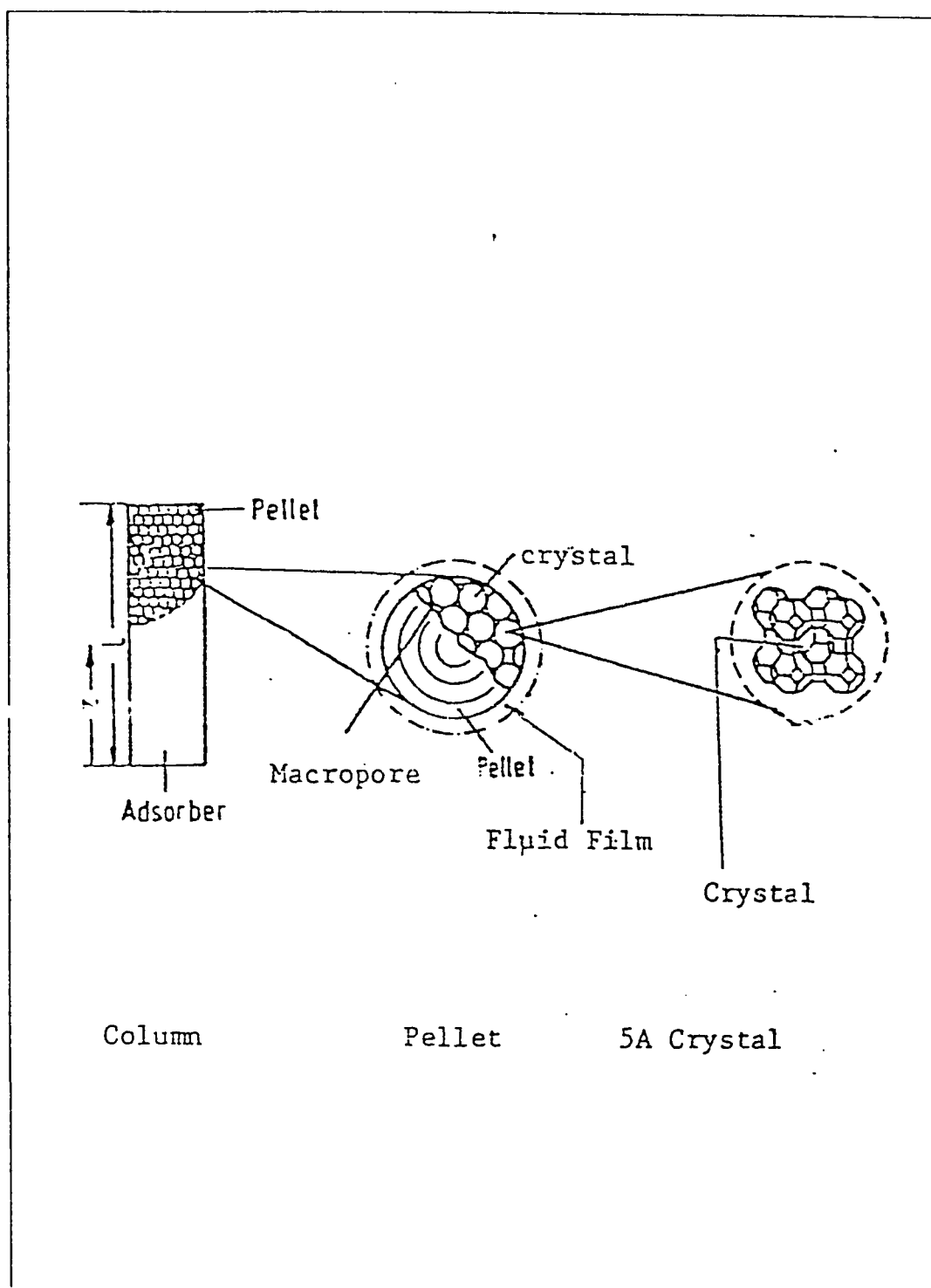


Fig. 1.1 Packed Adsorbent Column loaded with Pellets of zeolite 5A crystals.

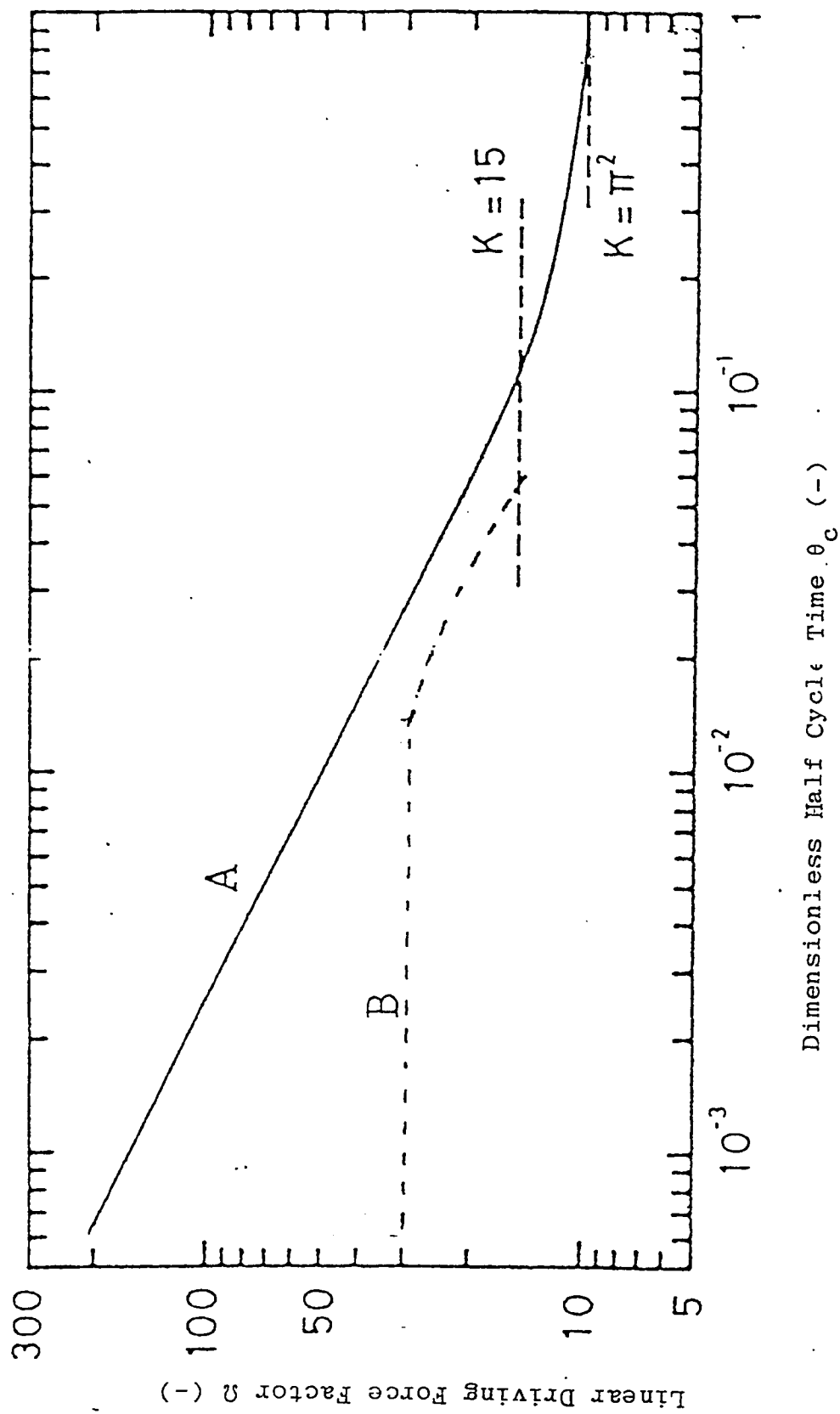


Fig 1.2 Linear Driving Force Approximation Factor as a Function of Dimensionless Half Cycle Time as studied by (A) Nakao & Suzuki and (B) Raghavan et al.

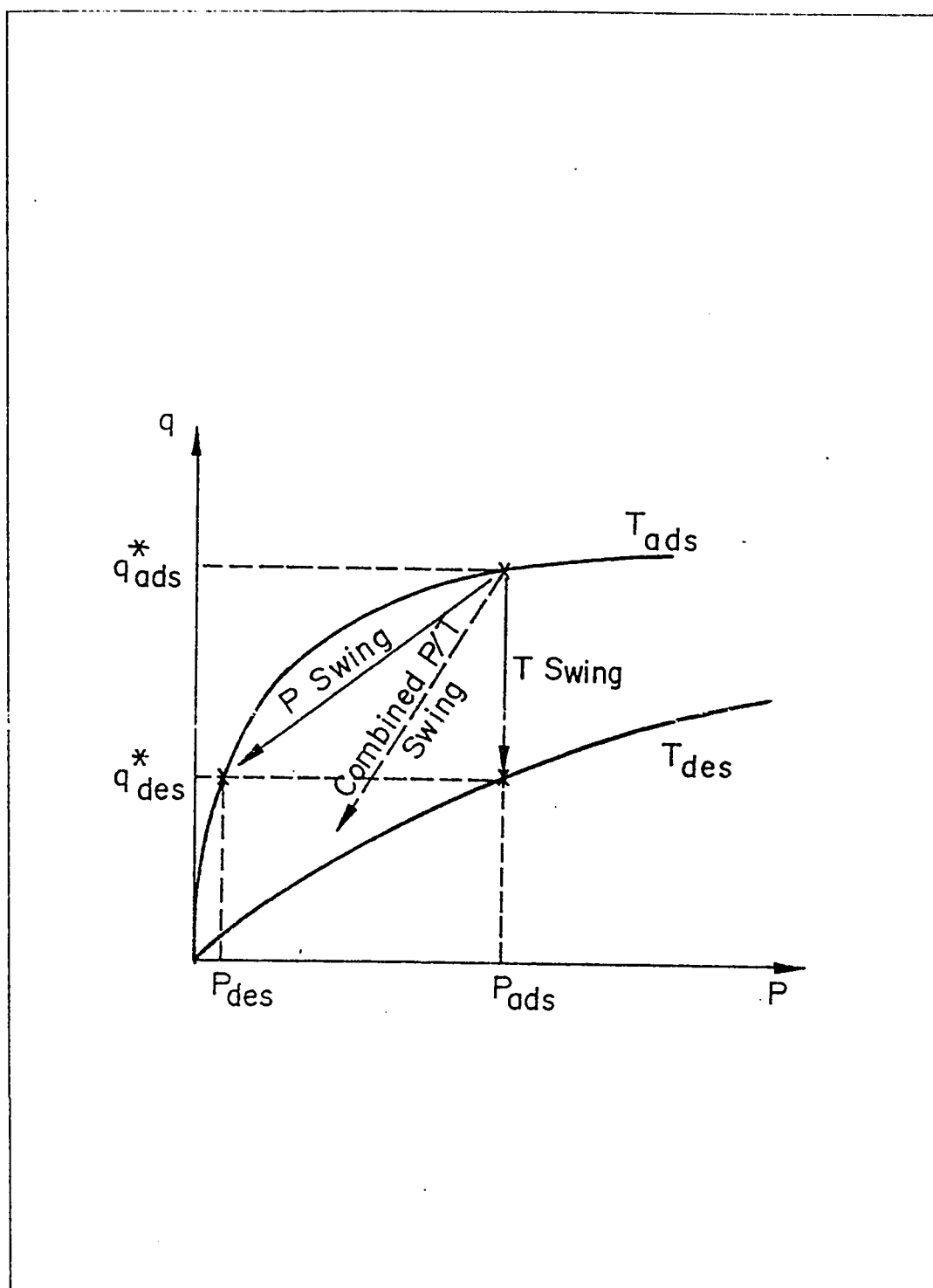


Fig. 1.3 Schematic Isotherm showing Pressure Swing, Thermal Swing and Combined Pressure-Temperature Swing Operation for an Adsorption Process

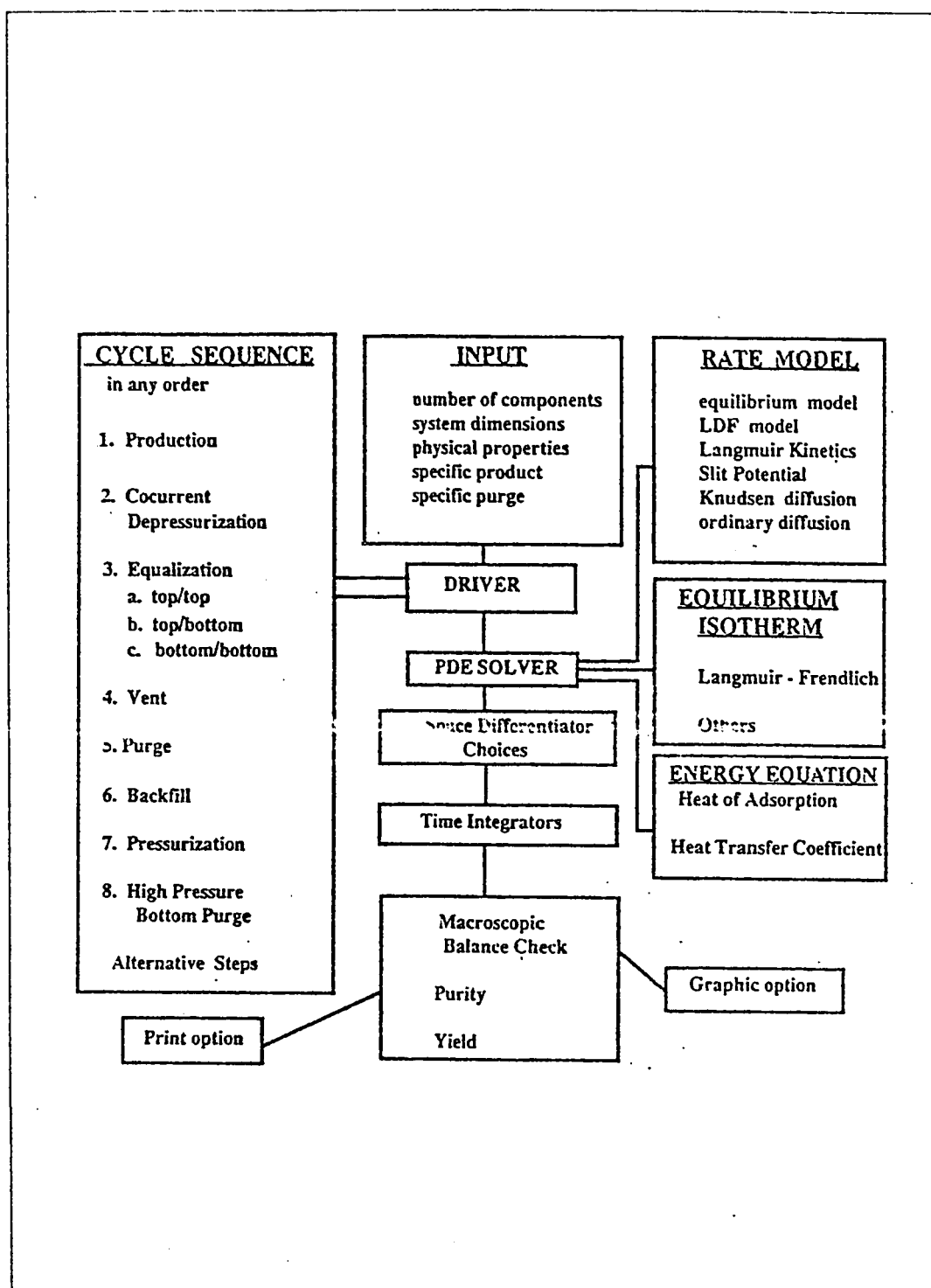


Fig 1.4 Program Flow Chart for a typical simulation of a PSA Process(9)

CHAPTER 2

ADSORPTIVE DIFFUSION OF BINARY MIXTURES IN MICROPOROUS CRYSTALS

2.1 INTRODUCTION

Adsorption is a widely used technique for gas separation(1). A variety of methods for using the adsorption techniques have been studied and put to use. Pressure swing adsorption is quite common among them(2). A relatively simple process, this is carried out using a packed bed consisting of adsorbent pellets. These pellets consists of microporous crystals typically zeolites, molecular sieves etc. which are binded together. A typical bed, pellet and crystal representation was given in Figure 1.1. A crystal is a basic unit where the actual process of adsorption occurs. These crystals are of regular molecular structure characterized in size and shape by the elements forming them. The size of a commercially available zeolite crystal is between 0.5 - 5.0 microns and the lattice parameter of its structure is about 12 Å ; hence the smallest crystal contains thousands of cavities, thereby justifying the diffusive transport within the crystals. Diffusion is the only internal resistance to mass transfer in the crystal. There can be external film mass and heat transfer resistance in case the crystal is suspended by itself in a gas stream.

The relative adsorption of a species in a gas mixture on the crystal depends on different factors such as:

- a) the size of gas molecule and size of crystals. If the size of the gas molecule is larger than the crystal opening no adsorption can occur for that species. This is referred to as a steric separation.
- b) adsorption affinity. If a particular species is more strongly adsorbed, then at equilibrium it will have a higher solid phase concentration. This is referred to as an equilibrium separation.
- c) diffusion characteristics. If the relative diffusion rates are quite different then this is referred to as a kinetic separation.

In practice when a mixture of gases have to be separated, selection of an adsorbent is based on the idea of steric separation which in most cases reduce the system effectively to a binary one. For a binary system either (b) or (c) may be applied depending on the requirements. An example of such a binary separation is of oxygen and nitrogen in air. Nitrogen is more strongly adsorbed at equilibrium in case of 4A and 5A zeolite while oxygen is a faster diffusing species in 4A zeolite only. In 5A both oxygen and nitrogen have almost the same diffusion rates. In case of carbon molecular sieve (CMS) the equilibrium capacities are same for both but oxygen is the faster diffusing species(3,4). Order of magnitude of the equilibrium and kinetic parameters for these cases are:

$$\text{In 5A zeolite } K_{O_2} < K_{N_2} \quad \frac{D}{r^2}|_{O_2} \approx \frac{D}{r^2}|_{N_2}$$

$$\text{In 4A zeolite } K_{O_2} < K_{N_2} \quad \frac{D}{r^2}|_{O_2} > > \frac{D}{r^2}|_{N_2}$$

$$\text{In CMS } K_{O_2} \approx K_{N_2} \quad \frac{D}{r^2}|_{O_2} > > \frac{D}{r^2}|_{N_2}$$

The interaction of kinetics and equilibrium is clear from the above schemes. Qualitative conclusions are difficult to make while quantitative conclusions need a proper modelling and solution of such systems. The objective of this study is to simulate the adsorption of a nitrogen-oxygen mixture on a 4A zeolite and CMS crystal under various practical conditions using a generalized model and note the effect on the adsorption selectivity.

2.2 LITERATURE REVIEW

Mathematical models for diffusion and their analytical solution and approximate solutions were presented by Crank (5) early in 1956. His work involved mainly one component systems. With the advances of computing devices, numerical solution of diffusion models were preferred since they are easier to obtain or in some cases the only way. The commonly used numerical methods for solving the partial differential equations of diffusion are finite difference or lately by collocation methods(6). For pure component sorption in a microporous spherical crystal, the diffusive transport equation under isothermal conditions is given by

$$\frac{\partial q}{\partial t} = \frac{1}{r^2} \frac{\partial}{\partial r} \left\{ r^2 D_c \frac{\partial q}{\partial r} \right\} \quad (2.1)$$

For the case of constant diffusivity, which is a reasonable approximation for small uptake rates the equation is

$$\frac{\partial q}{\partial t} = D_c \left\{ \frac{\partial^2 q}{\partial r^2} + \frac{2}{r} \frac{\partial q}{\partial r} \right\} \quad (2.2)$$

The initial and boundary conditions are as follows

$$\text{I.C.: } q(r_c, 0) = q_0,$$

$$\text{B. C.: } q(r_c, t) = q_0, \quad \left(\frac{\partial q}{\partial r} \right)_{r=0} = 0$$

The analytical solution for this case as well as several other cases such as sorption from a finite volume of gas phase is available in Crank(5). Approximate short and long time solutions have also been deduced. For a large step change the diffusivity changes with the concentration as proposed by Darken(7). Garg and Ruthven(8) studied the case when diffusivity varies with concentration based on Darken's relation and the adsorption equilibrium isotherm is Langmuir type. According to Darken's relation, the diffusivity expression and the diffusive transport equation are as follows:

$$D_c = D_0 \frac{d \ln P}{d \ln q} \quad (2.3)$$

The relation as applied to Langmuir type isotherm results as

$$D_c = D_0 \left\{ 1 - \frac{q}{q_s} \right\}^{-1} \quad (2.4)$$

and substitution in the diffusion equation leads to

$$\frac{\partial q}{\partial t} = \frac{D_0}{r^2} \frac{\partial}{\partial r} \left\{ \frac{r^2}{1 - \frac{q}{q_s}} \frac{\partial q}{\partial r} \right\} \quad (2.5)$$

A similar analysis was reported by Kocirik et al(9). When a large step change occurs, there is a possibility that the temperature in the microporous crystal may increase to an extent leading to nonisothermal conditions. In such a case an additional heat balance

equation needs to be solved. Also the adsorption equilibrium constant and the diffusivity will be a function of temperature. Ruthven and Lee(10) have studied such a situation wherein it is assumed that the temperature of the particle is constant throughout but different from the surroundings.

The above models are for sorption of a single component or a second inert component which does not affect the sorption rate. In case of both components being adsorbed or external mass transfer being significant, the model equations should be solved for the binary system. The model for the binary system is similar to that for the one component system except that the equilibrium relation is modified through a mixture isotherm. For the case of two component system the Langmuir adsorption isotherm can be written as

$$\frac{q_A}{q_s} = \frac{b_A P_A}{1 + b_A P_A + b_B P_B} \quad (2.6)$$

$$\frac{q_n}{q_s} = \frac{b_n P_n}{1 + b_A P_A + b_n P_n}$$

Hence the diffusion equations are coupled through the equilibrium relationship. Due to the complexity of the problem, diffusion in mixed adsorbed phase has been studied only to a limited extent. A theoretical study of diffusion in a binary adsorbed phase has been done by Round, Newton and Habgood(11) and independently reported by Karger and Bulow(12). In case of co-diffusion where both the components are competitively adsorbed the faster diffusing species is adsorbed initially and reaches a maximum after which it partially desorbs in favour of slower diffusing species to reach an equilibrium value lower than the maximum. Such behaviour has been observed for sorption of Nitrogen - Methane on 4A zeolite (13). A conclusion from this review is that although extensive work has been done for one component sorption in a microporous crystal, the binary system analysis remain elusive to a great extent. The present work is undertaken to model a binary adsorptive separation under various conditions. The analysis is based on a ratio, which is a normalized uptake of individual components.

2.3 MATHEMATICAL MODEL FOR ADSORPTION IN A CRYSTAL.

A mathematical model for sorption of a binary gas mixture on a microporous crystal under certain valid assumptions is developed for the most general condition, and solved for various limiting cases. The essential assumptions are

the spherical nature of the crystal, occurrence of radial micropore diffusion only and step change in the gas phase. The conditions arising for which the model is developed are variable intracrystalline diffusivity, non linear isotherm, non isothermal conditions and film resistance to heat and mass transfer. Following is a step by step development of the model presented for various cases.

Case I : Constant intracrystalline diffusivity, step change at surface, linear isotherm, isothermal conditions. The equations governing the diffusion process is written for a component as follows:

Mass balance

$$\frac{\partial q}{\partial t} = \frac{1}{r^2} \frac{\partial}{\partial r} \left\{ r^2 D_c \frac{\partial q}{\partial r} \right\}$$

Since the intracrystalline diffusivity is constant, it can be written for each component as follows:

Mass balances

$$\frac{\partial q_A}{\partial t} = D_A \left\{ \frac{\partial^2 q_A}{\partial r^2} + \frac{2}{r} \frac{\partial q_A}{\partial r} \right\}$$

$$\frac{\partial q_B}{\partial t} = D_B \left\{ \frac{\partial^2 q_B}{\partial r^2} + \frac{2}{r} \frac{\partial q_B}{\partial r} \right\}$$

Initial conditions:

$$q_A = q_B = 0$$

Boundary conditions:

At $r = 0$

$$\frac{\partial q_A}{\partial r} = \frac{\partial q_B}{\partial r} = 0 \quad (2.7)$$

At $r = r_0$

Equilibrium relationships:

$$q_A^* = K_A P_A, \quad q_B^* = K_B P_B \quad (2.8)$$

Defining the following dimensionless parameters :

$$Q_A = \frac{q_A}{q_A^*}, \quad Q_B = \frac{q_B}{q_B^*}$$

$$R = \frac{r}{r_0}, \quad \tau = \frac{D_A t}{r_0^2}$$

The above equations can be reduced to the following :

$$\frac{\partial Q_A}{\partial \tau} = \left\{ \frac{\partial^2 Q_A}{\partial R^2} + \frac{2}{R} \frac{\partial Q_A}{\partial R} \right\} \quad (2.9)$$

$$\frac{\partial Q_B}{\partial \tau} = \frac{D_B}{D_A} \left\{ \frac{\partial^2 Q_B}{\partial R^2} + \frac{2}{R} \frac{\partial Q_B}{\partial R} \right\} \quad (2.10)$$

$$\text{I. C. : } Q_A = Q_B = 0$$

$$\text{B. C.'s : At } R = 0$$

$$\frac{\partial Q_A}{\partial R} = \frac{\partial Q_B}{\partial R} = 0$$

$$\text{At } R = 1$$

$$Q_A = Q_B = 1$$

To evaluate the uptake ratio the following procedure is adopted

$$\frac{M_A}{M_B} = \frac{\int_0^{r_0} q_A r^2 dr}{\int_0^{r_0} q_B r^2 dr} = \frac{K_A P_A \int_0^1 Q_A R^2 dR}{K_B P_B \int_0^1 Q_B R^2 dR} \quad (2.11)$$

Define the normalised uptake ratio(NUR) as:

$$\left(\frac{M_A}{K_A P_A} \right) \left(\frac{K_B P_B}{M_B} \right) = \frac{\sum_1^7 W_i Q_{Ai}}{\sum_1^7 W_i Q_{Bi}} \quad (2.12)$$

where W's are the Gaussian Quadrature Weights at seven specific points and Q's are the corresponding concentrations.

Case (II) : Constant intracrystalline diffusivity, mass transfer resistance at the surface, linear isotherm, isothermal.

The governing equations are same as for case I except for the boundary conditions, given by Equation (2.8) which are rewritten as follows:

$$\text{At } r = r_0$$

$$D_A \frac{\partial q_A}{\partial r} = k \{q'_A - q_A\} \quad (2.13)$$

$$D_B \frac{\partial q_B}{\partial r} = k \{q'_B - q_B\} \quad (2.14)$$

Using the dimensionless number,

$$Bi_A = Bi = \frac{k r}{D_A}$$

the result is :

$$\text{At } R = 1$$

$$\frac{\partial Q_A}{\partial R} = Bi \{1 - Q_A\} \quad (2.15)$$

$$\frac{\partial Q_B}{\partial R} = \frac{D_A}{D_B} Bi \{1 - Q_B\} \quad (2.16)$$

Case III : Case I and Case II with non linear isotherm (Langmuir isotherm). The governing equations are the same except for the boundary conditions at the surface.

$$\text{At } r = r_0$$

$$\frac{q'_A}{q_s} = \frac{b_A P_A}{1 + b_A P_A + b_B P_B} \quad (2.17)$$

$$\frac{q'_B}{q_s} = \frac{b_B P_B}{1 + b_A P_A + b_B P_B} \quad (2.18)$$

The right hand side values of the above equations are constant. Defining the dimensionless variables as in Case I, the dimensionless equations and B.C.'s for both case I and II remain the same.

The uptake ratio in this case is :

$$\frac{M_A}{M_B} = \frac{\int_0^{r_0} q_A r^2 dr}{\int_0^{r_0} q_B r^2 dr} = \frac{b_A P_A}{b_B P_B} \frac{\int_0^1 Q_A R^2 dR}{\int_0^1 Q_B R^2 dR} \quad (2.19)$$

$$\left(\frac{M_A}{K_A P_A} \right) \left(\frac{K_B P_B}{M_B} \right) = \frac{\sum_1^7 W_i Q_{Ai}}{\sum_1^7 W_i Q_{Bi}} \quad (2.20)$$

Case IV : Variable Diffusivity, D_c is concentration dependent as follows:

$$D_c = D_0 \frac{d \ln P}{d \ln q}$$

where D_0 is the limiting diffusivity. In case of a linear isotherm, $q = KP$

$$\frac{d \ln P}{d \ln q} = 1$$

therefore D_c is independent of concentration. For a binary Langmuir isotherm the dependency is given by

$$D_A = D_{A_0} \left\{ \frac{1 - \frac{q_B}{q_s}}{1 - \frac{q_A}{q_s} - \frac{q_B}{q_s}} \right\} \quad (2.21)$$

With $Q_A = \frac{q_A}{q_s}$ and $Q_B = \frac{q_B}{q_s}$ the governing dimensionless equations are :

$$\frac{\partial Q_A}{\partial \tau} = \frac{1 - Q_B}{1 - Q_A - Q_B} \frac{\partial^2 Q_A}{\partial R^2} + \frac{1}{1 - Q_A - Q_B} \left\{ (1 - Q_B) \frac{\partial^2 Q_B}{\partial R^2} + Q_A \left(\frac{\partial Q_A}{\partial R} \right) \left(\frac{\partial Q_B}{\partial R} \right) \right\}. \quad (2.22)$$

$$\frac{\partial Q_B}{\partial \tau} = \frac{1 - Q_A}{1 - Q_A - Q_B} \frac{\partial^2 Q_B}{\partial R^2} + \frac{1}{1 - Q_A - Q_B} \left\{ (1 - Q_A) \frac{\partial^2 Q_A}{\partial R^2} + Q_B \left(\frac{\partial Q_B}{\partial R} \right) \left(\frac{\partial Q_A}{\partial R} \right) \right\} \quad (2.23)$$

B.C 's : At $R = 1$

$$Q_A = \frac{\dot{q}_A}{q_s} = \frac{b_A P_A}{1 + b_A P_A + b_B P_B} = \text{constant}$$

$$Q_B = \frac{\dot{q}_B}{q_s} = \frac{b_B P_B}{1 + b_A P_A + b_B P_B} = \text{constant}$$

The modified definition of Q_A , Q_B affects the uptake ratio as follows :

$$\frac{M_A}{M_B} = \frac{\int_0^1 q_A r^2 dr}{\int_0^1 q_B r^2 dr} = \frac{\int_0^1 Q_A R^2 dR}{\int_0^1 Q_B R^2 dR}$$

$$NUR = \left(\frac{M_A}{K_A P_A} \right) \left(\frac{K_B P_B}{M_B} \right) = \frac{b_B P_B}{b_A P_A} \frac{\sum_1^7 W_i Q_{Ai}}{\sum_1^7 W_i Q_{Bi}} \quad (2.24)$$

Case V : Case IV with mass transfer resistance on the surface. The relevant B. C.'s at the surface are

$$D_A \frac{\partial q_A}{\partial r} = k \{q_A^* - q_A\}$$

$$D_B \frac{\partial q_B}{\partial r} = k \{q_B^* - q_B\}$$

$$\frac{\partial Q_A}{\partial R} = Bi \left\{ \frac{q_A^*}{q_s} - Q_A \right\} \quad (2.25)$$

$$\frac{\partial Q_B}{\partial R} = \frac{D_A}{D_B} Bi \left\{ \frac{q_B^*}{q_s} - Q_A \right\} \quad (2.26)$$

Case VI : Case I to V with constant particle temperature different from the gas phase temperature. Additional equations for energy balance will be solved in this case using a dimensionless temperature defined as follows:

$$T = \frac{T_p}{T_o} \quad (2.28)$$

where

T_p = adsorbed phase temperature

T_o = gas phase temperature

The heat balance equation can be written as:

$$\rho_s \left\{ (-\Delta H_A) \left(\frac{3}{r_p} \right) D_{A,T} \left(\frac{\partial q_A}{\partial r} \right)_{r=r_0} + (-\Delta H_B) \left(\frac{3}{r_p} \right) D_{B,T} \left(\frac{\partial q_B}{\partial r} \right)_{r=r_0} \right\} =$$

$$\rho_s C_s \frac{\partial T_p}{\partial t} + h a (T_0 - T_p) \quad (2.29)$$

where I.C. $T_p = T_0$

The dimensionless form of the above equation is :

$$\frac{\partial T}{\partial \tau} = \frac{3(-\Delta H_A)q_s}{C_s T_0} \left\{ \frac{D_{A,T}}{D_{A,T_0}} \left(\frac{\partial Q_A}{\partial R} \right)_{R=1} + \left[\frac{-\Delta H_B}{-\Delta H_A} \right] \frac{D_{B,T}}{D_{A,T_0}} \left(\frac{\partial Q_B}{\partial R} \right)_{R=1} \right\} - \quad (2.30)$$

$$3 \frac{h}{\rho_s C_s} \frac{r_p}{D_{A,T_0}} (T - 1)$$

where

$$D_{A,T} = D_{A,T_0} \exp \left\{ \frac{E_A}{RT_0} \frac{T-1}{T} \right\} \quad (2.31)$$

$$D_{B,T} = D_{B,T_0} \exp \left\{ \frac{E_B}{RT_0} \frac{T-1}{T} \right\} , \quad \tau = \frac{D_{A,T_0} t}{r_p^2}$$

2.4 RESULTS AND DISCUSSION

The above mentioned cases were studied for two adsorption systems viz. O_2 , N_2 mixture on 4A zeolite and carbon molecular sieves. These systems are representative for air separation processes by pressure swing adsorption. The relevant parameters used for numerical computations are given in Table 2.1. Analysis of the models was done by solving the partial differential equations,

using collocation technique and IMSL Gear's routine for solving stiff ordinary differential equations. The resultant solutions were obtained in the form of semi logarithmic plots. The normalized uptake ratio, as defined earlier, was plotted on the linear scale versus the dimensionless time using logarithmic scale.

The normalised uptake ratio is a measure of the selectivity. The ultimate equilibrium value of this ratio is unity but when kinetics is controlling the adsorption, this indicates the preference for the faster diffusing species. Figs. 2.1 to 2.5 are typical plots generated for certain limiting cases described earlier.

Consider the most simple model with linear isotherm, fixed diffusivity and a step change occurring in the gas phase on the surface of the gas film or at the crystal surface in absence of mass transfer resistance. Fig. 2.1 and Fig. 2.2 shows the uptake curves from the solution of this model as applied to $O_2 - N_2$ mixture on CMS and 4A zeolite respectively. The film resistance is characterized by the Biot number, whose decreasing value indicates higher mass transfer resistance. As expected the normalised uptake ratio is directly proportional to the diffusivity ratio of the two species i.e. the diffusional time constants of the two species. With decreasing Biot number, which signifies a higher film resistance as compared to the internal diffusion resistance, the initial normalized uptake ratio decreases. Since mass transfer and diffusive resistance are additive, increase in the former decreases the effect of the latter hence the normalised uptake ratio decreases with increase in the mass transfer resistance signified by decreasing Biot number. Although individual uptakes may be affected with

pressure and composition the ratio remains independent of these parameters. The above analysis is valid for a non-linear isotherm as mentioned previously. Although the analysis for external mass transfer is done with a range of Biot number, the lowest physical value of this number is approximately 500, so that it can be assumed that zeolites and molecular sieve crystals are free of external mass transfer resistance.

In case of a large step change in the pressure the diffusivity becomes concentration dependent. Case IV and V are models in which the diffusivity is a function of the solid phase in accordance with Darken's relationship. Similar semi logarithmic plots (Figs. 2.3 and 2.4) for these cases shows that NUR is a strong function of pressure as well as composition. The mass transfer effect, though not physically realizable, is significant. Increased nitrogen composition reduces the NUR since it is the slower diffusing species. This effect is more prominent at high pressures. These effects are observed, in case of diffusivity being a function of solid phase composition, because coupling of equations is no longer limited to the crystal surface i.e. in the boundary conditions, but is now inherent in the mass balance equations within the crystals.

Large step change can lead to a temperature rise in the crystal giving rise to Case VI i.e. non isothermal model. Qualitatively it can be concluded that due to the small size of the crystal and a low value of $\frac{D}{r^2}$, the temperature rise is marginal. This case was solved and corresponding semi log plot is shown in Fig. 2.5, which indicates that even under a severe heat transfer conditions, the maximum

rise in temperature is about 12° C.

2.5 CONCLUSIONS

The simulation study of a binary gas mixture adsorbed on the crystal under variety of conditions was performed by developing a generalised model. Various limiting conditions and parameters likely to affect the process were considered. Various conclusions were drawn from this study based on the initial normalized uptake ratio(NUR). This decreases when the mass transfer resistance is significant. Also it is a function of diffusivity ratio in various adsorbents. It is independent of pressure, composition and non-linearity under conditions of fixed diffusivity. and is greatly dependent of pressure and composition, under conditions of concentration dependent diffusivity.

REFERENCES

- (1) Yang, R. T., Gas Separation by Adsorption Processes, Butterworths, 1987.
- (2) Ruthven, D. M., Principles of Adsorption and Adsorption Processes, John Wiley, New York, 1984.
- (3) H. S. Shin and K. S. Knaebel, AIChE J., 33, (4), 654, (1987).
- (4) Ruthven, D. M., N. S. Raghvan and Hassan, M. M., Chem. Engg. Sci., 41, 1325, (1986).
- (5) Crank, J., Mathematics of Diffusion, Oxford University Press, London, (1956).
- (6) N. S. Raghvan, M. M. Hassan, and D. M. Ruthven. AIChE J., 31, 385, (1985).
- (7) Darken, L., Trans. AIME, 174,184 (1948)
- (8) Garg, D. R. and Ruthven, D. M., Chem. Engg. Sci., 27, 417, (1972).
- (9) M. Kocirik, A. Zikanova, and J. Dubsky, Ind . Eng. Chem. Fund., 12, 440 (1973).
- (10) D. M. Ruthven, and L-K, Lee, AIChE J., 27, 654 (1981).
- (11) G. F. Round, H. W. Habgood and R. Newton, Sep. Sci., 1, 219 (1966).
- (12) J. Karger, and M. Bulow, Chem Eng. Sci., 30, 893 (1975).
- (13) H. W. Habgood, Can . J. Chem 36, 1384 (1958).

Table 2.1
Parameters used in the Computations

Adsorbent	Carbon molecular sieve
Temperature	45 °C
Equilibrium constant for N ₂	9.25
Equilibrium constant for O ₂	8.9
Diffusional time constant for O ₂	$3.728 \times 10^{-3} \text{ sec}^{-1}$
Diffusional time constant for N ₂	$1.171 \times 10^{-4} \text{ sec}^{-1}$
Adsorbent	Zeolite 4A
Temperature	45 °C
Equilibrium constant for O ₂	2.032
Equilibrium constant for N ₂	5.663
Diffusional time constant for O ₂	$1 \times 10^{-4} \text{ sec}^{-1}$
Diffusional time constant for N ₂	$1.6 \times 10^{-6} \text{ sec}^{-1}$

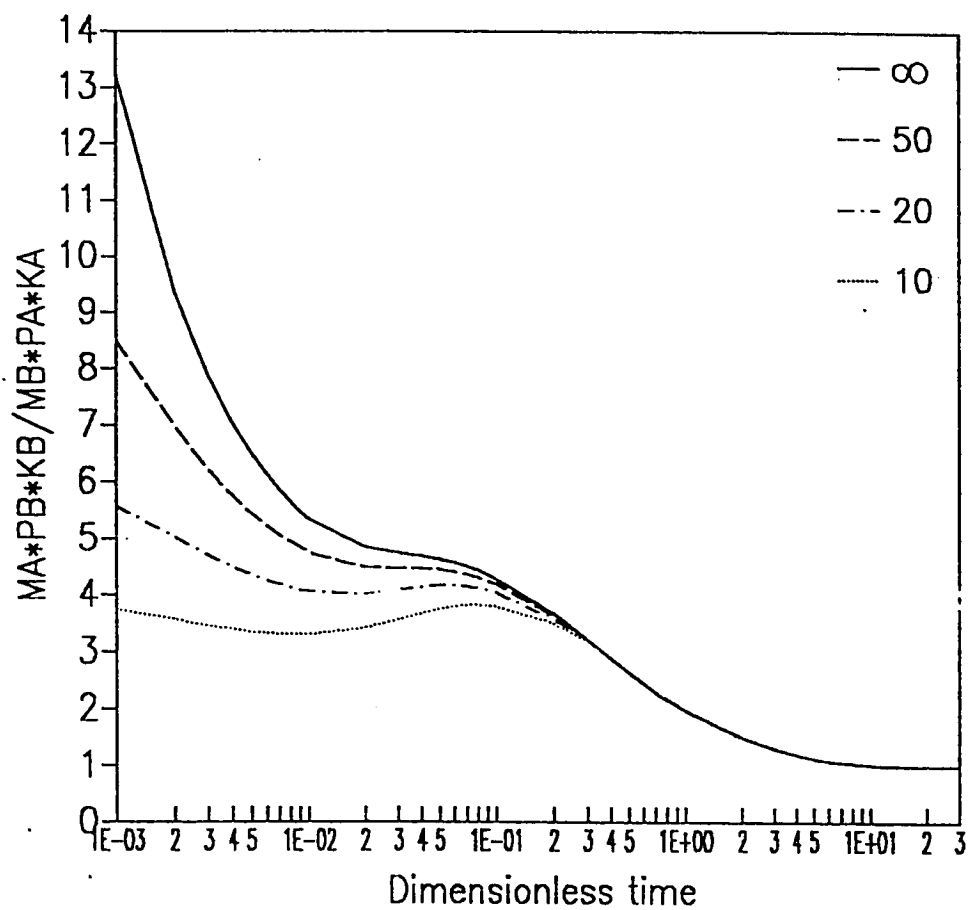


Fig. 2.1 Plot of Normalized Uptake Ratio with Dimensionless Time on CMS. Constant Diffusivity Case (Parameter is Biot No. of O_2 , $D_{O_2}/D_{N_2} = 31.82$)

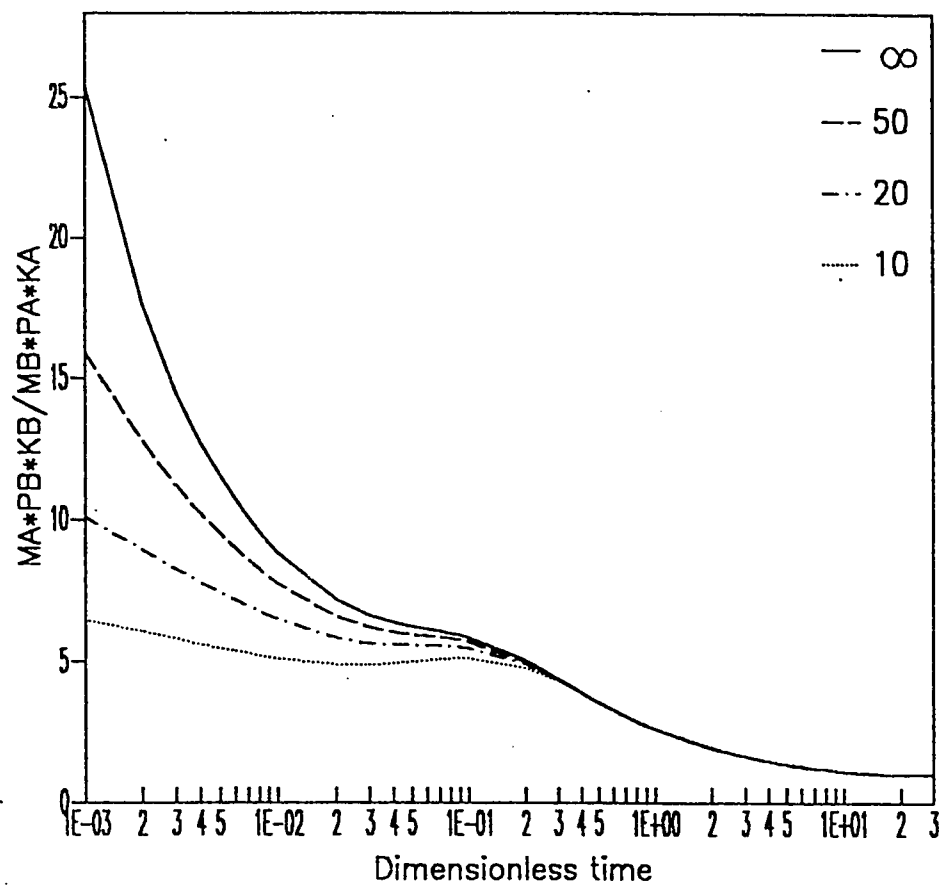


Fig. 2.2 Plot of Normalized Uptake Ratio with Dimensionless Time on CMS. Constant Diffusivity Case (Parameter is Biot No. of O_2 , $D_{O_2}/D_{N_2} = 62.5$)

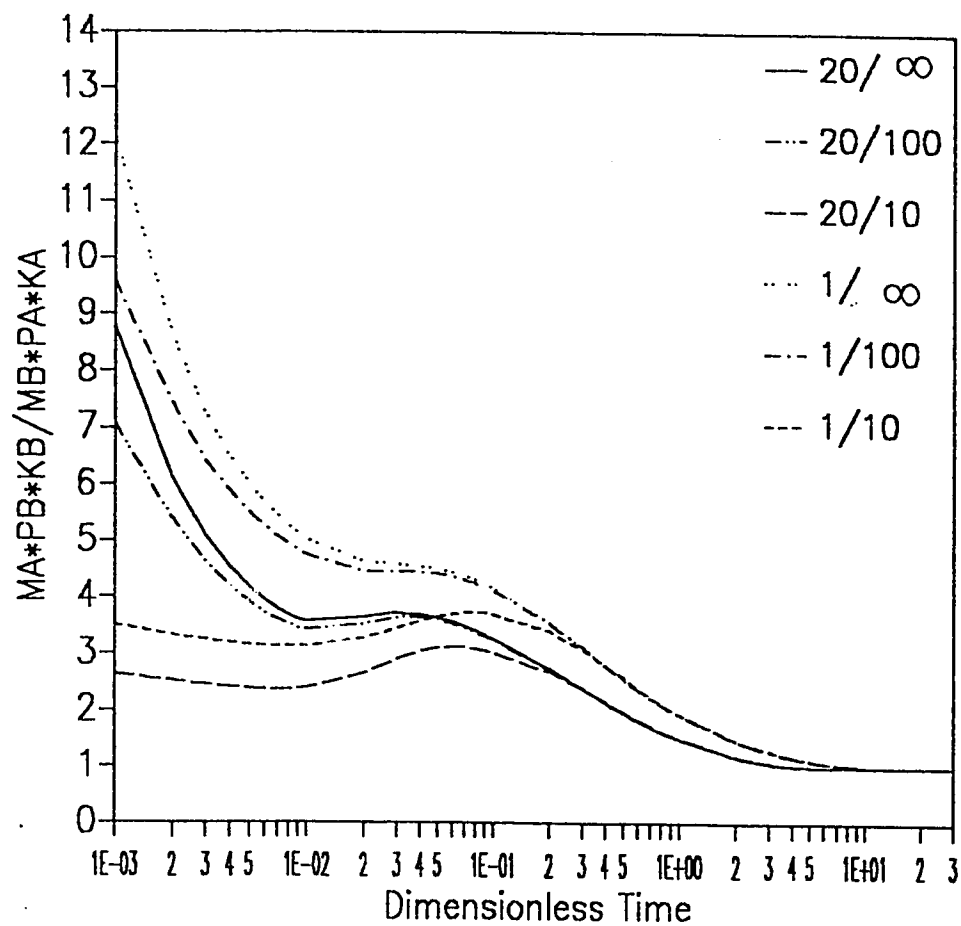


Fig. 2.3 Plot of Normalized Uptake Ratio with Dimensionless Time on CMS. Variable diffusivity Case (Parameter is Pressure (atm) / Biot No. of O_2 , $D_{O_2}/D_{N_2} = 31.82$)

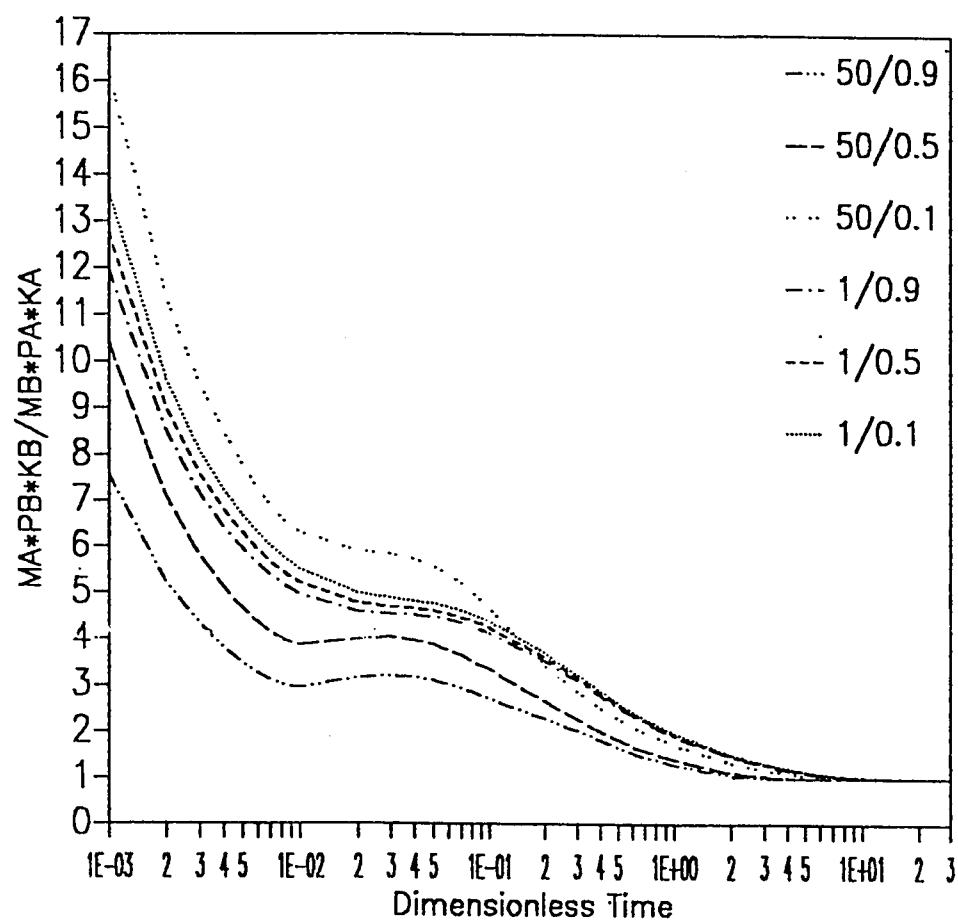


Fig 2.4 Plot of Normalized Uptake Ratio with Dimensionless Time on CMS. Variable Diffusivity & Feed concentration case. (Parameter is Pressure(atm)/ N_2 Mole Fraction)

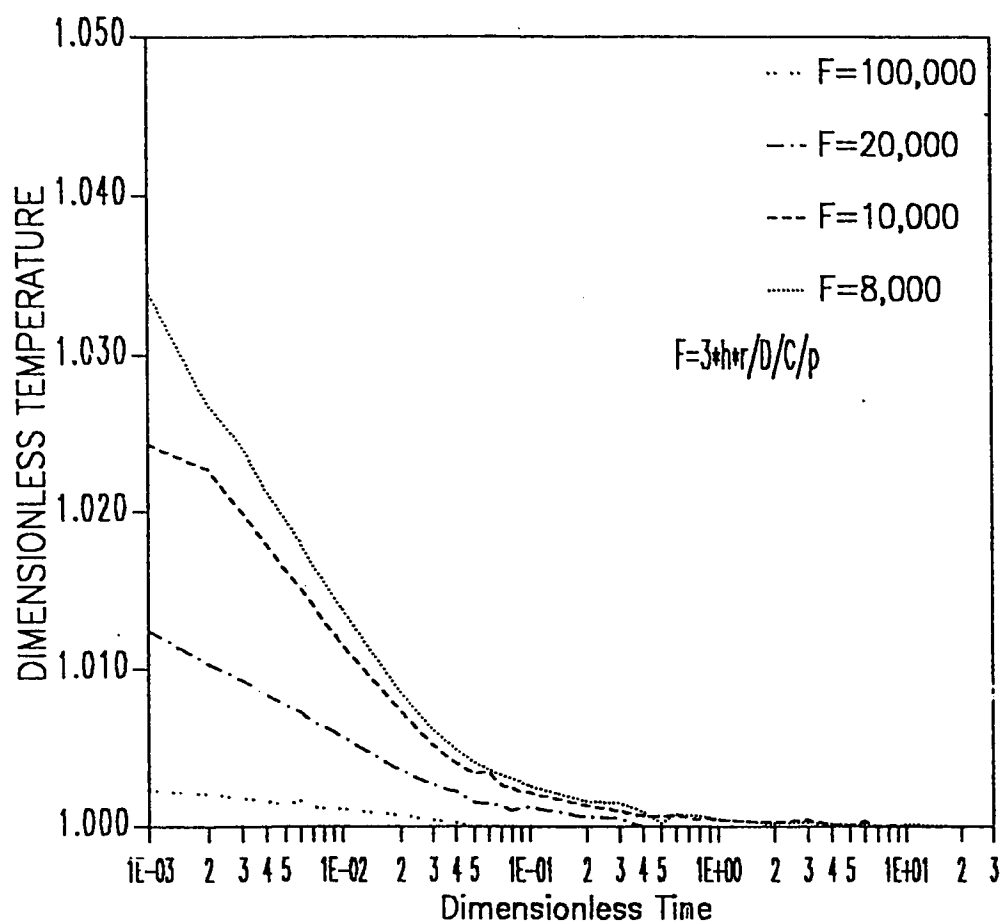


Fig. 2.5 Plot of Dimensionless Temperature with Dimensionless Time on zeolite 4A. Constant Diffusivity Case (Parameter is Diffusion to Thermal Time Constant)

CHAPTER 3

THEORETICAL STUDY OF NONLINEAR ISOTHERMAL PACKED BED ADSORBERS: COMPARISON OF PECLET AND CELL NUMBERS.

3.1 Introduction

Transport and flow models describing packed bed behaviour in reactors have many similarities. Two distinct approaches are observed, the quasi continuum dispersed plug flow model or the discrete cell approach model. Within each of the model systems, a subdivision into an equilibrium process or a non-equilibrium process is feasible, the latter due to mass transfer limitations. Further, models may involve linear or non-linear adsorption equilibria. The major difference between the adsorption and reaction processes is that adsorption is transient whereas the reaction process tends to be steady state.

In 1982, Hlavacek (1) reviewed fixed bed reactor models and classified them into eight categories presenting typical heat and mass balance expressions. The mass balance reactor models of Hlavacek (some titles revised) are presented in Table 3.1 together with the analog mass balance adsorber models. Like Hlavacek we observe that the first four models A-D are based on the quasicontinuum approach while models E-H follow the cell description approach. In reviewing these models, we will primarily restrict our comments to the adsorber models.

Model A, the simplest, entitled the piston flow model in reaction or equilibrium model in adsorption, considers only a convective mechanism of mass transfer neglecting gas to particle transport resistances or the effect of the dispersion process. The model is useful in estimating gross system behaviour. This equilibrium model has been recently revisited by Basmadjian and coworkers (2-5) who discuss separation of non-linear isotherms, and is also extensively used in pressure swing adsorption studies (6-10).

Inclusion of the dispersion effects gives Model B. This is a boundary value problem, requiring the assignment of the proper boundary conditions, the general consensus being that the constant flux Danckwert boundary conditions are the most reliable. Coppola and LeVan (11,12) discuss this model for adsorption in shallow and deep beds for both Langmuir and Freundlich isotherms. The width of the mass transfer zone at breakthrough decreases as the nonlinearity of the isotherm increases, until eventually the width becomes zero, as the isotherms approach irreversible isotherm behaviour. For deep beds breakthrough curves are shown to be much sharper than corresponding constant pattern profiles, especially for very favourable isotherms, as a result of the change in the velocity of the fluid phase concentration wave during breakthrough. Hlavacek (1) notes that the dispersed model, in reactors, failed to predict multiple propagating fronts, a concept that is worth examination in adsorption studies.

In model C, dispersion has been deleted and replaced by an overall mass transfer coefficient (gas to particle only in Hlavacek's case). For transfer of

solute to solid particle four rate mechanisms have been identified; diffusion from bulk fluid phase to adsorbent, diffusion within the pores of the adsorbent (macropore diffusion), surface or micropore diffusion and the kinetic rate of adsorption at the phase boundary. Breakthrough curves have been developed where each of the mechanisms control, where a combination of mechanisms control, and where the mechanisms have been combined into a lumped parameter linear driving force approximation for either linear or non linear equilibrium (13-29).

Model D, the most complicated of the quasicontinuum models includes both dispersion and an overall mass transfer coefficient. The model is solved for the combined individual resistances or frequently the dispersion coefficient is lumped into a linear driving force approximation (30-41). Also, frequently a step change boundary condition is substituted for the Danckwert's boundary condition presumably for long beds having a constant pattern solution or for case of analytic solution where the latter criterion is satisfied.

The empty volume between the catalyst or adsorbent particles can be considered as a perfectly mixed cell. Accordingly the mixing cell model is a good approximation of dispersion phenomena occurring in a packed bed, and for an infinite number of mixers the piston flow description results. Hlavacek reports four finite stage models in the reaction literature (models E to H) but only two of these models appear to have been used in the adsorption field.

The simplest adsorption mixing cell model, model E has no fluid to particle transport effects, and is simply an equilibrium model, first derived by Martin and Synge (42) and used extensively in chromatography by Giddings (44) . The equivalence of the discrete and continuous representations of a chromatographic system has been discussed by many authors. For a linear equilibrium system only, N the number of cells, and the axial Peclet number are related by expression $(N = Pe/2)$ (for example see Villermaux (43)). Cheng and Hill (50) use the linear equilibrium cell model to describe a PSA unit. The nonlinear equilibrium model has been discussed by Rodrigues and coworkers (47-49) using the Langmuir and BET isotherms. They show that the mass transfer zone width decreases as both the non-linearity increases at a constant loading, or as the loading increases for the same nonlinearity, giving a longer time to reach a fixed breakthrough point for favourable isotherms. Also, as the number of cells are increased , favourable isotherms approach plug flow and unfavourable isotherms decrease to a constant mass transfer zone width. Wicke (55) indicates that the depth of penetration of the longitudinal back diffusion is only a fraction of the pellet diameter even at low Reynolds number and it diminishes rapidly with increasing flow rate. Hlavacek (1) states that the addition of the second derivative term to describe the dispersion effects creates difficulty in kinetics since the model predicts backmixing, and that based on present experimental results the mixing cell model is a more physically sound description of a true mechanism of mass transfer.

If we have backflow between neighbouring stages, a mixing cell model with axial backflow, like model F, can be developed, but this does not appear to have been used in adsorption literature. In case of appreciable temperature gradient along the column length axial backflow may become important and under such circumstances this model would be useful.

Model G involves the addition of mass transfer resistances in the cell model. For linear isotherms the number of cells N is still equivalent to $Pe/2$ in the dispersion model with the mass transfer zone width adjusted for the extra mass transfer resistances (43). Rodrigues et al (47-49) have shown the effect of mass transfer alone or in combination with pellet diffusion, for the favourable non linear isotherm for the breakthrough curves. Do (53) has modelled fixed bed adsorbers with rectangular adsorption isotherm using $N = Pe/2$ to relate the number of cells to the dispersion effects.

For gaseous systems, if the empty cell volume between adsorbent particles is considered a perfectly mixed cell, the number of cells N can be related to the length of the bed L and the diameter of the particles d_p by the equation ($N = L/d_p$) providing the particle Reynolds number is greater than about 8 (45). Ikeda (46) has used this principle to model non-isothermal adsorption columns using the cell principle. Friday and LeVan (53) use a stage model, which is closely related to the cell model to model hot gas purge regeneration of adsorption beds. Finally Chirara and Kondo (51) divide PSA adsorption column into N cells and use a STOP-GO method to model the system, in which flow between cells is

stopped for a time increment Δt during which an amount adsorbed is calculated using a standard rate expression. Subsequently the pressure is calculated and an overall mass balance performed.

3.2 Mathematical Model

The model equations of the axial dispersed plug flow model and that of the cell model for both the equilibrium process and the non-equilibrium process is outlined below with the following assumptions:

- (1) The feed consists of a small concentration of a single adsorbable component in an inert carrier.
- (2) The system is isothermal with negligible pressure drop through the adsorbent beds.
- (3) The equilibrium isotherm is represented by a Langmuir expression.

Equilibrium Process

With the above assumptions the axially dispersed flow model equations can be written as:

Fluid phase:

$$-D_e \frac{\partial^2 C_A}{\partial z^2} + u \frac{\partial C_A}{\partial z} + \frac{\partial C_A}{\partial t} + \frac{(1-\epsilon)}{\epsilon} \frac{\partial q_A}{\partial t} = 0 \quad (3.1)$$

Adsorption equilibrium :

$$\frac{q_A^*}{q_{As}} = \frac{bC_A}{1 + bC_A} \quad (3.2)$$

Boundary conditions:

$$D_e \frac{\partial C_A}{\partial z} \Big|_{z=0} = -u \{ C_A|_{z=0^+} - C_A|_{z=0^-} \} \quad (3.3)$$

$$\frac{\partial C_A}{\partial z} \Big|_{z=1} = 0 \quad (3.4)$$

$$\begin{aligned} \text{with } C_A|_{z=0^-} &= C_{A0} \text{ (adsorption)} \\ &= 0 \text{ (desorption)} \end{aligned} \quad (3.5)$$

The cell model equations are

Fluid phase:

$$\frac{dC_{Ai}}{dt} + \frac{(1-\epsilon)}{\epsilon} \frac{dq_{Ai}^*}{dt} = \frac{u(C_{Ai-1} - C_{Ai})}{\Delta z} \quad (3.6)$$

Adsorption equilibrium:

$$\frac{q_{Ai}^*}{q_s} = \frac{bC_{Ai}}{1 + bC_{Ai}} \quad (3.7)$$

Boundary condition:

$$\begin{aligned} C_A|_{\text{feed}} &= C_{A0} \text{ (adsorption)} \\ &= 0 \text{ (desorption)} \end{aligned} \quad (3.8)$$

Non Equilibrium Process

For both models, a solid phase LDF approximation can be included to account for non-equilibrium process as follows:

$$\frac{dq_{Ai}}{dt} = k (q_{Ai}^* - q_{Ai}) \quad (3.9)$$

Equations 3.1 to 3.9 can be reduced to dimensionless form by the introduction of the following parameters:

$$\Phi_i = \frac{C_{Ai}}{C_{Ao}}, \quad \Psi_i = \frac{q_{Ai}}{q_{Ao}}, \quad \text{Pec} = \frac{uL}{D_e}, \quad \zeta = \frac{z}{L}$$

$$\lambda = \frac{bC_o}{1 + bC_o}, \quad \tau = \frac{t u}{L}, \quad \alpha = \frac{k L}{u}, \quad \beta = \frac{(1-\epsilon)}{\epsilon} K(1-\lambda)$$

The resulting equations are :

$$-\frac{1}{\text{Pec}} \frac{\partial^2 \Phi}{\partial \zeta^2} + \frac{\partial \Phi}{\partial \zeta} + \frac{\partial \Phi}{\partial \tau} + \beta \frac{\partial \Psi}{\partial \tau} = 0 \quad (3.10)$$

$$\Psi = \frac{\Phi}{1-\lambda-\lambda \Phi} \quad (3.11)$$

$$\frac{-1}{\text{Pec}} \frac{\partial \Phi}{\partial \zeta} \Big|_{\zeta=0} = \{ \Phi|_{\zeta=0} - \Phi|_{\zeta=0} \} \quad (3.12)$$

$$\frac{\partial \Phi}{\partial \zeta} \Big|_{\zeta=1} = 0 \quad (3.13)$$

with

$$\begin{aligned} \Phi|_{\zeta=0} &= 1 \quad (\text{adsorption}) \\ &= 0 \quad (\text{desorption}) \end{aligned} \quad (3.14)$$

$$\frac{d\Phi_i}{d\tau} + \beta \frac{d\Psi_i}{d\tau} = N \{ \Phi_{i+1} - \Phi_i \} \quad (3.15)$$

$$\frac{d\Psi_{Ai}}{d\tau} = \alpha \left\{ \frac{\Phi_{Ai}}{(1-\lambda - \lambda\Phi_{Ai})} - \Psi_{Ai} \right\} \quad (3.16)$$

$$\begin{aligned} \Phi|_{\text{feed}} &= 1 \quad (\text{adsorption}) \\ &= 0 \quad (\text{desorption}) \end{aligned} \quad (3.17)$$

For both processes the initial conditions are

$$\begin{aligned} \Phi = \Psi &= 0 \quad (\text{adsorption}) \\ &= 1 \quad (\text{desorption}) \end{aligned} \quad (3.18)$$

$\Phi = \Psi = 0$ implies an initially clean bed and $\Phi = \Psi = 1$ implies initially saturated bed at equilibrium with feed concentration

The axially dispersed plug flow model equations were solved using orthogonal collocation(Raghavan et al(56)). All equations were solved by Gear's method using the IMSL package.

3.3 Results and Discussion:

Numerical simulations were performed for the generation of breakthrough curves by the axial dispersed plug flow model and the cell model for sorption of methane and ethylene on 5A zeolite (equilibrium process), and for ethylene on 4A zeolite and oxygen on carbon molecular sieves(CMS) (non-equilibrium process) (helium is employed as a carrier gas). Previous studies of hydrocarbons in

4A and 5A zeolites (20,57,58,59) and oxygen in CMS (60) have shown that in 4A zeolite and in carbon molecular sieves intracrystalline diffusional resistance is high and likely to be rate controlling whereas in the wider lattice of the 5A zeolite the intracrystalline diffusion is rapid and the sorption is likely to be macropore diffusion controlled (59). The chosen systems therefore cover both extremes of micropore and macropore diffusion control.

The relevant data for all the systems are given in Table 3.2. The time between the dimensionless concentration level of 0.99 and 0.01 ($\tau_{0.99-0.01}$) was chosen as the criterion to find a correspondence between the Peclet number (l/uD_c) in the axial dispersed plug flow model and N of the cell model. For example for the same $\tau_{0.99-0.01}$ the adsorption and desorption curves for $\lambda = 0.5$ have been compared for both the models for oxygen on CMS in Figure 3.1. It may be observed that the generated curves for both models are coincidental for the same $\tau_{0.99-0.01}$.

The simulation runs were performed to find out $\tau_{0.99-0.01}$ for all the systems by both models for the various values of nonlinear parameter λ .

Figures 3.2 & 3.3 show the plot of $\tau_{0.99-0.01}$ vs. Peclet number or N for adsorption and desorption of methane and ethylene on 5A system for various values of λ using the axial dispersed plug flow model and cell model for an equilibrium process. It may be noted that the $\tau_{0.99-0.01}$ is different for adsorption and desorption except when $\lambda=0$ which corresponds to a linear isotherm. This difference can clearly be observed for ethylene on 5A at $\lambda = 0.92$ in Figure 3.3. In the case

of adsorption of methane on 5A zeolite it may be observed from Figure 3.2A that for the same value of Peclet number or N , $\tau_{0.99-0.01}$ decreases with the increase in the value of the nonlinear parameter λ . For the case of desorption (Figure 3.2B) $\tau_{0.99-0.01}$ increases with increase in λ .

Figures 3.4 & 3.5 show the plot of $\tau_{0.99-0.01}$ vs. Peclet number or N for adsorption and desorption of oxygen on carbon molecular sieves and ethylene on 4A respectively for different values of λ using the axial dispersed plug flow model and cell model for a non equilibrium process. For adsorption on the carbon molecular sieves, the mass transfer zone width first decreases and then increases as the non-linearity is increased (See Figures 3.4A and 3.4B). However for the ethylene 4A system the width increases as λ increases (Figure 3.5A). The reason is that for the carbon molecular sieve the non-linearity phenomena are initially controlling, and subsequently the rate phenomena control as λ is increased, whereas for ethylene 4A the rate is so slow it dominates throughout. For desorption the trends are similar to those described for the equilibrium process; however the extent of the breakthrough curve which is measured by $\tau_{0.99-0.01}$ is different being larger for the non-equilibrium process (See Figures 3.4C and 3.5B).

From Figure 3.2 to 3.5 plots may be obtained for the number of cells vs. Peclet number for the various cases considered. Such plots are shown in Figures 3.6 & 3.7 for methane on 5A and oxygen on carbon molecular sieves respectively. For the case of methane on 5A zeolite (equilibrium process), it may be observed from Figure 3.6 that during adsorption the ratio of Peclet number to N

shifts from a value of 2 at $\lambda = 0$ to unity when λ is high. On the other hand this ratio is 2 for desorption and is independent of λ . Ruthven (54) reported a ratio of Peclet number:N of 2 for linear systems ($\lambda=0$) and therefore the present study is consistent in this regard. Further, it may be considered that for all liquids where $\lambda \approx 1.0$ the ratio of Peclet number to N should be taken as unity for adsorption and 2 for desorption.

Figure 3.7 shows the plot of N vs. Peclet number for oxygen on carbon molecular sieves (non equilibrium process). The trend is similar to that observed for the equilibrium process. Similar plots for ethylene on 4A zeolite were obtained but due to very high mass transfer resistance $\tau_{0.99-0.01}$ was not affected by axial dispersion and therefore even one cell was found sufficient for such a process.

Care should be exercised in the specification of the mass transfer zone width in dealing with non-linear phenomena. A general rule is that the mass transfer zone width must be greater than the λ values involved i.e. for a λ value of 0.99 a mass transfer zone width of $\tau_{0.998-0.002}$ should be used to characterize. Otherwise erroneous results may occur. However with larger values of λ , accurate interpretation of results may be difficult due to tailing effects.

The results of this study will be useful for the simulation of adsorption system which needs repetitive calculation (e.g. Pressure swing adsorption, counter-current adsorption etc.). A detailed axial dispersion model solution takes

exceedingly long computational times which now may be reduced by use of cell models (using the right no. of cells) which takes relatively shorter times.

3.4 Conclusions

The equivalent Peclet and cell numbers associated with a definitive mass transfer zone width $\tau_{0.99-0.01}$ for both equilibrium and non-equilibrium processes have been evaluated for packed bed adsorbers having non-linear isotherm. For both the equilibrium and non-equilibrium processes, the ratio of Peclet number to N changes from a value of 2 at low λ (linear isotherm) to unity when λ is high ($\lambda = 0.85$) during adsorption. However, this ratio can be taken as 2 for all values of λ during desorption.

Hence we deduce that for liquids where $\lambda \approx 1.0$, the ratio of Peclet number to N should be taken as 1.0 during adsorption, and 2.0 during desorption.

REFERENCES

- (1) Hlavacek, V., "Fixed Bed Reactors, Flow and Chemical Reaction", in "Residence Time Distribution Theory in Chemical Engineering", Eds: A. Petho and R. D. Noble, published by Verlag Chemic, pages 103-111 (1982).
- (2) Coroyannakis, P. and Basmadjian, D., "Multicomponent Fixed Bed sorption : Selectivity reversal in isothermal binary systems: Equilibrium Theory and Experimental evidence", AIChE Sym. Ser. **81** (242), 9-16 (1985).
- (3) Basmadjian, D. and Coroyannakis, P., "Equilibrium Theory Revisited. Isothermal Fixed Bed Sorption of Binary Systems. I Solutes obeying the Binary Langmuir isotherms", Chem. Engg. Sci., **42** (7), 1723-1737 (1987).
- (4) Basmadjian, D. and Coroyannakis, P., "Equilibrium Theory Revisited. Isothermal Fixed Bed Sorption of Binary Systems. II Non - Langmuir solutes with Type I parent isotherms: Azeotropic systems", Chem. Engg. Sci., **42** (7), 1738-1752 (1987).
- (5) Basmadjian, D. and Coroyannakis, P., "Equilibrium Theory Revisited. Isothermal Fixed Bed Sorption of Binary Systems. III Solutes with Type I, Type II and Type IV Parent Isotherms. Phase Separation Phenomena.", Chem. Engg. Sci., **42** (7), 1753-1764 (1987).
- (6) Shendalman, L. H. and Mitchell, J. E., "A study of Heatless Adsorption in the model system CO₂ in He"- I, Chem. Engg. Sci., **27** , 1449-1458 (1972).
- (7) Chan, Y. I., Hill, F. B., and Wong, Y. W., "Equilibrium Theory of Pressure Swing Adsorption", Chem. Engg. Sci., **36** , 243-251 (1972).
- (8) Knäbel, K. S. and Hill, F. B., "Pressure Swing Adsorption: Development of an Equilibrium Theory for Gas Separations", Chem. Engg. Sci., **40** , 2351, (1985).
- (9) Nataraj, S. and Wankat, P. C., "Multicomponent Pressure Swing Adsorption", AIChE Sym. Ser. **78** (219), 29-38 (1982).
- (10) Underwood, R. P., "A model of Pressure Swing Adsorption Process for Non-Linear Adsorption Equilibrium", Chem. Engg. Sci., **41** (2), 409-411 (1986).

- (11) Coppola, A. P. and LeVan, M. D., "Adsorption with Axial Dispersion in Shallow Beds", *Chem. Engg. Sci.*, **38** (7), 991-997 (1983).
- (12) Coppola, A. P. and LeVan, M. D., "Adsorption with Axial Dispersion in Deep Beds", *Chem. Engg. Sci.*, **36** (6), 967-971 (1981).
- (13) Moon, H. and Tien, C., "Incorporation of the Potential Theory into Liquid Phase Multicomponent Adsorption Calculations", *Chem. Engg. Sci.*, **43** (6), 1269-1279 (1988).
- (14) Antonson, C. R. and Dranoff, J. S., "Nonlinear Equilibrium and Particle Shape Effects in Intraparticle Diffusion Controlled Adsorption", *Chem. Engg. Prog. Symp. Ser.*, **65** (96), 20-26 (1969).
- (15) Antonson, C. R. and Dranoff, J. S., "Adsorption of Ethane on Type 4A and 5A molecular sieve particles", *Chem. Engg. Prog. Symp. Ser.*, **65** (96), 27-33 (1969).
- (16) Gariepy, R. L. and Zwibel, I., "Adsorption of Binary Mixtures in Fixed Beds", *AIChE Sym. Ser.* **67** (117), 29-38 (1982).
- (17) Collins, H. W. and Chao, K. C., "A dynamic model for multicomponent fixed bed adsorption", *AIChE Sym. Ser.* **69** (134), 9-17 (1973).
- (18) Zwibel, I. and Schnitzer, J. J., "Desorption from Fixed Beds", *AIChE Sym. Ser.* **69** (134), 18-24 (1973).
- (19) Stuart, F. X. and Camp, D. T., "Solution of the Fixed Bed Physical Adsorption Problem with two significant rate controlling steps", *AIChE Sym. Ser.* **69** (134), 33-38 (1973).
- (20) Sheth, A. C. and Dranoff, J. S., "Adsorption of Ethylene on Type 4A molecular sieve particles", *AIChE Sym. Ser.* **69** (134), 76-81 (1973).
- (21) Wong, Y. W. and Niedzwieki, J. L., "A simplified model for multicomponent Fixed Bed Adsorption", *AIChE Sym. Ser.* **78** (219), 120-127 (1973).
- (22) Hasanain, M. A., Hines, A. L. and Cooney, D. A., "Adsorption Kinetics for Systems that exhibit Nonlinear Equilibrium", *AIChE Sym. Ser.* **79** (230), 60-66 (1983).
- (23) Rosen, J. B., *J. Chem. Phys.* **20** 387 (1952).
- (24) Razavi, M. S., McCoy, B. J. and Corbonell, R. J., "Moment Theory of Breakthrough Curves for Fixed Bed Adsorbers and Reactors", *Chem. Engg. Jour.*, **16** 211-222 (1978).

- (25) Garg, D. R. and Ruthven, D. M., "Theoretical Prediction of Break-through curves for molecular sieve adsorption columns. II General isothermal solution for micropore diffusion control", Chem. Engg. Sci., **28** , 799-805 (1974).
- (26) Garg, D. R. and Ruthven, D. M., "Sorption of CO₂ in Davison 5A molecular Sieve", Chem. Engg. Sci., **29** , 571 (1974).
- (27) Garg, D. R. and Ruthven, D. M., "The Performance of Molecular Sieve Adsorption Columns: systems with macropore diffusion control", Chem. Engg. Sci., **29** , 1961-1967 (1974).
- (28) Garg, D. R. and Ruthven, D. M., "Theoretical Prediction of Break-through curves for molecular sieve adsorption columns- I Asymptotic solutions", Chem. Engg. Sci., **28** , 791-798 (1973).
- (29) Garg, D. R. and Ruthven, D. M., "Linear Driving Force approximations for Diffusion Controlled Adsorption in Molecular Sieve Columns", AIChE J, **21** (1), 200-202 (1975).
- (30) Chung, I. J. and Hsu, H. W., "Analysis of Packed Bed Adsorption", Chem. Engg. Sci., **33** , 399-403 (1978).
- (31) Chao, R. and Hoelscher, H. E., "Simultaneous Axial Dispersion and Adsorption in Packed Beds", AIChE J, **12** 271-278 (1966).
- (32) Rasmusen, A., "Exact solutions of some models for the dynamics of fixed beds using Danckwert's inlet conditions", Chem. Engg. Sci., **41** (3), 599-600 (1986).
- (33) Rasmusen, A., "The effect of particles of variable size, shape and properties on the dynamics of fixed beds", Chem. Engg. Sci., **40** (4), 621-629 (1986).
- (34) Rasmusen, A., "The Influence of Particle Shape on the Dynamics of Fixed Beds", Chem. Engg. Sci., **40** (7), 1115-1122 (1985).
- (35) Liapis, A. I. and Rippin, D. W. T., "The simulation of binary adsorption in activated carbon columns using estimates of diffusional resistance within the carbon particles derived from batch experiments", Chem. Engg. Sci., **33** , 593-600 (1978).
- (36) Brown, N. L., Mullin, J. C. and Melshimer, S. S., "A Nonlinear Equilibrium Isothermal Fixed Bed Adsorption Model using Pulse Chromatographic Rate Measurements", AIChE Sym. Ser. **74** (179), 9-18 (1978).

- (37) LeVan, M. D., "Chanelling and Bed Diameter Effects in Fixed Bed Adsorber Performance", AIChE Sym. Ser. **80** (233), 34-43 (1984).
- (38) Raghavan, N. S. and Ruthven, D. M., "Numerical Simulation of a Fixed Bed Adsorption Column", AIChE J, **29**, (6), 922-925 (1983).
- (39) Hashimoto, N. and Smith, J. M., "Macropore Diffusion in Molecular Sieve Pellets by Chromatography", I & EC Fund. **12**, (3), 353-359 (1973).
- (40) Colwell, C. J. and Dranoff, J. S., "Nonlinear equilibrium and axial mixing effects in Intraparticle Diffusion Controlled Sorption by Ion Exchange Resin Beds", I & EC Fund. **8**, (2), 193-198 (1969).
- (41) Garg, D. R. and Ruthven, D. M., "Performance of Molecular Sieve Adsorption Columns: combined effects of mass transfer and longitudinal diffusion" Chem. Engg. Sci., **30**, 1192-1194 (1975).
- (42) Martin, M. J. P. and Synge R. L. M., Biochem J., **35**, 1358-1368 (1941).
- (43) Villiermaux, J., "Theory of linear Chromatography" in "Percolation Processes: Theory and Applications", Eds: A. E. Rodrigues and Tondueur D., pages 83-140, published by Sizthoff and Noordhoff, Netherlands (1981).
- (44) Giddings, J. C., "Dynamics of Chromatography. Part 1. Principles and Theory", Marcel Dekker, USA (1965).
- (45) Westerterp, K. R., Van Swaij, W. P. M. and Beenackers, A. A. C. M., "Chemical Reactor Design and Operation", John Wiley and Sons (1987).
- (46) Ikeda, K., "Performance of the Non-Isothermal Fixed Bed Adsorption Column with Nonlinear Isotherms", Chem. Engg. Sci., **34** (7), 941-949 (1979).
- (47) Rodrigues, A. E., "Modelling of Percolation Processes" in "Percolation Processes: Theory and Applications", Eds: A. E. Rodrigues and Tondueur D., pages 31-82, published by Sizthoff and Noordhoff, Netherlands (1981). Chem. Engg. Sci., **34** (7), 941-949 (1979).
- (48) Rodrigues, A. E. and Tondeur, D. J., J. Chem. Phys., **72** (6), 785 (1975).
- (49) Rodrigues, A. E. and Beira, E., "Staged approach to Percolation Process", AIChE J. **25** (3), 416-423 (1979).

- (50) Cheng, H. C. and Hill, F. B., "Recovery and Purification of Light Gases by Pressure Swing Adsorption", ACS Sym. Ser. **223** 195-212 (1983).
- (51) Chirara, K. and Kondo, A., "Simulation of Pressure Swing Adsorption - Three gas components and three adsorption columns" in Fundamentals of Adsorption" Ed. Liapis, A. I., published by Engineering Foundation, 345 East 47th St. NY p. 165-174 (1987).
- (52) Friday, D. K. and LeVan, M. D., "Hot Purge Gas Regeneration of Adsorption Beds with Solute Condensation: Experimental studies", AIChE J. **31** (8), 1322-1328 (1985).
- (53) Do, D. D., "Discrete Cell Model of Fixed Bed Adsorbers with Rectangular Adsorption Isotherms", AIChE J. **31** (8), 1329-1337 (1985).
- (54) Ruthven, D. M., "Principles of Adsorption and Adsorption Processes", Wiley Interscience, (1984).
- (55) Wicke, E., Adv. Chem. Ser. **148** p. 75, Am. Chem. Soc., Washington, D. C. (1975).
- (56) Raghavan, N. S., Hassan, M. M. and Ruthven, D. M., "Numerical Simulation of PSA system", AIChE J. **31** (3), 385-392 (1985).
- (57) Garg, D. R. and Ruthven, D. M., "Performance of Molecular Sieve Adsorption Columns with Micropore Diffusion Control", Chem. Engg. Sci., **29** , 517 (1974).
- (58) Yucel, H. and Ruthven, D. M., "Diffusion in 4A zeolite" J. Chem. Soc. Faraday Trans I. **76** ,60 (1980).
- (59) Yucel, H. and Ruthven, D. M., "Diffusion in 5A zeolite" J. Chem. Soc. Faraday Trans I. **76** , 71 (1980).
- (60) Ruthven, D. M., Raghavan, N. S. and Hassan, M. M. "Adsorption and Diffusion of Nitrogen and Oxygen in a Carbon Molecular Sieve", Chem. Engg. Sci., **41** (5), 1325-1341 (1985).

Table 3.1 : Transport Models describing Mass Transfer in Packed Catalytic Reactors and Adsorbers.

Specification	Reactors	Adsorbers
A. piston flow model	$-v \frac{dc_i}{dl} + R(c_i, T) = 0$	$-v \frac{\partial c_i}{\partial z} - \frac{\partial c_i}{\partial t} - \left(\frac{1-\epsilon}{\epsilon} \right) \frac{\partial q_i^*}{\partial t} = 0$
B. dispersion model	$D_e \frac{d^2 c_i}{dl^2} - v \frac{dc_i}{dl} + R(c_i, T) = 0$	$D_e \frac{\partial^2 c_i}{\partial z^2} - v \frac{\partial c_i}{\partial z} - \frac{\partial c_i}{\partial t} - \left(\frac{1-\epsilon}{\epsilon} \right) \frac{\partial q_i^*}{\partial t} = 0$
C. piston flow model with mass transfer	$-u \frac{dc_i}{dl} + k_c a(c_i - c_{is}) = 0$ $k_c a(c_i - c_{is}) - R(c_{is}, T_s) = 0$	$-v \frac{\partial c_i}{\partial z} - \frac{\partial c_i}{\partial t} - \left(\frac{1-\epsilon}{\epsilon} \right) k(q_i^* - q_i) = 0$
D. dispersion model with mass transfer	$D_e \frac{d^2 c_i}{dl^2} - u \frac{dc_i}{dl} + k_c a(c_i - c_{is}) = 0$ $k_c a(c_i - c_{is}) - R(c_{is}, T_s) = 0$	$D_e \frac{\partial^2 c_i}{\partial z^2} - v \frac{\partial c_i}{\partial z} - \frac{\partial c_i}{\partial t} - \left(\frac{1-\epsilon}{\epsilon} \right) k(q_i^* - q_i) = 0$
E. cell model	$vS(c_i^k - c_i^{k-1}) + VR(c_i^k, T_k) = 0$	$\frac{dc_i}{dt} + (1-\epsilon) \frac{dq_i^*}{dt} = \frac{Nv}{L} (c_{i-1} - c_i)$
F. cell model with axial mixing	$S(v(c_i^k - c_i^{k-1}) - q(c_i^{k-1} - c_i^k)) + VR(c_i^k, T_k) = 0$	
G. cell model with mass transfer	$uS(c_i^k - c_i^{k-1}) + V k_c a(c_i^k - c_{is}^k) = 0$ $k_c a(c_i^k - c_{is}^k) - R(c_{is}^k, T_s^k) = 0$	$\frac{dc_i}{dt} + \left(\frac{1-\epsilon}{\epsilon} \right) k(q_i^* - q_i) = \frac{Nv}{L} (c_{i-1} - c_i)$
H. cell model with mass transfer and axial mixing	$S(u(c_i^k - c_i^{k-1}) - q(c_i^{k-1} - c_i^k)) + V k_c a(c_i^k - c_{is}^k) = 0$ $k_c a(c_i^k - c_{is}^k) - R(c_{is}^k, T_s^k) = 0$	

Table 3.2: Parameters used in the Computations

Common Parameters:

Bed voidage	..	0.4
Non linearity Parameter	.. λ	0.1 0.95
Peclet Number	..	4 50
Number of Cells	..	2 30
Temperature	..	25 °C (Ambient)

Specific Parameters:

Feed Gas	Methane -Helium	Ethylene -Helium	Ethylene -Helium	Oxygen -Helium
Adsorbent	5A	5A	4A	CMS
(bq _s)	46.4	10463	571	9.25
Length/Velocity (sec)	--	5.64	6.18	25
k (cm/sec)	∞	∞	0.001	0.555

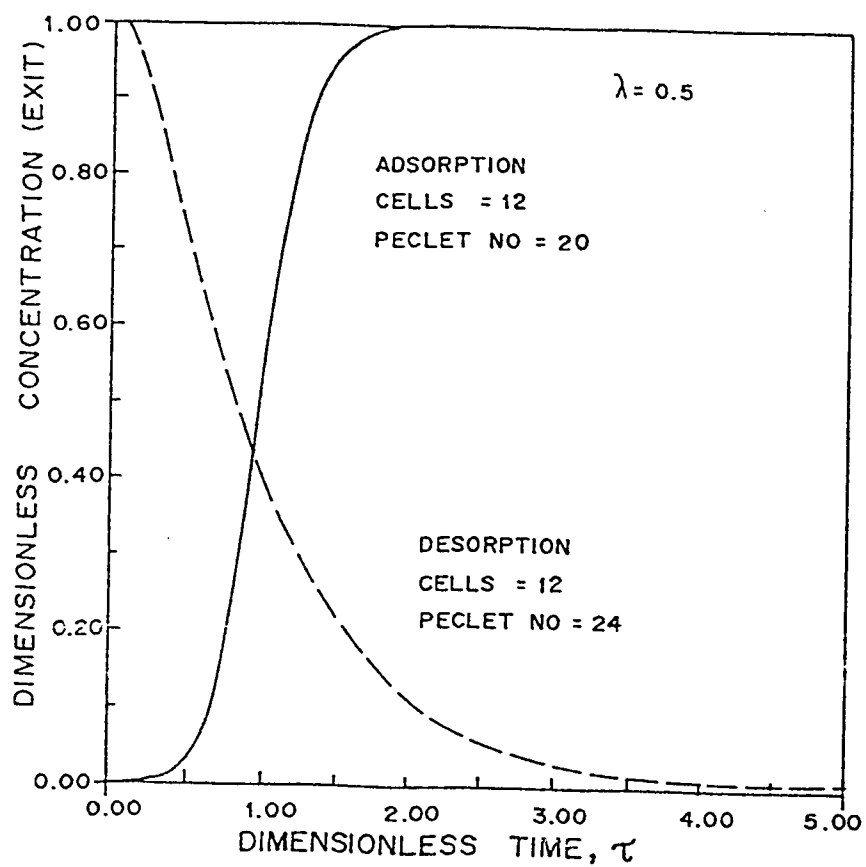


Figure 3.1 : Breakthrough curves - oxygen on carbon molecular sieves

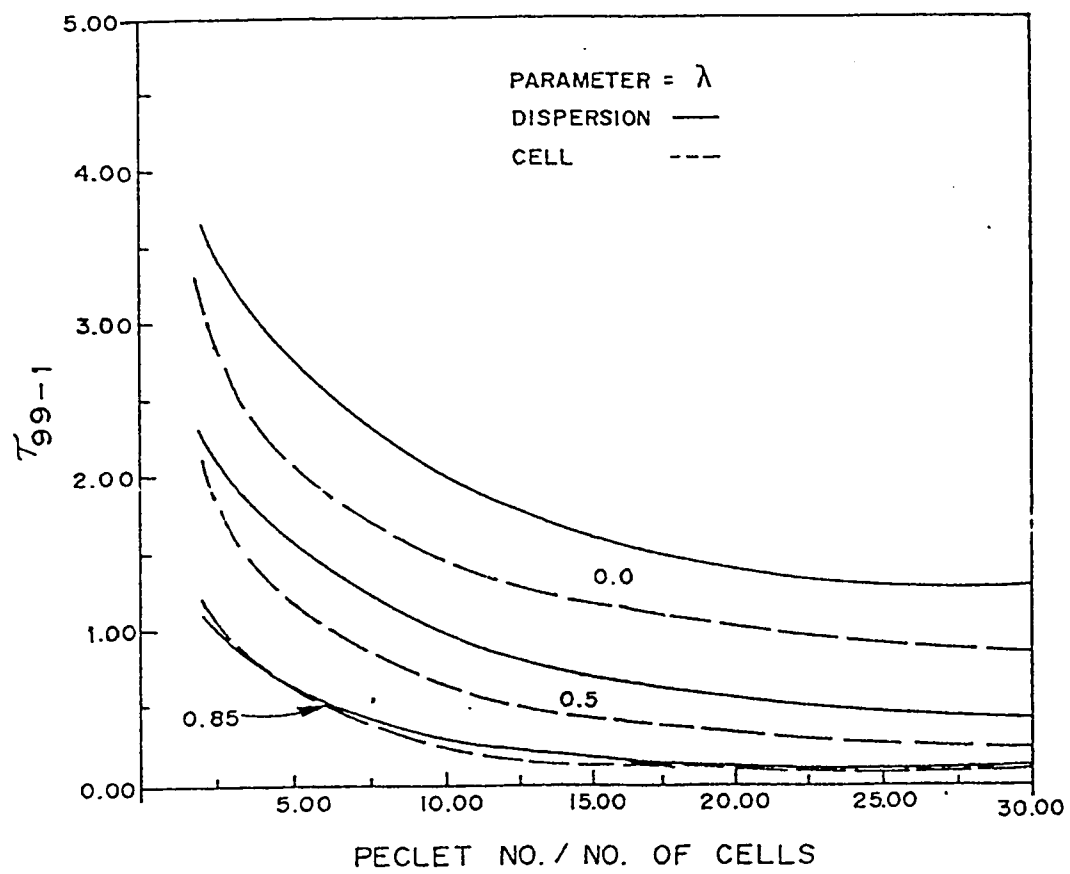


Figure 3.2A : Adsorption of methane on 5A zeolite - equilibrium model

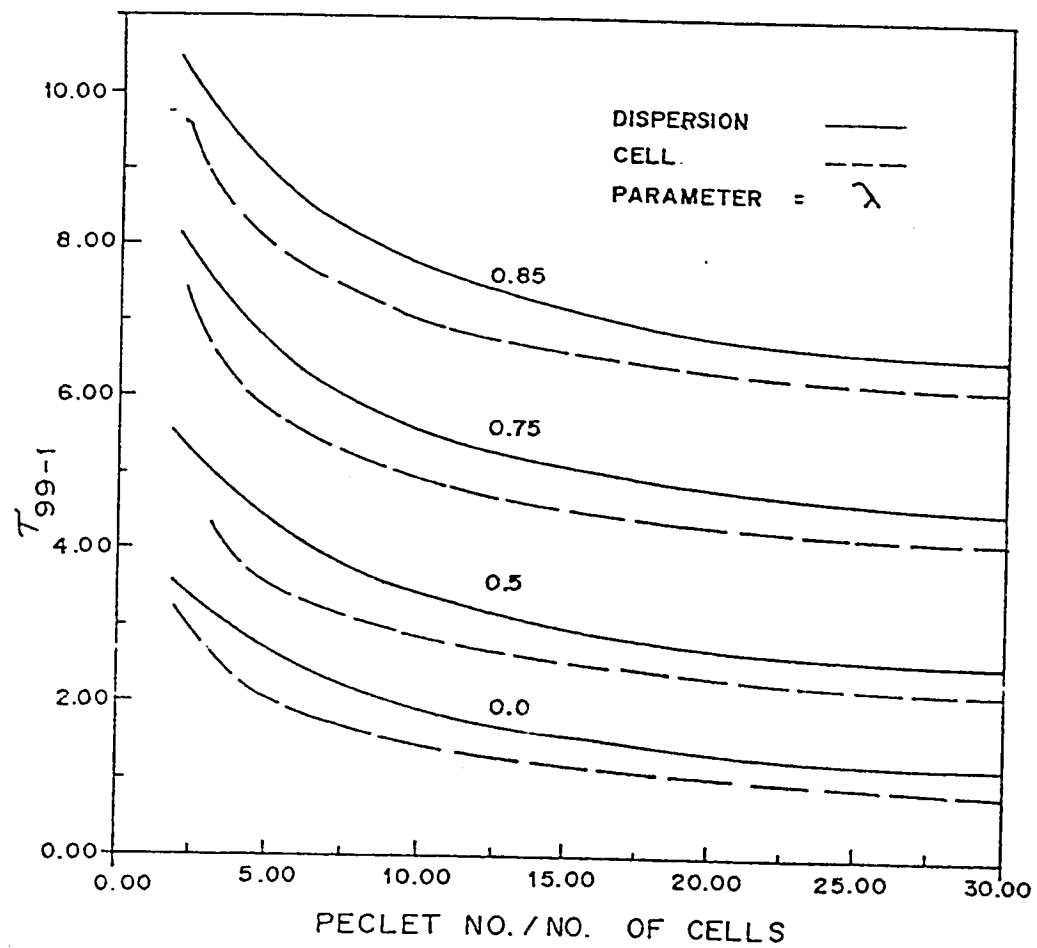


Figure 3.2B : Desorption of methane on 5A zeolite - equilibrium model

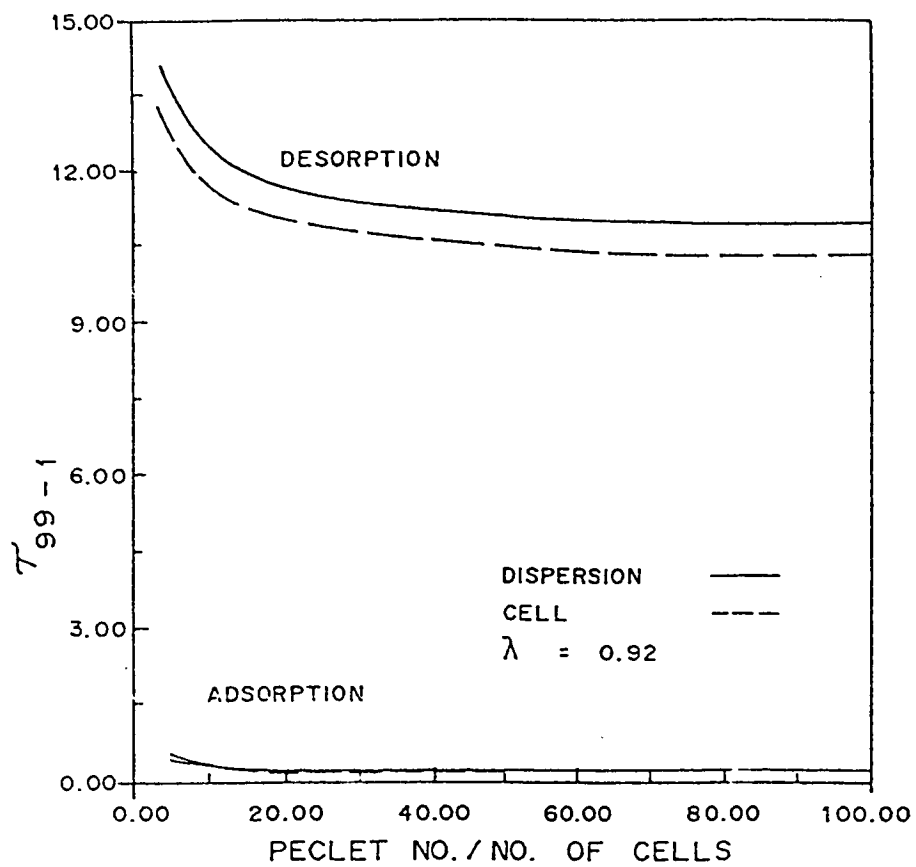


Figure 3.3 : Sorption of ethylene on 5A zeolite - equilibrium model

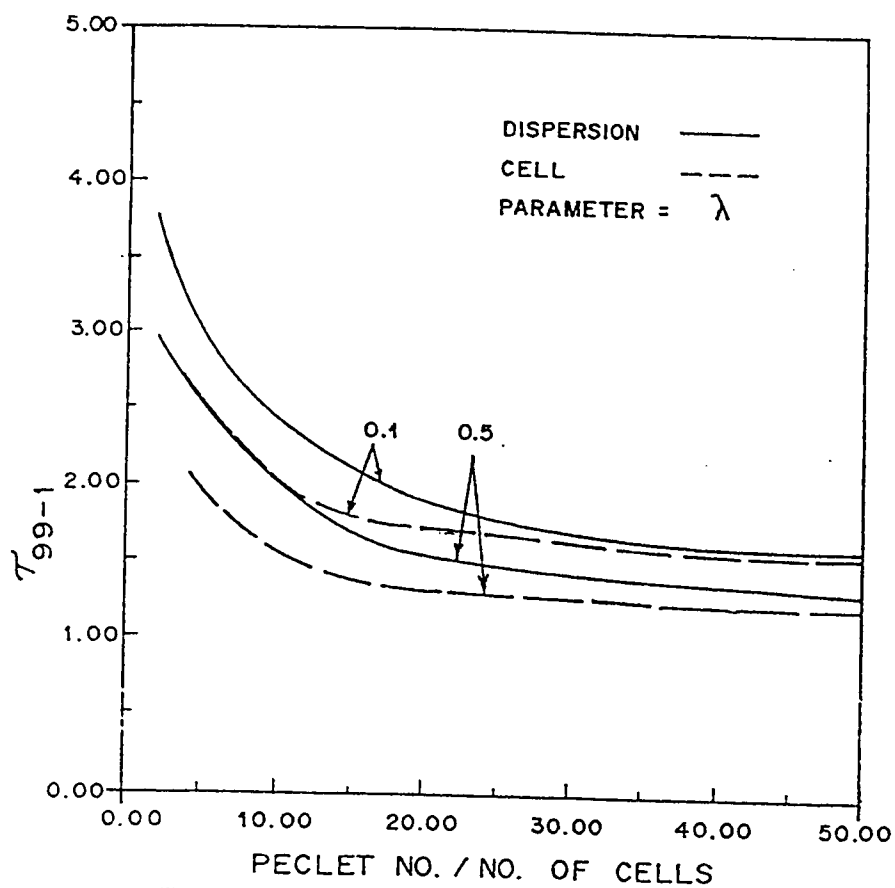


Figure 3.4A : Adsorption of oxygen on carbon molecular sieves - non equilibrium model

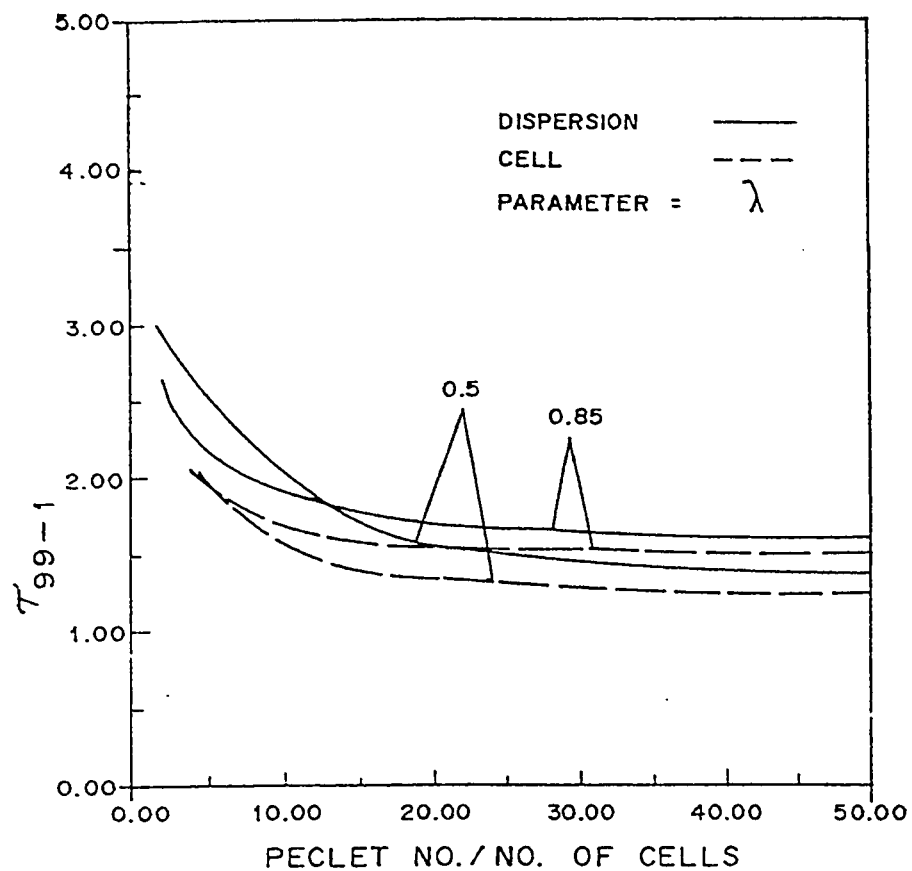


Figure 3.4B : Adsorption of oxygen on carbon molecular sieves - non equilibrium model

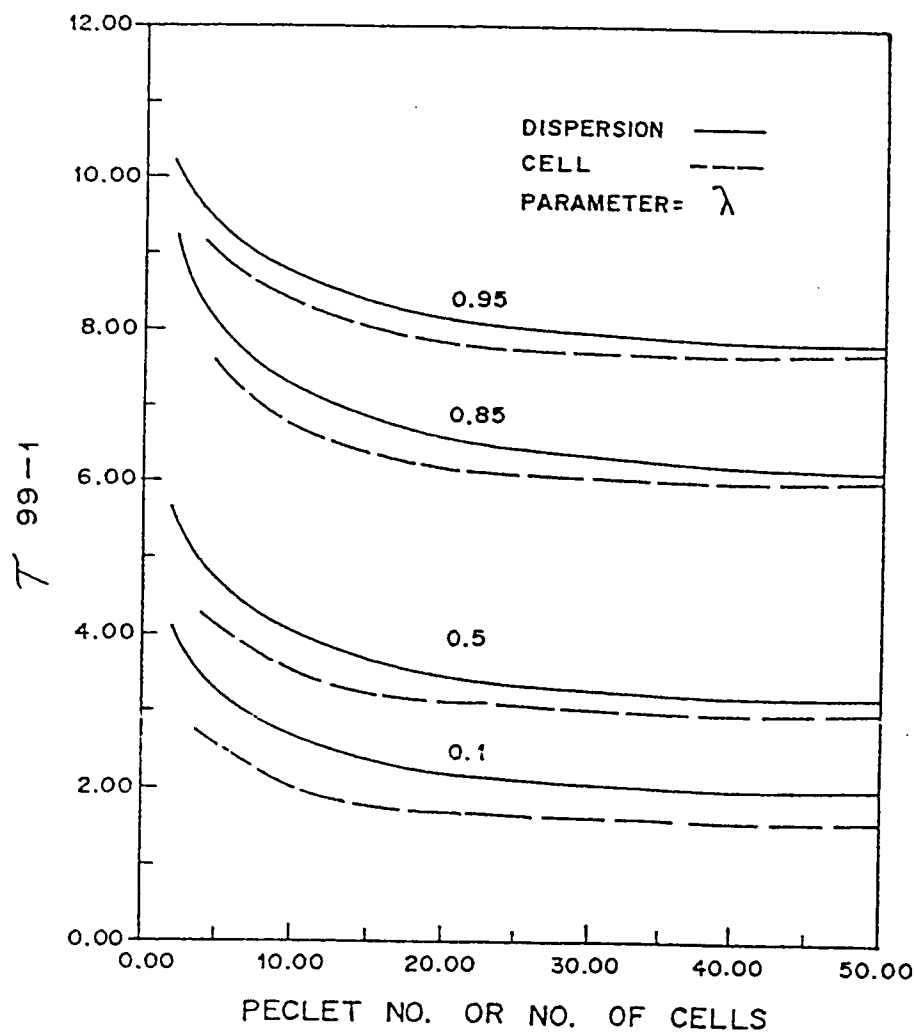


Figure 3.4C : Desorption of oxygen on carbon molecular sieves - non equilibrium model

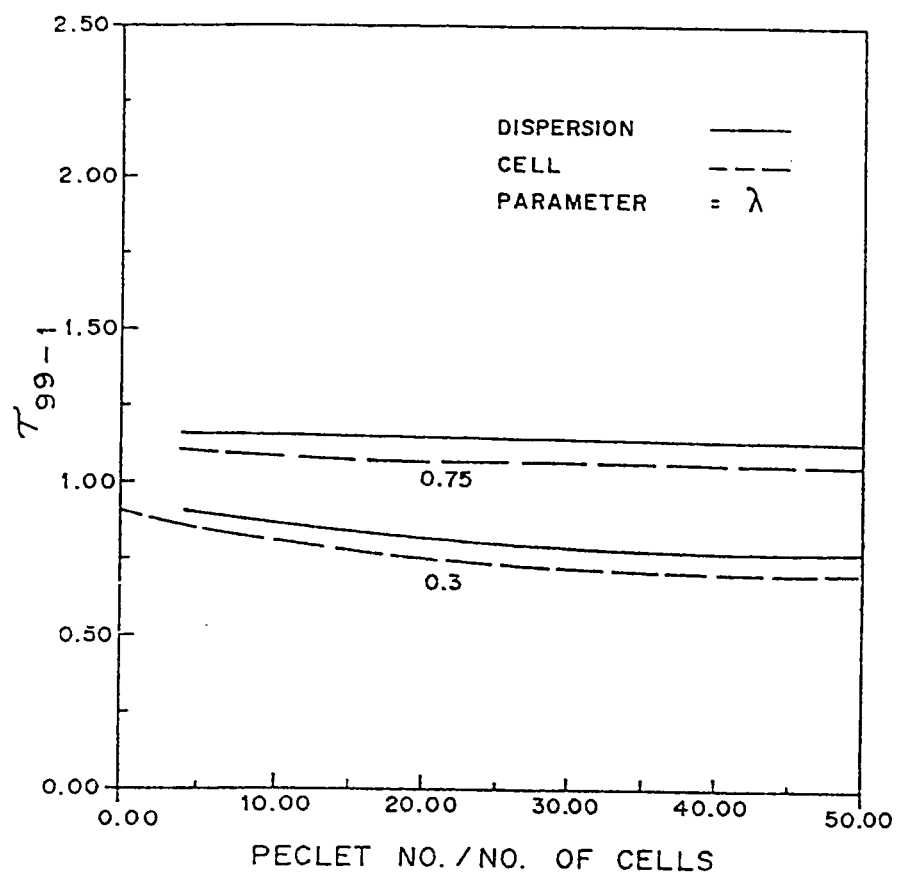


Figure 3.5A : Adsorption of ethylene on 4A zeolite - non equilibrium model

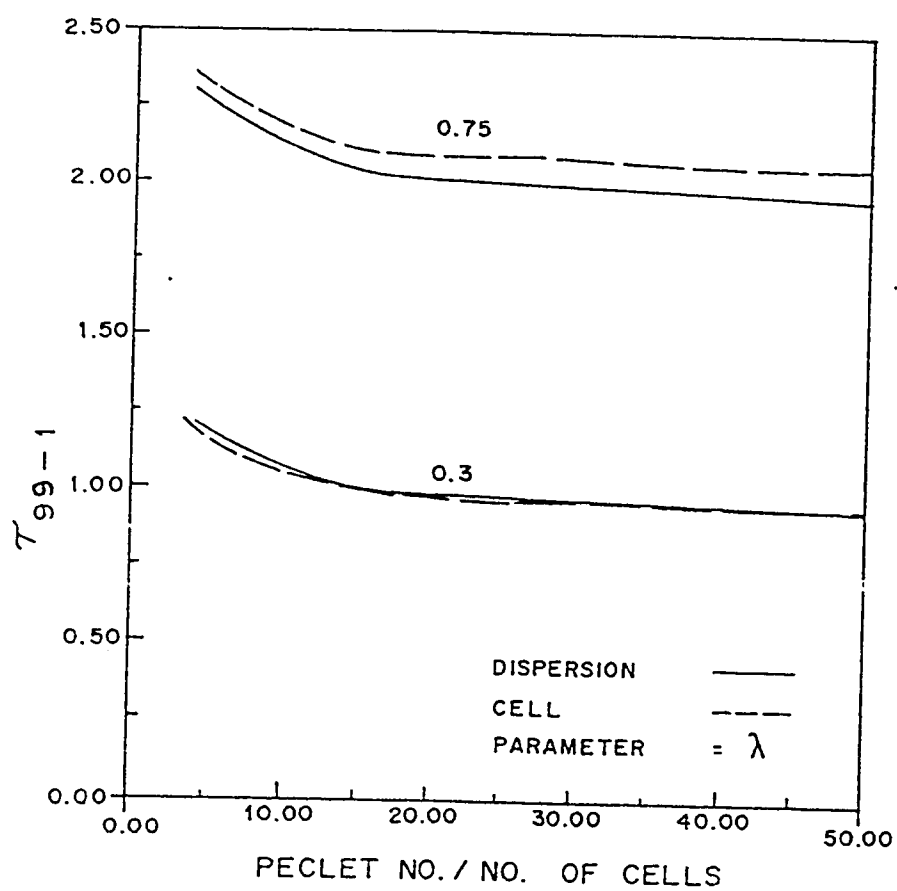


Figure 3.5B : Desorption of ethylene on 4A zeolite - non equilibrium model

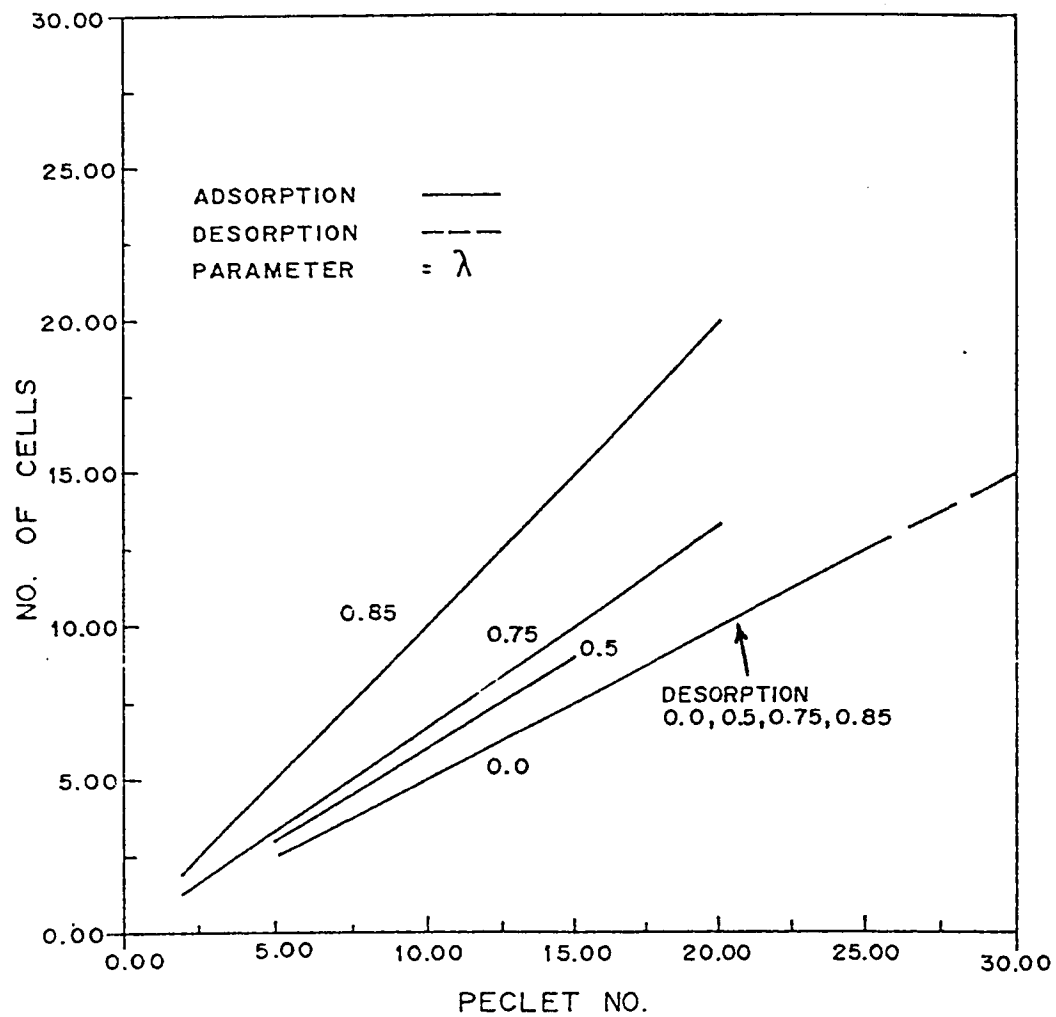


Figure 3.6 : Plot of peclet no. vs. no. of cells for methane on 5A zeolite - equilibrium model

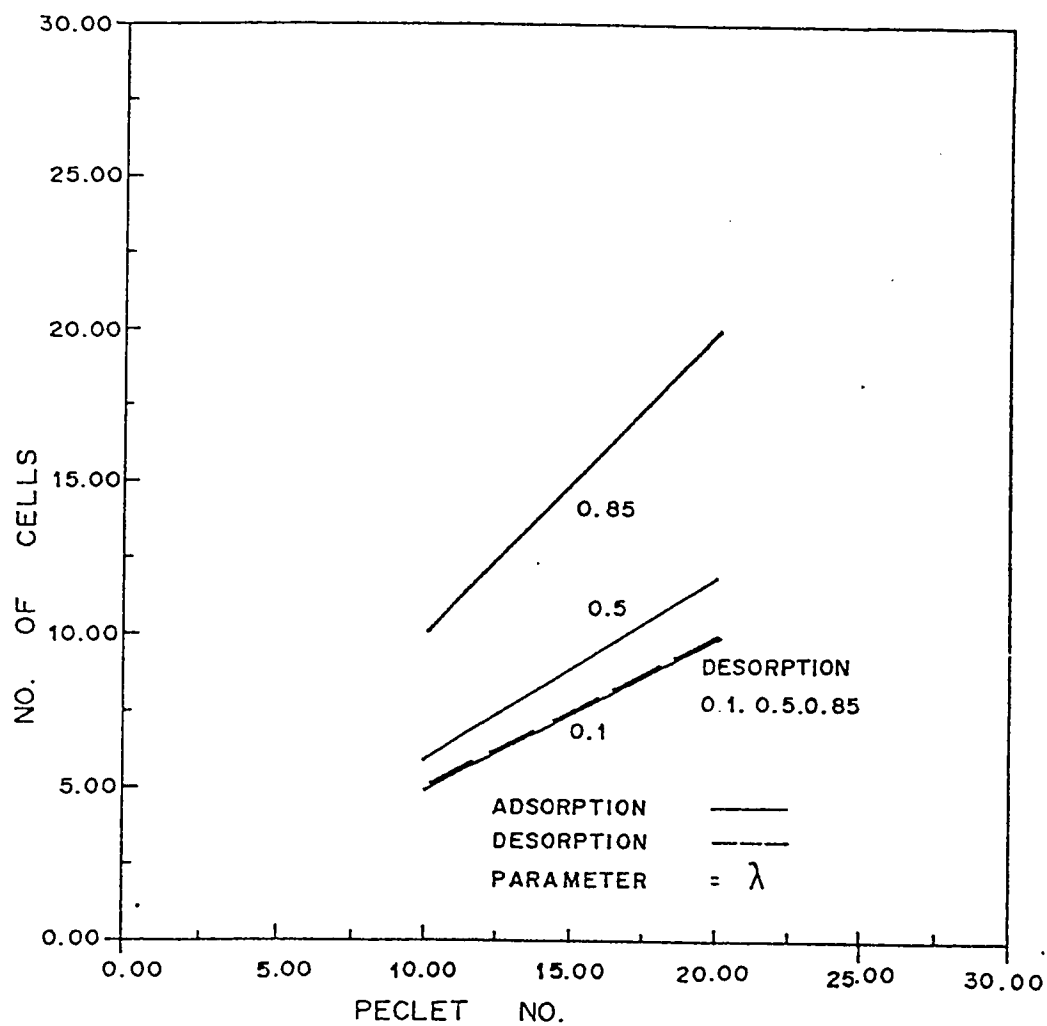


Figure 3.7 : Plot of peclet no. vs. no. of cells for oxygen on carbon molecular sieves - non equilibrium model

CHAPTER 4

EQUILIBRIUM AND KINETICS OF SORPTION OF NITROGEN AND METHANE ON ZEOLITE 4A AND CARBON MOLECULAR SIEVES

4.1 Introduction

The microporous adsorbents used in practical sorption processes are the traditional ones such as activated carbon, silica gel and the recently developed crystalline aluminosilicates or zeolites and carbon molecular sieves. A fundamental difference among them is pore size distribution which is spread over a few angstroms in the former while there is virtually no pore size distribution in the latter two. The micropore size in a zeolitic adsorbent is controlled by the crystal structure. A wide distribution in pore size results in little selectivity in adsorption of molecules of different sizes. Carbon molecular sieve, a coal based adsorbent prepared to circumvent the limitation of activated carbon, has a narrow distribution of pore size. The pore size ranges from 4 to 9 Angstroms.

The present chapter comprises a literature search and experiments to obtain the values of the equilibrium and kinetic parameters needed in the simulation of PSA separation of methane-nitrogen mixture on zeolite 4A and carbon molecular sieve. Since zeolite 4A is a standardized adsorbent the values are culled from a literature search. In the case of carbon molecular sieve, due to difficulty in reproducibility of production batches, experimental determination of data is preferable. The literature is limited to individual batch data.

4.2 Equilibrium and kinetic parameters for zeolite 4A

Adsorption equilibrium and kinetic parameters for zeolite 4A have been obtained by many workers (1-7), and the parameters to be used for the purpose of simulation in the subsequent chapters will be through the literature review of these studies. These parameters are presented mostly as graphical results. The equilibrium data obtained by these workers are summarized in Fig 4.1 for nitrogen and Fig 4.2 for methane which are plots of K_p vs. $\frac{1}{T}$ in semi logarithmic coordinates. The data have been regressed to give

$$K_{N_2} = 0.0206 \exp(3720/RT)$$

$$K_{CH_4} = 0.0345 \exp(3789/RT)$$

The sorption kinetic parameters such as zeolitic diffusivity and activation energy for nitrogen and methane as reported by various workers are tabulated in Table 4.1. Although the diffusivity values are varying for various authors, the diffusional time constant values are similar at 300 ° K.

4.3 Experimental techniques for sorption and equilibrium data:

The most common methods used for determination of adsorption equilibrium and kinetics are:

1.) Volumetric method

2.) Gravimetric method, and

3.) Chromatographic method

A brief description of these methods which were used in this study is presented.

4.3.1 Volumetric method

The constant volume experimental set up of Abdul-Rehman(8) is used for uptake measurements. It consists of a cylindrical cell containing adsorbent immersed in a constant temperature bath. A thermocouple close to the centre of the cell measures the temperature. The cell is connected to a series of empty cylinders through manual and control valves. The pressure in two of the cells can be monitored continuously via an electronic manometer. For uptake measurements the adsorbed cell pressure is continuously recorded on a strip chart recorder.

The cell is loaded with a known weight of the adsorbent. Regeneration of the adsorbent CMS is done at 80 ° C under a vacuum of approximately 10^{-3} torr. A differential step change is made by loading a known amount of pressurized adsorbate gas into this degassed and evacuated cell. The pressure drop is recorded continuously on a strip chart until there is equilibrium between the gas and the solid phase. Each step constitutes a data point in the isotherm. Analysis of the variation of pressure with time enables the kinetics to be established.

4.3.2 Gravimetric method

Uptake rate is measured gravimetrically using a Cahn RG recording electrobalance similar to that used by Loughlin(9).

The Cahn electrobalance is a precision instrument capable of continuously monitoring the weight changes as small as 10^{-7} gm. The balance has a loading loop and a tare loop. The balance can be operated under either atmospheric or vacuum conditions. A vibration free mounting of the balance is essential. The output from the balance is recorded continuously on a strip chart recorder. The hangdown tube which contained the balance pan is immersed in a water bath maintained at constant temperature. A high vacuum is maintained in the system by an Edwards diffusion pumping unit prior to the adsorption steps. A vacuum of 2×10^{-5} mbar was achieved during regeneration of the adsorbent CMS at a temperature of 80°C . The weight of the adsorbate for a step change is recorded continuously with time.

4.3.3 Chromatographic Method

A standard chromatographic method was used by Zahur(10). An experimental set up capable of injecting a step as well as pulse input to a packed column is used. The output stream is analysed with a GOWMAC 10-454 Thermal Conductivity Detector(TCD) block. The reference gas stream, helium, also serves as the carrier stream thereby eliminating flow fluctuations. The output from the TCD detector is obtained on a chart recorder and analysed further.

4.4 Equilibrium Results for Carbon Molecular Sieves:

Equilibrium data available in the literature for sorption in CMS are limited(11,12, 13). In addition, the data obtained by each author is limited to the specific CMS batch used in each particular study. However variations in equilibrium data between batches do not appear to be significant. CMS is a coal or polymer adsorbent and does not have a standard pore structure like zeolite adsorbents. The macropore size distribution for the CMS batch used in this study was measured by mercury porosimetry and the results are presented in Fig 4-3. The mean macropore radius was approximately 10,000 Å and the macropore volume is 275 mm³/gm. Porosity does not give the micropore distribution; typical estimates of this are 4-9 angstroms.

The limiting Henry constants K_p as measured chromatographically, volumetrically and gravimetrically for the sorption of N₂ and CH₄ are reported in Table 4.2 and are plotted on an Arrhenius plot in Fig. 4.4. Sorption of methane is higher by a factor of about 6 at room temperature decreasing as the temperature rises to about 1.5 @ 420 K. The limiting heats of sorption ($-\Delta H_o$) are 2.94 and 5.585 kcal/mole for N₂ and CH₄ respectively, similar to values reported in literature (see Table 4.2).

The adsorption isotherms at 25 °C were measured up to 10 atmospheres for both N₂ and CH₄ . The results are presented in Figs 4.5 and 4.6 respectively

together with the optimal Langmuir constants determined from the expression

$$\frac{q}{q_s} = \frac{b P}{1 + b P}$$

Reasonable agreement between data and the Langmuir fit may be observed.

The equilibrium data obtained in this work is compared to literature values in Table 4.4. For N_2 , the K_p values and for N_2 and CH_4 the b and q_s values determined here are comparable to reported values in the literature. Although there is no K_p value reported for CH_4 in the literature, the fact that the Langmuir constants b and q_s are similar indicates that the K_p values are comparable.

4.5 Kinetic results for the carbon molecular sieves

Representative uptake curves for the sorption of nitrogen and methane on CMS in volumetric apparatus are presented in Figs. 4.7 and 4.8. Detail on the actual experiments is provided in the appendices A.1.4, Runs 1-27. Carbon molecular sieve particles are known to be composed of microporous particles within a macroporous matrix. Accordingly two kinetic resistances can be identified, namely transport through the macropores followed by transport in the microporous matrix. The solution of of this dual kinetic problem was first developed by Ruckenstein et al(15) for a constant pressure system . This was simplified by Lee(16) who also derived the constant volume system solution

(Ruthven(17), pg 184). Ruthven et al(11) further simplified Lee's solution to allow for sudden significant uptake in the macropores before any diffusion into the micropores occurs. Typical results measured by these authors is shown in Fig. 4.9 together with the theoretical results based on a sudden sharp uptake by the macropore followed by slow diffusion in the micropores. A fractional uptake of 15 and 20% may be observed to occur at time zero in their work which is characteristic of rapid adsorption on the macropore walls. The uptake curves observed in this work (Figs. 4.7, 4.8) do not exhibit any sudden sharp uptake like that observed by Ruthven et al(11). An alternate model is required to explain the data found for the specific carbon molecular sieve used in this work.

The first model examined was that of standard Fickian diffusion in a sphere for a constant volume apparatus as derived by Crank(18; Pg 93). This model is not applicable as may be observed by examining Figs. 4.7 and 4.8 where the experimental data traverses the different finite volume uptake curves. The dual resistance constant volume model of Lee(15) was next examined and the results are shown in Fig. 4.10. Again no satisfactory match of theory and data was observed. This exhausted the known diffusion phenomena for carbon molecular sieves.

The uptake curves for methane at 25 ° C is plotted semilogarithmically in Figs. 4.11. This experiment took two weeks to measure but it is observed that for 90% of the uptake over a period of three days the fractional uptake is linear. Further data for different temperatures for both nitrogen and methane is pre-

sented in Figs. 4.12 and 4.13 and all are linear for an uptake of 90%. Between 90 and 100% some curvature is observed (see Fig. 4.14). The detailed data for these runs in addition to further measurements is presented in appendix A.1.4. The facts that these plots are linear initially suggests a rate law is limiting.

In the analysis of sorption on zeolites Karger and co-workers have shown that a barrier resistance exists at the surface, followed by diffusion within the crystal (19,20,21). The particular carbon molecular sieve sample used in this work appears to have similar kinetic characteristics, i.e. transport primarily controlled by a barrier resistance at the surface followed by diffusion. For 90% of the uptake the primary mechanism appears to be the barrier resistance. The appropriate sorption model for the system with the following assumption is then:

- (1) Finite system volume
- (2) Existence of barrier resistance at the surface.
- (3) Subsequent diffusion in a spherical microporous system by Fick's law
- (4) Isothermal
- (5) Constant diffusivity over the incremental step change in concentration.
- (6) Small step changes in concentration from C_i to C_0 , and adsorbing to a final pressure C_∞ .

The relevant equations are then

$$\frac{\partial q}{\partial t} = D \left\{ \frac{\partial^2 q}{\partial r^2} + \frac{2}{r} \frac{\partial q}{\partial r} \right\} \quad (4.1)$$

$$\frac{\partial q}{\partial r}(0,t) = 0 \quad (4.2)$$

$$D_c \frac{dq}{dr}(r_s,t) = k_b \{ q^*(t) - q(r_s,t) \} \quad (4.3)$$

where k_b is the barrier resistance in cm/s.

In the latter equation the expression for $q^*(t)$ derived from an overall balance on the gas phase volume, viz

$$4\pi r_s^2 N \int_0^t D_c \frac{\partial q(r_s,t)}{\partial r} dt = V \{ C(0^+) - C(t) \} \quad (4.4)$$

where N is the number of crystallite particles and

$$q^*(t) = K_p C(t) \quad (4.5)$$

The initial condition is $q(r,0) = K_p C(0^-)$.

Also, $C(0^-) = C_i$, $C(0^+) = C_0$, and $C(\infty) = C_\infty$.

This system of equations was solved by Huang and Li(22) who studied the ion exchange kinetics for calcium radiotracer in a batch system. However, instead of a barrier resistance, they postulated a film resistance at the surface for their system. The solution is

$$1 - \frac{M(t)}{M(\infty)} = \sum_{n=1}^{\infty} \frac{6\zeta^2\alpha(1+\alpha)}{(9+\alpha^2g_n^2+9\alpha)\zeta^2 - (6+\alpha)\alpha g_n^2\zeta + \alpha^2g_n^4} \exp(-g_n^2 T) \quad (4.6)$$

where g_n are the non-zero roots of the equation

$$\frac{\tan g_n}{g_n} = \frac{3\zeta - \alpha g_n^2}{(\zeta - 1)\alpha g_n^2 + 3\zeta} \quad (4.7)$$

and

$$\zeta = \frac{r_s k_b}{D_c}, \quad T = \frac{D_c t}{r_s^2} \quad \text{and} \quad \alpha = \frac{V}{V_s K_p}$$

are dimensionless groups. ζ In Huang and Li's work is defined as $r_s k_b / K_p D$, because equation 4.3 in their paper is defined in terms of bulk phase concentration. T is the usual dimensionless time group and α is the usual parameter that enables the total fractional uptake U to be calculated from

$$U = \frac{M(\infty)}{M(0)} = \frac{1}{1 + \alpha} \quad (4.8)$$

where $M(0)$ is the mass added at time zero and $M(\infty)$ is the mass adsorbed by the sample at final steady state.

ζ represents the relative importance of the barrier resistance and the diffusional resistance inside the microporous particle. Small values of ζ implies that the resistance inside the particle is insignificant and the adsorption rate is controlled by the barrier resistance. Large values of ζ imply that the mechanism of intraparticle resistance is the rate controlling step; as $\zeta \rightarrow \infty$, the equation simplifies to that given by Crank for intraparticle diffusion(18;Pg. 93).

$$1 - \frac{M(t)}{M(\infty)} = \sum_{n=1}^{\infty} \frac{6\alpha(1+\alpha)}{(9+9\alpha+\alpha^2 g_n^2)} \exp(-g_n^2 T) \quad (4.9)$$

where g_n are the non-zero roots of the equation

$$\frac{\tan g_n}{g_n} = \frac{3}{3 + \alpha g_n^2} \quad (4.10)$$

Huang and Li (22) solved equation 4.6 for various values of ζ and U . The smallest value of ζ used by them is 1.0. For this case their plots of $\ln\left(1 - \frac{M(t)}{M(\infty)}\right)$ vs. T are all linear over the entire range, similar to the plots shown in Figures 4.11, 4.12 and 4.13. The limiting values of ζ for film resistance for their work is probably $1/K_p$ but for a barrier resistance this could be much lower. The conclusion of semilogarithmic plots of $\left(1 - \frac{M(t)}{M(\infty)}\right)$ being linear versus T would still be valid. As ζ increases, Huang and Li's plot become non linear in the short time region and linear in the long time region similar to that shown in the Fig. 4.14. For $\zeta > 4$, the point of curvature is above values of $\left(1 - \frac{M(t)}{M(\infty)}\right) > 0.1$ which is not what is observed in this study suggesting that the appropriate value of ζ is somewhere between 0 and 4. At long times the solution of equation 4.6 reduces to the first term and becomes

$$1 - \frac{M(t)}{M(\infty)} = \frac{6\zeta^2\alpha(1+\alpha)}{(9+\alpha^2 g_1^2+9\alpha)\zeta^2 - (6+\alpha)\alpha g_1^2\zeta + \alpha^2 g_1^4} \exp(-g_1^2 T) \quad (4.11)$$

with g_1 given by

$$\frac{\text{tang}_1}{g_1} = \frac{3\zeta - \alpha g_1^2}{(\zeta - 1)\alpha g_1^2 + 3\zeta} \quad (4.12)$$

So a semilogarithmic plot of $\left(1 - \frac{M(t)}{M(\infty)}\right)$ versus t has an intercept of

$$\frac{6\zeta^2\alpha(1+\alpha)}{(9+\alpha^2g_1^2+9\alpha)\zeta^2 - (6+\alpha)\alpha g_1^2\zeta + \alpha^2g_1^4} \quad (4.13)$$

and a slope of

$$-g_1^2 D_c / r_s^2 \quad (4.14)$$

Knowing α , we can solve equations 4.12 and 4.13 for ζ and g_1 and hence obtain D_c / r_c^2 from equation 4.14.

An alternative procedure is to use a lumped parameter model for the initial region where the barrier resistance is dominant. For this system, the overall mass balance equations and initial conditions are

$$V_s \frac{dq(t)}{dt} = -V \frac{dC(t)}{dt} = A \underline{j} \quad (4.15)$$

where

$$\underline{j} = k_g (q^* - q)$$

with

$$C(0^-) = C_i, \quad C(0^+) = C_0, \quad C(\infty) = C_\infty$$

$$q'(t) = K_p C(t) \text{ and } q(t) = K_p C^*(t)$$

Substituting

$$-V \frac{dC(t)}{dt} = A \underline{j} \quad (4.16)$$

$$= A k_s K_p (C - C^*) \quad (4.17)$$

In the case of a finite volume system, the initial and final concentrations C_i , C_∞ , q_i and q_∞ are constant, but C^* varies during the adsorption step. The overall concentration in the gas and solid phases may be related at any instant of time by

$$V (C_0 - C) = V_s (q - q_0)$$

$$V (C_0 - C_\infty) = V_s (q_\infty - q_0) \quad (4.18)$$

$$V (C - C_\infty) = V_s (q_\infty - q)$$

Physically these equations indicate that what has been transferred from the gas phase must be in the solid phase. Substituting in the mass balance equation gives

$$\frac{dC}{dt} = - \frac{A k_s K_p}{V} (1 + \alpha) (C - C_\infty) \quad (4.19)$$

$$= -\frac{Ak_s}{V_s} \left(\frac{1+\alpha}{\alpha} \right) (C - C_\infty) \quad (4.20)$$

Solving using the initial and final conditions gives

$$\ln \left(\frac{C - C_\infty}{C_0 - C_\infty} \right) = -\frac{Ak_s}{V_s} \left(\frac{1+\alpha}{\alpha} \right) t \quad (4.21)$$

In terms of fractional uptake this reduces to

$$\ln \left(1 - \frac{M_t}{M_\infty} \right) = -\frac{Ak_s}{V_s} \left(\frac{1+\alpha}{\alpha} \right) t \quad (4.22)$$

so that semilogarithmic plots for a volumetric system have a slope

$$k_v = \frac{Ak_s}{V_s} \left(\frac{1+\alpha}{\alpha} \right) \quad (4.23)$$

The volumetric slope k_v was extracted from the initial rate data and is tabulated in Table 4.3 for the different temperatures for methane and nitrogen.

Zahur(10) also measured the transport rate of nitrogen into the carbon molecular sieve particles used in the study. Using a chromatographic method, he abstracted the rate constant from the second moment equation

$$\frac{\sigma^2 L}{2\mu^2 v} = \frac{D_L}{v^2} + \frac{\epsilon}{1 - \epsilon} \frac{1}{k_c K_p} \quad (4.24)$$

where k_c is the chromatographic rate constant. The rates measured for nitrogen are also reported in Table 4.3 as k_c . In his study Zahur used crushed particles of approximately 0.0425 cm whereas the volumetric measurement were carried out

on particles of 0.233 cm. Uptake rates of methane via chromatography was too slow to measure on the carbon molecular sieve particles used in this study. The surface resistance from the volumetric and chromatographic data were calculated using the equations

$$k_s = \frac{\alpha k_v d_{p1}}{6(1 + \alpha)} \quad (4.25)$$

$$k_s = \frac{k_c d_{p2}}{6} \quad (4.26)$$

The resulting data is tabulated in Table 4.3 and is plotted in Fig 4.15. The volumetric and chromatographic data are observed to be in good agreement, and although different particle sizes have been used in the two methods. This indicates that surface resistance controls the rate constants and are independent of r^2 . The surface resistance may be correlated by an expression of the form

$$k_s = k_{os}^* \exp\left(-\frac{E}{RT}\right)$$

and the best fit lines are shown in Fig 4.15 with the data. The high values of the activation energy E of 8.11 kcal/mol and 13.96 kcal/mol for nitrogen and methane respectively indicate that this is an activated process rather than a normal diffusion process. The activation energies are compared with the diffusional activation energies against Van der Waals diameter for diffusion in 4Å and 5Å zeolites and 5Å carbon molecular sieves as presented by Ruthven(17) in Fig 4.16 and against the isotheric heat of adsorption presented by Chihara et al (15) in Fig

4.17. The conclusion from these comparisons appears to be that the carbon molecular sieve used in this study has a pore opening somewhat smaller than 4Å which appears to be the cause of the high activation energy needed for the transport process. For comparison of uptake rate in sec^{-1} with literature values, the rate constant k may be defined analogous to the literature as

$$k = 15 \frac{D_c}{r_c^2}$$

and for this study as

$$k = \frac{6k_s}{d_p} \text{ with } d_p = 0.233 \text{ cm.}$$

Values of k so calculated are presented in Table 4.4 for both methane and nitrogen and the measured rates in this study are the lowest reported. This is consistent with a smaller pore opening carbon molecular sieve as noted above. The D_c/r_s^2 values for methane and nitrogen are tabulated in Table 4.5. These are calculated from equations 4.12, 4.13, 4.14. The temperature dependency of D_c/r_s^2 for methane is plotted in Fig 4.18. An activation energy of 12.563 Kcal/mol is close to that obtained for the barrier resistance.

4.6 Conclusions

The carbon molecular sieve sample used in this study has similar equilibrium properties to samples reported in the literature but has significantly differ-

ent kinetic properties. The equilibrium of nitrogen and methane is Langmuir like having similar Henry constants and saturation values to other samples.

The kinetics do not appear to be diffusionally controlled as reported by other workers. Further the rates are significantly slower indicating that the micropore opening may be less than 4\AA . A coupled resistance mechanism comprising a dominant barrier resistance on the surface and a micropore diffusion resistance within the crystal is proposed to model the uptake data. Subsequently a diffusional resistance appears to control the adsorption rate. The observed phenomena are similar to Huang and Li's model with their film resistance replaced by a barrier resistance.

References

- (1) Habgood, H. W., Can. J. Chem., 36, 1384 (1958)
- (2) Harper, R.J., Stifel, G. R., and Anderson, R. B., Can. J. Chem., 47, 4661 (1969)
- (3) Ruthven, D. M. , and Kumar, R., Ind. Eng. Chem. Fundamen., 19, 27 (1980)
- (4) Eagen, J. D., and Anderson, R. B., J. Colloid. Interface Science., 50, 419 (1975)
- (5) Yucel, H., and Ruthven, D. M., J. Chem. Soc. Faraday Trans. I, 76, 60 (1980).
- (6) Ruthven, D. M., and Derrah, R. I., J. Chem. Soc. Faraday Trans. I, 71, 2031 (1975).
- (7) Ruthven, D. M., and Haq, N., J. Colloid. Interface Science., 112, 154 (1986)
- (8) Abdul-Rehman, H. B., M. S. Thesis, KFUPM, Dhahran, (1988).
- (9) Loughlin K. F., Ph. D. Thesis, Univ. of New Brunswick, (1970).
- (10) Zahur, M., M. S. Thesis, KFUPM, Dhahran, (1991).
- (11) Ruthven, D. M., Raghvan, N. S., and Hassan, M. M., Chem. Eng. Sci., 41, 1325 (1986).
- (12) Ackley, M., and Yang, R. T., AIChE J., 36, 1229 (1990).
- (13) Kapoor, A., and Yang, R. T., Chem. Eng. Sci., 44, 1723 (1989).
- (14) Chihara, K. and Suzuki, M., AIChEJ, 24, 243, (1978).
- (15) Ruckenstein, E., Vaidyanathan, A. S., and Youngquist, G. R., Chem. Eng. Sci., 26, 1306 (1971).
- (16) Lee, L. K., AIChE J., 24, 531 (1978).

- (17) Ruthven, D. M., Principles of Adsorption and Adsorption Processes, John Wiley & Sons, (1984).
- (18) Crank, J., Mathematics of Diffusion, (1954).
- (19) Karger J., and Caro J., J. Chem. Soc. Faraday Trans. I, 73,1363 (1977).
- (20) Bulow, M., Struve, P., Finger, G., Redszus, C., Ehrhardt, K., Schirmer, W. and Karger J., J. Chem. Soc. Faraday Trans. I, 76,597 (1980).
- (21) Karger J., and Pfeifer, H., J. Chem. Soc. Faraday Trans., 87(13),1989 (1991).
- (22) Huang, T. and Li, K, Ind. Eng. Chem. Fundam., 12(1), 50 (1973).
- (23) Hassan M. M., Ph. D. Thesis, Univ. of New Brunswick, (1985).

TABLE 4.1 Activation Energy, E, Preexponential Factor, D., Crystal diameter and Diffusional Time Constant at 300 K of Nitrogen and Methane in 4A Zeolite

Sorbate	Reference	Temperature Range ° K	E kcal/mole	D. cm ² / sec	Crystal dia. microns	D/r ² *10 ⁴ @ 300° K sec ⁻¹
N ₂	(3)	304 - 363	6.06	2.96 x 10 ⁻⁶	3.5	37.2
	(5)	243 - 323	5.58	1.3 x 10 ⁻⁵	7.3, 21, 34	42.0
	(1)	194 - 273	4.07	2.3 x 10 ⁻⁹	0.5	39.8
	(6)	215 - 279	6.13	8.32 x 10 ⁻⁷	3.4	9.84
	(4)	195 - 223	8.21	1.8 x 10 ⁻³	4.1	446.
	(7)	298 - 363	4.46	3.39 x 10 ⁻⁷	3.7	55.7
CH ₄	(3)	305 - 366	6.74	4.1 x 10 ⁻⁷	3.5	1.64
	(5)	273 - 323	5.75	9.1 x 10 ⁻⁷	7.3, 21, 34	4.42
	(1)	194 - 273	7.42	5.8 x 10 ⁻⁸	0.5	3.64
	(4)	263	6.30	-	4.1	-
	(7)	273 - 323	4.54	4.47 x 10 ⁻⁸	3.7	6.43

TABLE 4.2 Summary of the Henry Constant Measurements for
the Sorption of Nitrogen and Methane on CMS

Temp.	K _p			K ₀ * 10 ³	-ΔH ₀ kcal/mole	
K	Chromat.	Vol.	Grav.			
Nitrogen						
283			14.4 15.8	60	2.94	
298		7.58	10.25 10.48			
298.5		10.47				
323	7.38	6.693 6.675	5.39 5.31 6.40			
348	6.15					
352		4.25 4.34 4.51				
353	6.16	4.22	3.69 3.76			
375	5.24					
Methane						
297.7 323 351.4 400 420		46.83 28.5 16.09 4.49 3.29			4.337	5.585 5.10 ⁽²⁾

Note : (1) Regression Correlation Coefficient for Nitrogen Data is 0.906
Regression Correlation Coefficient for Methane Data is 0.9914
(2) Q st -RT values reported by Chihara et al for CMS(14).

TABLE 4.3 Summary of the Rate Data Measurements for the Sorption of Nitrogen and Methane on CMS

Temp.	Volumetric		Chromat.			
K	$k_v \times 10^2$ s ⁻¹	$k_s \times 10^4$ cm/s	$k_c \times 10^2$ s ⁻¹	$k \times 10^4$ cm/s	$k'_{os} \times 10^4$ cm/s	E kcal/mol
Nitrogen						
298	0.151	0.371				
323	0.36 0.34	1.0 0.947	2.1	1.49		
348			3.18	2.25		
352	0.87 0.87 0.87	2.66 2.66 2.66			34.37	8.11
353	0.968	2.97	3.645	2.58		
373			3.645	4.59		
420	9.5	32.3				
Methane						
	$k_v \times 10^4$	$k_s \times 10^6$				
297.7	0.212	0.27				
323	0.61	0.936				
351.4	1.8	3.977			3247	13.96
400	30	90.55				
420	65. 55.7	209.46 179.53				

- Note : (1a) Correlation coefficient for k_s for N₂ is $r=0.95$
 (1b) Correlation coefficient for k_s for CH₄ is $r=0.9936$
 (2) $k_s = \frac{k_v d_p / 6}{\frac{K_p V_s}{V} + 1}$ with $d_p = 0.233$ cm, $V_s = 39.17$ cm³, $V = 668.2$ cm³
 except for 297.7 °K, CH₄ data where $V = 1046.2$ cm³
 (3) $k_s = k_c d_p / 6$ with $d_p = 0.0425$ cm.

TABLE 4.4 Comparison of Equilibrium and Kinetic Parameters Reported in the Literature with Results of this Study on CMS

Sorbate	Reference	Temperature °K	k sec ⁻¹	K _p	b atm ⁻¹	q _s mmole/cc	Method
N ₂	(10)	303	0.011	8.93	-	-	Chromat.
	(12)	295	0.0014	-	0.2475	1.64	Grav.
	(11)	299	0.0018	9.6	-	-	Chromat.
	Pres. Study	298	0.0010	8.6	0.26	1.82	Volumetric
CH ₄	(12)	295	5.1 x 10 ⁻⁵	-	0.5882	2.55	Grav.
	(13)	298	7.5 x 10 ⁻⁵	-	0.607	2.308	Grav.
	Pres. Study	298	4.82 x 10 ⁻⁶	54.1	0.62	2.55	Volumetric

Notes: (1) For literature values, $k = 15 D_g/r_c^2$
 (2) For comparison with column studies $k = 6 k_g/d_p$ with $d_p = 0.233$ cm

TABLE 4.5 Diffusion Time Constant of Methane and Nitrogen in Carbon Molecular Sieves
based on Long Time Solution of the Barrier Resistance Model

Sorbate	Temperature K	Slope sec ⁻¹	Intercept	α	ξ	g_1	D_e/r_s^2 sec ⁻¹
CH ₄	323	-3 x 10 ⁻⁵	0.296	0.598	0.315	4.569	1.43 x 10 ⁻⁶
	351.4	-1.5 x 10 ⁻⁴	0.7	1.060	0.542	4.623	7.02 x 10 ⁻⁶
	400	-9.7 x 10 ⁻⁴	0.165	3.799	1.387	4.807	4.20 x 10 ⁻⁵
	420	-4.1 x 10 ⁻³	0.42	5.185	2.000	4.932	1.69 x 10 ⁻⁴
N ₂	323	-2.5 x 10 ⁻⁵	0.569	2.554	1.163	4.763	1.10 x 10 ⁻⁴

Notes: (1) The slope and intercept are obtained from the semilogarithmic plot of the long time solution.

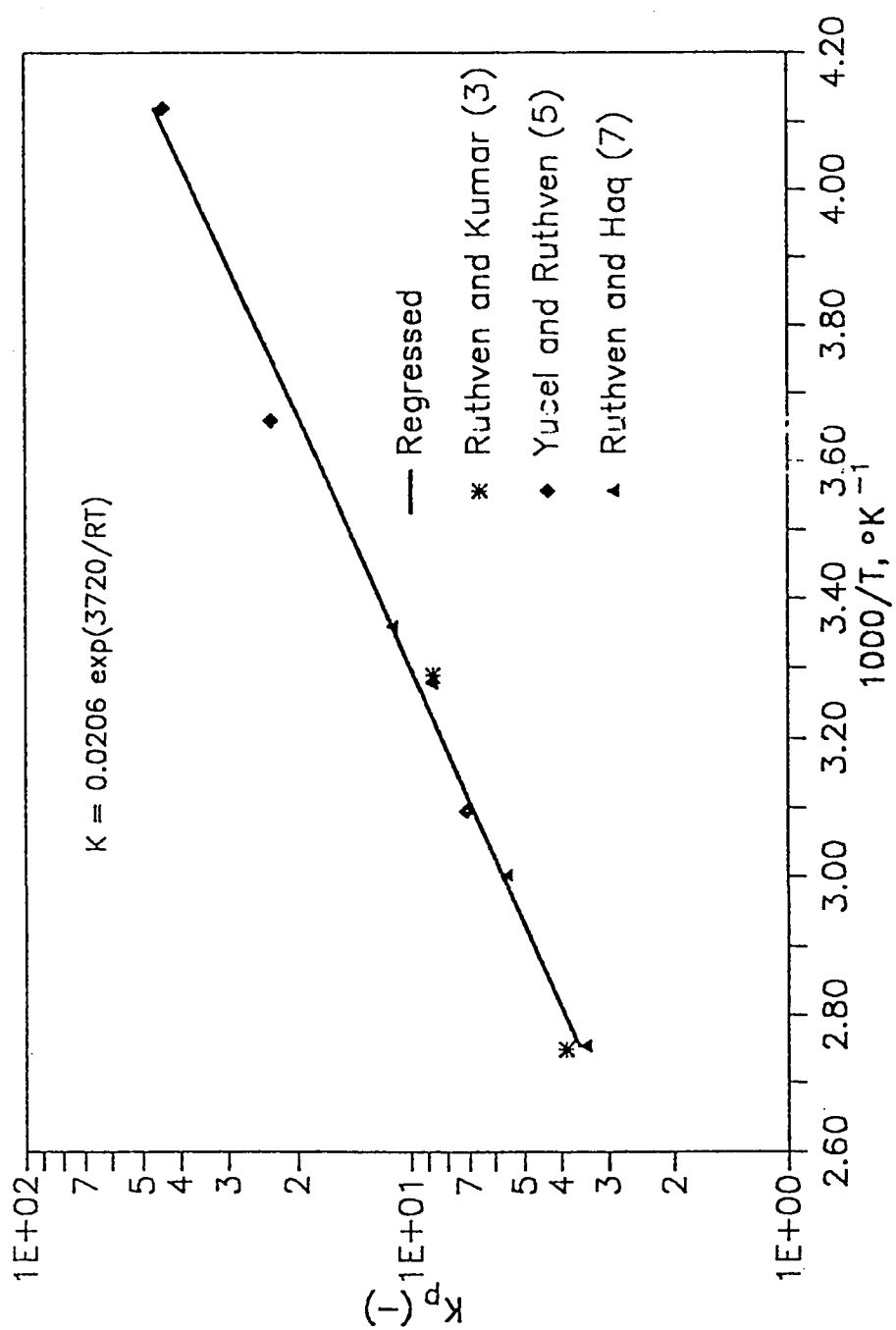


Fig 4.1 Temperature Dependence of Henry constants for Sorption of Nitrogen in 4A zeolite

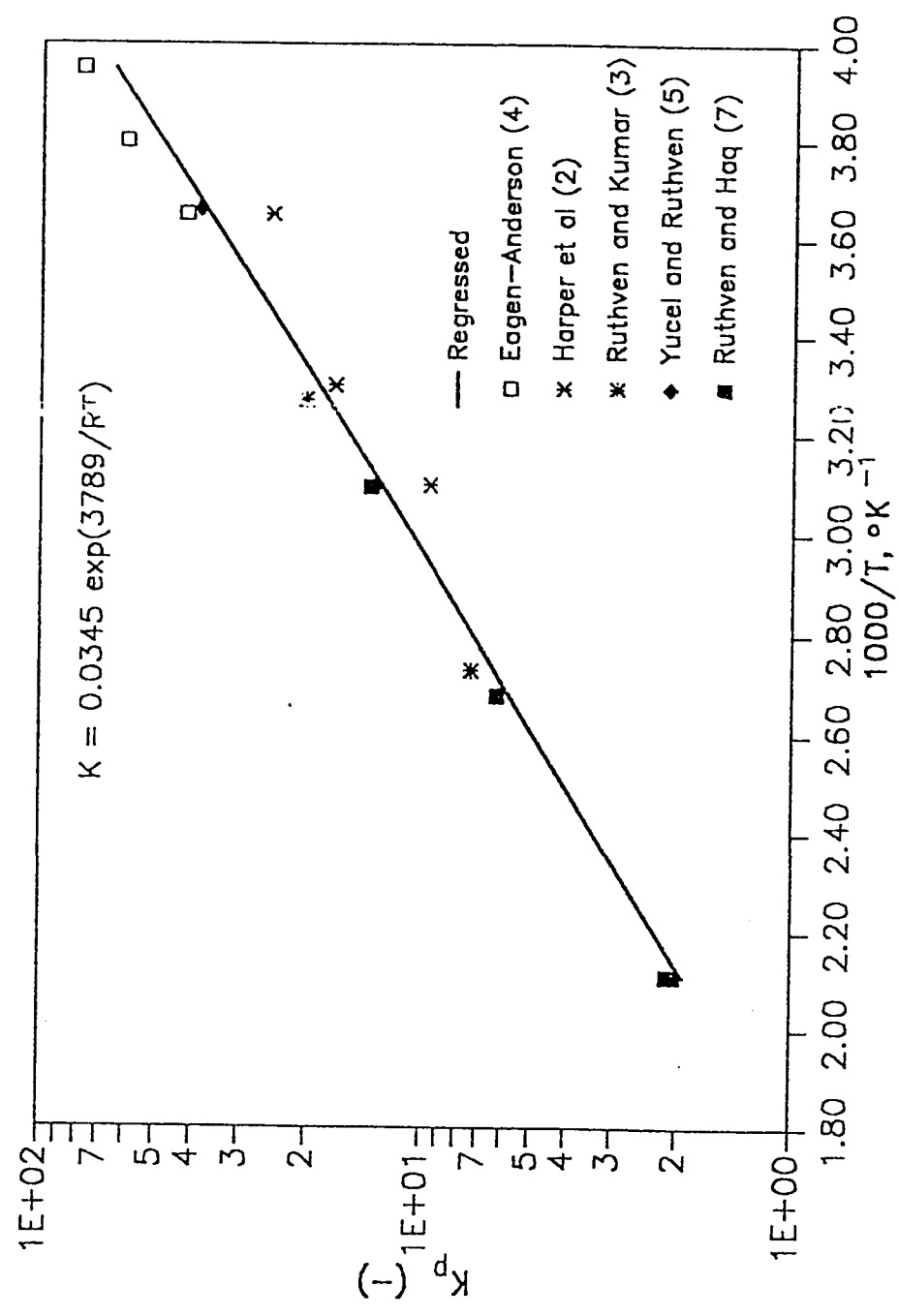


Fig 4.2 Temperature Dependence of Henry constants for Sorption of Methane in 4A zeolite

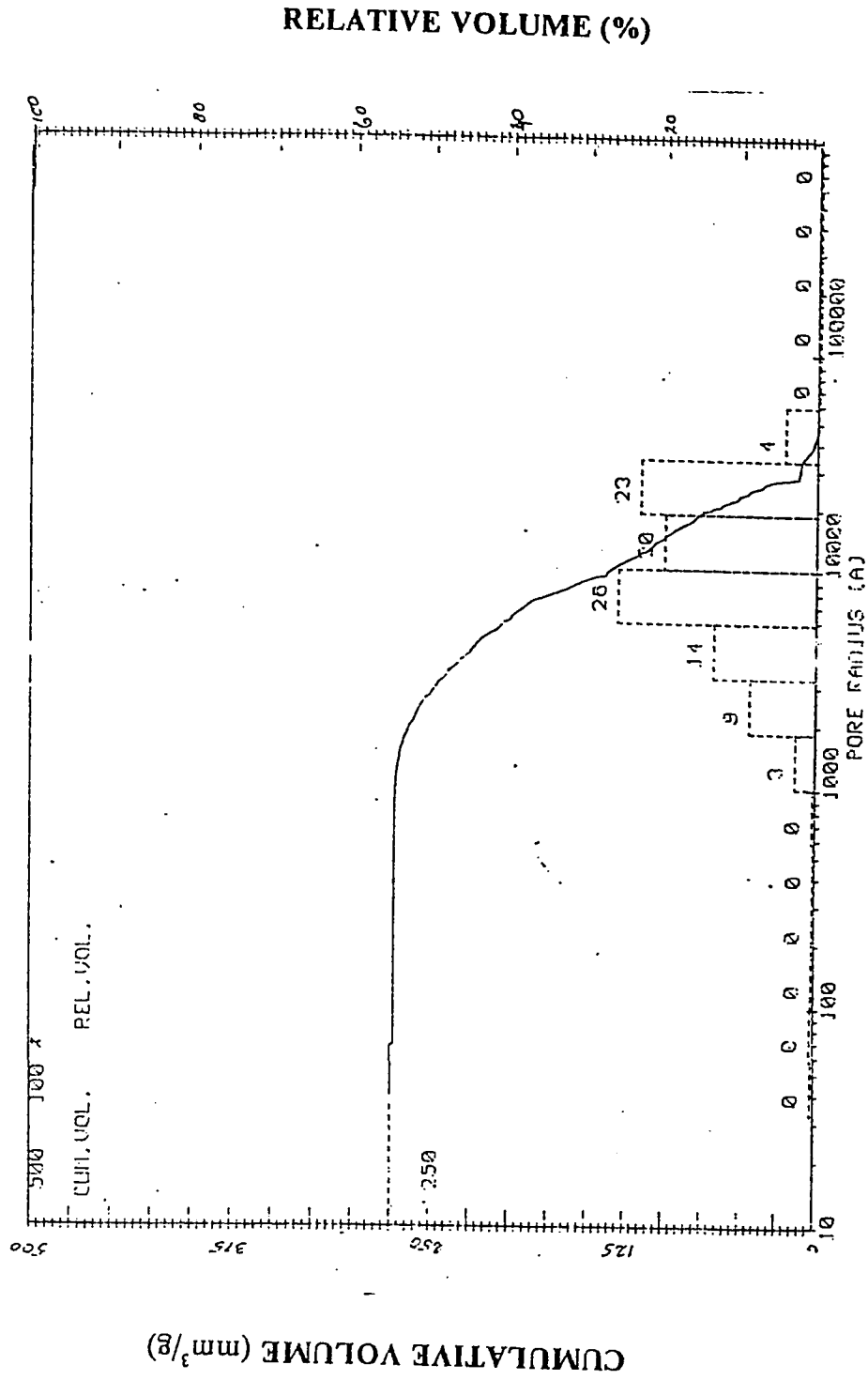


Fig 4.3 Plot of Cumulative and Relative Volumes vs. Pore Radius for the CMS sample used in this study

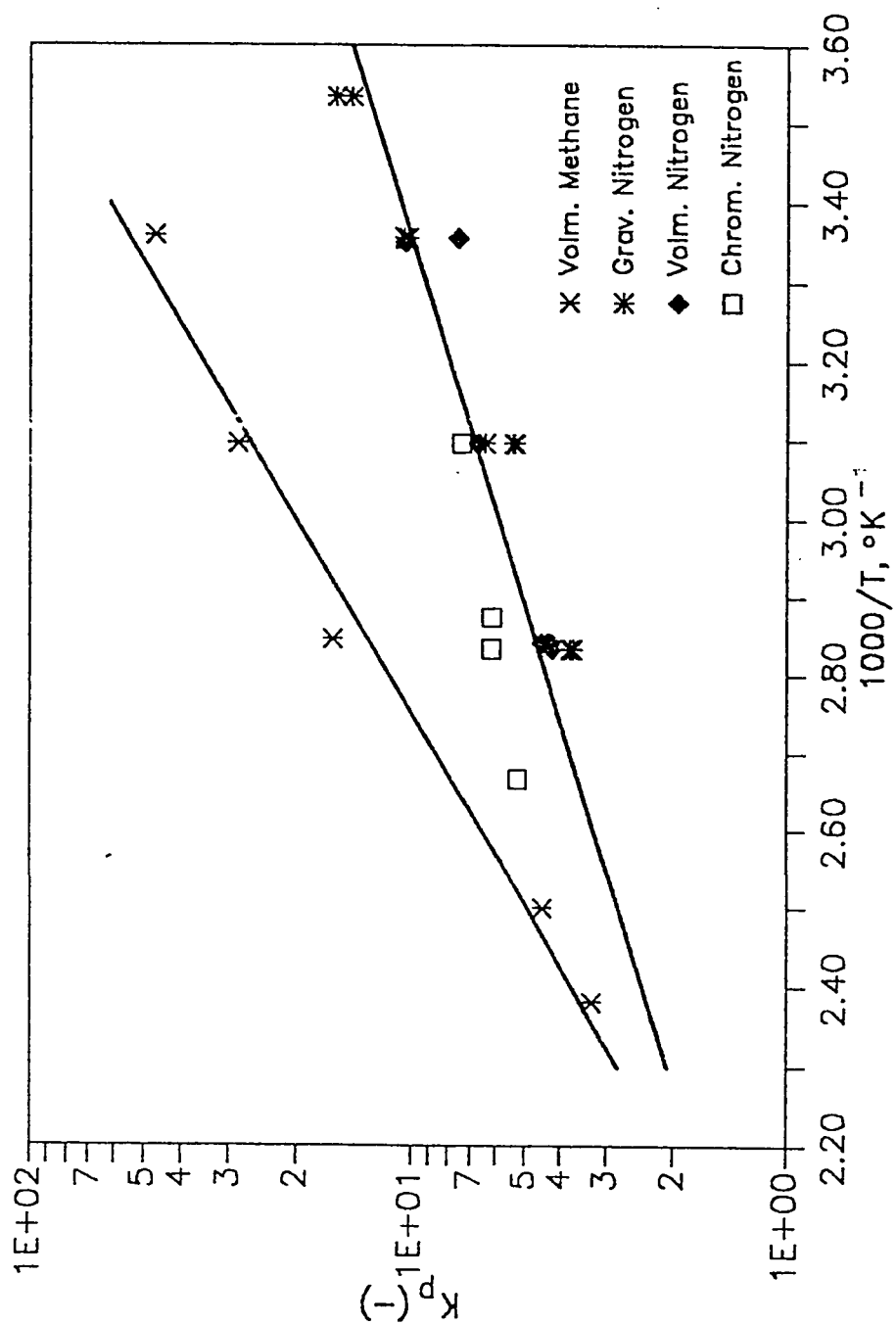
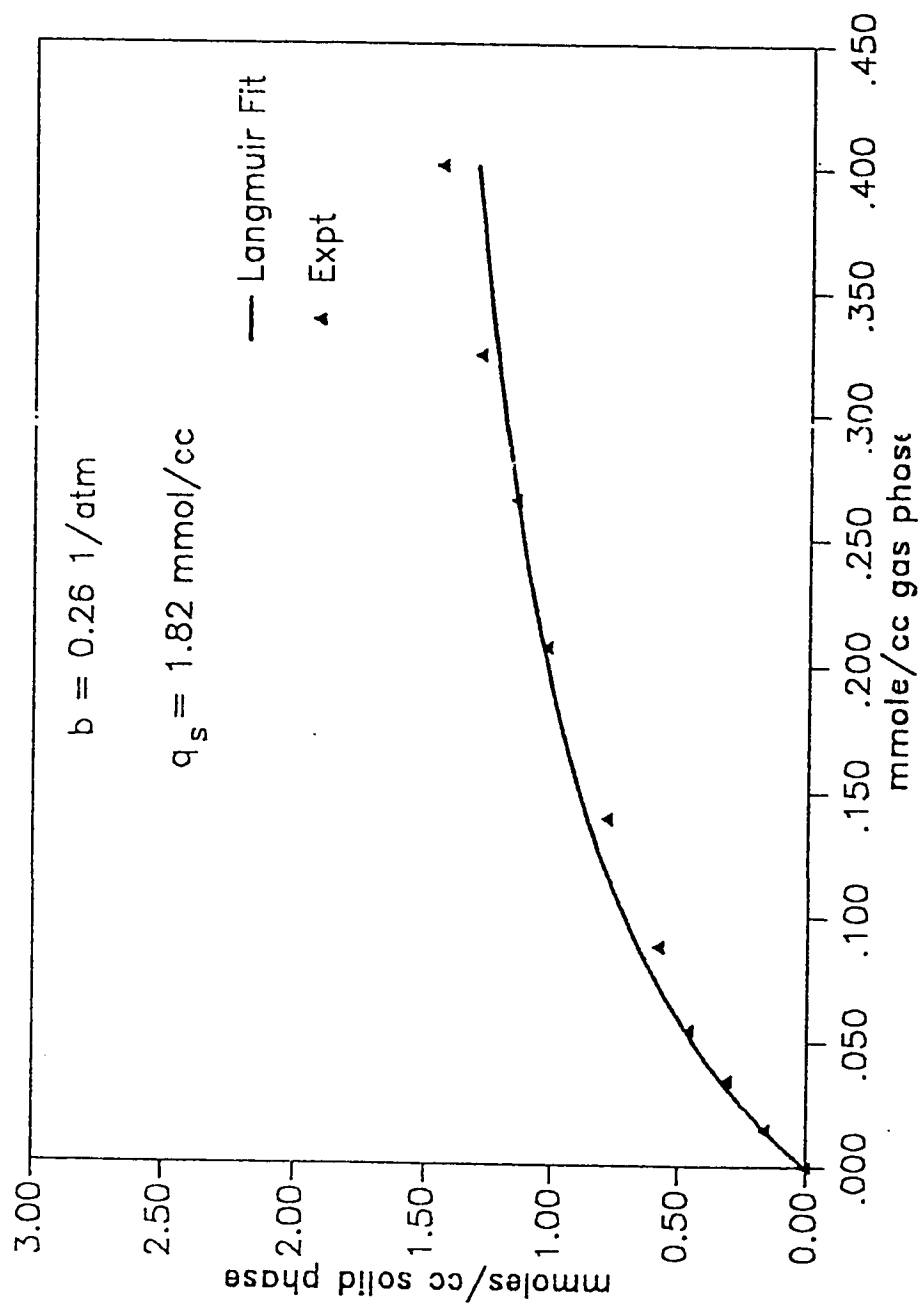
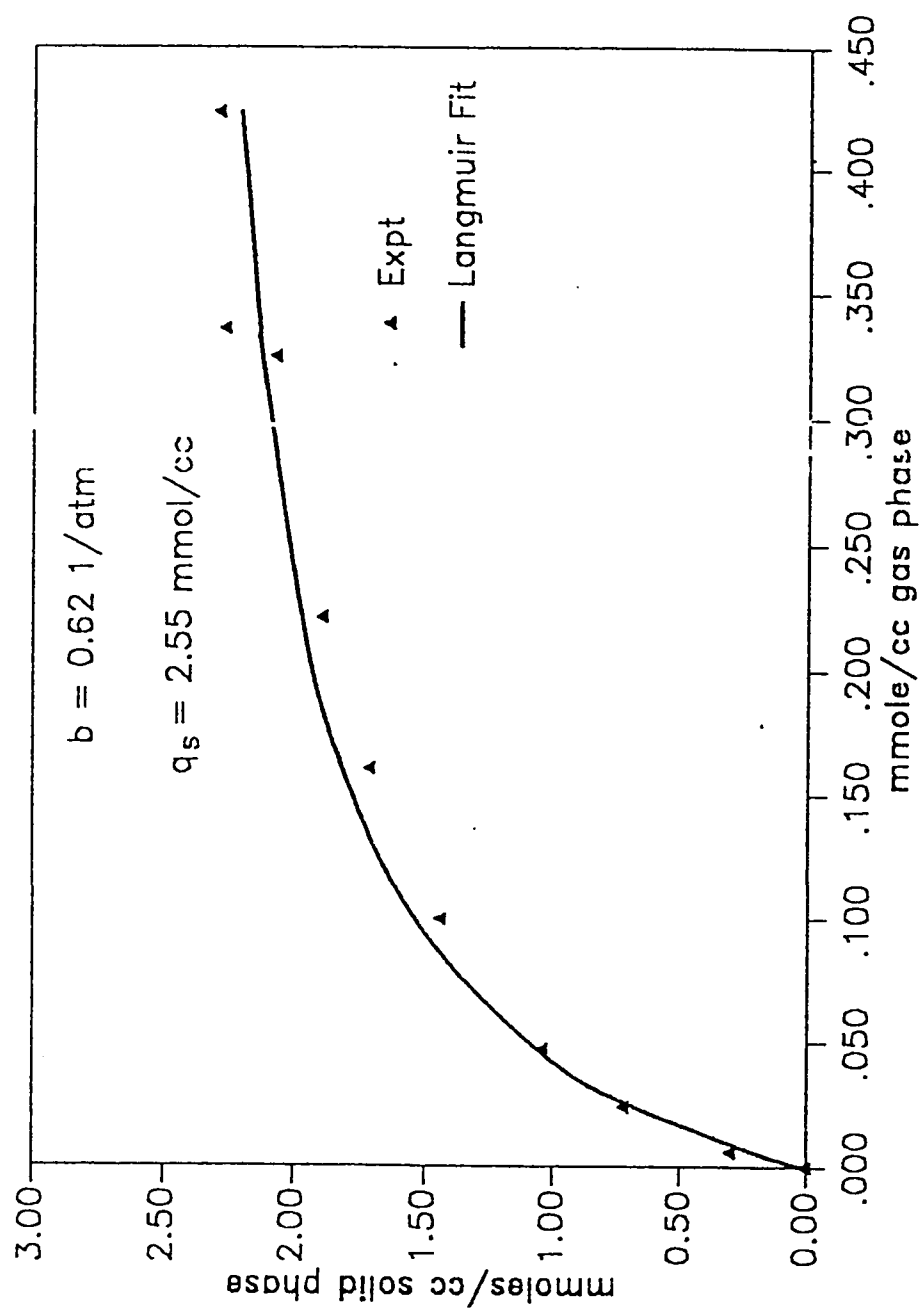


Fig 4.4 Vant Hoff Plot of the Henry Constants K_h vs. $1/T$ for Nitrogen and Methane Sorption on CMS.



FILE: ison2/fig4.5

Fig 4.5 Equilibrium Isotherm of Nitrogen on CM5 at 25°C



FILE:isoch4/fig46

Fig 4.6 Equilibrium Isotherm of Methane on CMS at 25°C

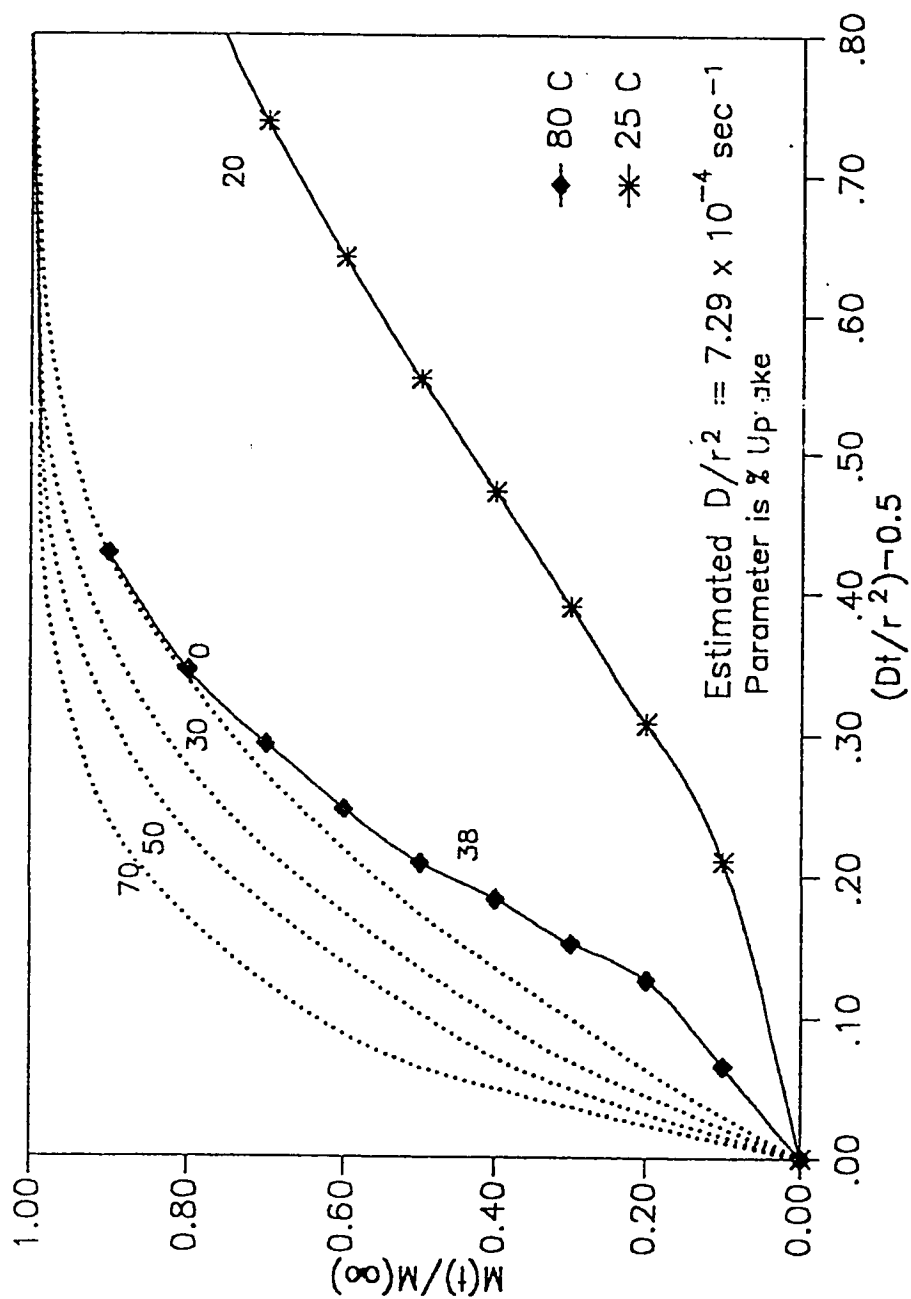


Fig 4.7 Comparison of volumetric uptake rates with standard solution of Fick's Law for diffusion in spheres for Nitrogen at 25 and 80 °C on 2.33 mm pellets

22/fig47

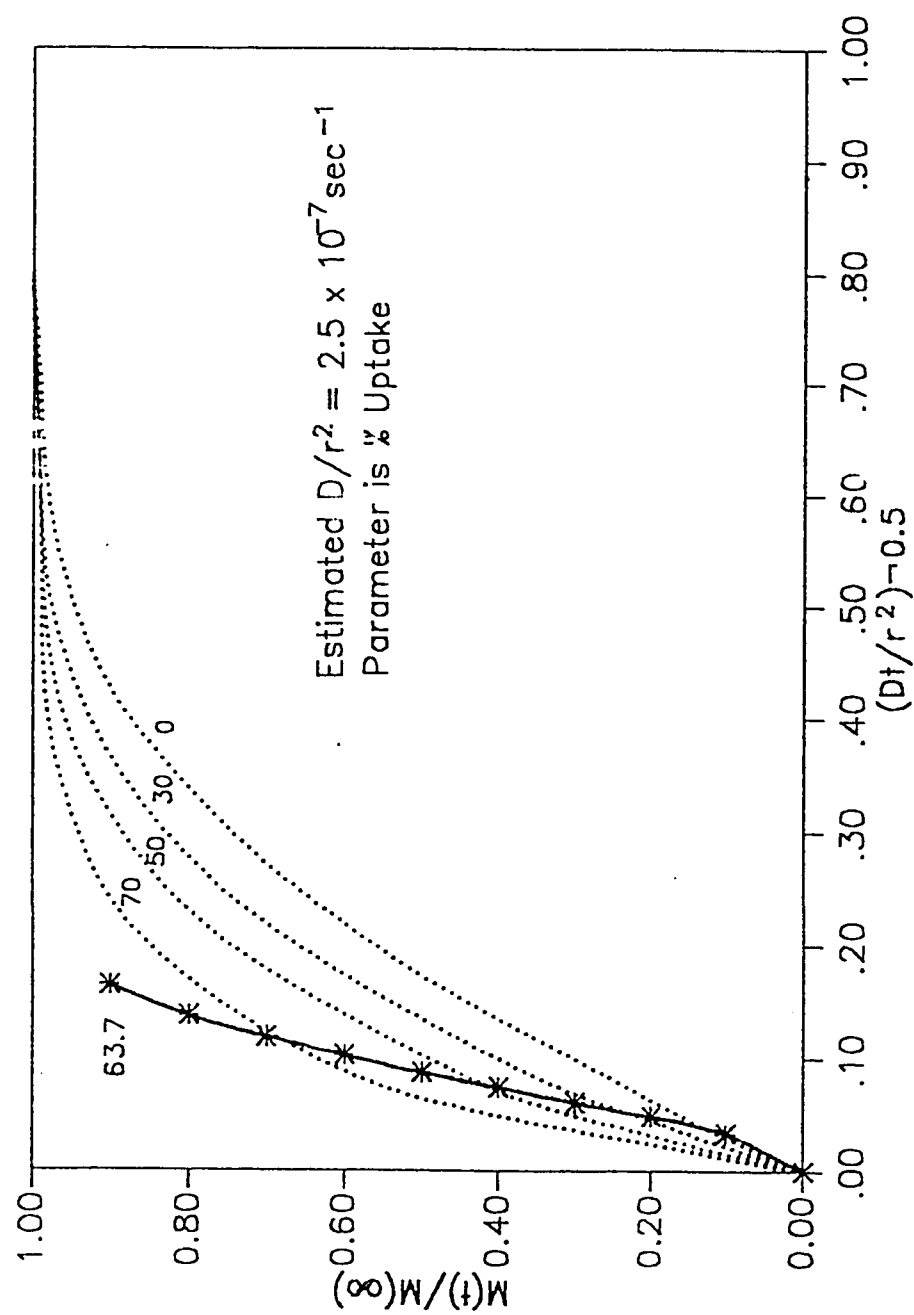


Fig 4.8 Comparison of volumetric uptake rates with standard solution of Fick's Law for diffusion in spheres for Methane at 25 °C on 2.33 mm pellets

-Ernk90ch

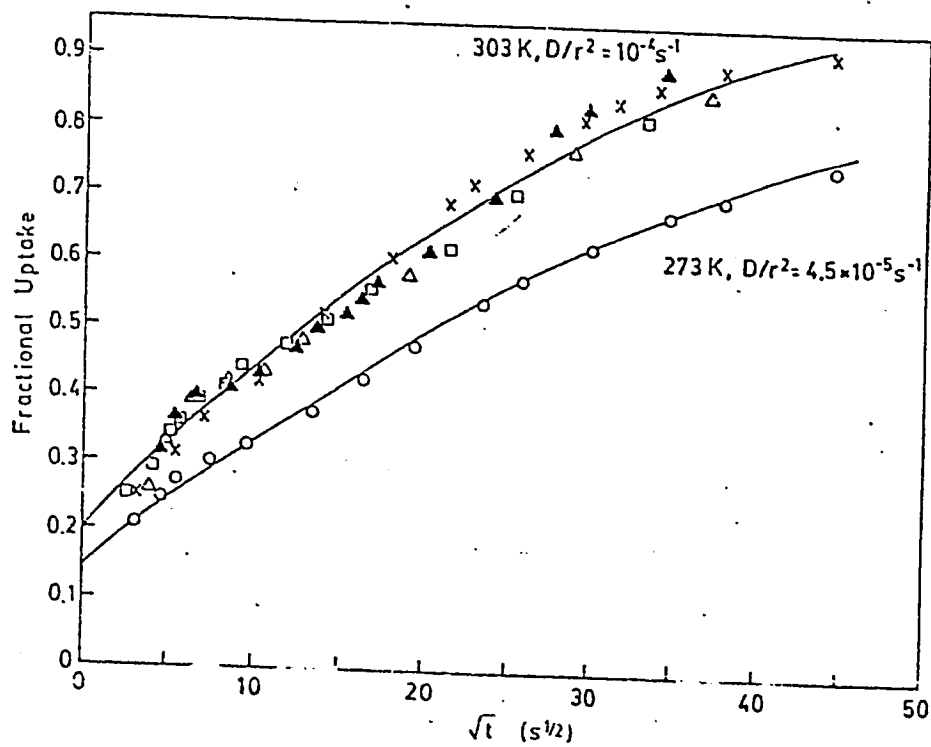


Fig 4.9 Experimental uptake curves for Nitrogen on CMS reported in the literature. 3 mm pellet at 303K, \blacktriangle ; 30-60 mesh at 303 K, \square , \triangle , \times ; 30-60 mesh at 273 K, \circ ; Reproduced from Ph.D. Thesis of Hassan(23)

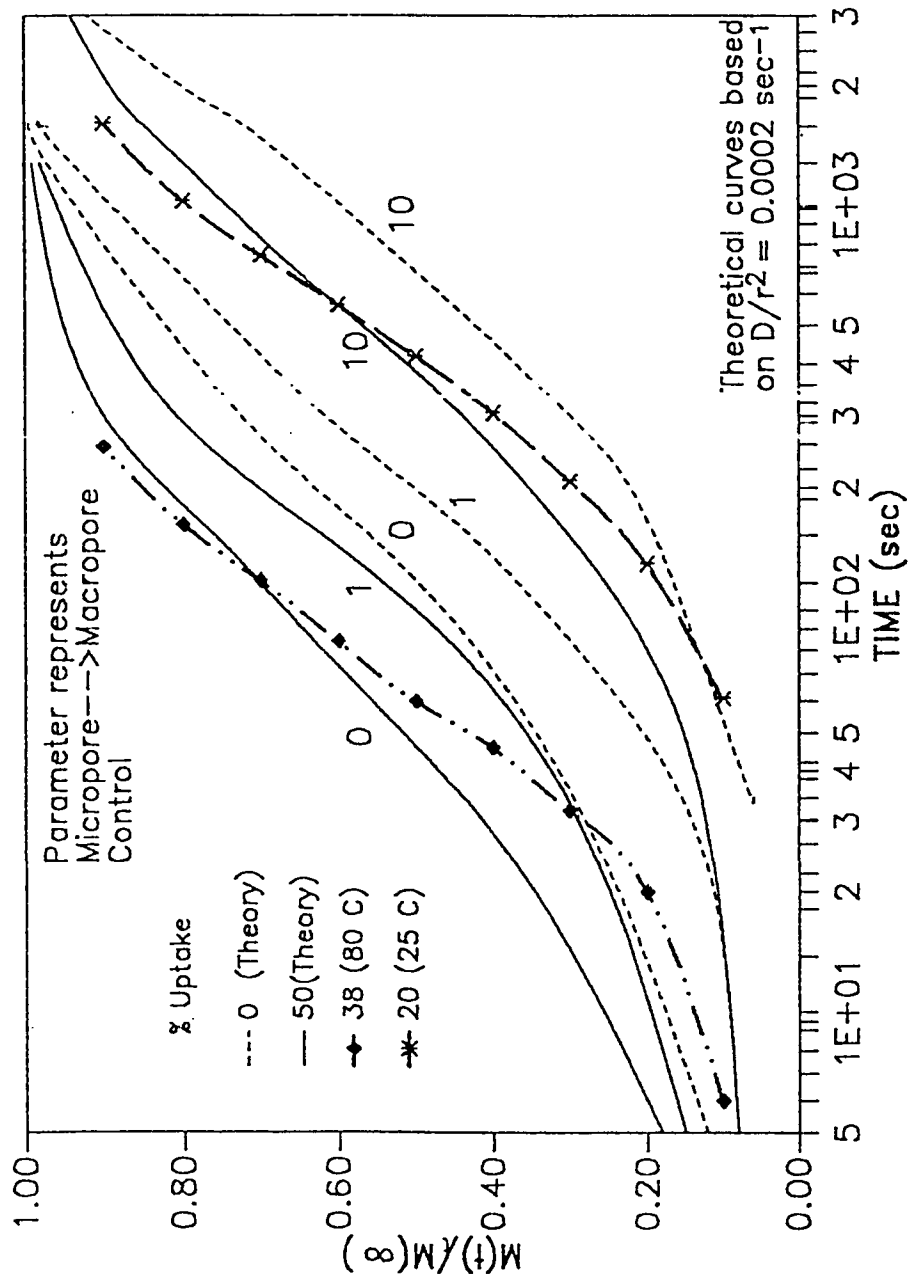
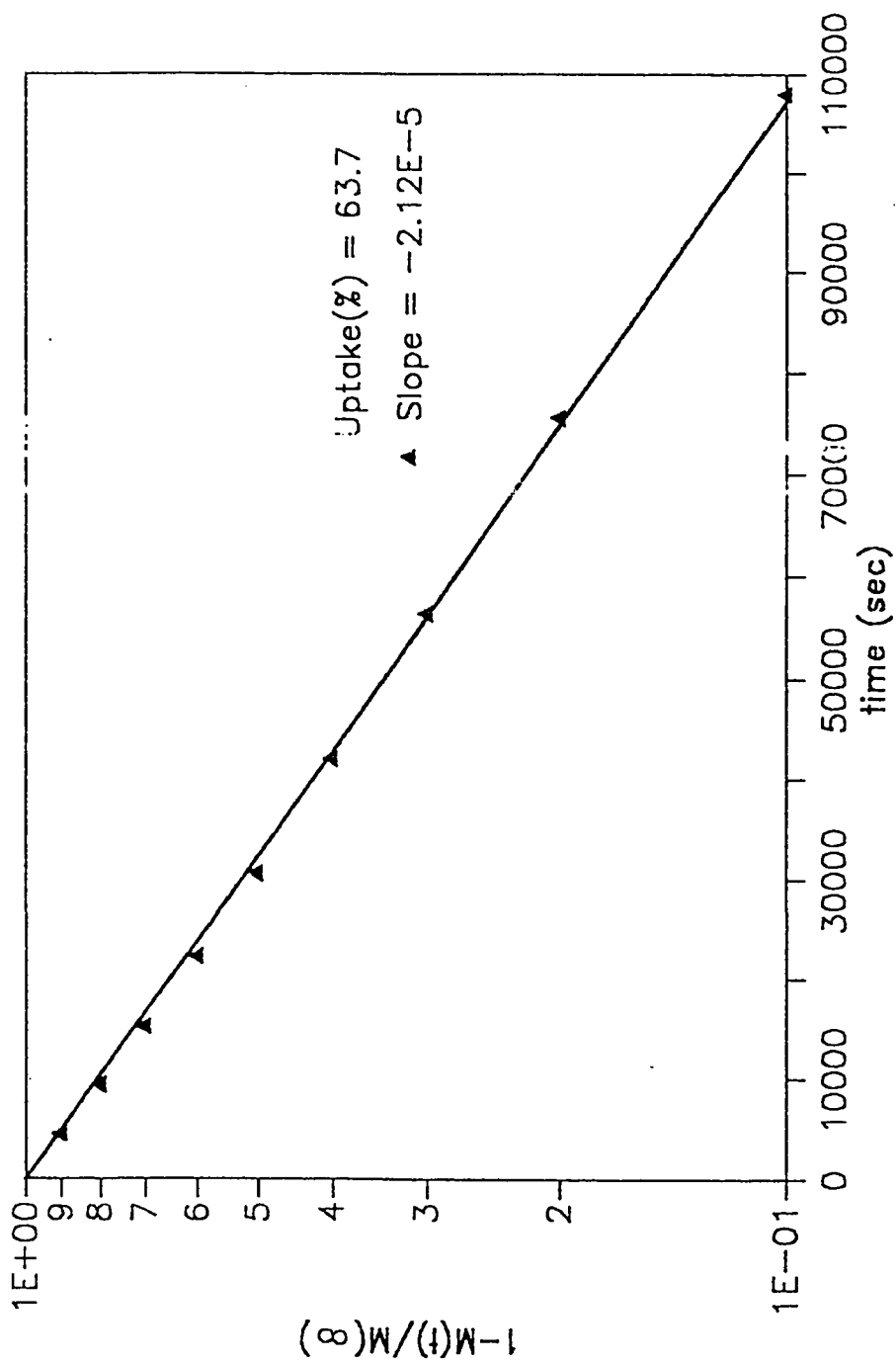


Fig 4.10 Comparison of volumetric uptake curves of Nitrogen on 2.33 mm pellets with standard solution assuming both macropore - micropore diffusional resistances.



FILE:kflth2/thfg411

Fig 4.11 Semi-logarithmic plot of volumetric uptake rate of methane on 2.33 mm pellets on CMS at 25 °C

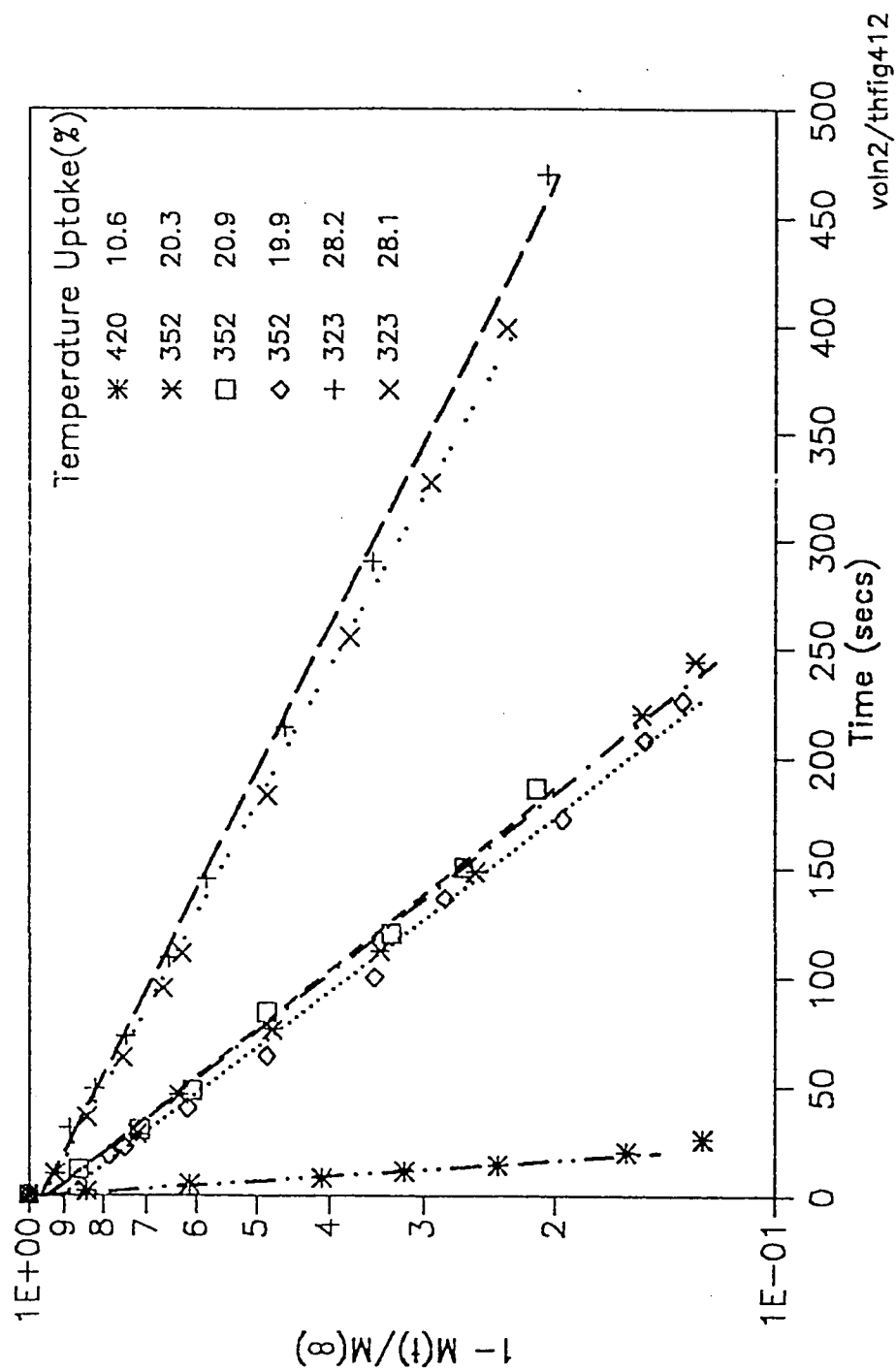


Fig 4.12 Semilogarithmic plot of volumetric uptake rate of nitrogen on 2.33 mm pellets on CMS at 323, 352 and 420 °K

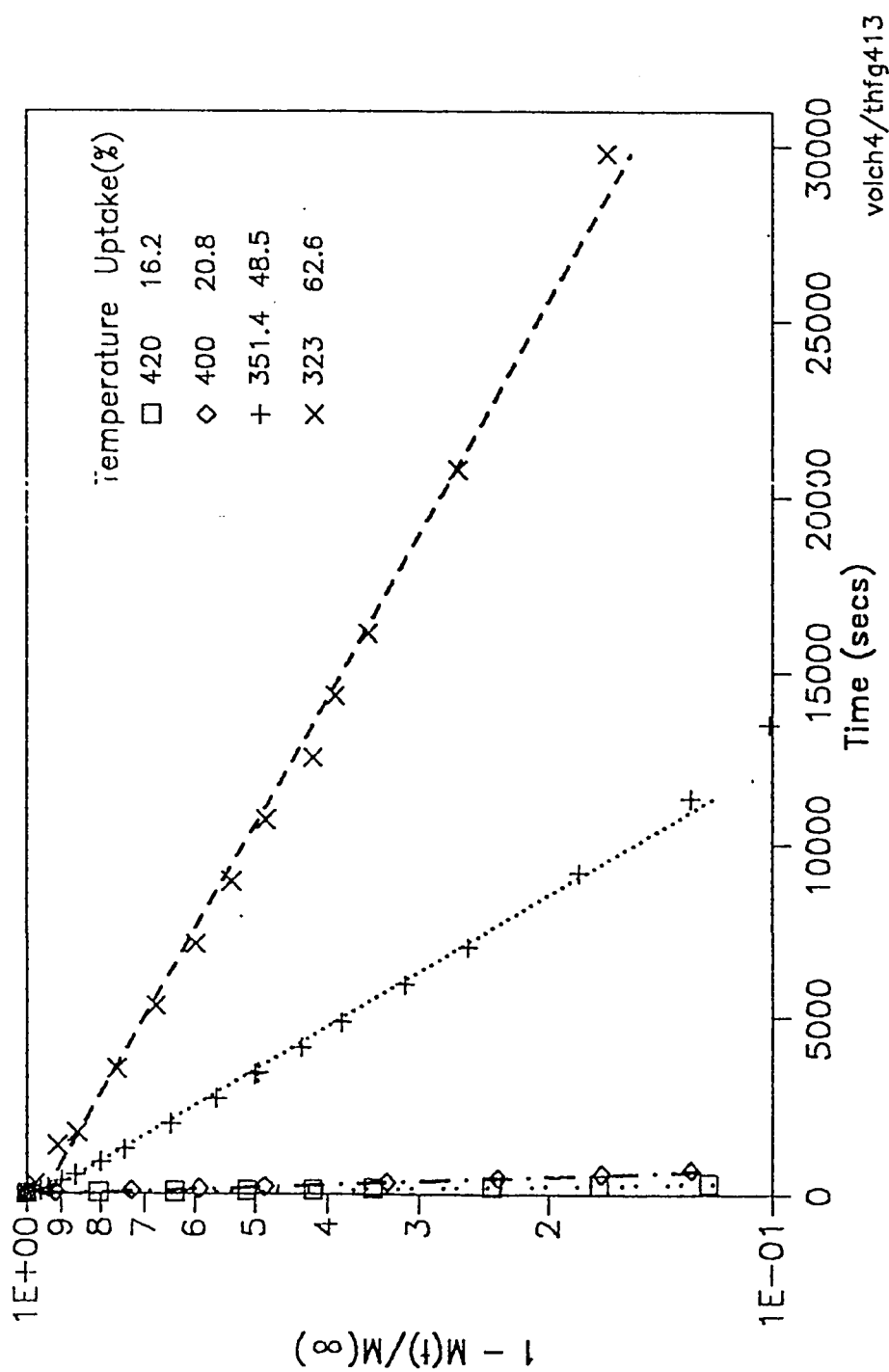


Fig 4.13 Semilogarithmic plot of volumetric uptake rate of methane on 2.33 mm pellets on CNIS at 323, 351.4, 400 and 420 °K

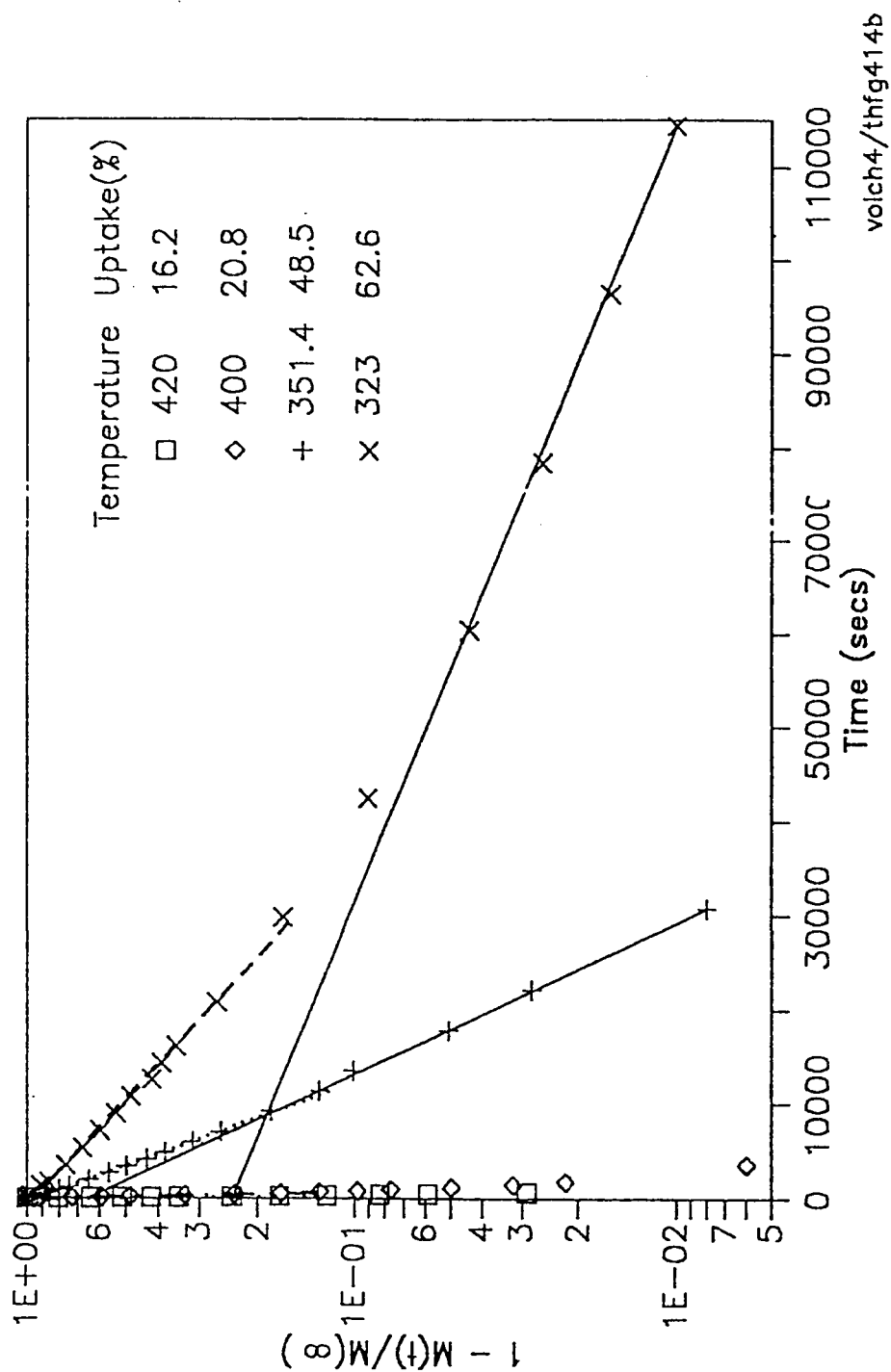


Fig 4.14 Semilogarithmic plot of volumetric uptake rate of methane on 2.33 mm pellets on CMS at 323, 351.4, 400 and 420 °K showing both regions of the curve

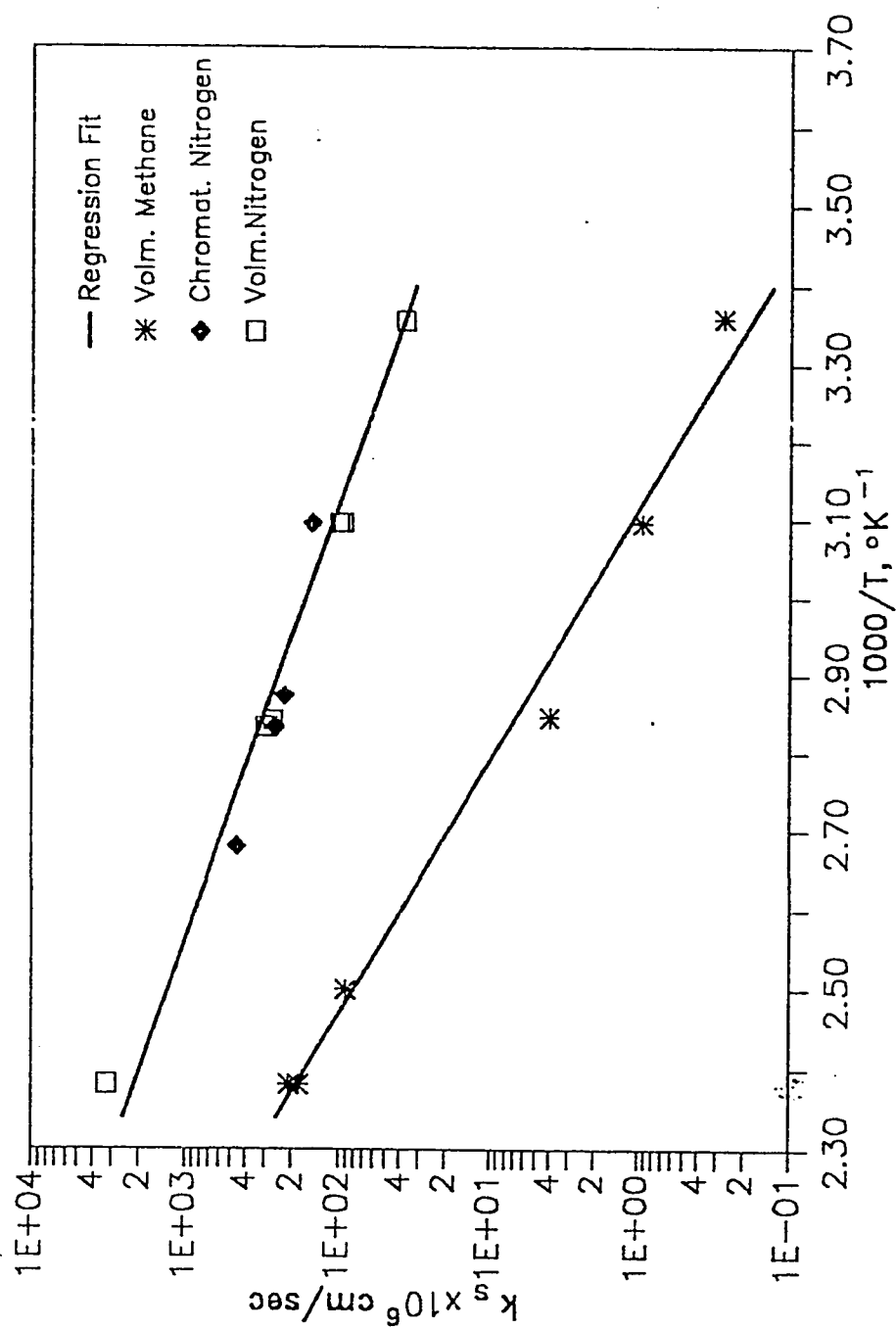


Fig 4.15 Semilogarithmic plot of rate values k_s versus $1/T$ for volumetric and chromatographic data

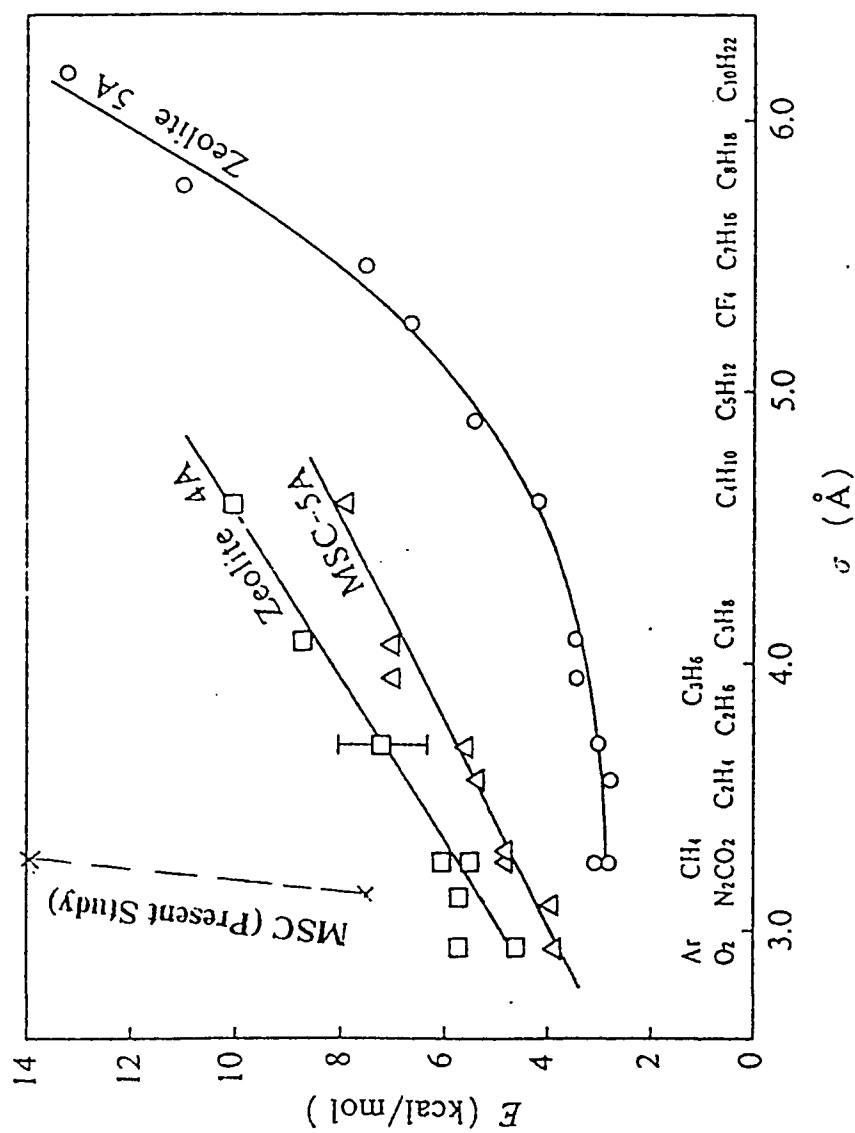


Fig 4.16 Comparison of activation energy obtained in this work and reported literature value for diffusional activation energy with van der Waals diameter for diffusion in 4A and 5A zeolites and 5A molecular sieve {Data abstracted from Ruthven, D., Principles of Adsorption and Adsorption Processes, pg.148, John Wiley & Sons, New York(1985)}

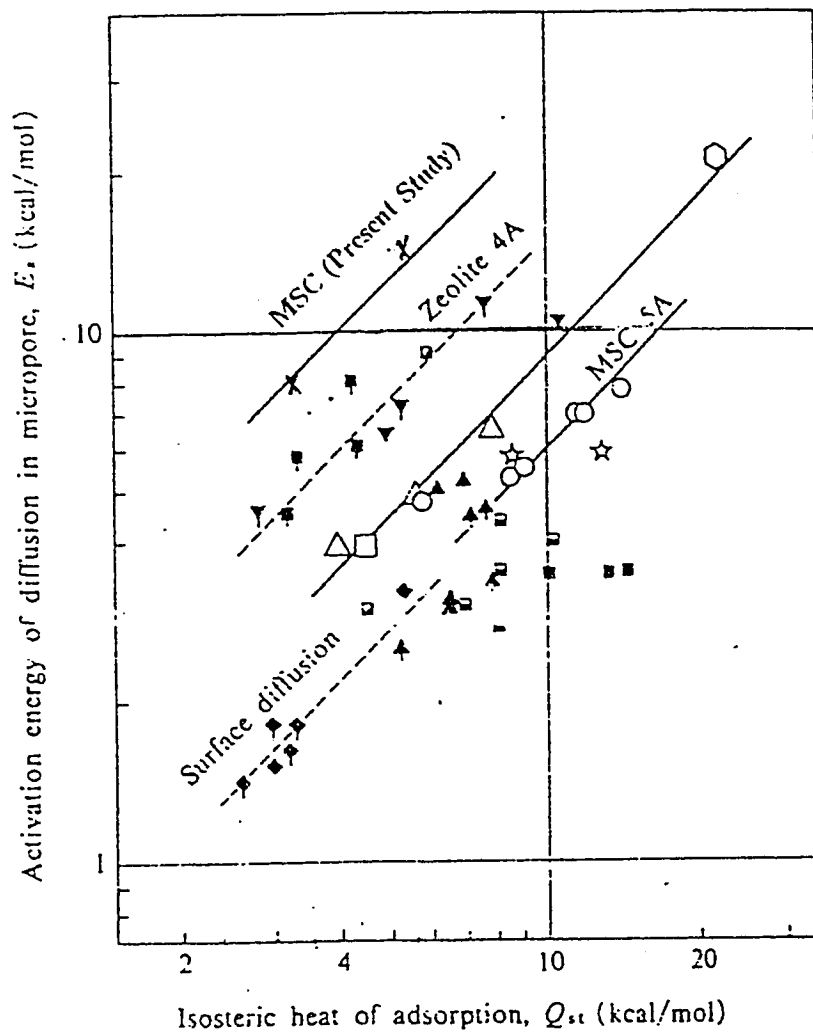


Fig 4.17 Correlation of activation energy for this work and activation energy for micropore diffusion reported in the literature with isosteric heat of adsorption {Data abstracted from Chihara, K. et al, AIChE Journal 24, 243(1978)}

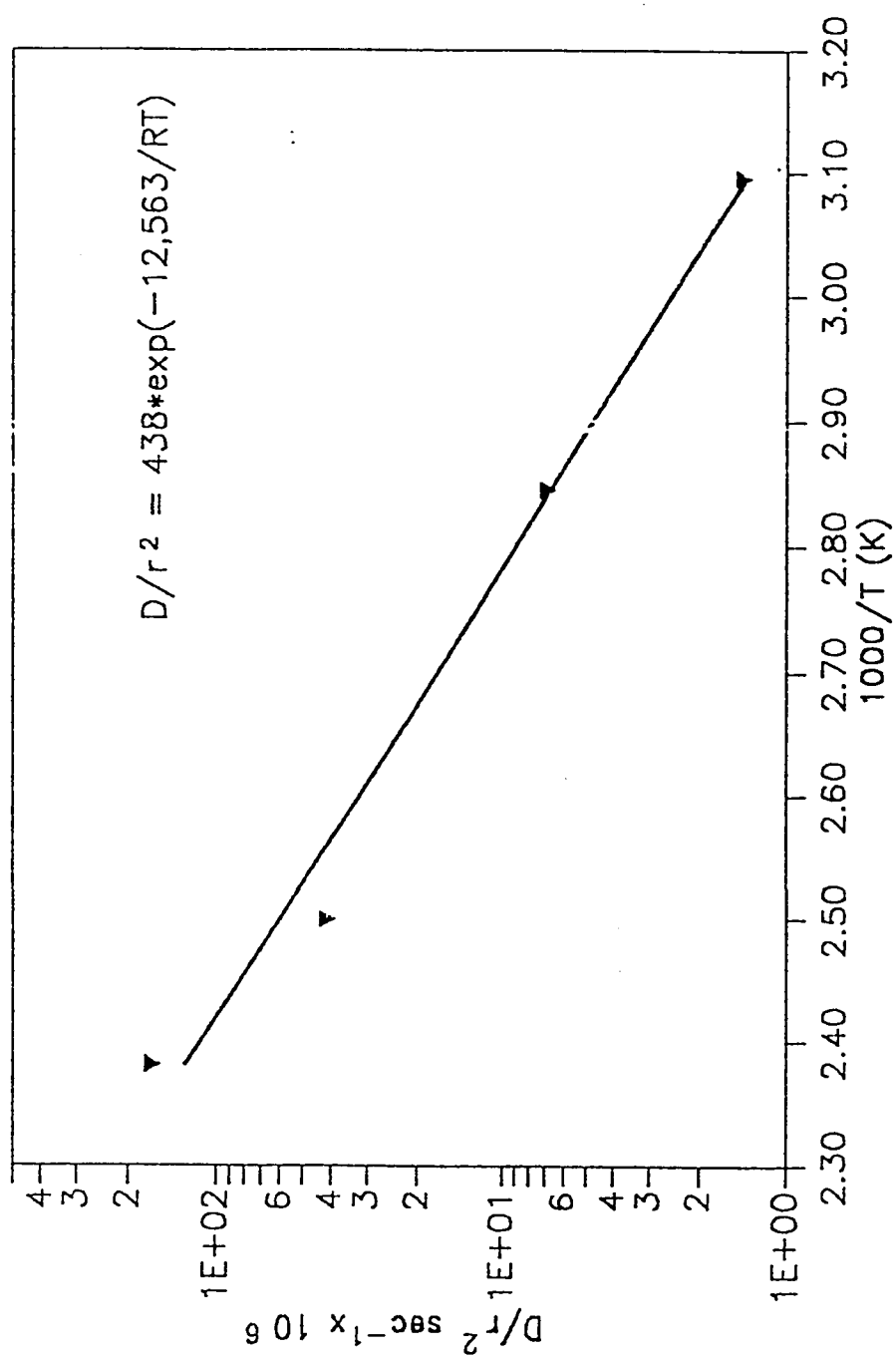


Fig 4.18 Temperature Dependence of Diffusional Time Constant of Methane in Carbon Molecular Sieve

CHAPTER 5

PSA SEPARATION OF METHANE - NITROGEN MIXTURES ON CARBON MOLECULAR SIEVES

5.1 Introduction

Pressure swing adsorption processes are widely used for gas separation. Among the most frequent bulk applications are oxygen nitrogen separation from air, paraffin mixture separation, removal of trace gases such as oxides of nitrogen or hydrogen sulfide from bulk gas streams and air drying. Another potential application in the oil refining industry is enrichment of associated gas, essentially a methane nitrogen mixture with the objective of reducing N_2 content. PSA separation for this mixture is primarily effected by kinetic selectivity since equilibrium selectivity yields a product richer in nitrogen, which is less strongly adsorbed than methane while steric selectivity is applicable only in case of molecules quite different in size.

Kinetic separation is achieved, in principle, by virtue of difference in diffusion rates which is higher for nitrogen, a smaller molecule, as compared to methane. Although simple in principle, it is a difficult separation in practice since the absolute value of the diffusional time constants are quite low and hence large column length to velocity ratio and adsorption time are required to achieve the objective. Another factor is the adverse equilibrium selectivity towards methane thereby reducing the separation efficiency. The choice of adsorbent

with this gas mixture is between 4A zeolite, which has a pore opening sufficient to give a different diffusion resistance to nitrogen and methane, and carbon molecular sieve (CMS), a carbon based adsorbent tailored to a specific narrow pore size distribution for obtaining high selectivity. A further advantage of CMS is that it is far less hydrophilic than 4A zeolite. In this chapter a brief review of PSA processes using CMS is presented. This is followed by experimental PSA results obtained for two model gas methane nitrogen mixtures (8% and 40% nitrogen in methane) under various conditions of flowrates, pressure, purge to feed ratio and cycle time. The results are interpreted using the dynamic PSA model of Hassan(1).

5.2 Literature Review

Activated carbon was long known for its sieving properties but successful control of its pore size distribution was only achieved in mid 70's by Walker et al.(2) and Jungsten(3). This helped in developing processes based on the property of molecules selectively penetrating the sieves. The difference in ability of each gas to penetrate the adsorbent is the basis of kinetic selectivity. Carbon molecular sieves are mainly used for obtaining nitrogen from air through a kinetic separation in which oxygen diffuses faster leaving high purity nitrogen as a product using PSA processes, and they have been studied quite extensively (4-7,9-11) for this separation. Hassan et al.(4) obtained an efficient kinetic separation with a high pressure nitrogen product with 1-2 % residual oxygen. Also a simplified dynamic model for the PSA process was developed based on the lin-

carized mass transfer rate expression and binary Langmuir equilibrium. Constant pressure was assumed during adsorption and desorption steps but variation in velocity due to adsorption was considered. Later the cycle was modified to include pressure equalization and no purge (5). Ruthven and Farooq(6) studied air separation on CMS and 4A zeolite achieving a good separation on both adsorbents. Kapoor and Yang(7) studied the kinetic separation of another important model mixture of methane and carbon dioxide, similar to landfill gas, using carbon molecular sieve, the advantage of this separation being that carbon dioxide diffuses faster and adsorbs more strongly than methane. Nitrogen methane mixture separation using the PSA process has been studied by Kadlec and Turnock(8) on 5A zeolite using a periodic sorption process based on equilibrium selectivity. Recently Ackley and Yang(9) studied the kinetic separation of methane and nitrogen on CMS using a single column PSA unit using a 50/50 feed mixture. Purity up to 80% was obtained. Vacuum desorption was used. Zahur(10) studied oxygen nitrogen separation on the same CMS batch used in the present study. High purity N_2 (residual $O_2 \approx 2\%$) product was obtained indicating a good kinetic separation.

5.3 Theoretical Modeling and Simulation

A simple two bed PSA process (see Fig 5.1) operated in a cyclic manner as shown in Fig 5.2 comprises four basic steps:

- 1.) High pressure feed flows through bed 2 where the faster diffusing (or more strongly adsorbed) species is preferentially removed leaving a raffinate stream richer in the other species. A fraction of the raffinate is let down to a lower pressure for purging bed 1.
- 2.) Bed 1 is pressurised with the feed at high pressure while bed 2 is depressurised in the reverse direction to a lower operating pressure (atmospheric). Neither product or purge stream flows during this step.
- 3.) Step 1 repeated with bed 1 and bed 2 reversed.
- 4.) Step 2 repeated with bed 1 and bed 2 reversed.

For the simulation of a kinetic separation process the two main approaches are the rigorous pore diffusion model as presented by Raghavan et al.(11), Shin and Knaebel(12) and Farooq and Ruthven(13), or the linear driving force approximation(LDF) model as presented by Hassan et al.(4,5), Kapoor and Yang(7) and Farooq and Ruthven(14). The pore diffusion model is quite rigorous and closer to reality but is quite cumbersome to solve particularly for a new system while the LDF model is easier to solve and gives reasonably good results. For the simulation of methane nitrogen separation on carbon molecular sieve the model developed by Hassan et al.(4), for use in nitrogen separation from air on CMS, is employed with the following general assumptions:

- (1) The system is assumed isothermal with total pressure remaining constant throughout the high pressure and low pressure operations (Steps 1 and 3).

- (2) The flow velocity varies during the adsorption and desorption steps along the bed as determined by the mass balance.
- (3) The flow pattern is described by the axial dispersed plug flow model
- (4) The equilibrium relationships for both methane and nitrogen are of the binary Langmuir type.
- (5) The mass transfer rates are represented by linear driving force rate expressions and the rate coefficients are taken to be the same for both high pressure and low pressure steps. This is a reasonable assumption when the mass transfer rate is controlled by micropore diffusion which may be concentration dependent or where a barrier resistance exists.

For the blowdown step, the following approximations are introduced

- (1) The gas phase mole fractions at the end of the blowdown step remain the same at each and every position in the bed as was prevailing at the end of the preceding high pressure flow adsorption step but the total pressure is reduced instantaneously from the high pressure P_H to the purge pressure P_L .
- (2) The solid phase concentrations are assumed to remain frozen during this step.

For the pressurization step, the following approximations are introduced:

- (1) During pressurization by the feed, the fluid phases remaining in the bed from the preceding low pressure purge flow operation are pushed in

plug flow towards the closed end of the bed through a fraction of the length given by $(1 - P_I/P_{II})$. The rest of the length of bed is filled with pressurised feed. This was also observed by Fernandez and Kenney(15).

- (2) The solid phase concentrations remain unchanged at the values prevailing at the end of the preceding low pressure purge flow.

Subject to these assumptions the dynamic behaviour of the system may be described by the following set of equations (A for Methane and B for Nitrogen):

Step 1: High pressure flow in bed 2 and low pressure (purge) flow in bed 1.

External fluid phase in bed 2:

$$\frac{\partial C_{A2}}{\partial t} - D_{1,2} \frac{\partial^2 C_{A2}}{\partial z^2} + v_2 \frac{\partial C_{A2}}{\partial z} + C_{A2} \frac{\partial v_2}{\partial z} + \left(\frac{1-\epsilon}{\epsilon} \right) \frac{\partial q_{A2}}{\partial t} = 0 \quad (5.1)$$

$$\frac{\partial C_{B2}}{\partial t} - D_{1,2} \frac{\partial^2 C_{B2}}{\partial z^2} + v_2 \frac{\partial C_{B2}}{\partial z} + C_{B2} \frac{\partial v_2}{\partial z} + \left(\frac{1-\epsilon}{\epsilon} \right) \frac{\partial q_{B2}}{\partial t} = 0 \quad (5.2)$$

$$C_{A2} + C_{B2} = C_{HP} = \text{constant} \quad (5.3)$$

Adding equations (5.1) and (5.2) and considering equation (5.3) gives

$$C_{HP} \frac{\partial v_2}{\partial z} + \left(\frac{1-\epsilon}{\epsilon} \right) \frac{\partial q_{A2}}{\partial t} + \left(\frac{1-\epsilon}{\epsilon} \right) \frac{\partial q_{B2}}{\partial t} = 0 \quad (5.4)$$

Solid phase in bed 2:

$$\frac{\partial q_{A2}}{\partial t} = k_A (q_{A2}^* - q_{A2}) \quad (5.5)$$

$$\frac{\partial q_{B2}}{\partial t} = k_B (q_{B2}^* - q_{B2}) \quad (5.6)$$

$$q_{A2}^* = \frac{b_A q_{AS} C_{A2}}{1 + b_A C_{A2} + b_B C_{B2}} \quad (5.7)$$

$$q_{B2}^* = \frac{b_B q_{BS} C_{B2}}{1 + b_A C_{A2} + b_B C_{B2}}$$

Boundary conditions:

$$D_{1,2} \frac{\partial C_{A2}}{\partial z} \Big|_{z=0} = -v_H [C_{A2} \Big|_{z=0} - C_{A2} \Big|_{z=0^+}] \quad (5.8)$$

$$\frac{\partial C_{A2}}{\partial z} \Big|_{z=1} = 0 \quad (5.9)$$

External fluid phase in bed 1:

$$\frac{\partial C_{A1}}{\partial t} - D_{1,1} \frac{\partial^2 C_{A1}}{\partial z^2} + v_1 \frac{\partial C_{A1}}{\partial z} + C_{A1} \frac{\partial v_1}{\partial z} + \left(\frac{1-\epsilon}{\epsilon} \right) \frac{\partial q_{A1}}{\partial t} = 0 \quad (5.10)$$

$$\frac{\partial C_{BI}}{\partial t} - D_{L1} \frac{\partial^2 C_{BI}}{\partial z^2} + v_1 \frac{\partial C_{BI}}{\partial z} + C_{BI} \frac{\partial v_1}{\partial z} + \left(\frac{1-\epsilon}{\epsilon}\right) \frac{\partial q_{BI}}{\partial t} = 0 \quad (5.11)$$

$$C_{AI} + C_{BI} = C_{I,P} = \text{constant} \quad (5.12)$$

Adding equations (5.10) and (5.11) and considering equation (5.12) gives

$$C_{I,P} \frac{\partial v_1}{\partial z} + \left(\frac{1-\epsilon}{\epsilon}\right) \frac{\partial q_{AI}}{\partial t} + \left(\frac{1-\epsilon}{\epsilon}\right) \frac{\partial q_{BI}}{\partial t} = 0 \quad (5.13)$$

Solid phase in bed 1:

$$\frac{\partial q_{AI}}{\partial t} = k_A (q_{AI}^* - q_{AI}) \quad (5.14)$$

$$\frac{\partial q_{BI}}{\partial t} = k_B (q_{BI}^* - q_{BI}) \quad (5.15)$$

where,

$$q_{AI}^* = \frac{b_A q_{AS} C_{AI}}{1 + b_A C_{AI} + b_B C_{BI}} \quad (5.16)$$

$$q_{BI}^* = \frac{b_B q_{BS} C_{BI}}{1 + b_A C_{AI} + b_B C_{BI}}$$

Boundary conditions:

$$D_{L1} \left. \frac{\partial C_{AI}}{\partial z} \right|_{z=0} = -v_L [C_{AI}|_{z=0^-} - C_{AI}|_{z=0^+}] \quad (5.17)$$

where,

$$C_{A1}|_{z=0} = C_{A2}|_{z=L, P=P_L} \quad (5.18)$$

$$\left. \frac{\partial C_{A1}}{\partial z} \right|_{z=L} = 0 \quad (5.19)$$

The initial conditions for the startup of the cyclic operation were both beds saturated at their respective pressures, i.e. bed 2 at high pressure and bed 1 at low pressure. The concentration of the gas phase in both the columns is at feed conditions but at the column pressure while the corresponding solid phase concentration is given by the Langmuir isotherm.

Step 2: Blowdown of bed 2 and pressurization of bed 1.

These conditions are not solved in the model but implemented according to the approximations stated earlier.

Steps 3 and 4 are essentially the same except for the reversed flow directions.

The above equations are written in dimensionless form (see Appendix A-3) and solved by the method of orthogonal collocation to give the velocity as well as the gas and solid phase concentration profiles as a function of dimensionless bed distance for the real time simulation.

The essential parameters in the model are the axial dispersion coefficients, D_L , the Langmuir constants b_A , b_B , q_{As} , q_{Bs} and the rate constants k_A , k_B . The axial dispersion coefficient is calculated according to the following equation suggested by Ruthven(16).

$$D_L = 0.7 * D_m + 0.5 * 2 * R_p v, \quad (5.20)$$

The Langmuir constants b_A , b_B , q_{As} , q_{Bs} are determined by experimentally gravimetric and volumetric methods. Literature data are not used due to the non uniformity in CMS synthesis. The data so obtained is presented in Table 5.1. The other essential parameter in the model is the rate coefficient in the mass transfer rate expression given by (5.14) and (5.15). This is a simplified expression lumping the mass balance within the particle by an overall uptake. Generally in a practical kinetic separation process the fluid film resistance and macropore resistance are not significant as compared to the micropore diffusion hence this rate coefficient is normally expressed as a function of the diffusional time constant:

$$k = \Omega \frac{D}{r^2} \quad (5.21)$$

The factor Ω was generally taken as 15 for most applications following Gluckauf's study(17), although this was derived for an isolated particle and only valid for $Dt/r^2 > 0.1$. Applicability of Ω , known as the LDF approximation, to cyclic sorption process was studied by Nakao and Suzuki(18) who concluded

that the factor was cycle time dependent and had a value of 15 at $Dt/r^2 \approx 0.1$. Raghavan et al(11) studied this factor for a PSA application and concluded that it depended on cycle time and to a lesser extent on the degree of non-linearity of the isotherm and the nature of the diffusion mechanism. The value of Ω varied from 40 at low cycle times to less than 15 at large cycle times. The results of these studies are shown in Fig 1.2. Recently Buzanowaski and Yang(19,20) presented the LDF approximation as a sum of two terms. The second term was added to account for the cycle time variations. The use of this approximation is cumbersome.

The most recent simulation study of Farooq and Ruthven(21) comprised solving a kinetically controlled PSA system for a binary Langmuir system with full binary diffusion equations, accounting for the concentration dependency of micropore diffusion. A key conclusion of their study was that a constant diffusivity diffusion model, with calibrated effective diffusivities, provides no further improvement over the constant diffusivity LDF model with calibrated Ω values. This conclusion along with advantage of computation time places the LDF model as a preferable alternative.

For the present study the values of the barrier and diffusional resistance were experimentally determined and reported in Chapter 4. The overall rate constant was determined from these combined resistances using equation 4.25. The overall resistance used in the simulation are given in Table 5.1. For comparison with the standard Ω factor in the PSA model, a new factor Φ is defined

as follows :

$$\Phi \equiv \Omega / 15 \quad (5.22)$$

which is a function of dimensionless cycle time θ_c defined as follows:

$$\theta_c \equiv k t_{1/2} / 15 \equiv D t_{1/2} / r^2 \quad (5.23)$$

The solution of these model equations is discussed later in the chapter.

5.4 Apparatus:

A schematic diagram of the two column PSA unit is shown in Fig. 5.1 and details of instrument specifications are listed in Appendix A-2. The two stainless steel columns (internal dia. 3.45 cm, length 51 cm.) were packed with a known amount of carbon molecular sieves (Table 5.1). Both the columns are connected at one end by 1/4 " stainless steel(SS) tubing through a pair of three way solenoid valves, one for introduction of the feed stream to either of the columns and the other for releasing the purge stream from either of the columns. The feed gas flow is monitored by an electronic mass flow indicator and controller from the high pressure cylinder. The purge gas, apart from a portion going to the sampling loop for analysis, flows to the flare system through a mass flow indicator. At the other end of each column the product stream is divided into two parts, one part going to the other column as a purge gas through a two way solenoid valve and a manual control valve, and the other to the flare system and the sampling loop through a solenoid valve and a mass flow indicator. Sequen-

tial switching of the two and three way solenoid valves was controlled by an Xanadu universal programmable timer. The flow rates of feed, product and purge streams were monitored and controlled using Matheson flow indicators and controllers and the corresponding continuous output obtained on strip chart recorders. Typical outputs are shown in Figs. 5.3 and 5.4. Pressure was monitored by an Edwards electronic manometer through a transducer. The product and purge stream were analysed by withdrawing gas samples through a manual sampling loop on Gow Mac gas chromatograph. A 20 % chromosorb column along with a Thermal Conductivity Detector was used and a typical output from the Hewlett Packard Integrator is shown in Fig. 5.5.

5.5 Procedure

The packed columns were purged overnight with helium flowing through it to remove the adsorbed gases. The experiments were performed with two model feeds (40% and 8% nitrogen in methane) and in accordance with the two bed PSA cycle consisting of adsorption, blowdown, desorption and pressurisation steps described in detail later in the chapter. The feed rate control valve was fully open since the pressure was controlled. Feed was introduced at high pressure in one column while the other column was desorbed, in most of the runs, by blowdown and purging, at atmospheric pressure, with a part of the product stream. Continuous methane or nitrogen analysis, highly desirable, was not possible and accordingly the product and purge stream were analysed intermittently using the gas chromatograph. The actual concentration was corrected based on

a previous calibration. Sampling time was limited to one sample every 2-3 minutes; hence a sample was taken 2 sec prior to the end of adsorption or desorption step. In case of short cycle time a sample was analysed once every 3 - 4 cycles. Due to these limitations the results were studied for cyclic steady state conditions, however, some samples were analysed during the initial unsteady state period. In some cases samples were also analysed for the complete duration of the cycle after the cyclic steady state conditions were reached.

Flow rates did not reach steady values for the adsorption and desorption step in case of short cycle time of 60 sec but was steady for larger cycle time of 300 sec. and above. At cyclic steady state conditions a concentration profile for the duration of a cycle was obtained to account for the concentration variation during the course of the cycle. The data and parameters used in the experiments are listed in Table 5.1. The raw data obtained from the experimental runs is listed in Appendix A.1.1.

5.6 Results and Discussion

A summary of the experiments performed on the column PSA units is presented in Table 5.2. The essential parameters for each block of runs are tabulated. The essential parameters in PSA that affect the separation are the cycle time, length to velocity ratio, high to low pressure ratio, and purge to feed ratio. The present experimental data was studied for different L/v ratios, purge to feed

ratios and cycle time since the results of a trial run indicated that high pressure did not affect the separation significantly. For this reason the pressure ratio was kept at 3 to 1. for all the runs. Runs 1-6, 7-12, 13-24 and 25 are four sets of experiments with different operating conditions. The effect of cycle time on the exit methane concentration was studied in each set with the remaining operating conditions fixed at tabulated values. In the first set of 6 experiments (Runs 1-6) with $L/v_{II} \approx 25$ it was observed that at a low cycle time (60 sec) the exit methane concentration was lower than the feed but with increasing cycle time the methane concentration increased to reach an optimum at 180 sec. This behaviour is expected in a kinetic separation as increased time for sorption initially leads to increased sorption of the faster diffusing species but further time increase results in competitive diffusion of the slower diffusing species. In the next set (Runs 7-12) the inlet velocity during adsorption was reduced i.e. $L/v_{II} \approx 40$ and the purge to feed ratio was increased as compared to the earlier set. Both these factors improved the separation as expected. Also the optimum cycle time was higher at 240 sec (Run 11) with a higher concentration. In the third set of experiments (Runs 13-24), the velocity was further reduced so that $L/v_{II} \approx 69$ and the purge to feed ratio was slightly less than the second set. The exit methane concentration in this set spanned from 48 % at a cycle time of 60 sec (Run 13) to an optimum of 76 % at 540 sec (Run 21). A comparison of Runs 5,10,16 which have the same cycle time indicates an optimum L/v_{II} exists. Run 25 was done with a limiting low velocity, for the existing experimental setup, and also at a low purge to feed ratio compared to all the earlier sets. The

exit concentration was the same as Run 22, which has the same cycle time, indicating that a lower purge is offset by a higher L/v_{II} ratio. The purge concentration was also measured in this run and it showed a concentration higher than the feed, which is not expected in a case when the product concentration is higher than the feed. This was attributed to the sampling time and is discussed later. Runs 26-30 were performed with the other model feed (8% nitrogen in methane) with the same operating parameters as Run 25 and the trend was similar to the earlier sets. The optimum cycle time was 720 sec. The purge concentration is higher than the feed in these cases also.

The sampling of product and purge was limited to a maximum of one per cycle for cycle times greater than 240 sec and one per 3-4 cycles for shorter cycle times. The exit concentration presented in Table 5.2, were measured 2 seconds prior to the end of the sorption step to provide the best available concentration measurement for each step. In order to ascertain the behaviour of the exit concentration profile at cyclic steady state typical product and purge profiles, during the course of a cycle, for cycle times of 100 sec (Run 26) and 600 sec (Run 25) were measured and are shown in Figs 5.6 and 5.7 respectively. The purge concentration for the 100 sec cycle oscillated about the feed level while the product concentration oscillated below the feed level and vice versa for the 600 sec cycle. The concentration at half cycle, at 288 sec for the 600 sec cycle, matched the tabulated sample value and is also higher than the feed at that instant. This explains the unusual purge concentration observed. Note that the average purge concentration is approximately 53%.

The discussion so far has been limited to the cyclic steady state experimental conditions but the concentrations were also measured prior to reaching these conditions. The experimental product and purge concentration profile along with the simulated theoretical curves (discussed later) as a function of the number of cycles for various runs are shown in different figures as follows :

- (1) Runs 1-6 in Fig. 5.8 (product only)
- (2) Runs 7-12 in Fig. 5.9 (product only)
- (3) Runs 13-18 in Fig. 5.10 (product only)
- (4) Runs 19-24 in Fig. 5.11 (product only)
- (5) Run 25 in Fig. 5.12 (product and purge)
- (6) Runs 26-30 in Fig. 5.13 (product only)
- (7) Runs 26-30 in Fig. 5.14 (purge only)

A general observation from these figures is that the exit concentration, initially at feed conditions, moves monotonically to the steady state conditions. In all the runs the steady state conditions were reached in 8 to 12 cycles. The cyclic steady state product concentration for the four sets of experiments (Runs 1-6, 7-12, 13-24, 26-30) comprising both model feeds are plotted along with the theoretical curves, discussed later, as a function of cycle time in Fig 5.15.

The simulation studies for the experiments discussed above were performed based on the mathematical model described earlier in the chapter. Five point

orthogonal collocation technique was used and the corresponding ordinary differential equations were solved using Gear's method. The theoretical curves obtained were plotted along with the experimental data. The main parameters needed for the model were the dispersion coefficients, adsorption equilibrium constants and mass transfer rate constants. The dispersion coefficients were computed through a correlation described earlier while the equilibrium and mass transfer rate constants were experimentally determined and the data is presented in Table 5.1. The mass transfer rate constants tabulated were determined experimentally from the volumetric uptake rates in a particle subjected to a step change boundary condition. The basis for using these rate constants for a cyclic PSA process comes from previous studies and the discussion of this follows.

The mass transfer rate process in an adsorption process is described by either a rigorous pore model or a simplified expression relating the uptake in a particle to the bulk flow concentration. The approaches for the latter method, reviewed by Yang(22), are the two term driving force, linear driving force or the non linear driving force approximation. Two term as well as the linear driving force approximation were suggested by Gluckauf and resulted from the solution of the uptake rate in a spherical particle for different increases in bulk phase concentration. The solution for $Dt/r^2 > 0.1$ is

$$\frac{\partial \bar{q}}{\partial t} = \frac{\pi^2 D}{r^2} (q^* - \bar{q}) + \left(1 - \frac{\pi^2}{15}\right) \frac{\partial q^*}{\partial t} + \text{higher derivatives} \quad (5.24)$$

This is the two term approximation and it simplifies to the linear driving force (LDF) approximation if the conditions in the interior are close to equilibrium (for large D or at long time) as

$$\frac{\partial \bar{q}}{\partial t} = \frac{15 D}{r^2} (q^* - \bar{q}) \quad (5.25)$$

The term $15D/r^2$ is the mass transfer rate constant equivalent to the value tabulated in Table 5.1. This approximation predicts lower uptakes if the amount adsorbed is small. For a step function change in concentration Vermuelen(23) derived the following non linear approximation:

$$\frac{\partial \bar{q}}{\partial t} = \frac{\pi^2 D}{r^2} \frac{(q^{*2} - \bar{q}^2)}{2\bar{q}} \quad (5.26)$$

This approximation is good for a steep isotherm. Among the approximations, LDF is sufficient in most cases. The applicability of the LDF mass transfer rate approximation to a cyclic process was studied by Nakao and Suzuki(18) by comparing the uptake in a spherical particle under cyclic step change in gas phase concentration using the rigorous and LDF models. It was observed that the factor Ω was a function of cycle time as shown in Fig. 1.2 and was 15 for conditions close to those specified by Gluckauf. This was further studied for application to a PSA process by Raghavan et al.(11). This was to account for the interactions in a packed bed which may be absent for an isolated particle. The result is also shown in the same figure and it indicates that at a lower

dimensionless half cycle time (0.1 to 1×10^{-4}) the value of Ω increases and levels off at 30 at approximately a half cycle time of 0.01 . This establishes that the tabulated rate constants equivalent to $15D/r^2$, are good for a basis in PSA modelling but may need adjustment to correlate the data.

Simulation of Runs 13-24 was performed using the linear driving force rate constants tabulated in Table 5.1. This is equivalent of $\Omega = 15$ or $\Phi = 1$. This set of runs was chosen due to a wide span of exit methane concentration obtained by just varying the cycle time. The corresponding result is plotted in Fig. 5.16, the curve with legend 1/1. The legend signifies Φ used for methane and nitrogen respectively. The simulated concentration is much lower than the experimental results and not sensitive to cycle time. The next step was to assume that Φ varies as cycle time similar to Ω . With this assumption and for a typical adsorption step of 234 sec (cycle time of 540 sec) the Ω value for methane and nitrogen according to Raghvan's Plot (Fig. 1.3) is 30 and 15 respectively. The corresponding Φ is 2 and 1 respectively. The dimensionless half cycle time for these points is 6.9×10^{-5} and 0.014 . These factors did not yield satisfactory results. Indeed values of Φ of 10 and 20 for both methane and nitrogen, as shown by the curves 10/10 and 20/20, predicted the results at specific cycle times but not in general. The trend among these curves shows that a higher value of the factor predicted accurately at a higher cycle time. This was contrary to the earlier studies discussed above in which Ω decreased with cycle time. The factor, Φ , for nitrogen was more sensitive as compared to methane

since varying the factor for methane between 1 and 125 had no significant effect on the predictions while varying it for nitrogen between 1 and 30 was sufficient to predict the results satisfactorily except for shorter cycle times. It may be noted that for all positive values of Φ the lowest predicted concentration limits to the feed concentration. The lower limit of Φ was retained as unity for this reason. In this model an increase in Φ physically means a lower mass transfer resistance. Since the predicted concentration were lower than expected for methane the obvious deduction was to increase the theoretical methane resistance or decrease the theoretical nitrogen resistance. These two alternatives were examined by fixing the nitrogen factor at a specific value and varying the factor for methane and vice versa. The first alternative is represented by the M/24 curve where the factor for methane was varied from 1075 to 125 in accordance with Suzuki et al's plot and for nitrogen fixed at 24. From the curve it is evident that the predictions were not satisfactory. The second alternative was represented by 1/N curve where Φ for methane was retained as 1 since it had no significant effect on the cycle time and for nitrogen it was varied from 1 to 30 to correlate satisfactorily except for shorter cycle times. The experimental data obtained at shorter cycle times are expected to be under unsteady and developing conditions and hence not reliable for correlation purposes. This shows up in the tabulated results of Runs 7,8,13,14 and 26.

The value of Φ for Runs 13-24 and the corresponding cyclic steady state concentrations for this set are tabulated in Table 5.2. The results are also plot-

ted in Figs. 5.10, 5.11 and 5.16 and a good fit is observed. These values for Φ were used for other data sets (Runs 1-6, 7-12, 25, 26-30) and the corresponding cyclic steady state concentration are also tabulated in Table 5.2. The theoretical concentration curves so obtained are plotted with the corresponding experimental data in Figs. 5.8 to 5.15 for the runs in which the product concentration is more than the feed concentration. Purge concentration is plotted for Runs 25-30 since it was only measured for these runs. A plot of Φ for both methane and nitrogen versus dimensionless half cycle time in Fig 5.17 indicates a linear relationship for values of θ_c greater than 0.0045. The minimum value of Φ used was 1. The dimensionless half cycle time was calculated according to equation 5.23. The LDF factor Ω , used by Suzuki and Raghavan and its equivalent in the present study $15*\Phi$ were plotted as a function of the dimensionless half cycle time in Fig 5.18. The unusual behaviour of the present results are obvious and indicates that the controlling mechanism is not only an internal diffusion process. This is consistent with the results of the adsorption uptake experiments which indicate that the controlling mechanism is a barrier resistance coupled with micropore diffusion.

The theoretical curves plotted along with the experimental data as a function of cycles elapsed in Figs 5.8-5.15 are consistent with the experimental data. The theoretical concentrations for Runs 13-24 fits the data quite well except for shorter cycle times while deviations in case of other sets are observed because of a common Φ used for all sets, assuming it to be a cycle time dependent parame-

ter. The trend was acceptable for the entire range of data and no unusual behaviour was observed. The deviations were also noticeable due to the magnified scale for individual sets. The cyclic steady state data plotted collectively on Fig 5.15 shows that the predicted results seems quite reasonable. Plot of concentration as a function of L/v_{II} ratio with cycle time as a parameter is shown in Fig 5.19. The experimental and theoretical results do not show the same trend. The experimental data indicates an optimum L/v_{II} for each cycle time while the simulated results predicts a monotonic increase with L/v_{II} and is in agreement at L/v_{II} of 68.7. A possible reason for such a behavior is the assumption that Φ is only a function of cycle time. Since Φ was correlated based on runs with L/v_{II} of 68.7 agrees with the experimental data it is likely that Φ is a coupled function of cycle time and L/v_{II} . No functionality was obtained due to lack of sufficient data and back up from literature. Qualitatively variation in cycle time and L/v_{II} have opposing effects on the adsorption and desorption steps; hence an optimum is expected in these parameters.

Typical theoretical gas and solid phase concentration profile and the velocity profile as a function of time (No. of cycles) and also as a function of dimensionless distance are plotted in Figs. 5.20-5.27. These results were obtained during the simulation of Run 21. Fig 5.20 shows the gas phase methane concentration at the end of the adsorption step along the column for specific cycles while Fig 5.21 shows the same at specific locations in the column with time. A monotonically increasing profile is observed along the column which reaches the cyclic

steady state in 4-5 cycles. Fig 5.22 shows the solid phase methane concentration at the end of the adsorption step along the column for specific cycles while Fig 5.23 shows the same at specific locations in the column with time. A reduction in concentration from the initial saturated condition, higher at the entrance than the exit, is seen. This is expected since the saturated conditions are not reached during cycling. The solid and gas phase methane concentration are in tune along the length of the column. Fig 5.24 and 5.25 show similar plots for the solid phase nitrogen concentration at the end of adsorption step. In this case the reduction in concentration is less near the entrance and more towards the exit which is expected due to the corresponding gas phase profile. Fig 5.26 shows the normalized velocity profile at the end of the adsorption step along the length of the column for different cycles while Fig 5.27 shows the same with time at specific locations in the column. The reduction in velocity due to adsorption is evident and the profile reaches steady state in 4-5 cycles.

The velocity used in the experiment was the limiting value for the existing L/v_H ratio. The only other way to increase the L/v_H ratio is by using a longer column. The purge to feed ratio used was also on the high side and further increase renders the process impractical. An alternative method is to have unequal sorption time either by using more than two columns or on a single column set up. These modifications could lead to higher product concentrations of methane.

5.7 Conclusions

Experimental PSA studies were done with two model methane nitrogen feeds (8% and 40% nitrogen in methane) using a two column set up with carbon molecular sieves. A four step PSA cycle was used. Exit methane concentration spanned from 48% to 76% for the 60% feed and up to 96% for the 92% feed. An optimum cycle time as well as L/v_{II} ratio was observed for a set of operating conditions.

Simulation studies to interpret the experimental results were done with an LDF dynamic model. The parameters for the simulation were experimentally determined. Correlation of data based on the micropore diffusion LDF approximation, Ω , was not possible but with an equivalent factor $15*\Phi$ based on a dual resistance model the results were in fair agreement in lieu of the simplified model. This factor increased linearly for dimensionless half cycle time > 0.0045 . The hypothesis of barrier resistance control rather than micropore diffusion control gives significantly different results for the LDF parameter. Correlation results were consistent with cycle time but not with L/v_{II} . A possible reason is that Φ is a coupled function of cycle time and L/v_{II} .

REFERENCES

- (1) Hassan, M. M., Ph. D. Thesis, University of New Brunswick, Canada (1985).
- (2) Walker, P. L., Austin, L. G., and Nandi, S. P., Chemistry and Physics of Carbon, vol. 2, Marcel Decker (1966).
- (3) Jungsten, H., Carbon, 15,273(1977).
- (4) Hassan, M. M., Ruthven, D. M., and Raghavan, N. N., Chem. Engg. Sci., 41, 1333, (1986).
- (5) Hassan, M. M., Raghavan, N. S.,and Ruthven, D. M., Chem. Eng. Sci., 42, 2037, (1987).
- (6) Ruthven, D. M., and Farooq, S., Gas Separation and Purification, 4, (3), 141 (1990).
- (7) Kapoor, A., and Yang, R. T., Chem. Eng. Sci., 44, 1723, (1989).
- (8) Kadlec, R. H., and Turnock, P. H., AIChE J. 17, 335 (1971).
- (9) Ackley, M. W., and Yang, R. T., AIChE J., 36, (8), 1229, (1990).
- (10) Zahur, M., M. S. Thesis, KFUPM, Dhahran, 1991.
- (11) Raghavan, N. S.,Hassan, M. M., and Ruthven, D. M., Chem. Eng. Sci., 41, 2787, (1986).
- (12) Shin, H. S., and Knaebel, K. S., AIChE J., 33, (4), 654, (1987).
- (13) Farooq, S., and Ruthven, D. M., Chem. Eng. Sci., 46, 2213, (1991).
- (14) Farooq, S., and Ruthven, D. M., Chem. Eng. Sci., 45, 107, (1990).
- (15) Fernandez, G. F., and Kenney, C. N., Chem. Engg. Sci., 38, 827, (1983).
- (16) Ruthven, D. M., Principles of Adsorption and Adsorption Processes, John Wiley, New York, 1984.
- (17) Glueckauf, E., Trans. Faraday Soc., 51, 1540 (1955).
- (18) Nakao, S. I., and Suzuki, M., J. of Chem. Engg. Japan 16, 114, (1983).

- (19) Buzanowaski, M. A., and Yang, R. T., Chem. Eng. Sci., 44, 2683, (1989).
- (20) Buzanowaski, M. A., and Yang, R. T., Chem. Eng. Sci., 46, 2589, (1991).
- (21) Farooq, S. and Ruthven D. M., Chem. Eng. Sci., 46, 2213, (1991).
- (22) Yang, R. T., Gas Separation by Adsorption Processes, pgs. 125-133, Butterworths (1987).
- (23) Vermuelen, T., Ind. Eng. Chem., 45, 1664, (1953).

Table 5.1
Experimental Conditions and Parameters used
in the simulation for two column PSA Unit.

Feed gas composition, either	60%CH ₄ , 40%N ₂
or	92%CH ₄ , 8%N ₂
Column length (two column unit)	51 cm
Cross sectional area	9.35 cm ²
Bed voidage	0.4
Adsorbent	Carbon molecular sieve
Amount in each column	360 grams
Particle size	3.18 mm pellets
Equilibrium constant for CH ₄	54.14
Equilibrium constant for N ₂	9.88
Saturation concentration for CH ₄	0.00255 $\frac{\text{mole}}{\text{cm}^3}$
Saturation concentration for N ₂	0.00182 $\frac{\text{mole}}{\text{cm}^3}$
Barrier Resistance for CH ₄	4.82 x 10 ⁻⁶ sec ⁻¹
Barrier Resistance for N ₂	9.99 x 10 ⁻⁴ sec ⁻¹

Table 5.2 : Summary of two column experiments with Molecular Sieve Carbon

Initial bed conditions: Saturated with feed at high and low pressure respectively.

Purge gas: Portion of the high pressure product exit stream.

Run No.	Temp. ° C	Feed concn. CH ₄	velocity cm/sec	$\frac{P_H}{P_L}$	Purge to feed ratio	Cycle time sec.	Product concn. exptl.	Purge concn. exptl	LDF parm. CH ₄ / N ₂	Product concn. theor.
1	25	60	2.01	3:1	2.02	60	60.15	-	1/1	60.32
2						100	63.85	-	1/1	60.58
3						120	64.83	-	1/1	60.60
4						180	66.22	-	1/3	61.78
5						240	65.59	-	1/3	61.73
6						300	65.35	-	1/7	63.19
7	25	60	1.29	3:1	2.28	60	46.32	-	1/1	60.45
8						120	57.79	-	1/1	60.93
9						180	66.76	-	1/3	62.76
10						240	69.84	-	1/3	62.71

(...contd.)

Table 5.2 (contd.)

Run No.	Temp. ° C	Feed concn. CH ₄	velocity cm/sec	$\frac{P_{H_2}}{P_{L_2}}$	Purge to feed ratio	Cycle time sec.	Product concn. exptl.	Purge concn. exptl.	LDF parm. CH ₄ N ₂	Product concn. theor.
11						300	68.67	-	1/7	65.20
12						360	67.39	-	1/11	66.62
13	25	60	0.74	3:1	2:1	60	48.12	-	1/1	59.28
14						120	57.91	-	1/1	61.11
15						180	64.72	-	1/3	64.40
16						240	64.47	-	1/3	64.40
17						300	68.45	-	1/7	68.57
18						360	71.71	-	1/11	71.64
19						420	74.39	-	1/16	74.55
20						480	75.33	-	1/19	75.54

(...contd.)

Table 5.2 (contd.)

Run No.	Temp. °C	Feed concn. CH ₄	velocity cm/sec	$\frac{P_H}{P_L}$	Purge to feed ratio	Cycle time sec.	Product concn. exptl.	Purge concn. exptl.	LDF parm. CH ₄ /N ₂ theor.	Product concn. theor.
21						540	75.84	-	1/22	75.52
22						600	75.34	-	1/23	75.20
23						660	74.95	-	1/26	74.91
24						720	74.27	-	1/30	74.46
25	25	60	0.62	3:1	1.79	600	75.21	63.21	1/23	65.43
26	25	92	0.62	3:1	1.79	100	87.58	91.44	1/1	92.12
27						300	93.90	89.77	1/7	93.70
28						600	96.15	92.20	1/13	94.56
29						720	96.25	92.70	1/30	94.55
30						840	95.79	92.92	1/37	94.40

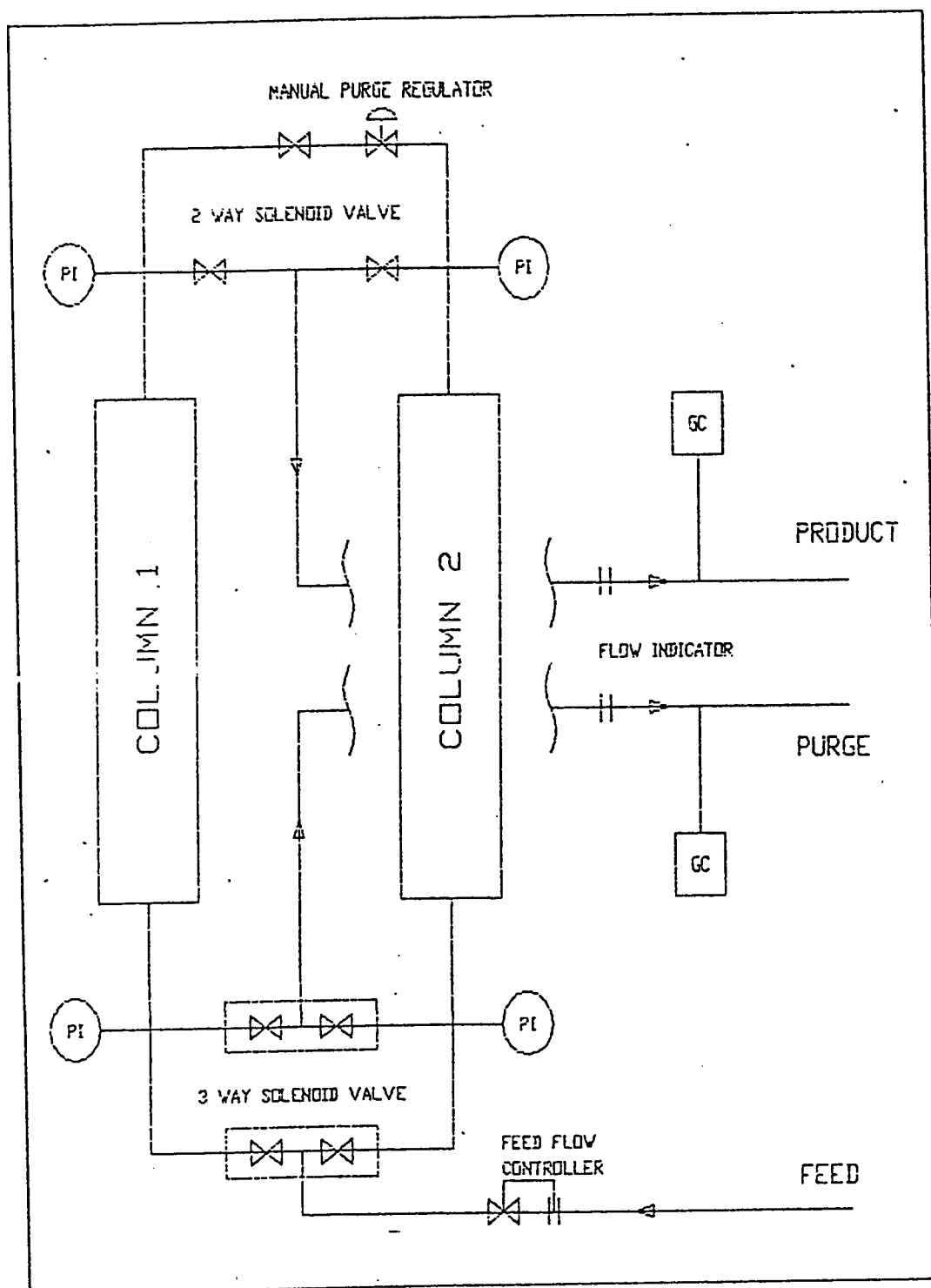


Fig 5.1 Schematic Diagram of the Two Column PSA Experimental Unit

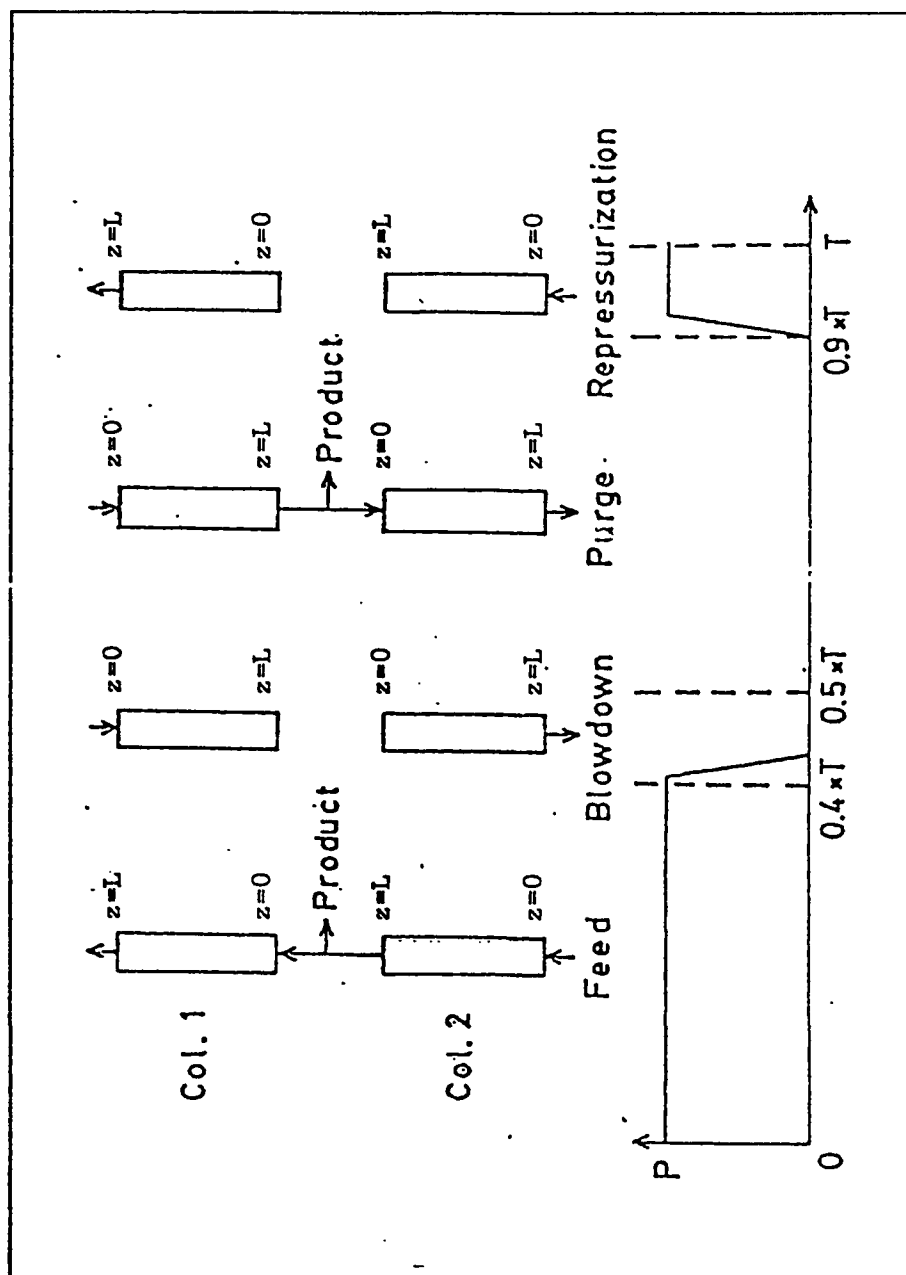


Fig. 5.2 Schematic diagram of the steps involved in PSA cycle

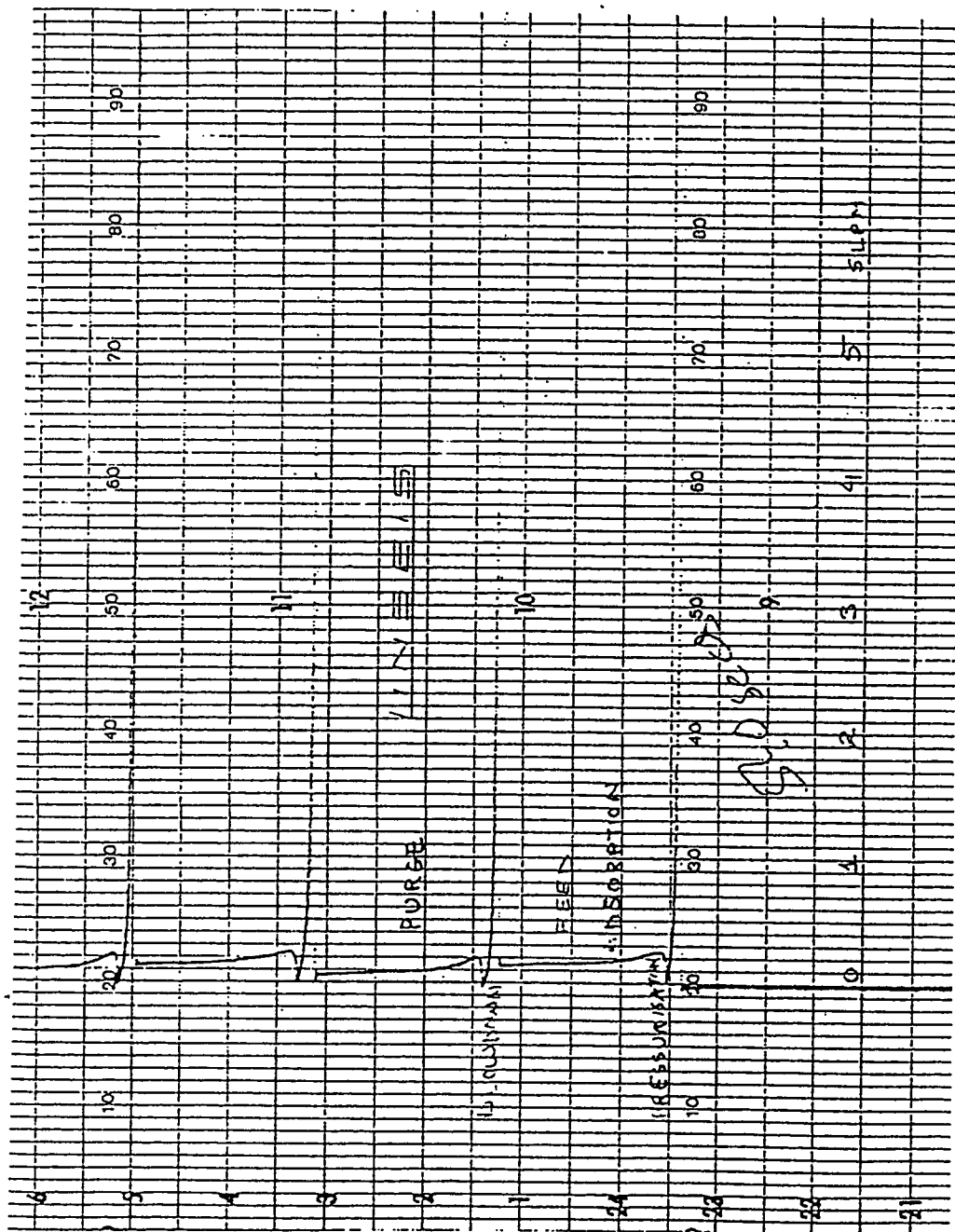


Fig 5.3 Feed Flow during the course of a 540 sec Cycle

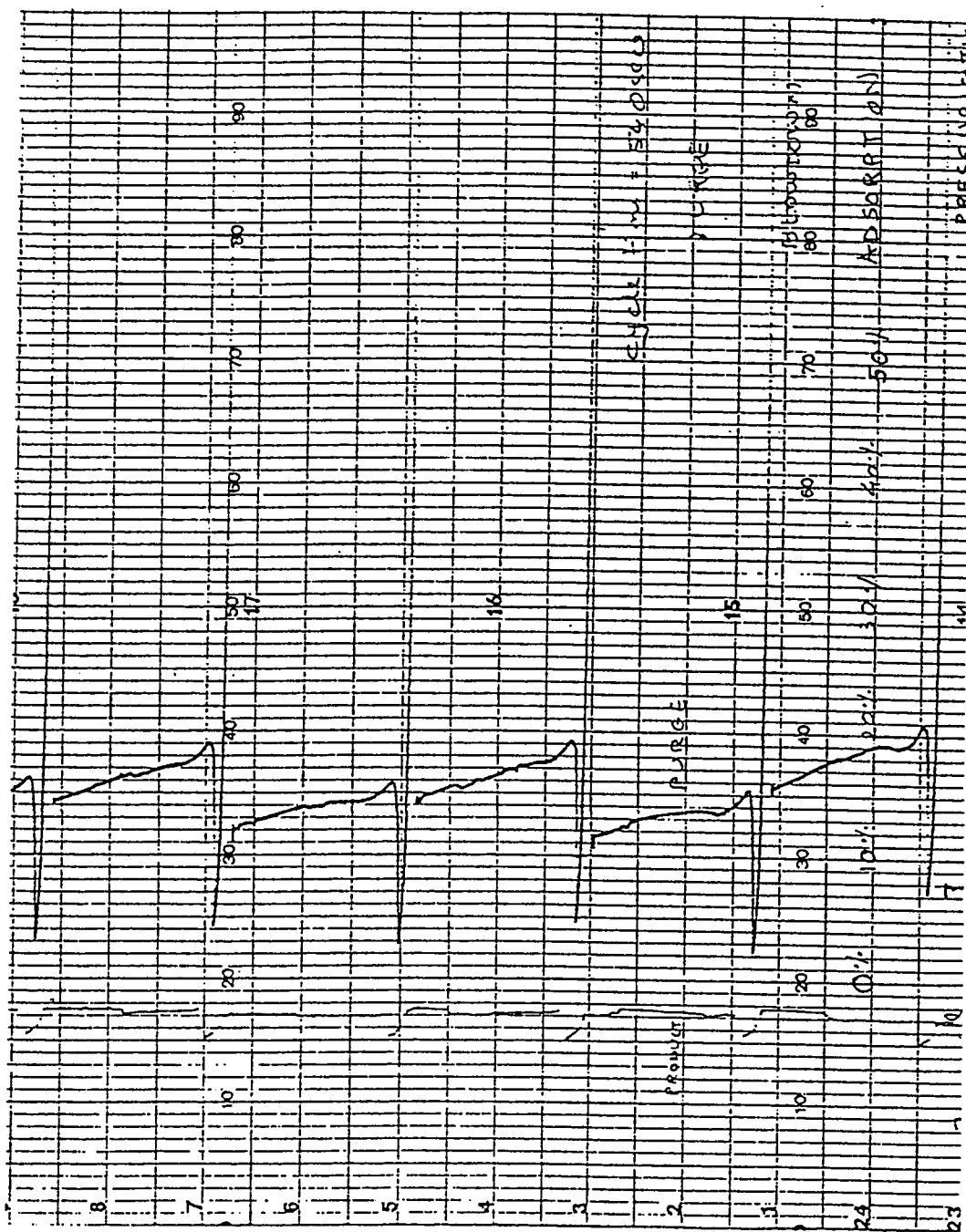


Fig 5.4 Product and Purge Flow during the course of a 540 sec Cycle

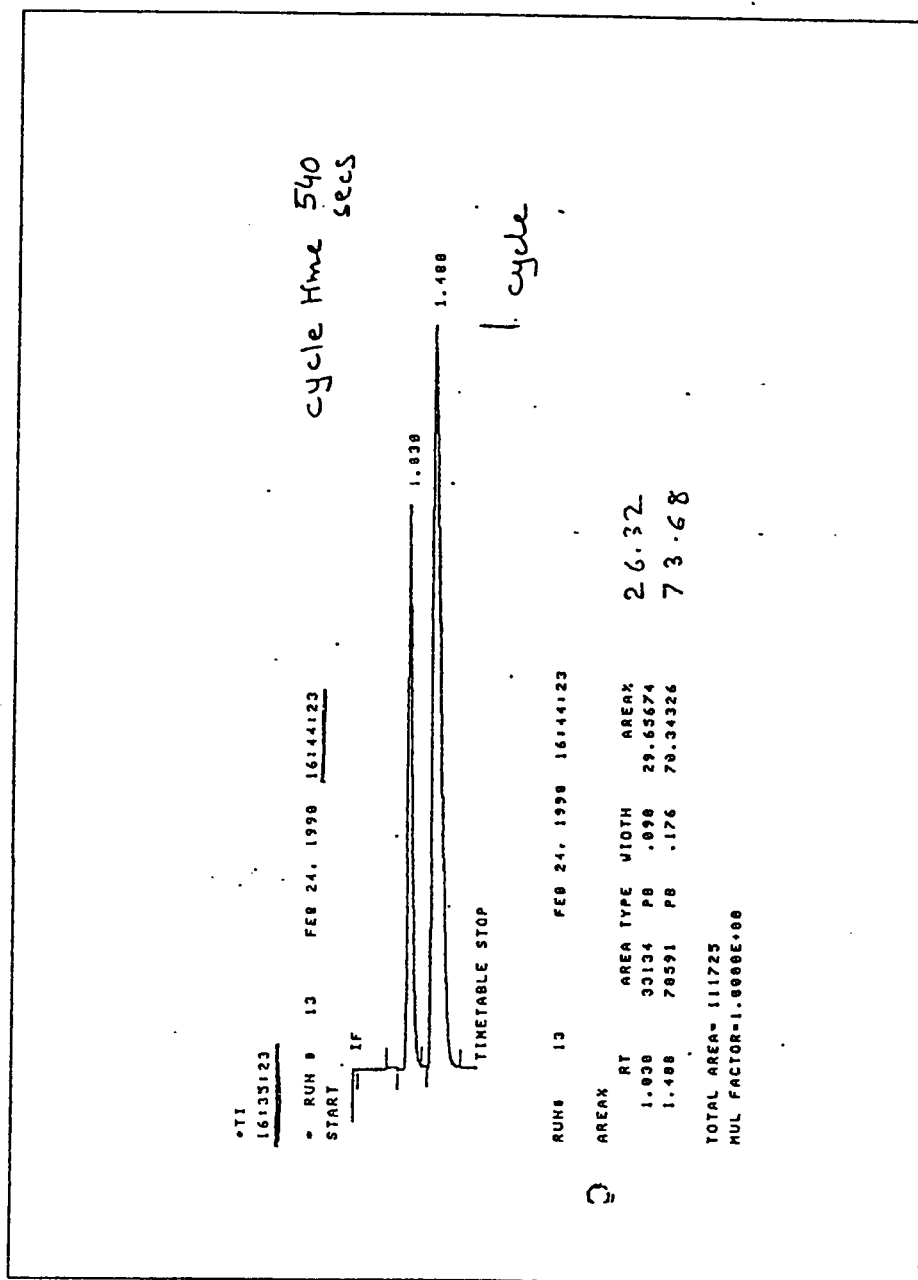
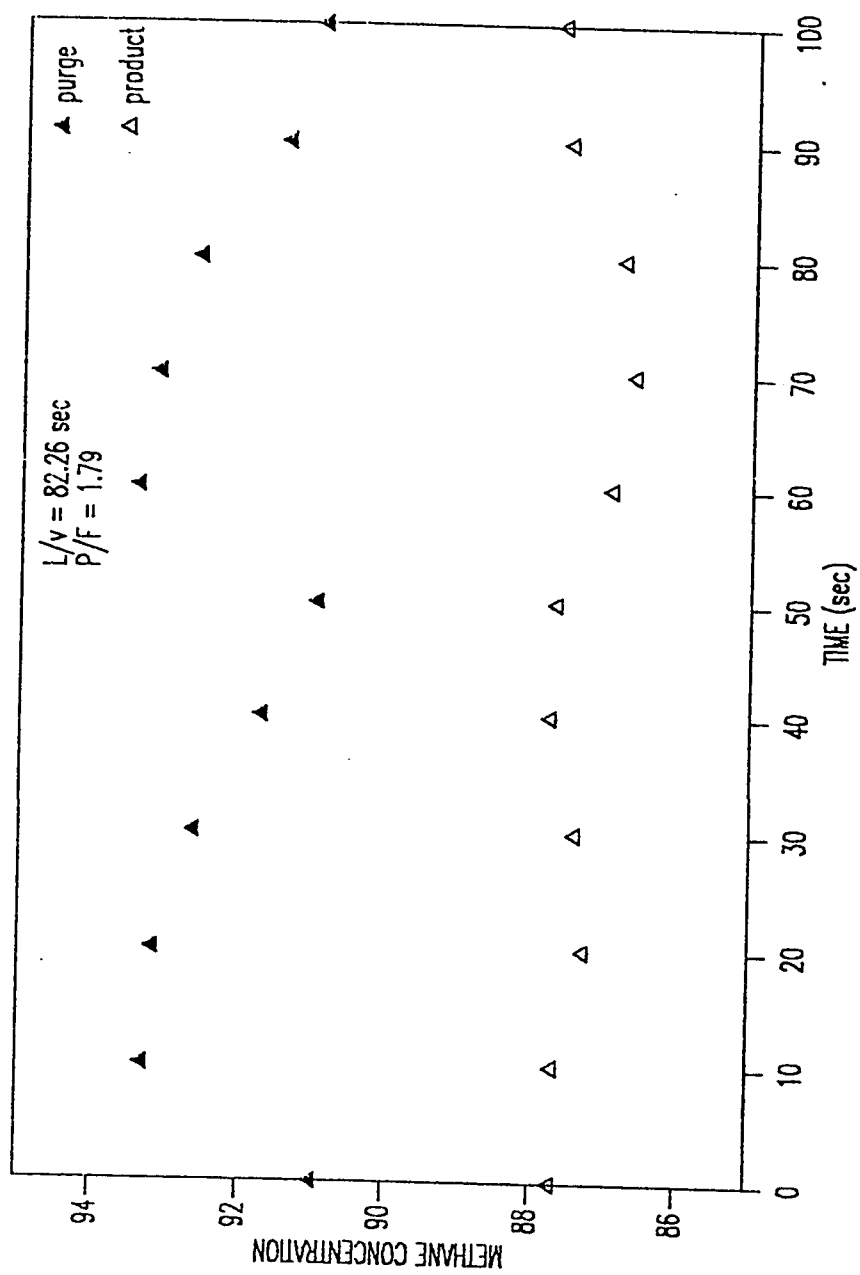


Fig. 5.5 Typical output from an Integrator of a Gas Chromatograph



file:csml420b

Fig 5.6 Methane concentration during the course of a 100 sec. cycle (Run 26)

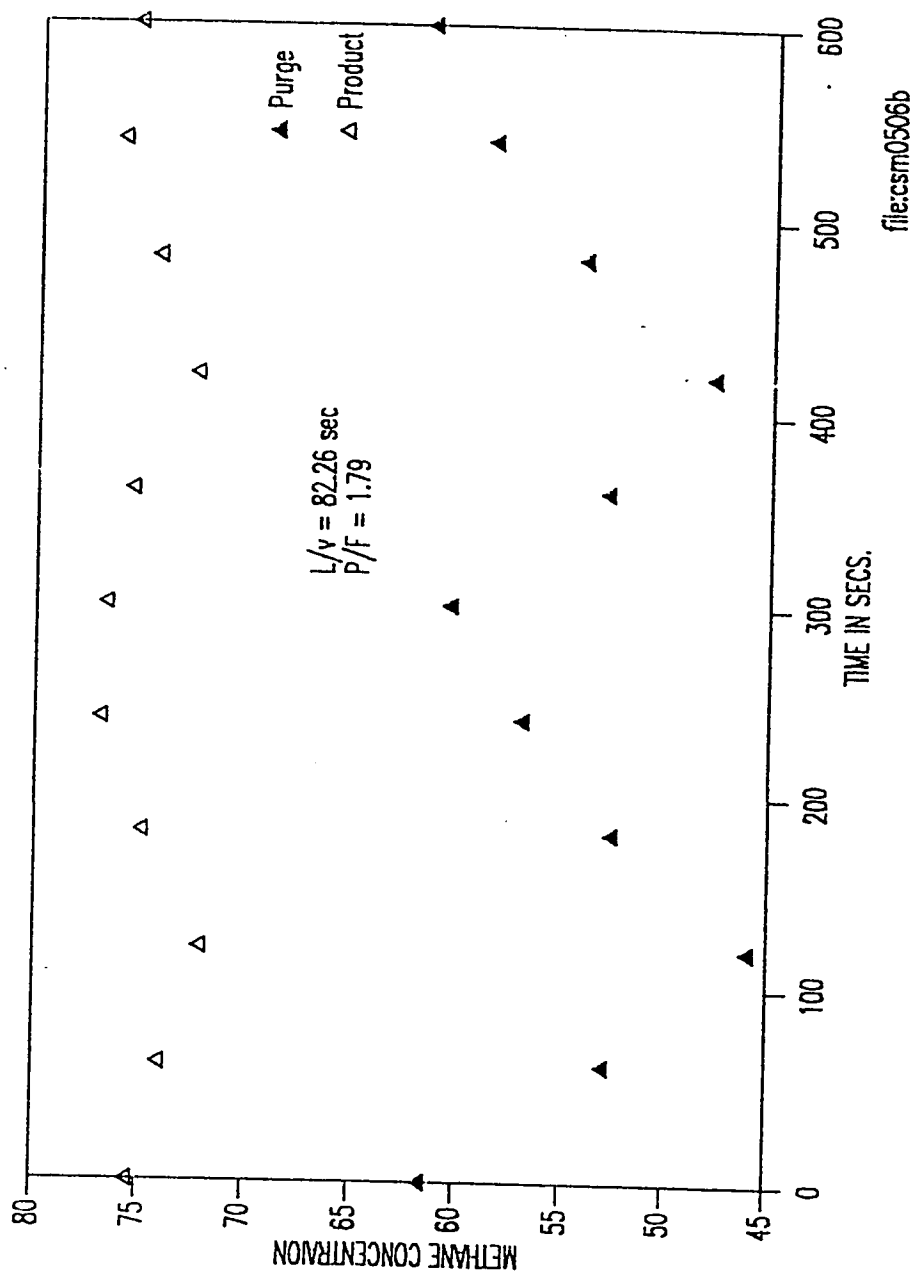


Fig 5.7 Methane concentration during the course of a 600 sec. cycle (Run 25)

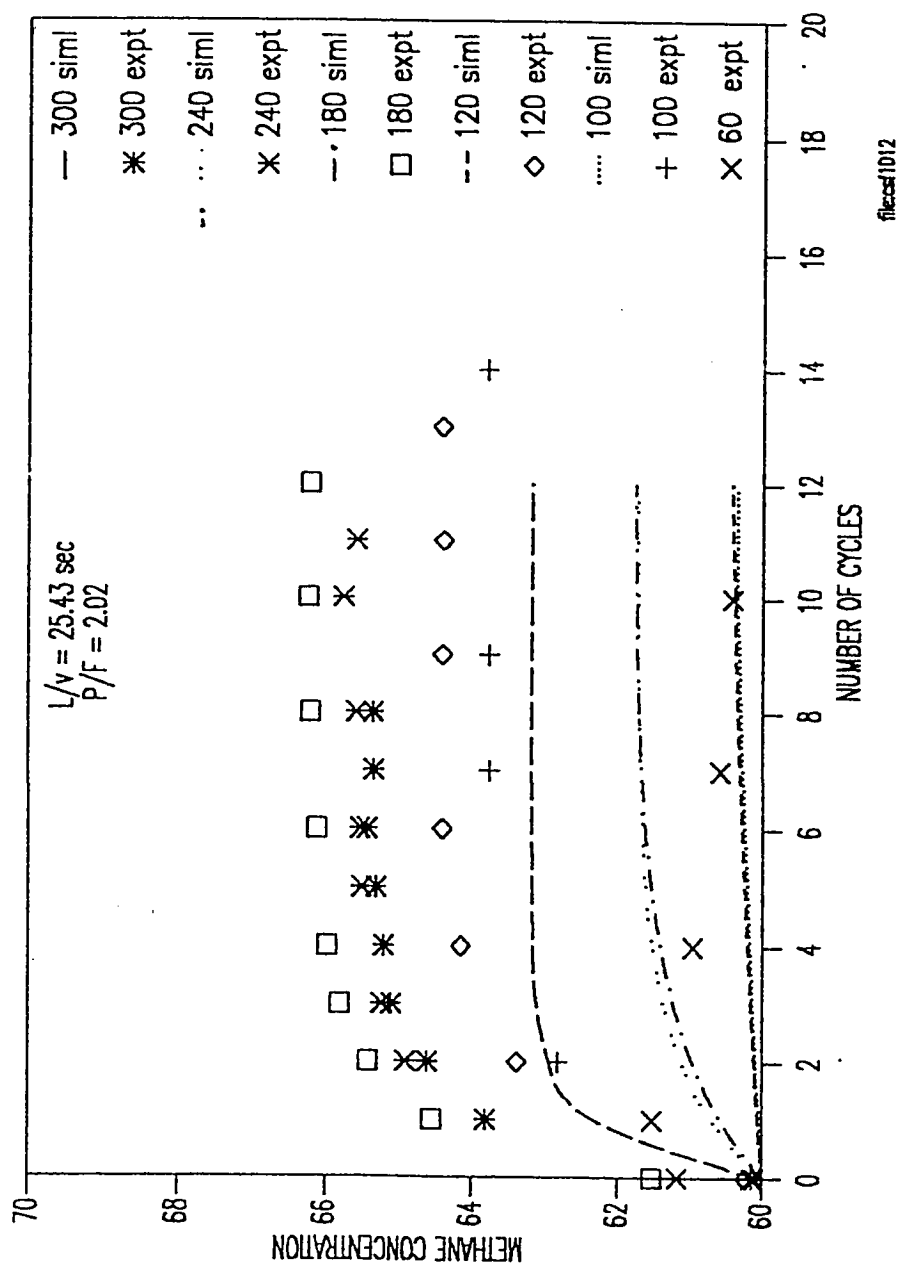
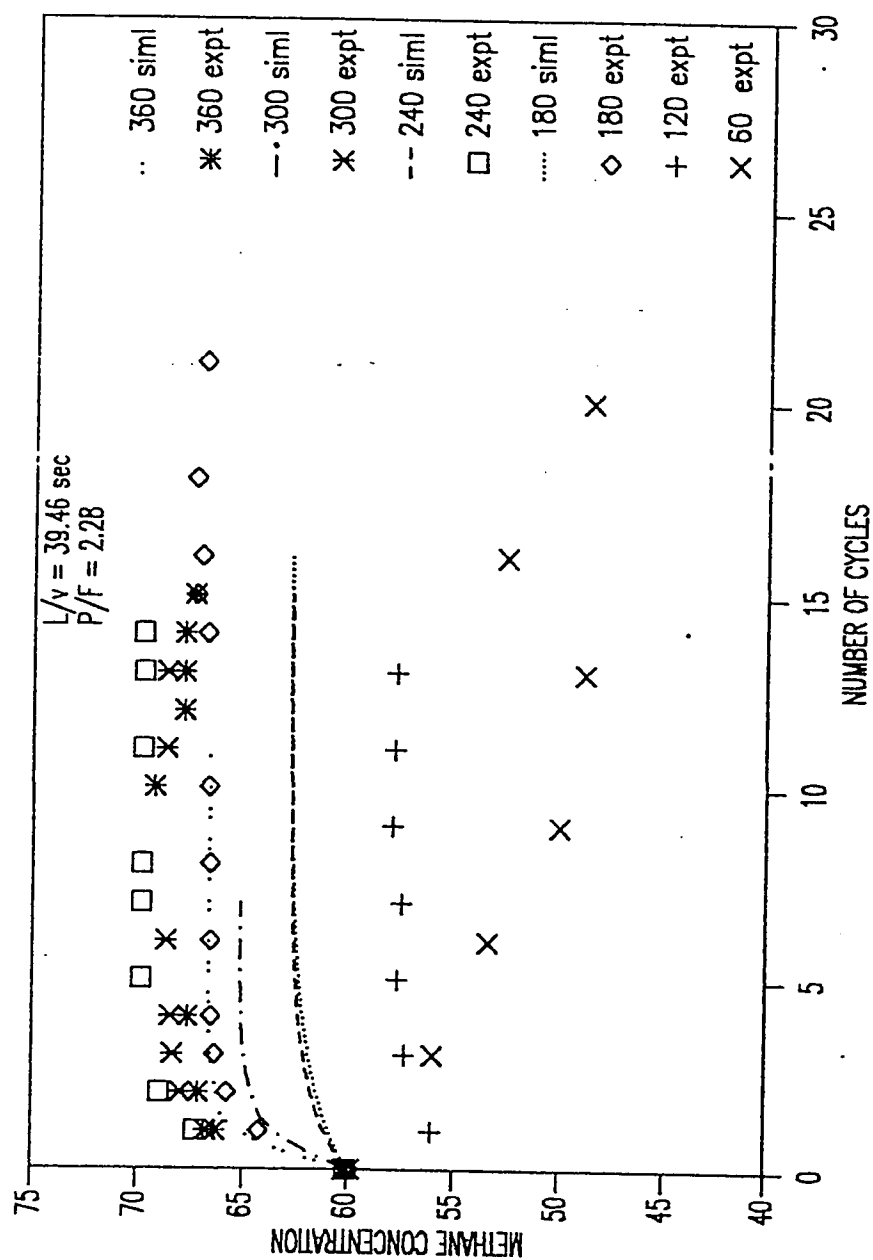


Fig 5.8 Exit Experimental and Simulated Product Concentration
2 sec. prior to the end of the Adsorption step as a function of
No. of Cycles (Runs 1-6). Parameter is cycle time



filed/1214

Fig 5.9 Exit Experimental and Simulated Propanol Concentration 2 sec. prior to the end of the Adsorption step as a function of No. of Cycles (Runs 7-12). Parameter is cycle time

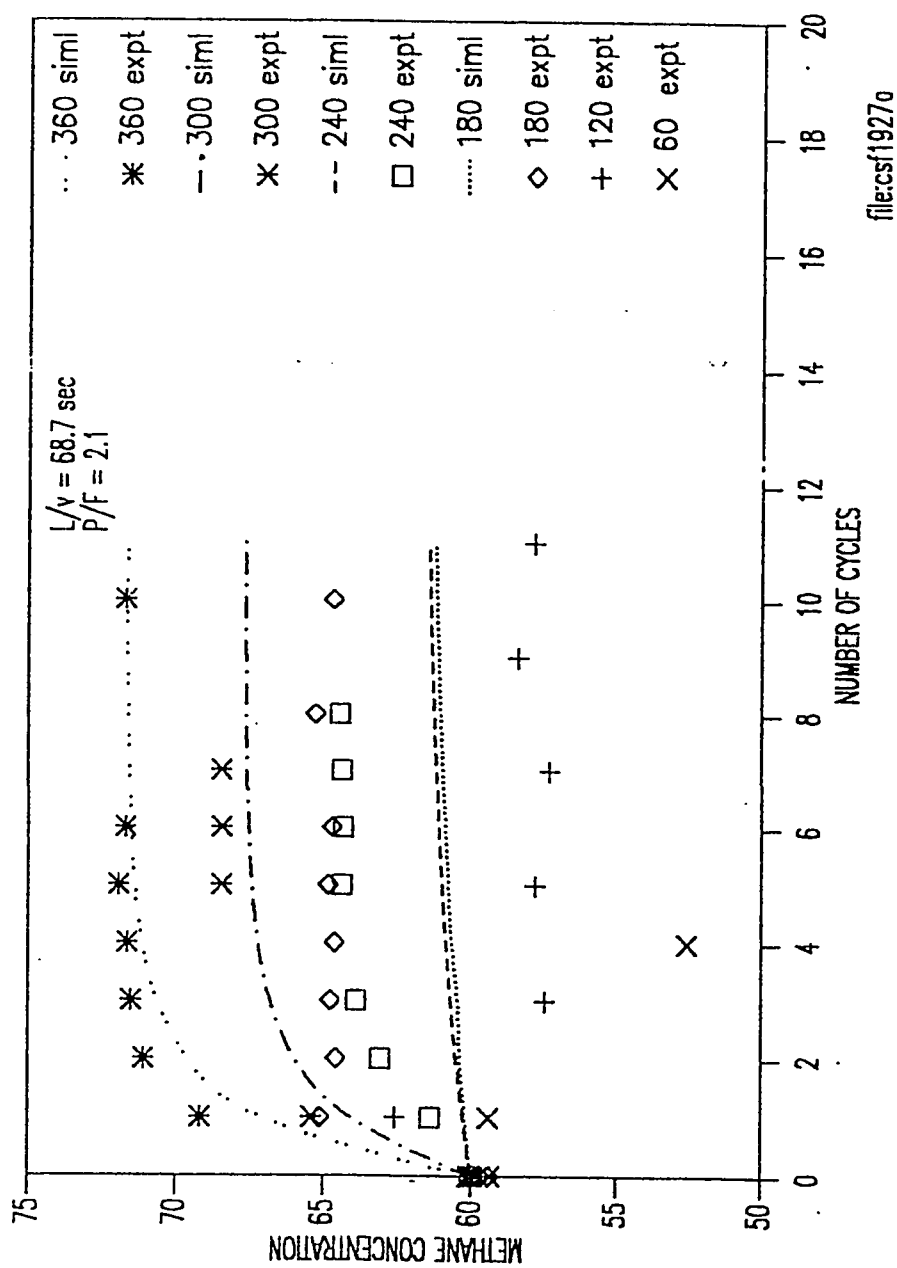


Fig 5.10 Exit Experimental and Simulated Product Concentration 2 sec. prior to the end of the Adsorption step as a function of No. of Cycles (Runs 13-18). Parameter is cycle time

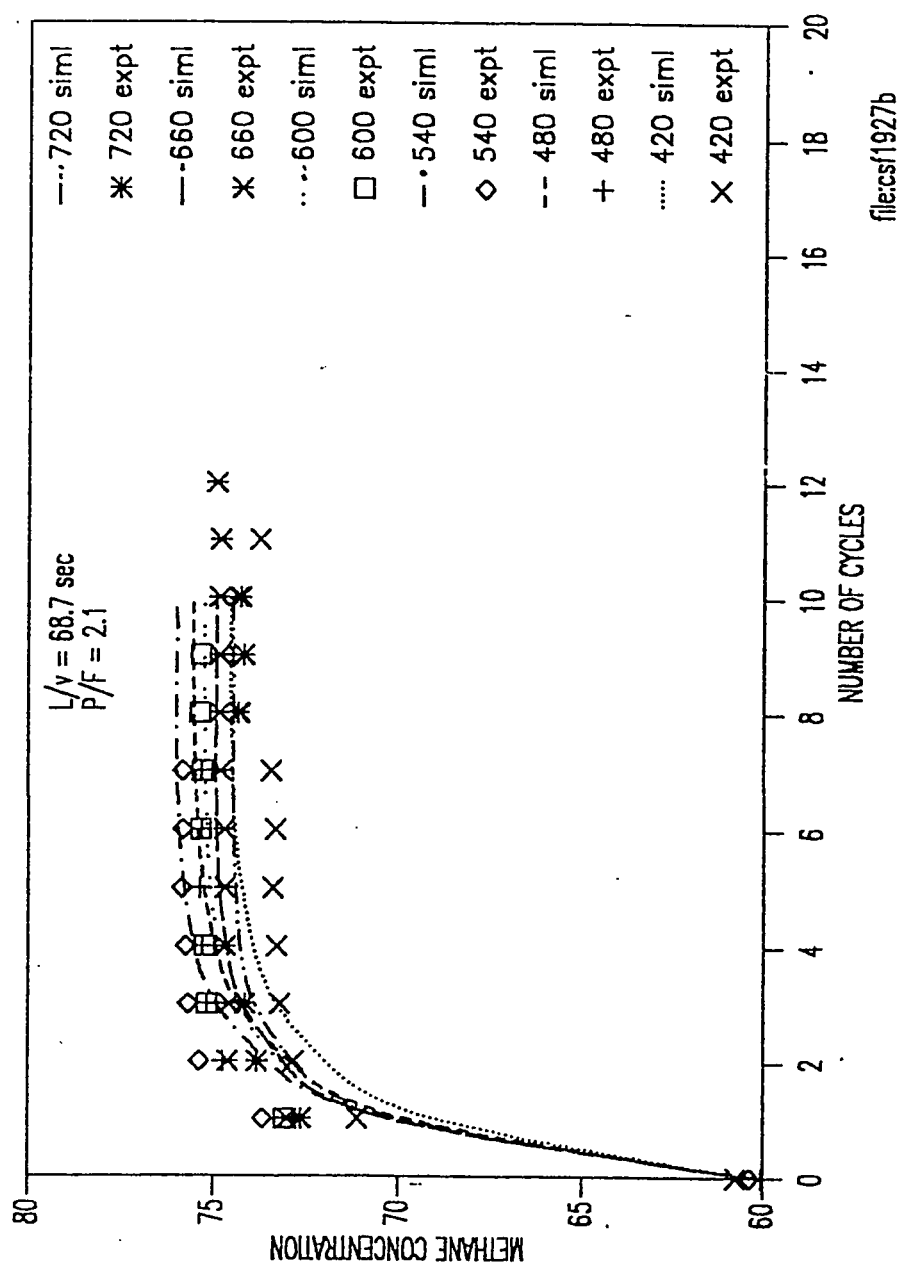
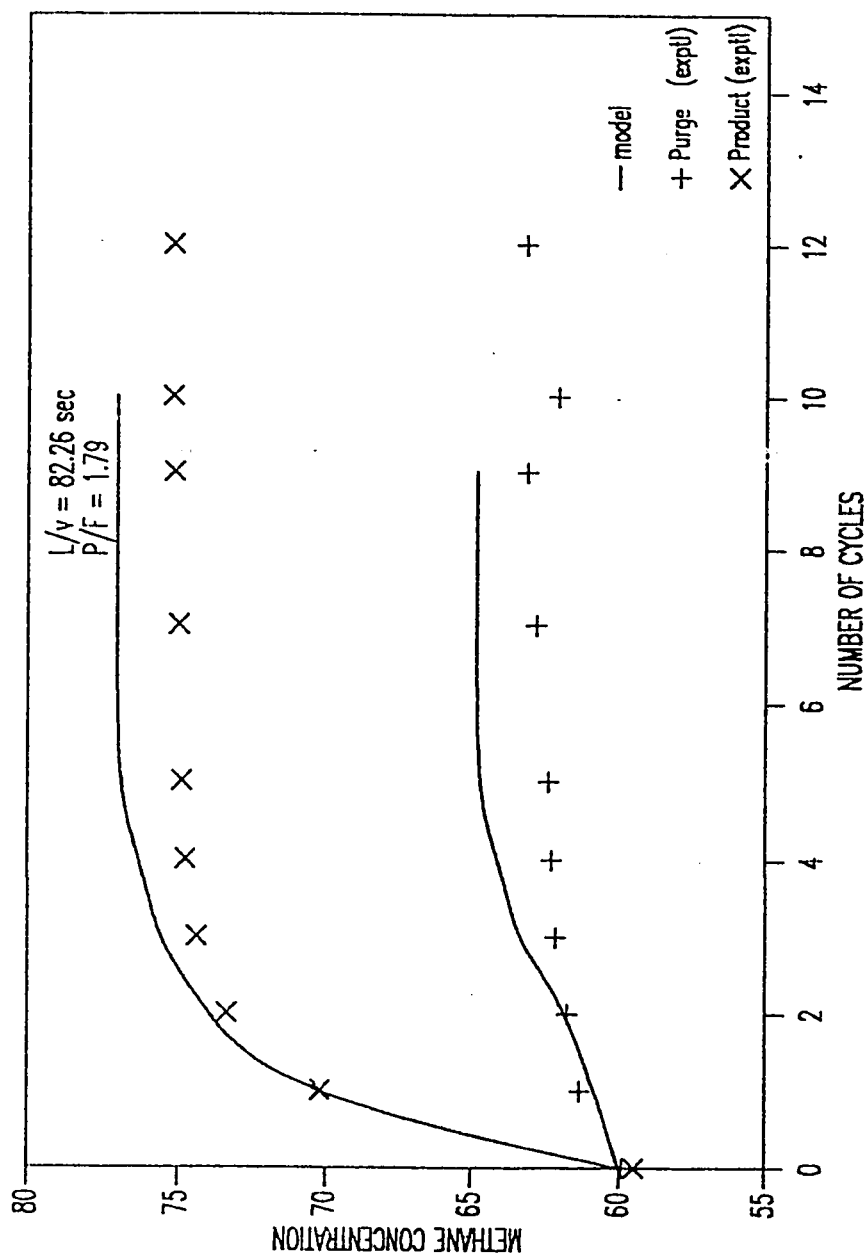


Fig 5.11 Exit Experimental and Simulated Product Concentration
2 sec. prior to the end of the Adsorption step as a function of
No. of Cycles (Runs 19-24). Parameter is cycle time



file:csrm0506a

Fig 5.12 Exit Experimental and Simulated, Product and Purge, Concentration 2 sec. prior to the end of the Sorption step as a function of No. of Cycles (Run 25)

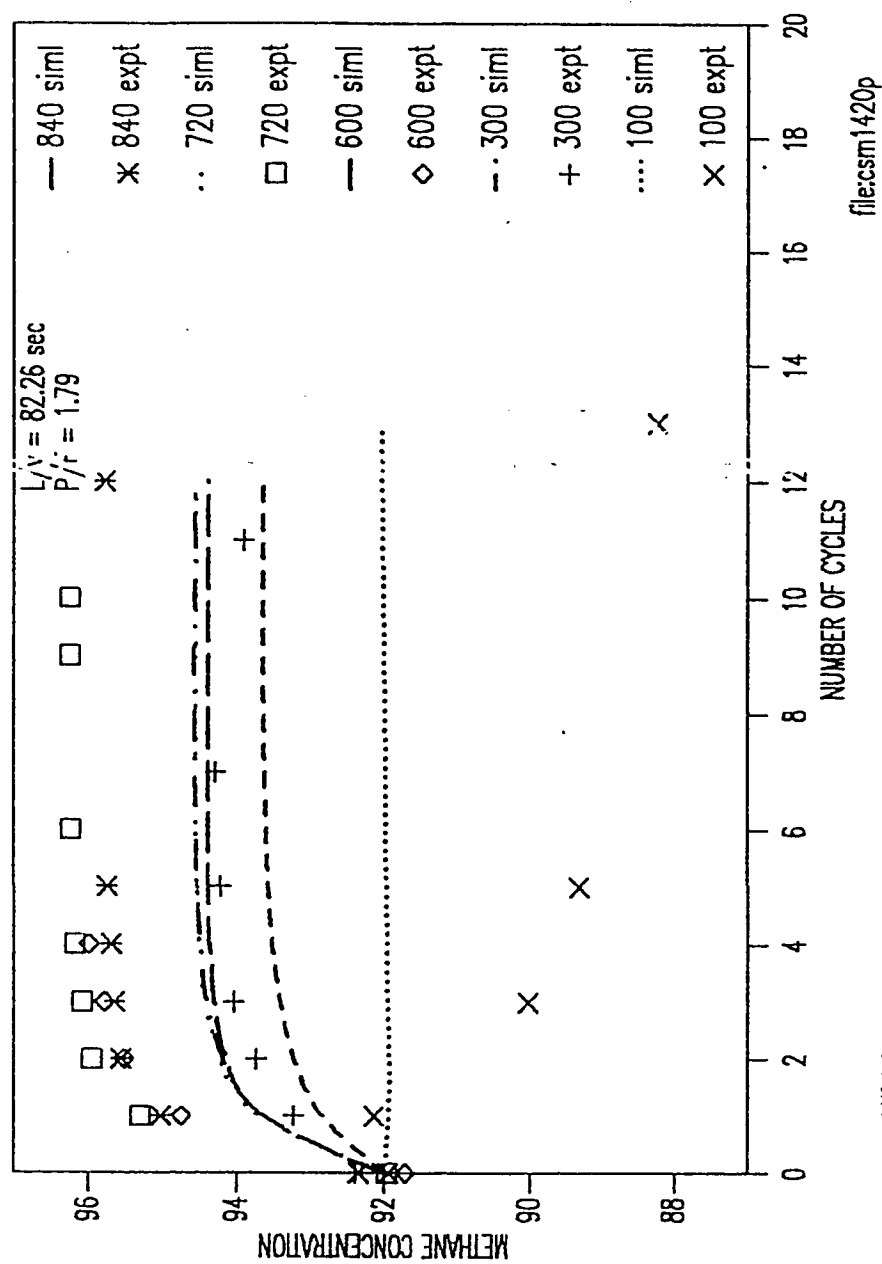


Fig 5.13 Exit Experimental and Simulated Product Concentration 2 sec. prior to the end of the Adsorption step as a function of No. of Cycles (Runs 26-30). Parameter is cycle time

file:csml420p

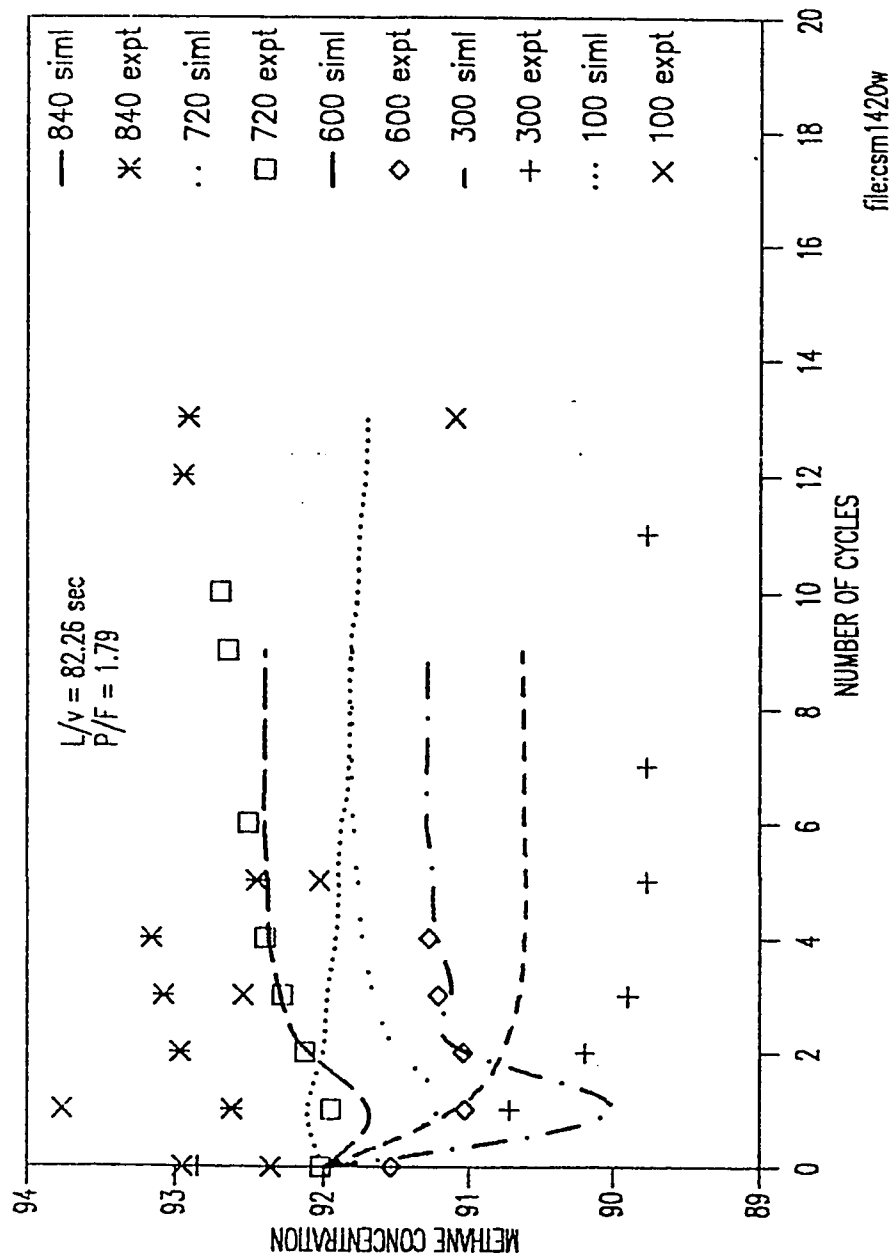


Fig 5.14 Exit Experimental and Simulated Purge Concentration 2 sec. prior to the end of the Adsorption step as a function of No. of Cycles (Runs 26-30). Parameter is cycle time

file:csml420w

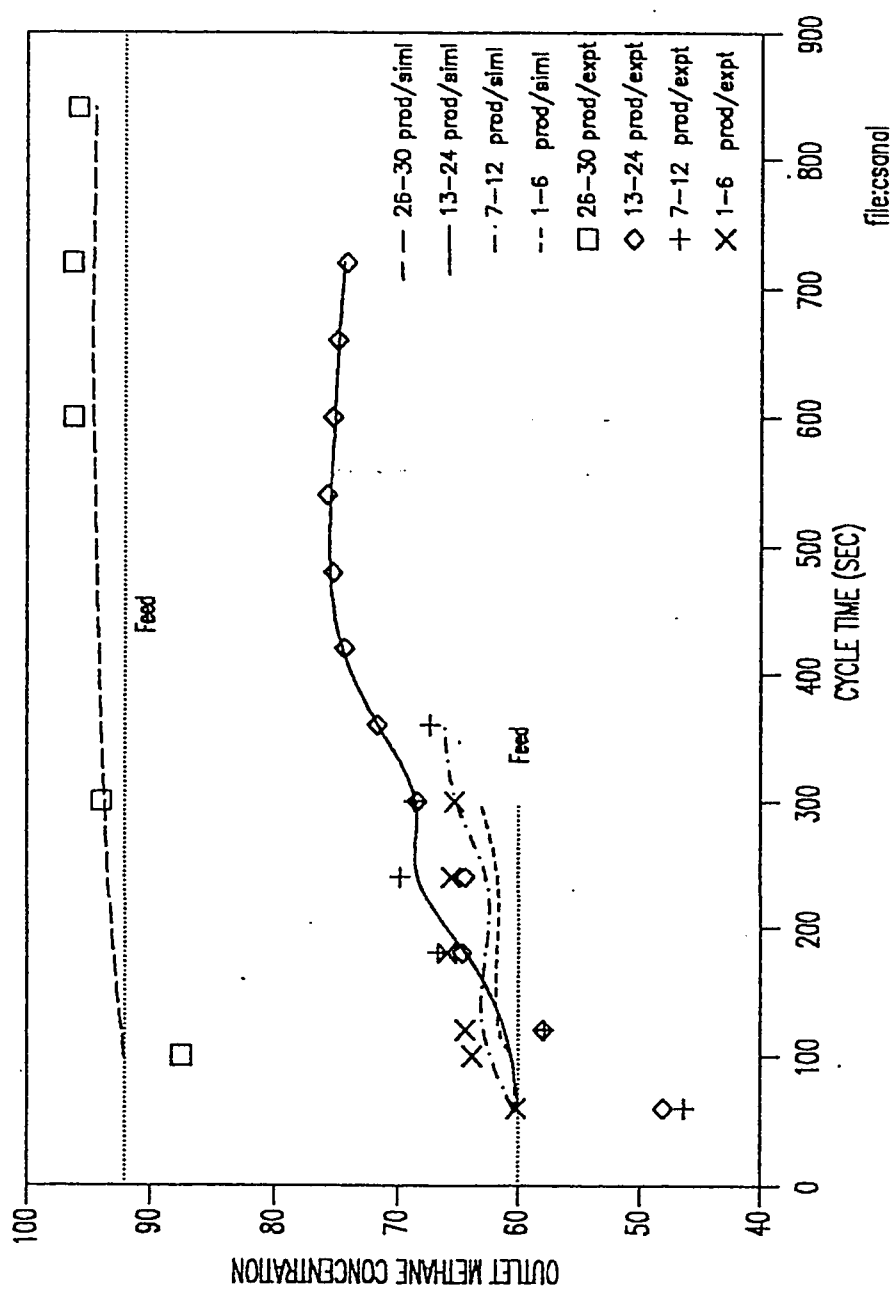
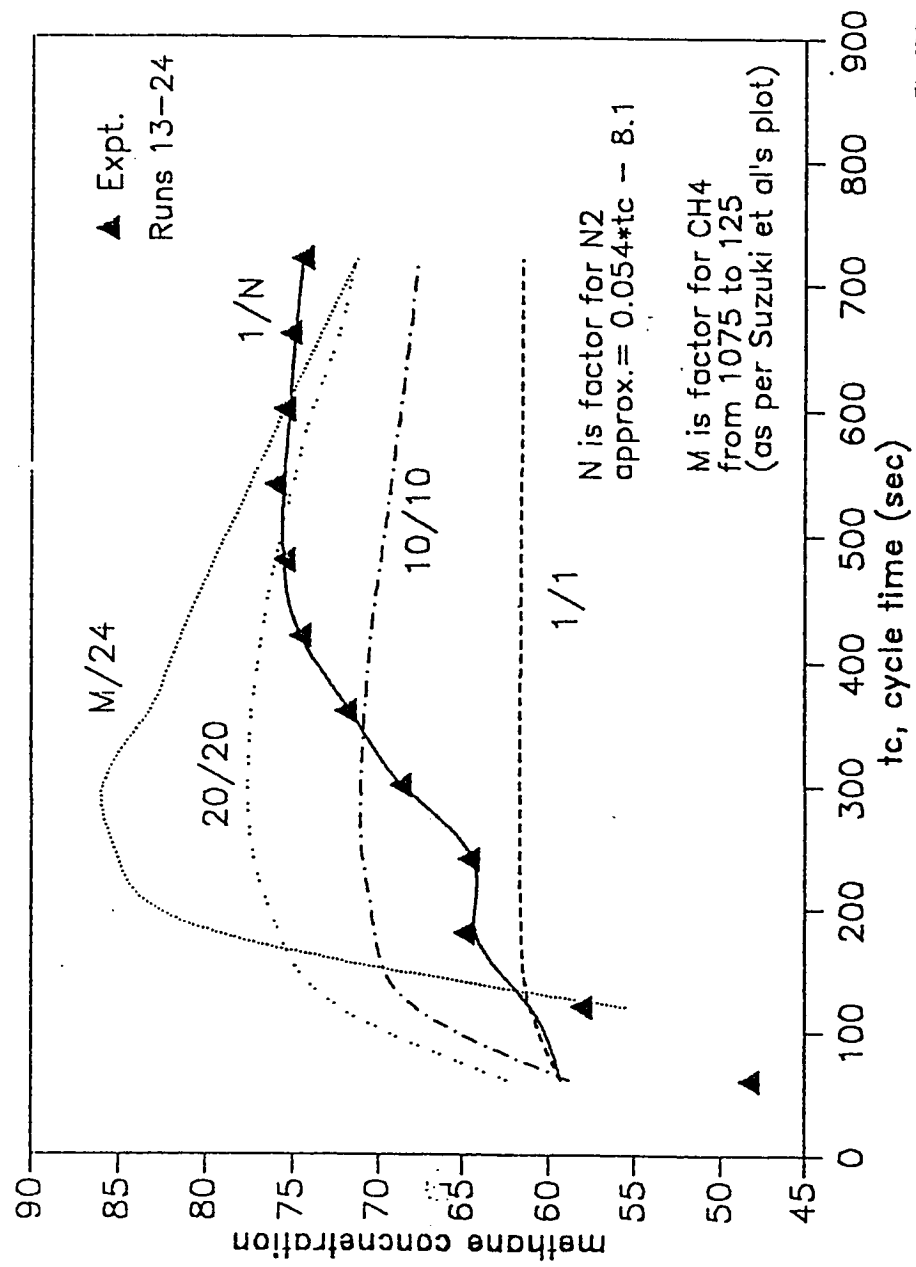


Fig 5.15 Exit Experimental and Simulated Product Concentration at Cyclic steady state as a function of cycle time (Runs 1-30).



file:f22

Fig 5.16 Theoretical Exit Methane Concentration as a function of Cycle time with ϕ factor for Methane/Nitrogen as parameter

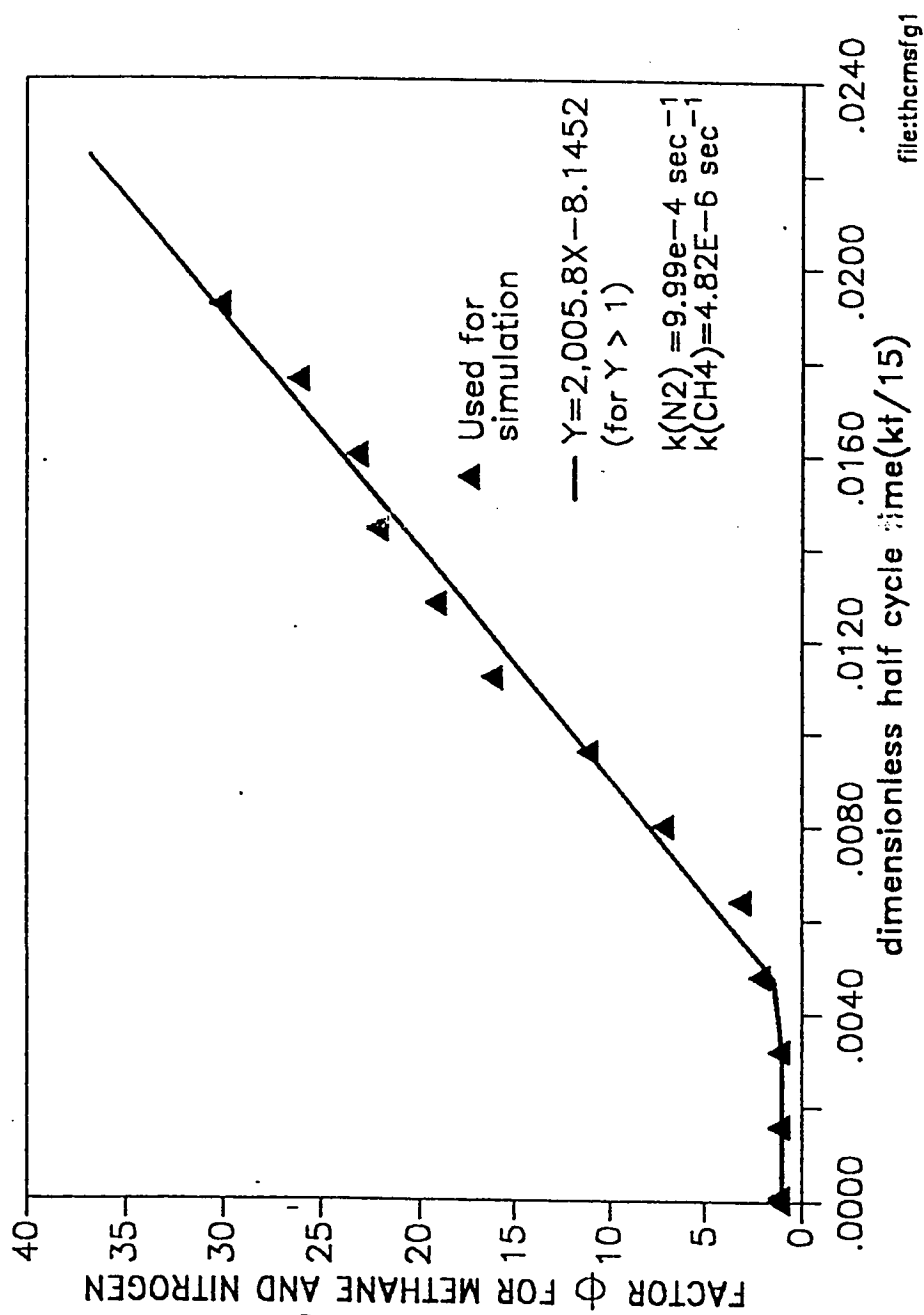


Fig.5.17 Plot of Methane and Nitrogen factor (Φ) as a function of Dimensionless Half Cycle time

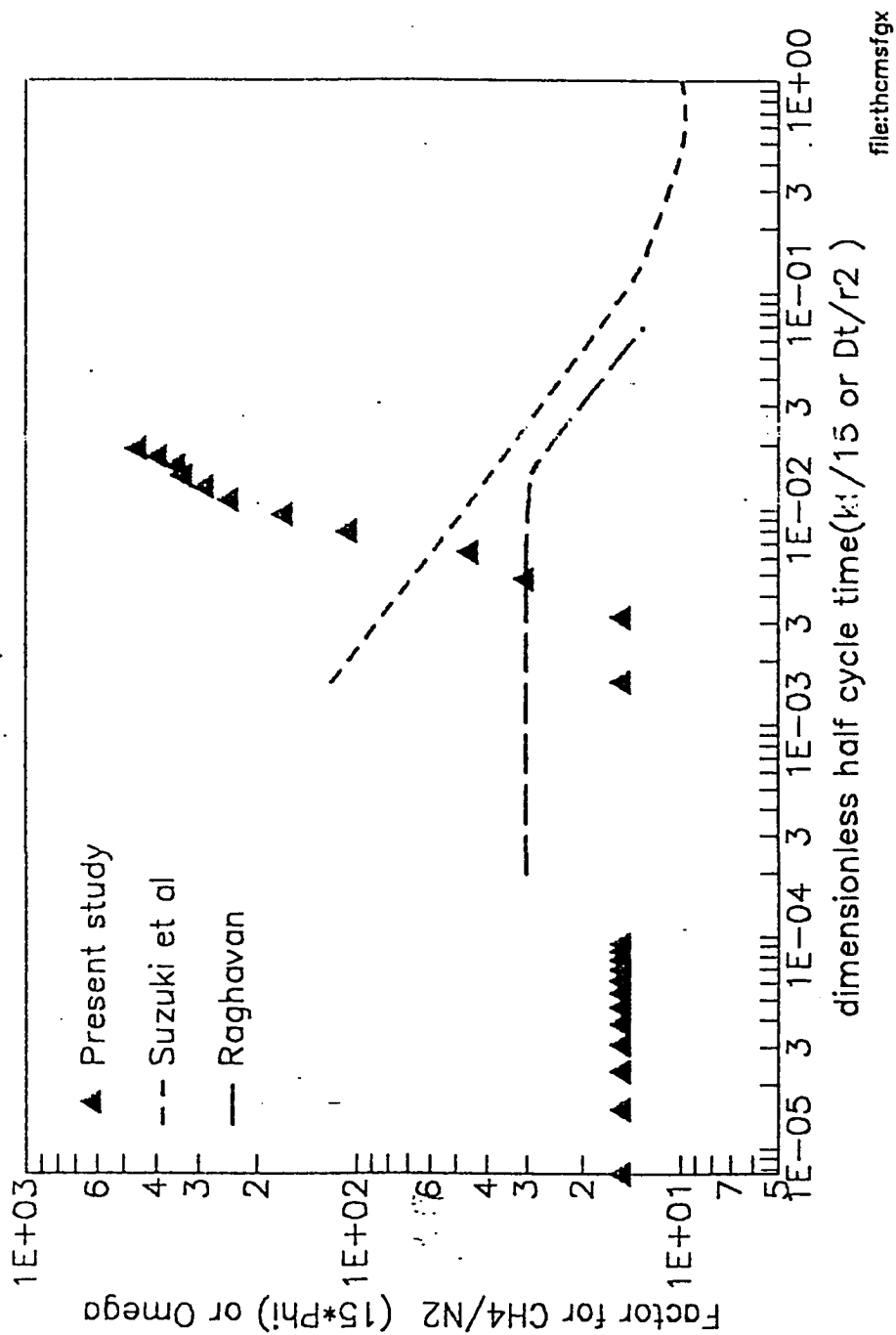


Fig 5.18 Plot of equivalent Methane and Nitrogen (15*Phi) factor along with LDF factor of Suzuki et al(18) and Raghavan et al(11) as a function of Dimensionless half Cycle time

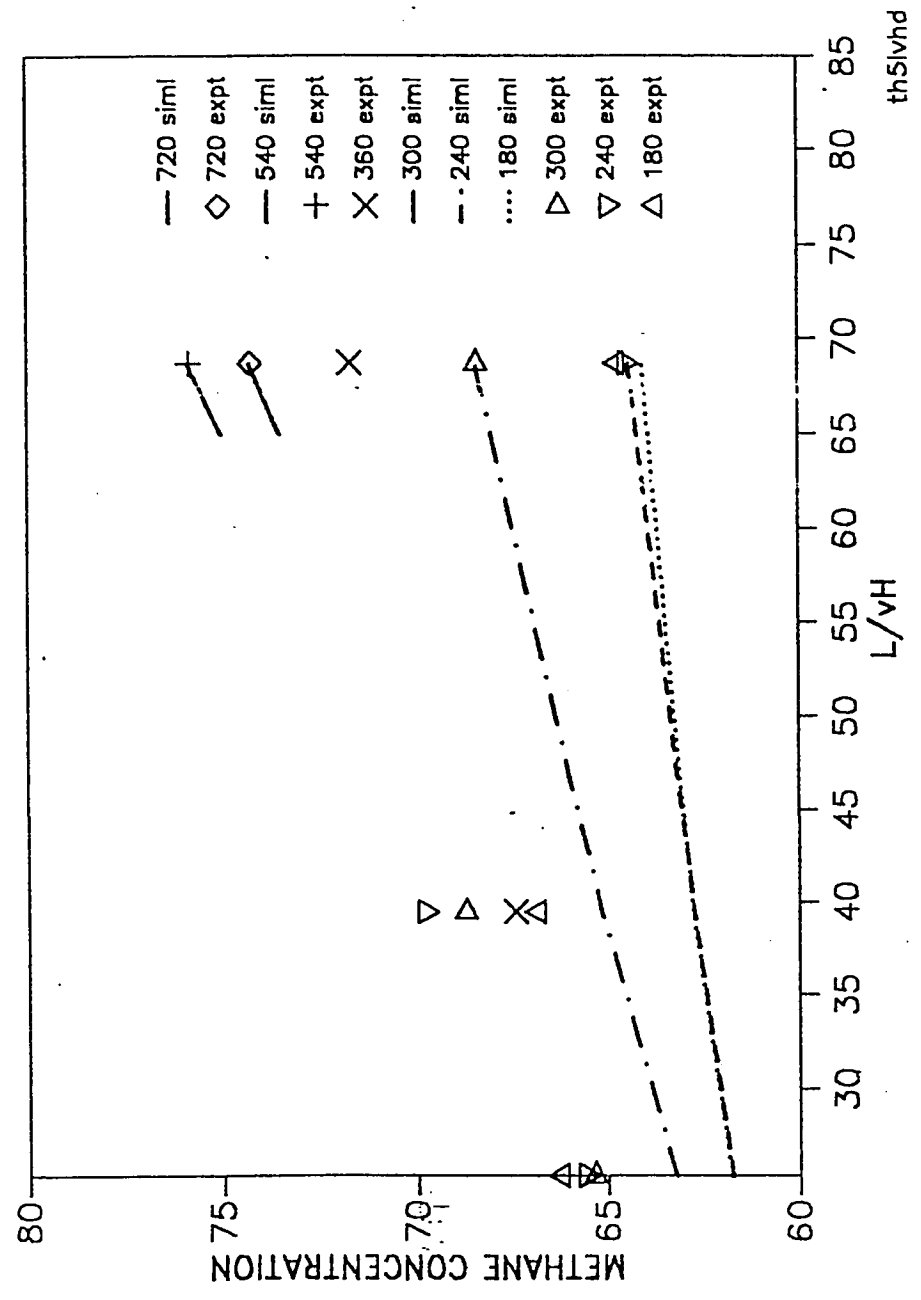


Fig 5.19 Exit Methane Concentration as a function of L/v_H with Cycle time as a parameter

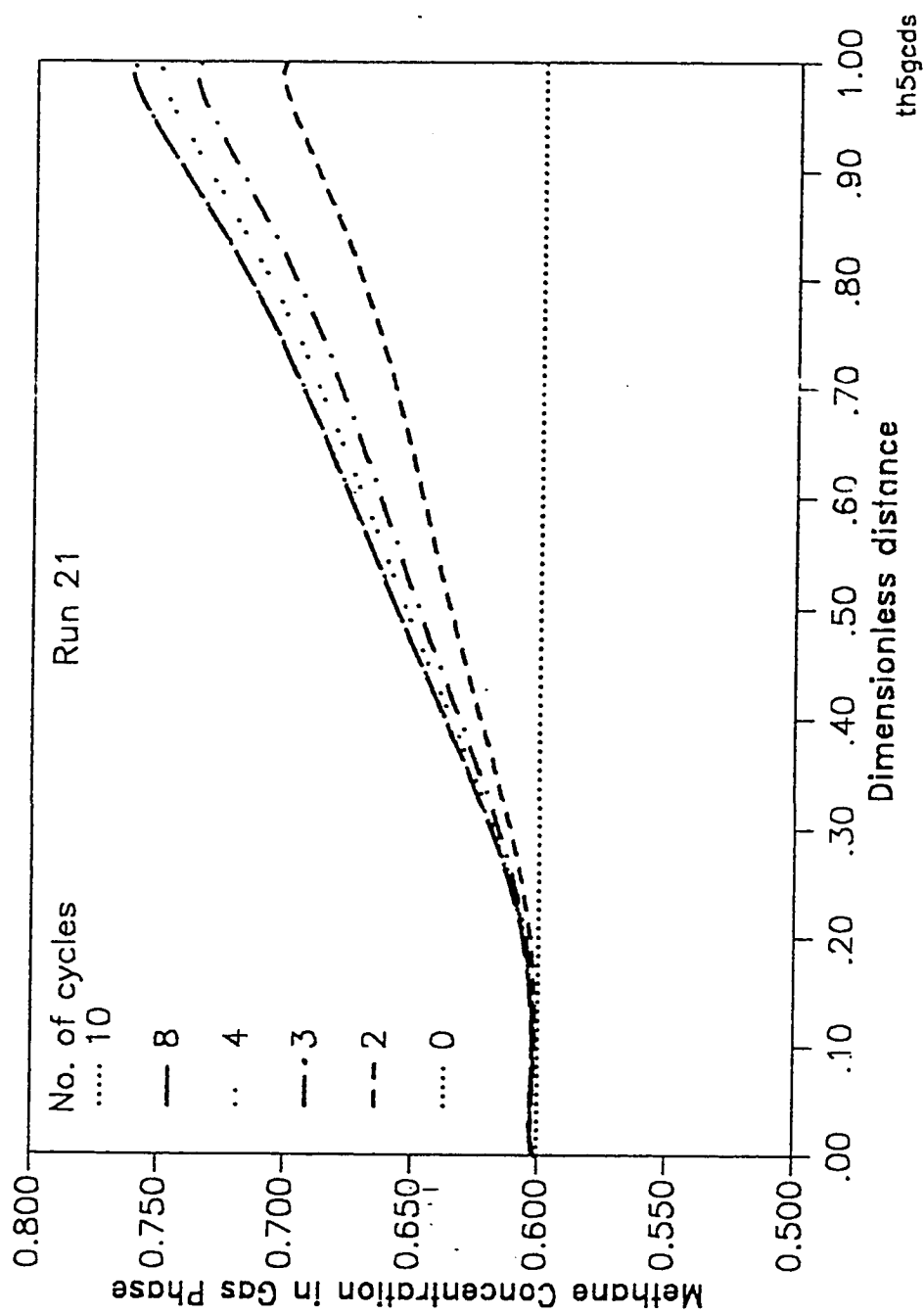


Fig 5.20 Methane Concentration in Gas Phase along the Column with No. of Cycles as a parameter

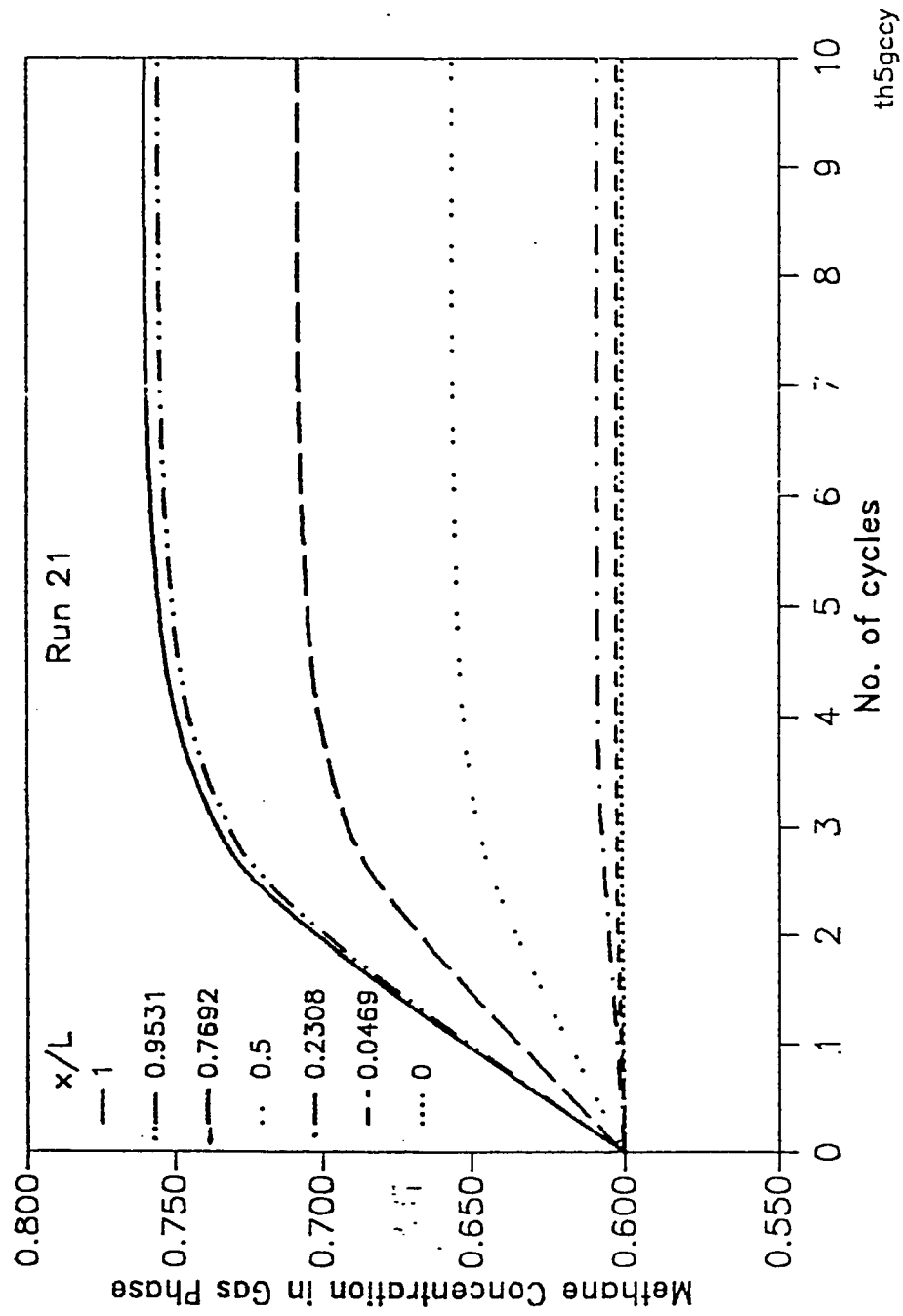


Fig 5.21 Methane Concentration in Gas Phase at specific points in the Column as a function of No. of Cycles

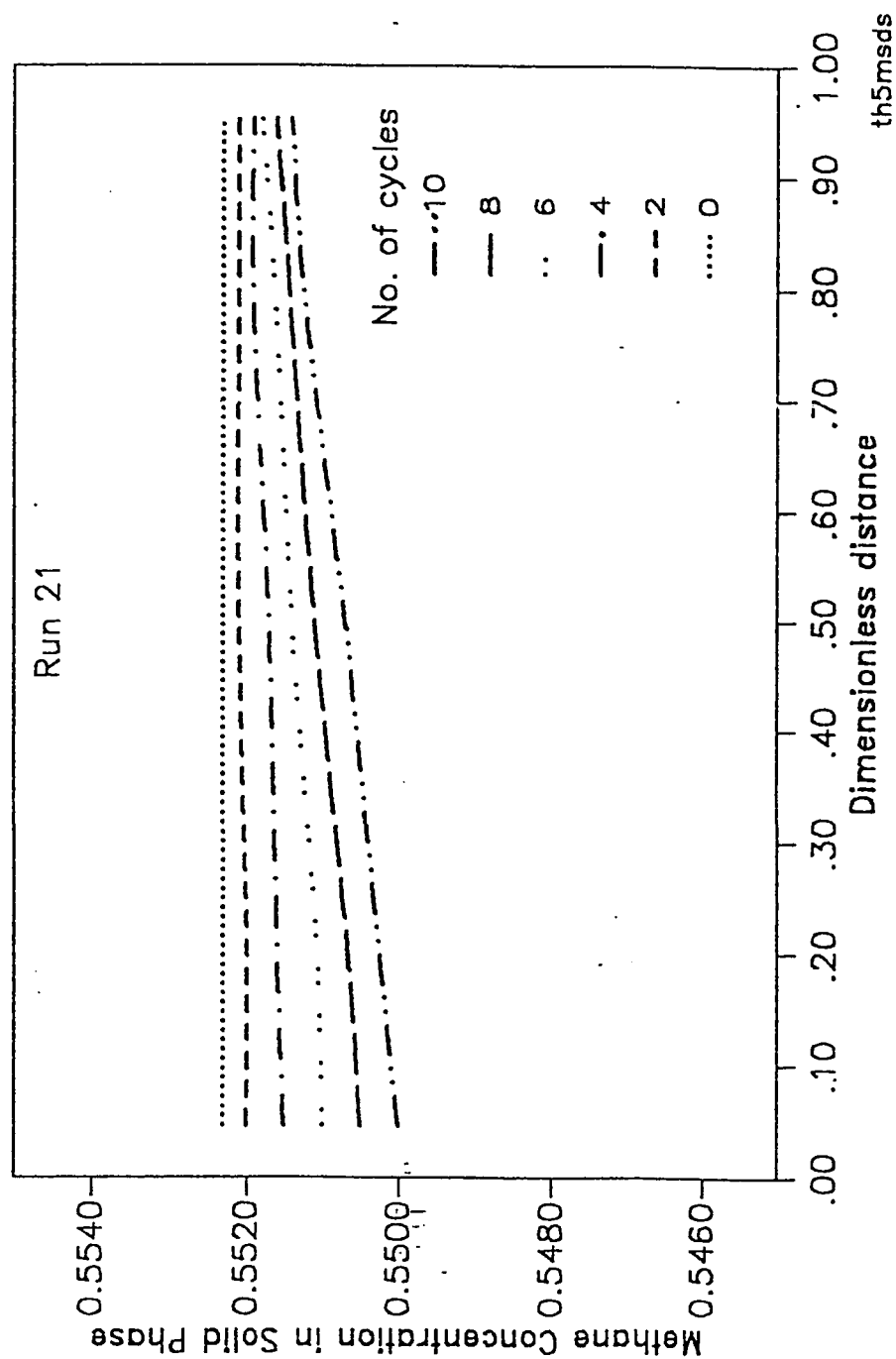


Fig 5.22 Methane Concentration in Solid Phase along the Column with No. of Cycles as a parameter

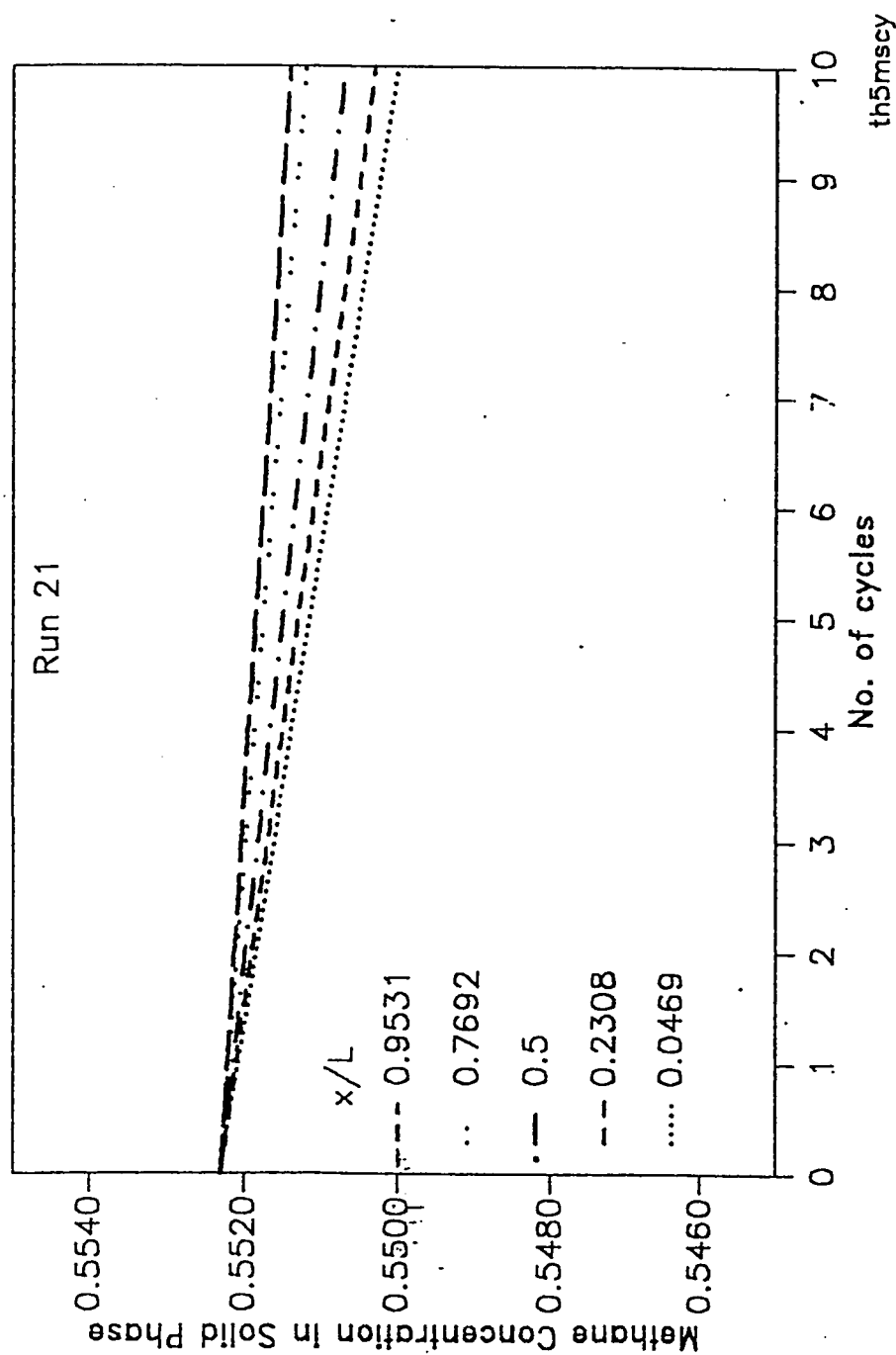


Fig 5.23 Methane Concentration in Solid Phase at specific points in the Column as a function of No. of Cycles

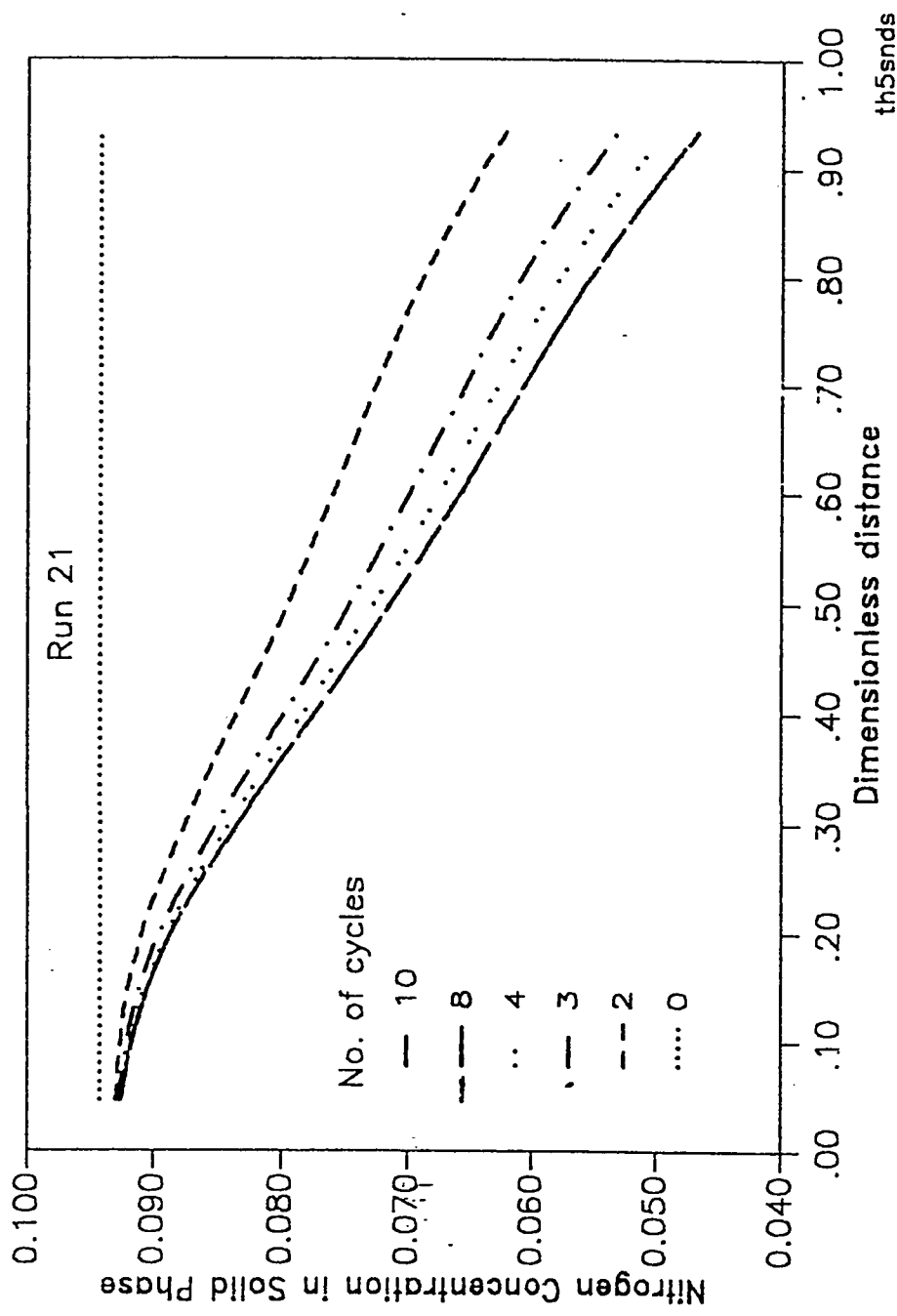


Fig 5.24 Nitrogen Concentration in Solid Phase along the Column with No. of Cycles as a parameter

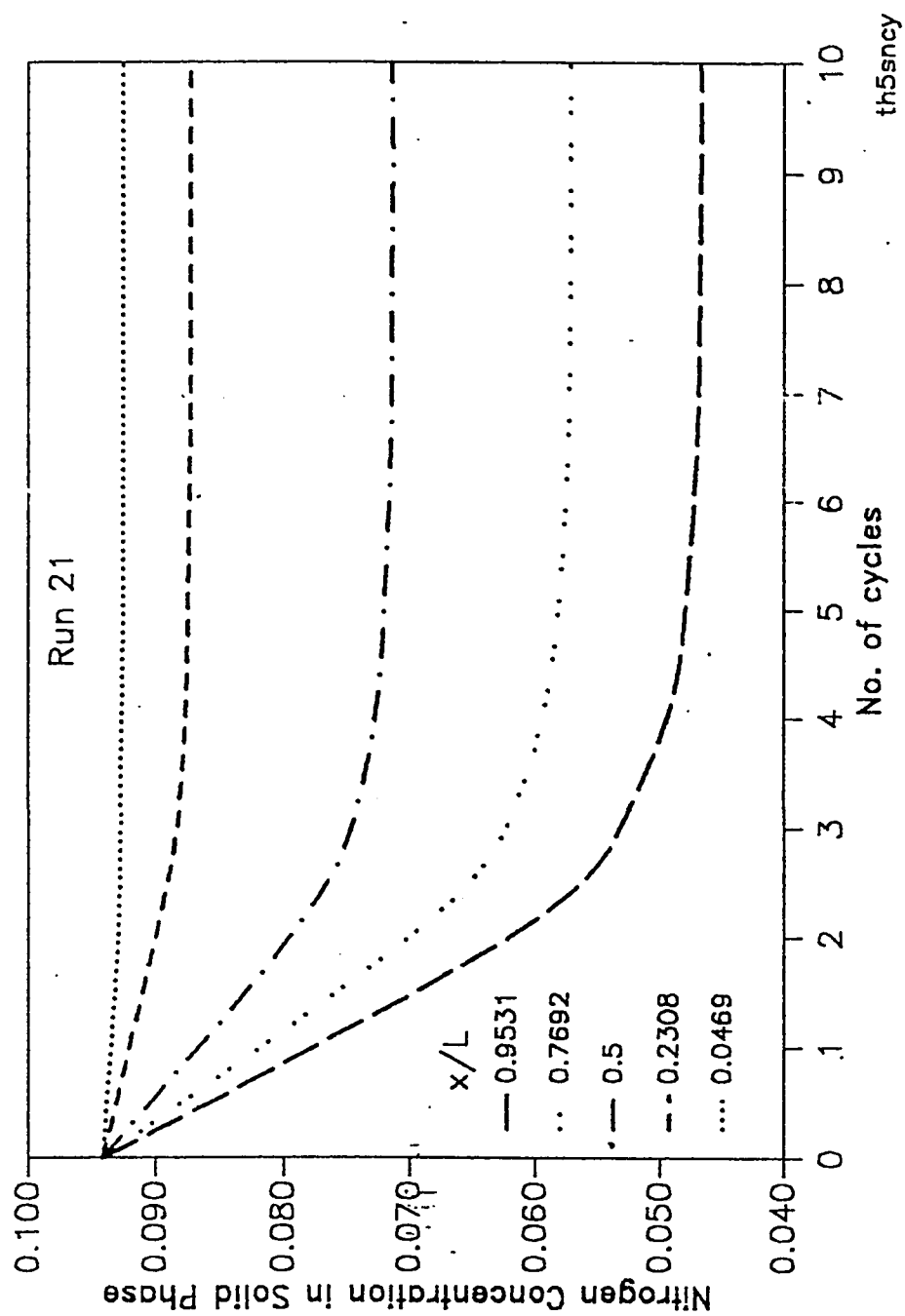


Fig 5.25 Nitrogen Concentration in Solid Phase at specific points in the Column as a function of No. of Cycles

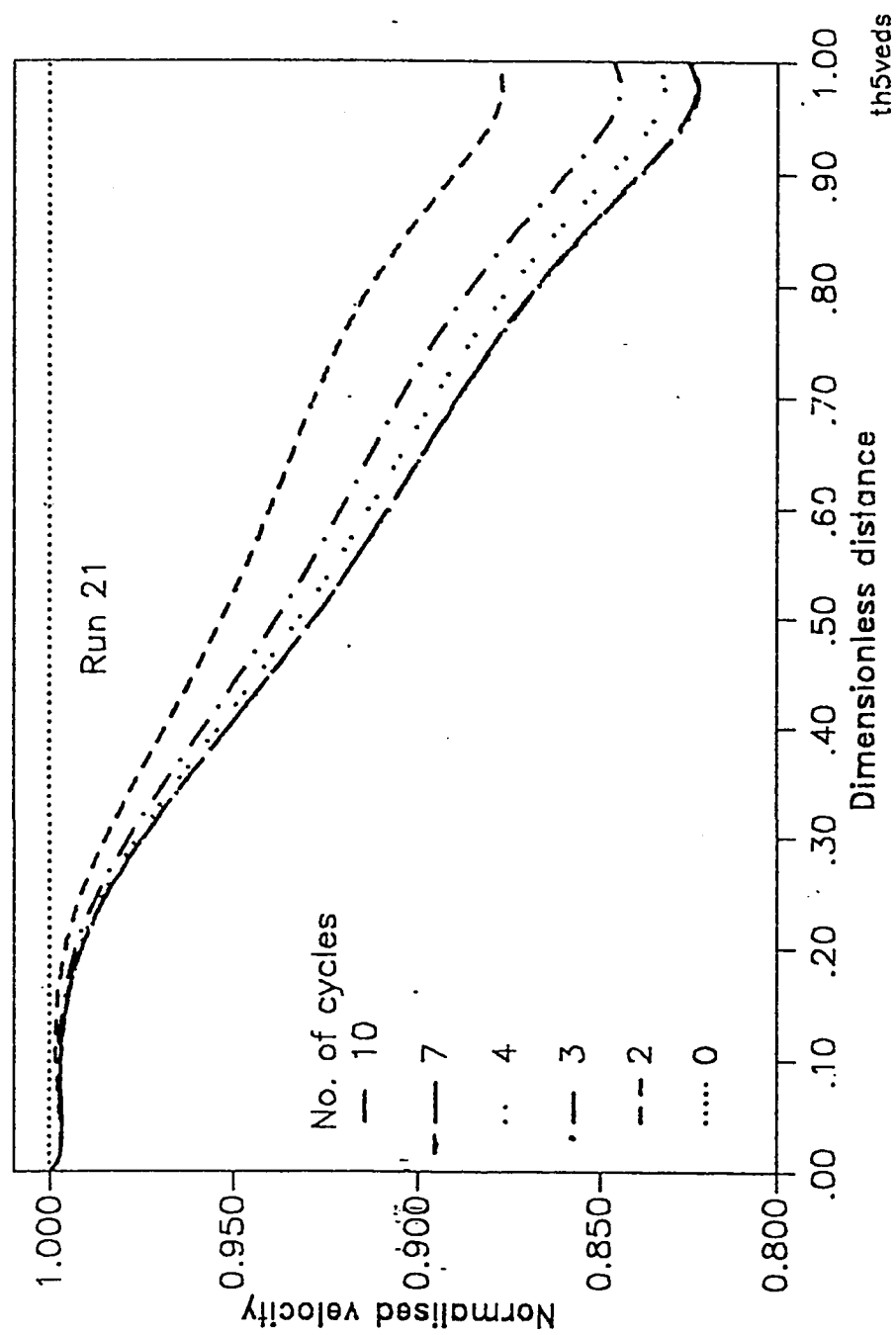


Fig 5.26 Normalised Velocity Profile along the Column with No. of Cycles as a parameter

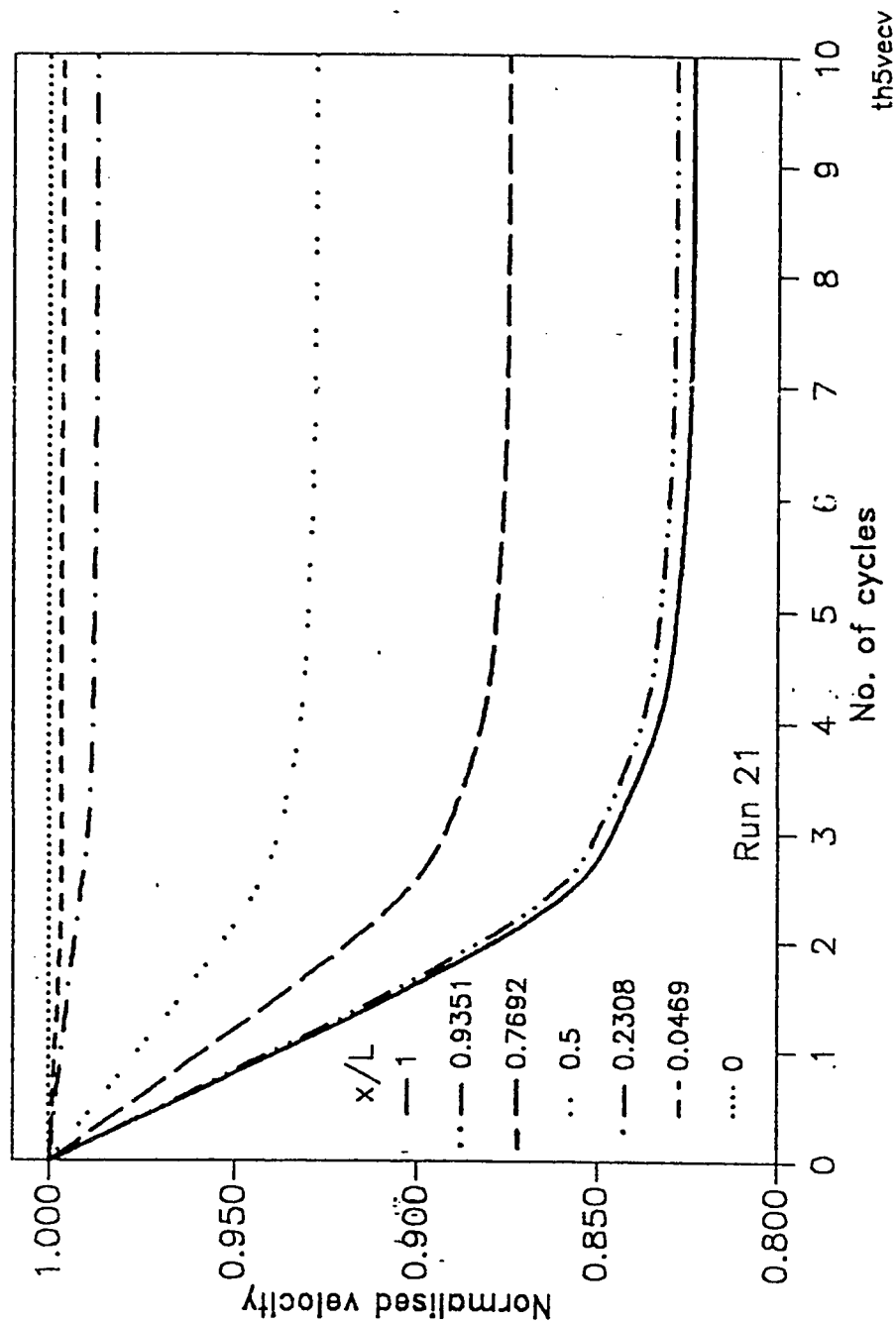


Fig 5.27 Normalised Velocity Profile at specific points in the Column as a function of No. of Cycles;

CHAPTER 6

PSA SEPARATION OF METHANE - NITROGEN MIXTURES ON ZEOLITE 4A

6.1 Introduction

Kinetic separation is achieved, in principle, by virtue of difference in diffusion rates which is higher for nitrogen as compared to methane in 4A zeolite. Although simple in principle it is a difficult separation in practice. The only kinetic PSA separation using zeolite 4A that is studied in the literature is air separation. In case of nitrogen methane mixture no previous study has been done using 4A zeolite but some study has been reported using carbon molecular sieve as presented in the earlier chapter. An advantage of 4A zeolite over carbon molecular sieve is the uniformity of pore opening leading to better selectivity. In this chapter a brief review of PSA processes using 4A zeolite is presented followed by PSA experiments performed using model methane nitrogen mixtures under various conditions of flowrates, pressure, purge to feed ratio and cycle time. Also an existing kinetically based separation model is applied to fit the experimental data.

6.2 Literature Review

Kinetic separation of binary mixtures using PSA has been studied and exploited in a limited way. The earliest study on the concept for producing

nitrogen from air using zeolite 4A came from Keller as a patent (1). Separation of air using molecular sieve carbon (MSC) is an example of commercialization of a kinetic separation process(2). Shin and Knaebel studied nitrogen separation from air with 4A zeolite theoretically(3) and tested the model with experiments on air separation using sieve RS-10 (4). Keller and Yang(5) experimentally studied the separation of nitrogen from air with 4A zeolite with regards to improving the nitrogen recovery by introducing a delay step, cocurrent and counter current blowdown. Kapoor and Yang (6) studied the kinetic separation of landfill gas into methane and carbon dioxide by MSC. Zahur (7) studied air separation with 4A zeolite to recover both oxygen and nitrogen by adjusting the operating parameters. It is evident from this brief review that most experimental and theoretical studies on 4A zeolite are dedicated to air separation and till date no experimental or theoretical study on methane - nitrogen separation with 4A zeolite has been done.

6.3 Theoretical Modeling and Simulation

For the simulation of a kinetic separation process the two main approaches are the rigorous pore diffusion model as presented by Raghavan et al.(8), Shin and Knaebel(3) and Farooq and Ruthven(9), or the linear driving force(LDF) model approximation as presented by Hassan et al.(10,11), Kapoor and Yang(6) and Farooq and Ruthven(12). The pore diffusion model is quite rigorous and closer to reality but is quite cumbersome to solve particularly for a new system

while the LDF model is easier to solve and gives reasonably good results. For the simulation of methane nitrogen separation on 4A zeolite the model developed by Hassan et al.(10), for use in nitrogen separation from air on MSC has been used.

The model equations were formulated in chapter 5, were written in a dimensionless form (see Appendix A.3) and solved by the method of orthogonal collocation to give the velocity as well as the gas and solid phase concentration profiles as a function of dimensionless bed distance for the real time simulation.

The essential parameters in the model are axial dispersion coefficient, D_L , the Langmuir constants b_A , b_B , q_{As} , q_{Bs} and the linear driving constants k_A , k_B . The axial dispersion coefficient is calculated using equation 5.20. The Langmuir constants were estimated in Chapter 4. It is worthwhile to mention that although the Henry law constant for methane and nitrogen are reported in the literature, the fit to a Langmuir isotherm is not exact and hence these values were used as a guideline for simulation studies and modified within limits. The ratio of $K_{CH_4} : K_{N_2}$ was retained as 3 as observed in the reported data.

One of the key parameter in a kinetic separation simulation is the estimation of linear driving force (LDF) constants k_{CH_4} and k_{N_2} . This LDF constant is a lumped parameter of the various resistances added together. Assuming that micropore diffusion controls the process, the LDF approximation for a component A is written as

$$k_A = \Omega_A \frac{D_{cA}}{r_c^2}$$

The value of Ω_A was obtained by Gluckauf(13) to be 15 for the spherical diffusion in a sphere for a step change boundary conditions. Later this was modified, for cyclic adsorption processes through a study of a single particle under cyclic boundary conditions, by Nakao and Suzuki(14). They observed a cycle time dependency and conclude that a value of 15 is only true for the case when θ , the half cycle time, is close to 0.1. This study was done on single component adsorption. For low cycle time, the value of Ω was as high as 100 while the lower limit was about π^2 . Lately Buzanowaski and Yang(15,16) presented the LDF approximation as a sum of two terms. The second term was added to account for the cycle time variations. In the present study the Ω parameter for both components was taken as 15 based on Gluckauf's approximation to begin with and subsequently adjusted.

6.4 Apparatus

6.4.1 Two Column PSA unit.

The two column unit described in Chapter 5 was used for the experiments. The only obvious modification was to pack it with 4A zeolite rather than CMS. Details on the columns are given in Table 6.1.

6.4.2 Description of a Single column PSA unit.

A schematic diagram of a single column PSA unit is shown in Fig. 6.1. The stainless steel column (dia. 3.45 cm, length 35 cm.) was packed with Linde 4A zeolite. The column was connected at one end by 1/4 " SS tubing through a three way solenoid valve for introduction of the the high pressure feed stream to the column and release of the blowdown and purge. The feed gas enters through an electronic mass flow indicator and controller from the high pressure cylinder. At the other end of each column a three way solenoid valve either directs the product to the the flare system through a sampling loop, or introduces a purge gas through an electronic mass flow indicator and controller and a two way solenoid valve.

Sequential switching of the two and three way solenoid valves was controlled by Xanadu universal programmable timer. The flow rates of feed, product and purge streams were monitored and controlled using Matheson flow indicators and controllers and the corresponding continuous output obtained on strip chart recorders. The product and purge stream were analysed by withdrawing gas samples through a manual sampling loop on Gow Mac gas chromatograph and the output obtained through Hewlett Packard Integrator. Details of the instrument specifications are listed in Appendix A.2.

6.5. Procedure

6.5.1 Two Column Unit:

The packed columns were regenerated overnight at 150° C with helium flowing through it to remove the adsorbed moisture ($\approx 22\%$). The experiments were performed with two model feeds (40% and 8% nitrogen in methane) and in accordance with the usual two bed four step PSA cycle described in the earlier chapter. Feed was introduced at high pressure in one column while the other column was desorbed, in most of the runs, by blowdown and purging with a part of the product stream at atmospheric pressure. In some of the runs vacuum blowdown and purge was used. Continuous methane or nitrogen analysis, although very much desired, was not possible and as a result the product and purge stream were analysed intermittently. Sampling time was limited to one every 2-3 minutes; hence only one sample was taken at a time when the sorption step was about to end i.e. 2 sec prior to the end of adsorption or desorption step. In case of short cycle time a sample was analysed once every 3 - 4 cycles. Sampling was not done for the vacuum desorption step. The necessary data and parameters used in the experiments are listed in Table 6.1. The raw data obtained from the experimental runs are listed in Appendix A.1.

6.5.2 Single column Unit:

The packed column was regenerated overnight at 150° C with helium flow to remove the adsorbed moisture ($\approx 22\%$). The experiments were performed with two model feeds (40% and 8% nitrogen in methane) and in accordance with the usual one bed PSA cycle. Feed was introduced at high pressure from the bottom of the column while the top of the column was shut during pressurization step and open during the adsorption step to withdraw the product. During blowdown the bottom of column is either opened to atmosphere or vacuum while the top of the column is shut. In case of atmospheric purge, gas is introduced from the top while the bottom is open to atmosphere. In case of vacuum purging the condition is same as blowdown. The product and purge stream were analysed periodically. Sampling time was limited to one every 2-3 minutes. A sample was taken 2 sec prior to the end of adsorption or desorption step. In case of short cycle time a sample was analysed once every 3 - 4 cycles. Sampling of the purge was not done for the vacuum desorption step. The necessary data and parameters used in the experiments are listed in Table 6.1. The raw data obtained from the experimental runs is listed in Appendix A.1.

6.6 Results and Discussion

PSA experiments were performed in two column as well as single column units with the basic objective of reducing nitrogen in the high pressure product stream. The experiments were done in the two column set up initially and later

followed with single column unit. Although a continuous methane analysis for the product and purge was desirable, the analysis in the present study was intermittent as it was done by gas chromatograph. Due to this limitation the results were studied for cyclic steady state conditions; however, samples were also analysed during the initial unsteady state period. In some cases samples were also analysed for the complete duration of the cycle after the cyclic steady state conditions were reached. The raw experimental data is presented in Appendix A.1. A summary of the two column experiments is presented in Table 6.2. The essential parameters studied along with the cyclic steady state concentration as well as maximum concentration during the cycle are presented. The maximum concentration during the course of a cycle at cyclic steady state, when measured, is shown in the last column of the Table and it is tabulated as the steady state concentration otherwise. Runs 1-24 were performed at ambient temperature and Runs 25, 26 at 90°C. A general observation for all the runs indicate that exit methane concentration is close to as well as less than the feed concentration. This indicated that there was practically no separation and the effect of varying parameters such as cycle time (Run 1-6), purge to feed ratio (Runs 2-4 and 7-9) also had practically no effect on the separation. Different velocities i.e. different $\frac{L}{v_H}$ ratio and pressure also has no effect on the separation. The reasons that lead to such behaviour are :

- 1.) Kinetics is favouring nitrogen which is diffusing faster than methane while equilibrium is favouring methane which is more strongly adsorbed. This opposing behaviour reduces the separation selectivity. Similar situation is observed in case of air separation on zeolite 4A.
- 2.) High pressure exit stream used as a low pressure purge is not rich enough in methane to clean the other column of nitrogen and this spiraling effect tends to lower separation efficiency.
- 3.) The adsorption and desorption time are always the same for a two column system due to symmetry of operations and this limitation is a handicap in system where the adsorption and desorption times are different.

The first reason is ruled out since in case of a kinetic separation with increasing cycle time there should be a rise in methane exit concentration till an optimum is reached after which there will be a decline. This behaviour can be explained because more nitrogen diffuses with increased time to the limit when sufficient methane starts diffusing and getting adsorbed. This was not observed as indicated by Runs 1-6. The second reason was ruled out from the results of Runs 24-26. In these runs the columns were saturated with pure methane prior to cycling thereby maintaining a high concentration of methane in the purge stream for the first few cycles but the cyclic steady state concentration was no different from the earlier case. Vacuum purging was not used for the two col-

umn unit since it reduces to two single column setup in series but with a limitation of equal adsorption and desorption time. This alternative was explored on the single column unit later on. Since no separation had been obtained on the two column units, single column experiments were performed to study the effect of the different adsorption and purge times, and the effect of pure gases as purge and vacuum purge.

Results of the single column PSA experiments are summarized in Table 6.3. The objective of these experiments were to study the effect of methane, helium and vacuum purging as well as different adsorption and purge duration on the methane nitrogen separation. Runs 1-4 were performed using methane as a purge gas. In Run 1 the overall concentration of methane entering the column, 60% in the feed and pure methane in the purge, is about 73%. A cyclic steady state exit concentration of 82% (Run 1) and a peak concentration of 94% implies an effective enrichment of more than 9%. Also for Runs 2-4 a similar calculation indicates that enrichment occurs. Use of methane as a purge gas confirms that separation is viable provided better desorption of nitrogen is achieved. Since methane is the desired end product, use of pure methane as purge is not of much importance. The other alternative was to use helium, an inert gas, as a purge. Runs 5-24, 43-45 were done using helium as a purge gas under various operating conditions. Run 5 was done under conditions of equal adsorption and purge duration using helium as a purge. No enrichment of methane was observed. In Run 6, the purge period is thrice the adsorption time and

also the latter is same as Run 5 as the cycle time is doubled. A 7% increase in the methane concentration is observed. A longer period for purging the bed is needed because of two factors. First, the diffusion favours nitrogen while equilibrium favours methane but this is true also for oxygen nitrogen separation on zeolite 4A and yet it is possible to separate them with symmetric operations. This is due to the second reason namely that the absolute value of the adsorption equilibrium constants for methane and nitrogen are much higher than nitrogen and oxygen and hence a larger amount of these species are adsorbed.

Improvement in the separation due to a longer purge duration was further refined by merging the pressure and adsorption step which in effect gives more time for the adsorption step. Runs(7-24) were performed with this option. Runs 7-13 indicates for the effect of cycle time showing the expected gradual increase in methane concentration till an optimum of 77% (Run 11) is achieved and then a drop further on. Comparison of Runs 9-11 and 14-16 indicate that a higher pressure ratio is not favourable. From Runs 7-13 and Runs 21-24 the expected improvement in concentration due to a higher L/v_H for the same purge flow rate was observed. The purge to feed ratio is different in the two cases.

Another alternative to inert gas purging was vacuum. Although this process implies an extra energy input it is used as a viable alternative when high pressure product used as a purge stream is not sufficient to clean the bed. Runs 25-42 were performed with vacuum purge. Runs 21-24 and 25-29 indicate the

relative performance of the inert gas and vacuum purging. Vacuum purging, although less efficient, is preferable to inert gas purging since the latter introduces an extra component in the mixture. With the exception of cycle time there is a negligible effect of pressure (Runs 26-27 and 31-32) or L/v_{II} (Runs 30-33 and 34-36) on the exit concentration.

Runs 41-45 were done for the model feed containing 92% methane in nitrogen. Observations were similar to those obtained above. The experimental results from two column and single column units were quite apart. There was depletion from 60% in feed to 55% in product in the former and enrichment up to 82% in the latter.

Simulation and correlation of this diverse experimental data was done using the mathematical model described earlier in the chapter which was solved using orthogonal collocation. The parameters needed for this dynamic model were the axial dispersion coefficient, adsorption equilibrium as well as the mass transfer coefficients. For a start these were either computed through correlations (e.g. D_L) described earlier or taken from literature (D/r^2 , b , q_s), as presented in Chapter 4, and listed in Table 6.1. The mass transfer coefficients for the solid phase were described by the linear driving force approximation and is related to the diffusional time constant as $\Omega D/r_c^2$, where Ω is a function of dimensionless cycle time and was described earlier. This parameter varies with cycle time and is adjusted for each cycle time. Simulation using the above data was performed

based on Run 4 of the single column experiment. Two column experiments were not chosen because of poor separation. Result of the simulation indicated a 95 % exit concentration as compared to the 78% in the experiment suggesting that the model cannot be used as a predictive tool based on literature data as stated.

The difference in the simulated and experimental results makes it necessary to review the the assumptions and the approximations in the model and also the parameter data taken from literature. The approximation of frozen solid phase concentration during pressurization and blowdown, although more valid for shorter cycle times, was introduced for simplifying the model. Assumption of Langmuir isotherm as a non linear equilibrium relationship for methane and nitrogen is for the sake of convenience and is reasonable. The mass transfer rates represented by linear driving force approximation is a simplification of the rigorous pore diffusion model and mass transfer therein is a function of the controlling micropore diffusion resistance. The equilibrium and kinetic parameters for methane and nitrogen on the zeolite 4A sample used in the experiments were not experimentally determined but were abstracted from the literature, from the range of values, as presented in Chapter 4. These values were used as a guideline to begin with and are subject to change within practical limits. From the discussion it is evident that in order to correlate the data, with this simplified model, the effect of essential parameters need to be tested. Among the parameters L/v_H and dispersion coefficient are fixed in the model and hence the remaining parameters that can be adjusted are the adsorption equilibrium constants

and mass transfer rate constants.

The effect of varying Ω for each component, keeping the D/r^2 fixed, in the mass transfer rate constant, $\Omega D/r^2$, was studied for Run 4. The equilibrium constants for methane and nitrogen were fixed at 27 and 9 respectively and Ω factor, obtained from Fig 1.2, were 45 and 15 according to Suzuki's plot and 30 and 15 according to Hassan et al's plot for an adsorption step of 24 seconds. The exit concentration, shown in Table 6.4 for these conditions is 94% and is far greater than the experimental value of 78%. The simulated exit concentration, by varying Ω_{N_2} from 1 to 15 and the $\Omega_{CH_4} : \Omega_{N_2}$ ratio from 1 to 6, are also shown in the Table 6.4. This data is plotted in Fig. 6.2. The experimental and simulated data are in good agreement for the following combination

- 1.) $\Omega_{N_2} = 2$ and a wide range of Ω_{CH_4}
- 2.) $\Omega_{CH_4} : \Omega_{N_2}$ at 5 and Ω_{N_2} from 2 to 15.
- 3.) $\Omega_{CH_4} : \Omega_{N_2}$ at 6 and Ω_{N_2} from 2 to 6.

Since only Ω factors were varied a definite combination cannot be made at this stage, however it is clear that Ω_{N_2} is a sensitive parameter. A further study of the effect of equilibrium constants and the behaviour of these combinations on the simulation of the other runs both on single as well as two column units is necessary prior to any conclusions.

It is evident from the above results that Ω 's are lower than the literature values. An alternative is to use lower values of adsorption equilibrium constant, hereafter referred to as K . Table 6.5 illustrates the effect of reducing the values of K from 27 and 9 to 3 and 1 for methane and nitrogen respectively. For this case Ω_{N_2} is between 10 and 15 and the methane to nitrogen Ω ratio in the range of 1 to 3 results in good agreement between experiment and simulation. This data is plotted alongside the earlier data in Fig. 6.2 and the complementary effect of mass transfer and equilibrium is evident.

The simulation was further studied for several combination of K values and Ω ratios with $\Omega_{N_2} = 3$ and the data is presented in Table 6.6. Ω_{N_2} was kept 3 and not 15 because the latter is not acceptable for the two column simulation, as discussed later. The above study establishes the acceptable range of the K and Ω values for further correlation of different runs with varying L/v_{II} and D_I values but the same cycle time. The three set of options for fitting the experimental data of Run 4 are :

- (1) Equilibrium constants at the reported values of 27 and 9 for methane and nitrogen respectively and $\Omega_{N_2} = 2$ and a wide range of Ω_{CH_4} value.
- (2) Equilibrium constants at a low value of 3 and 1 for methane and nitrogen respectively and $\Omega_{N_2} = \Omega_{CH_4} \approx 15$
- (3) Equilibrium constants at the reported values of 27 and 9 for methane and nitrogen respectively and $\Omega_{N_2} \approx 15$ and $\Omega_{CH_4} \approx 75$.

In order to select a set of optimized parameters for correlating the other data, the first option is most suited for the following reasons. The second option implies a lower equilibrium adsorption, a possibility when pores are blocked or the sieve has some moisture due to improper regeneration. This was not the case since fresh zeolite was regenerated at 200 °C with helium. The third option is an effective reduction in the mass transfer resistance to methane(higher Ω), based on the literature data, while the first option is an increase in the mass transfer resistance to nitrogen. The latter is more likely either due to coupling effect of a binary mixture or some unaccounted resistance. Also the value of Ω is based on a study of single component diffusion in a spherical particle(13). The third option does not yield acceptable results for two column simulation as discussed later. The first option was henceforth used as a basis for optimizing the parameters.

The parameter Ω_{N_2} is the critical parameter and was the criteria for optimization. With Ω_{CH_4} at 15 and varying Ω_{N_2} , from 2 to 15, Runs 1-3 of the single column experiments were simulated and the results form a part of Table 6.7. The K values were fixed at 24 and 8, although one set was tested for a different K value(27:9). Simulation with values of $\Omega_{N_2} = 10, 15$ and $\Omega_{CH_4} = 50, 55, 75$ were also performed for reasons to follow and these are in good agreement with the experimental data. The Root Mean Sum of Square(SS) for each combination is obtained and is plotted only for the case when all parameters are fixed

except Ω_{N_2} . The plot in Fig 6.3 goes through a minima at $\Omega_{N_2} \approx 3$. The simulation was also performed for Runs 19, 16, 20, 23 of the two column experiments with $\Omega_{N_2} = 3, 4.5$, and 15 and the results are presented in Table 6.8. The results are in good agreement for the first two values but lead to unacceptable results for $\Omega_{N_2} = 15$ and $\Omega_{CH_4} = 75$. This leads to the conclusion that although $\Omega_{N_2} = 15$ is the literature supported value, it is not applicable and instead a lower value of $\Omega_{N_2} = 3$ is appropriate for the diverse experimental results.

The low value of 3 for Ω_{N_2} is justified by the fact that the D/r^2 values for the 4A zeolite were abstracted from literature (Table 4.1) and not measured for the current study. A glance at Table 4.1 indicates a wide variation in these values obtained by different workers. The abstracted value is on the higher side and if the actual sample value is lower it would result in a higher Ω value in the results.

Simulation was restricted to these runs since the Ω value for different cycle time had to be optimized separately and fitted with the data making it a repeat exercise. The program based on the model presented in the earlier section was not applicable in case of vacuum desorption as well as three component system with helium as inert. However the main objective of simulating the diverse data under different conditions using the same model and parameters was achieved.

The experimental and simulated product concentration is shown in Fig 6.4 for Run 4 (single column). The model shows a lag in reaching the cyclic steady state (after 5 cycles experimentally) but considering the simplification in the model this is a satisfactory fit.

The gas phase profile for methane and the solid phase profile for methane and nitrogen at the end of the adsorption step, in a single column experiment (Run 4), are shown in Figs 6.5 to 6.10 respectively. The K and Ω values were fixed at 27 and 15 for methane and 9 and 3 for nitrogen respectively for these plots. Figs 6.5 to 6.7 are plots of the axial profiles of the gas and solid phase for methane and nitrogen at different cycles during the course of the experiment while Figs 6.8 to 6.10 are plots of the gas and solid phase profiles for methane and nitrogen, at specific locations in the column, with progressing cycles during the course of the experiment. The solid phase solution is only for the interior points. The initial saturated bed condition is obvious from the uniform concentration in the solid phase and the gas phase at the feed concentration throughout the column. The gas phase profiles are shown in Figs 6.5 and 6.8. Axial profile in Fig 6.5 indicates a breakthrough half way down the column with a slight dip close to the entrance and a steady rise towards the exit with regard to methane concentration. The slight dip could be either due to more nitrogen in the gas phase as a result of displacement desorption or a numerical offset. Approach to cyclic steady state conditions also is evident. The solid phase concentration profiles of methane and nitrogen indicates the transition from saturation at the

start to the cyclic steady state conditions. Equilibrium concentration in the solid phase exists at zero time and drops with cycling for both for methane and nitrogen indicating the unsteady conditions prevailing during the adsorption step. In case of nitrogen (Figs 6.7 and 6.10) it drops both with time and distance but reaches cyclic steady state conditions in 10 cycles and has a lower value near the exit corresponding to a low gas phase concentration. In case of methane (Figs 6.6 and 6.9) it drops initially both with time and distance but increases later on to values both lower and higher than the initial saturation. This is consistent with the higher gas phase concentration near the exit. Cyclic steady state conditions are reached more slowly as compared to nitrogen due to slower diffusion and stronger adsorption.

This simulation was not performed for runs with helium and vacuum purging since the model is not applicable to these cases. In case of inert gas purging along with two adsorbable components, the system is a two transition system with two individual mass transfer zones and the model required is beyond the scope of the present study but a recommendation for future study. In case of vacuum purging since there is no purge gas entering the bed from one end and the gas in the bed is being removed through vacuum at the other end, the fluid phase mass balance and the boundary conditions for the blowdown and purge step of the present model needs to be changed. The pressure drop across the bed will be of the same order of magnitude as the absolute pressure leading to variable pressure during the course of the purge step. Also the approximations introduced during blowdown are not applicable due to variable pressure.

Simulation of the one and two column experiment resulted in the linear driving force parameter, Ω , for nitrogen to be lower than expected by a factor of 5. This reduces Ω to a correlative tool rather than a predictive tool. A reason for this could be a higher value of the D/r^2 for the 4A zeolite, used in the experiment, than the available literature data. A recommendation in this context is to measure the diffusional time constant of nitrogen and methane in this particular zeolite sample after which further comments on Ω can be made.

The present study was done on a two column unit without much success: a good degree of separation was obtained on single column by using different step duration, vacuum and inert gas purging. The other way to obtain a higher purity is to either use multiple columns, three and more, and manipulate the operation for a longer purge step to adsorption time ratio.

6.7 Conclusions

Experimental PSA studies were done separately on single and two column units packed with zeolite 4A adsorbent. Two model methane nitrogen feeds (8% and 40% nitrogen in methane) were studied. In the two column experiments a four step PSA cycle was used with a portion of high pressure product as purge gas. Experiments were performed at ambient temperature with the exception of two runs at 90 ° C. No significant separation was achieved even with limiting values of L/v_{II} purge to feed ratio. It was concluded that the desorption time

was insufficient. Unequal sorption time was not possible with two column operations; hence single column experiments were performed in the usual 4 step cycle. Pure methane was used as the purge gas. An effective enrichment of 21% was obtained (with 60% methane feed). Experiments with unequal adsorption and desorption time with helium as well as vacuum purging were performed. Helium purge pushed concentration up to 85% while vacuum desorption was less effective and the concentration reached 74%. For the 92% feed the concentrations achieved were 96.5% and 95.5% respectively.

Simulation studies to interpret the selected experimental results were done with an LDF kinetic model. Simulation with vacuum desorption and helium purging were not considered due to non applicability of the model at present. The LDF approximation based on micropore diffusion time constant, obtained from literature, predicted a very high concentration ($> 94\%$). The effects of modifying the equilibrium and kinetic parameter was studied and the LDF factor for nitrogen, Ω_{N_2} , was found to be most sensitive. An optimised low value of 3 (instead of 15) correlated the diverse results in acceptable limits. The low value suggests a lower diffusional time constant data than in the literature for this particular sample.

REFERENCES

- (1) Keller II, G. E., and Kuo, C. A., U. S. Patent 4,354,859 (1982).
- (2) Yang, R. T., Gas Separation by Adsorption Processes, Butterworths, 1987.
- (3) Shin, H. S., and Knaebel, K. S., AIChE J., 33, (4), 654, (1987).
- (4) Shin, H. S., and Knaebel, K. S., AIChE J., 34, (9), 1409, (1988).
- (5) Keller II, G. E., and Yang R. T., New Directions in Sorption Technology, pgs. 61-67, Butterworths, 1989.
- (6) Kapoor, A., and Yang, R. T., Chem. Eng. Sci., 44, 1723, (1989).
- (7) Zahur, M., M. S. Thesis, KFUPM, Dhahran, 1991.
- (8) Raghvan, N. S., Hassan, M. M., and Ruthven, D. M., Chem. Eng. Sci., 41, 2787, (1986).
- (9) Farooq, S., and Ruthven, D. M., Chem. Eng. Sci., 46, 2213, (1991).
- (10) Hassan, M. M., Ruthven, D. M., and Raghvan, N. N., Chem. Engg. Sci., 41, 1333, (1986).
- (11) Hassan, M. M., Raghvan, N. S., and Ruthven, D. M., Chem. Engg. Sci., 42, 2037, (1987).
- (12) Farooq, S., and Ruthven, D. M., Chem. Eng. Sci., 45, 107, (1990).
- (13) Glueckauf, E., Trans. Faraday Soc., 51, 1540 (1955).
- (14) Nakao, S. I., and Suzuki, M., J. of Chem. Engg. Japan 16, 114, (1983).
- (15) Buzanowaski, M. A., and Yang, R. T., Chem. Eng. Sci., 44, 2683, (1989).
- (16) Buzanowaski, M. A., and Yang, R. T., Chem. Eng. Sci., 46, 2589, (1991).
- (17) Fernandez, G. F., and Kenney, C. N., Chem. Engg. Sci., 38, 827, (1983).

Table 6.1
Experimental Conditions and Parameters
used in the simulation for two column
and single column PSA Unit.

Feed gas composition	60%CH ₄ , 40%N ₂ 92%CH ₄ , 8%N ₂
Column length (two column unit)	51 cm
Column length (single column unit)	35 cm
Cross sectional area of both units	9.35 cm ²
Bed voidage	0.4
Adsorbent	4A zeolite
Amount in each column of two column unit (before regeneration)	430 grams
Amount in single column unit (before regeneration)	292 grams
Particle size	3.18 mm pellets
Equilibrium constant for CH ₄	24
Equilibrium constant for N ₂	8
Saturation constant for CH ₄ & N ₂	0.005 $\frac{\text{mole}}{\text{cm}^3}$
Diffusional time constant for CH ₄ (D/r ²)	6.28 x 10 ⁻⁴ sec ⁻¹
Diffusional time constant for N ₂ (D/r ²)	5.52 x 10 ⁻³ sec ⁻¹

Table 6.2 : Summary of two column experiments with zeolite 4A

Run No.	Temp. ° C	Feed concn. CH ₄	velocity cm/sec	$\frac{P_H}{P_L}$	Purge to feed ratio	Cycle time sec.	Purge gas	Initial bed condition	Step duration ratio(*)	Concn. steady state	Concn. profile max.
1	25	60	0.62	3:1	2.14	30	product	sat/feed	1:4:1:4	54.56	54.56
2						60	product	sat/feed	1:4:1:4	53.05	53.05
3						90	product	sat/feed	1:4:1:4	53.79	53.79
4						120	product	sat/feed	1:4:1:4	55.00	55.00
5						180	product	sat/feed	1:4:1:4	58.31	58.31
6						240	product	sat/feed	1:4:1:4	60.56	60.56
7	25	60	0.62	3:1	1.71	60	product	sat/feed	1:4:1:4	54.12	54.12
8						90	product	sat/feed	1:4:1:4	53.42	53.42
9						120	product	sat/feed	1:4:1:4	54.05	54.05
10	25	92	0.53	3:1	2.17	60	product	sat/feed	1:4:1:4	90.21	90.21
11						90	product	sat/feed	1:4:1:4	90.53	90.53
12						120	product	sat/feed	1:4:1:4	90.57	90.57

(*) Pressurisation:adsorption:blowdown:purge

(...contd.)

Table 6.2 (contd.)

Run No.	Temp. ° C	Feed concn. CH ₄	velocity cm/sec	$\frac{P_H}{P_L}$	Purge to feed ratio	Cycle time sec.	Purge gas	Initial bed condition	Step duration ratio	Concn. steady state	Concn. profile max.
13	25	92	1.19	4:1	2.17	30	product	sat/feed	1:4:1:4	90.85	90.85
14						30	product	sat/feed	1:4:1:4	90.94	90.94
15	25	60	0.75	4:1	2.92	30	product	sat/feed	1:4:1:4	54.60	54.60
16	25	60	0.94	2:1	1.24	60	product	sat/feed	1:4:1:4	56.11	56.74
17						90	product	sat/feed	1:4:1:4	57.85	57.85
18						40	product	sat/feed	1:4:1:4	56.53	56.87
19	25	60	1.26	2:1	0.88	60	product	sat/feed	1:4:1:4	56.25	56.25

(...contd.)

Table 6.2 (contd.)

Run No.	Temp. ° C	Feed concn. CH ₄	velocity cm/sec	$\frac{P_H}{P_L}$	Purge to feed ratio	Cycle time sec.	Purge gas	Initial bed condition	Step duration ratio	Concn. steady state	Concn. profile max.
20	25	60	0.76	2:1	1.24	60	product	sat/feed	1:4:1:4	53.34	53.72
21						90	product	sat/feed		53.31	53.95
22	25	60	0.51	3:1	1.85	90	product	sat/feed	1:4:1:4	52.66	52.80
23	25	60	0.67	2:1	0.93	60	product	sat/feed	1:4:1:4	53.60	53.60
24	25	60	0.94	2:1	1.0	60	product	sat/methane	1:4:1:4	53.65	53.65
25	90	60	0.94	2:1	1.14	60	product	sat/methane	1:4:1:4	57.39	57.39
26	90	60				30	product	sat/methane	1:4:1:4	54.42	54.42

Table 6.3 : Summary of single column experiments with zeolite 4A

Run No.	Temp. ° C	Feed concn. CH ₄	velocity cm/sec	$\frac{P_H}{P_L}$	Purge to feed ratio	Cycle time sec.	Purge gas	Initial bed condition	Step duration ratio(*)	Concn. steady state	Concn. profile max.
1	26	60	1.26	2:1	0.93	60	methane	sat/feed	1:4:1:4	81.64	94.42
2	26	60	0.58	2:1	2.03	60	methane	sat/feed	1:4:1:4	98.82	98.82
3	26	60	1.57	2:1	0.45	60	methane	sat/feed	1:4:1:4	77.32	77.32
4	26	60	0.95	2:1	0.74	60	methane	sat/feed	1:4:1:4	77.48	77.48
5	26	60	0.95	2:1	1.08	60	helium	sat/feed	1:4:1:4	55.71	55.71
6						120	helium	sat/feed	1:2:1:6	59.94	62.26
7	26	60	1.26	2:1	0.81	120	helium	sat/feed	3:1:6	64.08	64.08
8						150	helium	sat/feed	3:1:6	70.02	70.63
9						180	helium	sat/feed	3:1:6	73.87	73.87

(*) Pressurisation:adsorption:blowdown:purge / Adsorption:blowdown:purge

(...contd.)

Table 6.3 (contd.)

Run No.	Temp. ° C	Feed concn. CH ₄	velocity cm/sec	$\frac{P_H}{P_L}$	Purge to feed ratio	Cycle time sec.	Purge gas	Initial bed condition	Step duration ratio	Concn. steady state	Concn. profile max.
10						210	helium	sat/feed	3:1:6	76.62	76.62
11						240	helium	sat/feed	3:1:6	77.52	77.52
12						270	helium	sat/feed	3:1:6	75.62	75.62
13						300	helium	sat/feed	3:1:6	76.95	76.95
14	26	60	1.26	4:1	0.81	180	helium	sat/feed	3:1:6	71.72	71.72
15						210	helium	sat/feed	3:1:6	74.03	74.03
16						240	helium	sat/feed	3:1:6	73.77	74.54
17	26	60	0.88	3:1	1.16	210	helium	sat/feed	3:1:6	74.08	74.45
18						240	helium	sat/feed	3:1:6	76.40	76.55

(...contd.)

Table 6.3 (contd.)

Run No.	Temp. ° C	Feed concn. CH ₄	velocity cm/sec	$\frac{P_H}{P_L}$	Purge to feed ratio	Cycle time sec.	Purge gas	Initial bed condition	Step duration ratio	Concn. steady state	Concn. profile max.
19						270	helium	sat/feed	3:1:6	77.49	77.26
20						300	helium	sat/feed	3:1:6	77.83	77.91
21	26	60	0.88	2:1	1.16	300	helium	sat/feed	3:1:6	65.76	75.06
22						360	helium	sat/feed	3:1:6	80.72	80.72
23						390	helium	sat/feed	3:1:6	82.67	82.36
24						420	helium	sat/feed	3:1:6	82.28	82.63
25	26	60	0.88	2:0.1	vac	240	---	sat/feed	3:1:6	72.83	72.88
26						300	---	sat/feed	3:1:6	74.18	74.18
27						330	---	sat/feed	3:1:6	74.22	74.32

(...contd.)

Table 6.3 (contd.)

Run No.	Temp. ° C	Feed concn. CH ₄	velocity cm/sec	$\frac{P_H}{P_L}$	Purge to feed ratio	Cycle time sec.	Purge gas	Initial bed condition	Step duration ratio	Concn. steady state	Concn. profile max.
28						360	---	sat/feed	3:1:6	74.55	74.55
29						390	---	sat/feed	3:1:6	74.21	74.56
30	26	60	0.88	3:0.1	vac	270	---	sat/feed	3:1:6	73.44	73.42
31						300	---	sat/feed	3:1:6	73.85	73.85
32						330	---	sat/feed	3:1:6	73.66	73.86
33						420	---	sat/feed	3:1:6	72.10	72.10
34	26	60	1.26	3:0.1	vac	210	---	sat/feed	3:1:6	72.06	72.40
35						240	---	sat/feed	3:1:6	72.00	72.17
36						360	---	sat/feed	3:1:6	73.44	72.64

(...contd.)

Table 6.3 (contd.)

Run No.	Temp. ° C	Feed concn. CH ₄	velocity cm/sec	$\frac{P_H}{P_L}$	Purge to feed ratio	Cycle time sec.	Purge gas	Initial bed condition	Step duration ratio	Concn. steady state	Concn. profile max.
37	26	60	1.26	2:0.1	vac	210	---	sat/feed	3:1:6	72.13	72.29
38						240	---	sat/feed	3:1:6	73.19	73.24
39						270	---	sat/feed	3:1:6	73.69	73.81
40						300	---	sat/feed	3:1:6	73.86	73.86
41	26	92	1.22	2:0.1	vac	270	---	sat/feed	3:1:6	95.47	95.55
42						300	---	sat/feed	3:1:6	95.50	95.55
43	26	92	1.22	2:1	0.84	300	helium	sat/feed	3:1:6	96.35	96.43
44						300	helium	sat/feed	3:1:6	96.50	96.50
45						330	helium	sat/feed	3:1:6	96.32	96.46

**Table 6.4 : Simulated exit concentration in a single column experiment
as a function of Ω factor of nitrogen and methane.**

Run No. : 4
 Feed velocity = 0.95 cm/sec
 Purge to feed ratio = 0.74
 $K_{\text{CH}_4} : K_{\text{N}_2}$ = 27 : 9
 Expt. exit concn. = 0.78

Ω_{N_2}	Ratio of $\Omega_{\text{CH}_4} : \Omega_{\text{N}_2}$					
	1	2	3	4	5	6
1	0.70	0.70	0.71	0.71	0.72	0.72
2	0.77	0.79	0.80	0.81	0.80	0.79
3	0.82	0.85	0.85	0.83	0.81	0.79
4	0.86	0.88	0.87	0.84	0.81	0.78
5	0.89	0.89	0.88	0.85	0.81	0.77
6	0.90	0.90	0.89	0.86	0.81	0.77
8	0.92	0.92	0.90	0.87	0.81	0.75
10	0.94	0.94	0.92	0.88	0.81	0.75
15	0.95	0.96	0.94	0.90	0.82	0.73

**Table 6.5 : Simulated exit concentration in a single column experiment
as a function of Ω factor of nitrogen and methane.**

Run No. : 4
 Feed velocity = 0.95 cm/sec
 Purge to feed ratio = 0.74
 $K_{\text{CH}_4} : K_{\text{N}_2}$ = 3 : 1
 Expt. exit concn. = 0.78

Ω_{N_2}	Ratio of $\Omega_{\text{CH}_4} : \Omega_{\text{N}_2}$					
	1	2	3	4	5	6
7	0.71	0.72	0.72	0.74	0.75	0.75
10	0.74	0.76	0.78	0.79	0.80	0.81
13	0.77	0.80	0.82	0.83	0.83	0.82
15	0.78	0.82	0.84	0.85	0.84	0.82

**Table 6.6 : Simulated exit concentration in a single column
experiment as a function of Henry Law constants and Ω
factor of nitrogen and methane.**

Run No. : 4
 Feed velocity = 0.95 cm/sec
 Purge to feed ratio = 0.74
 Expt. exit concn. = 0.78

Henry Law constant at 25 C		Ratio of $\Omega_{\text{CH}_4} : \Omega_{\text{N}_2}$ with $\Omega_{\text{N}_2} = 3$		
K_{N_2}	K_{CH_4}	3	4	5
5	15	0.81	0.82	0.82
6	18	0.83	0.83	0.82
7	21	0.84	0.84	0.82
8	24	0.85	0.84	0.82
9	27	0.85	0.85	0.83

**Table 6.7 : Experimental and simulated exit concentration
in a single column along with sum of squares**

Run No.	4	1	3	2		
vel (cm/sec)	0.95	1.26	1.57	0.58		
Purge/feed ratio	0.74	0.93	0.45	2.03		
Exptl. exit concn.	0.78	0.82	0.77	0.98		
$\Omega_{CH_4} : \Omega_{N_2}$	$K_{CH_4} : K_{N_2}$	Simulated exit concn.				SS [@]
15:2	24:8	0.78	0.81	0.68	0.84	0.213
15:3	24:8	0.82	0.86	0.76	0.87	0.144
15:4.5	24:8	0.86	0.91	0.84	0.92	0.172
15:4.5	27:9	0.87	0.91	0.84	0.91	0.183
15:7.5	24:8	0.92	0.95	0.90	0.94	0.254
15:15	24:8	0.95	0.97	0.95	0.97	0.303
50:10	24:8	0.81	0.88	0.80	0.88	0.142
55:10	24:8	0.78	0.85	0.76	0.85	0.157
75:15	24:8	0.81	0.88	0.79	0.88	0.140

$$@ \text{ SS} = \sqrt{\sum \left[\frac{C_{A, \text{expt}}}{C_{A, \text{theory}}} - 1 \right]^2}$$

Table 6.8 : Experimental and simulated exit concentration in a two column unit along with sum of squares

Run No.	19	16	20	23
vel(cm/sec)	1.31	0.93	0.76	0.67
Purge/feed ratio	0.88	1.24	1.24	0.93
Exptl. concn.	0.56	0.56	0.53	0.54

$\Omega_{\text{CH}_4}:\Omega_{\text{N}_2}$	$K_{\text{CH}_4}:K_{\text{N}_2}$	Simulated exit concn.				SS [@]
15:3	24:8	0.49	0.49	0.49	0.51	0.225
15:4.5	24:8	0.57	0.57	0.58	0.59	0.120
75:15	24:8	0.21	0.20	0.20	0.24	3.21

$$@ \text{SS} = \sqrt{\sum \left(\frac{C_{A, \text{expt}}}{C_{A, \text{theory}}} - 1 \right)^2}$$

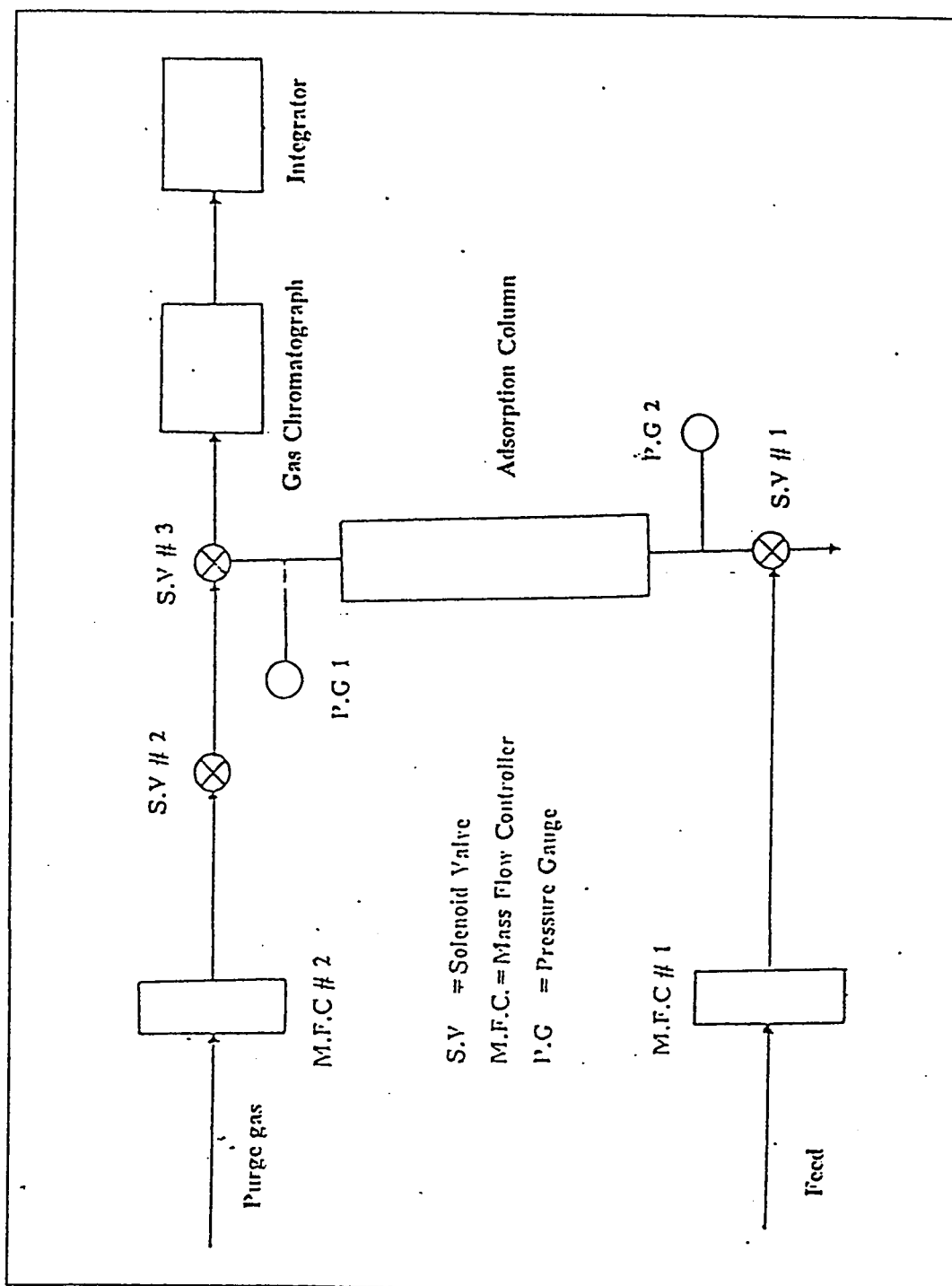


Fig. 6.1 Schematic diagram of the Single Column PSA experimental unit

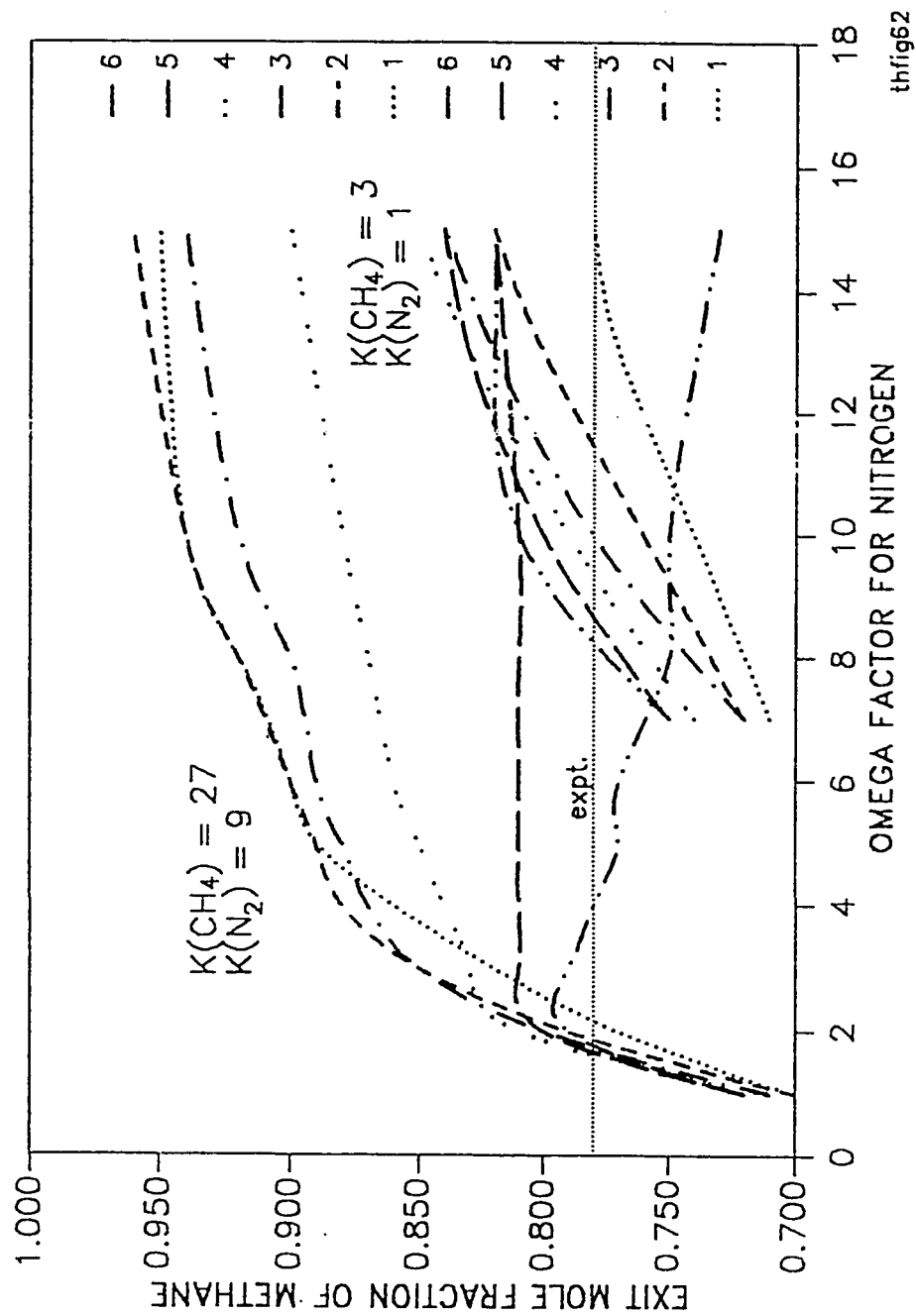


Fig. 6.2 Plot of exit concentration vs. Ω factor for nitrogen.
 Parameter is Ω ratio of methane to nitrogen.
 Two sets of curves for different values of equilibrium constants.

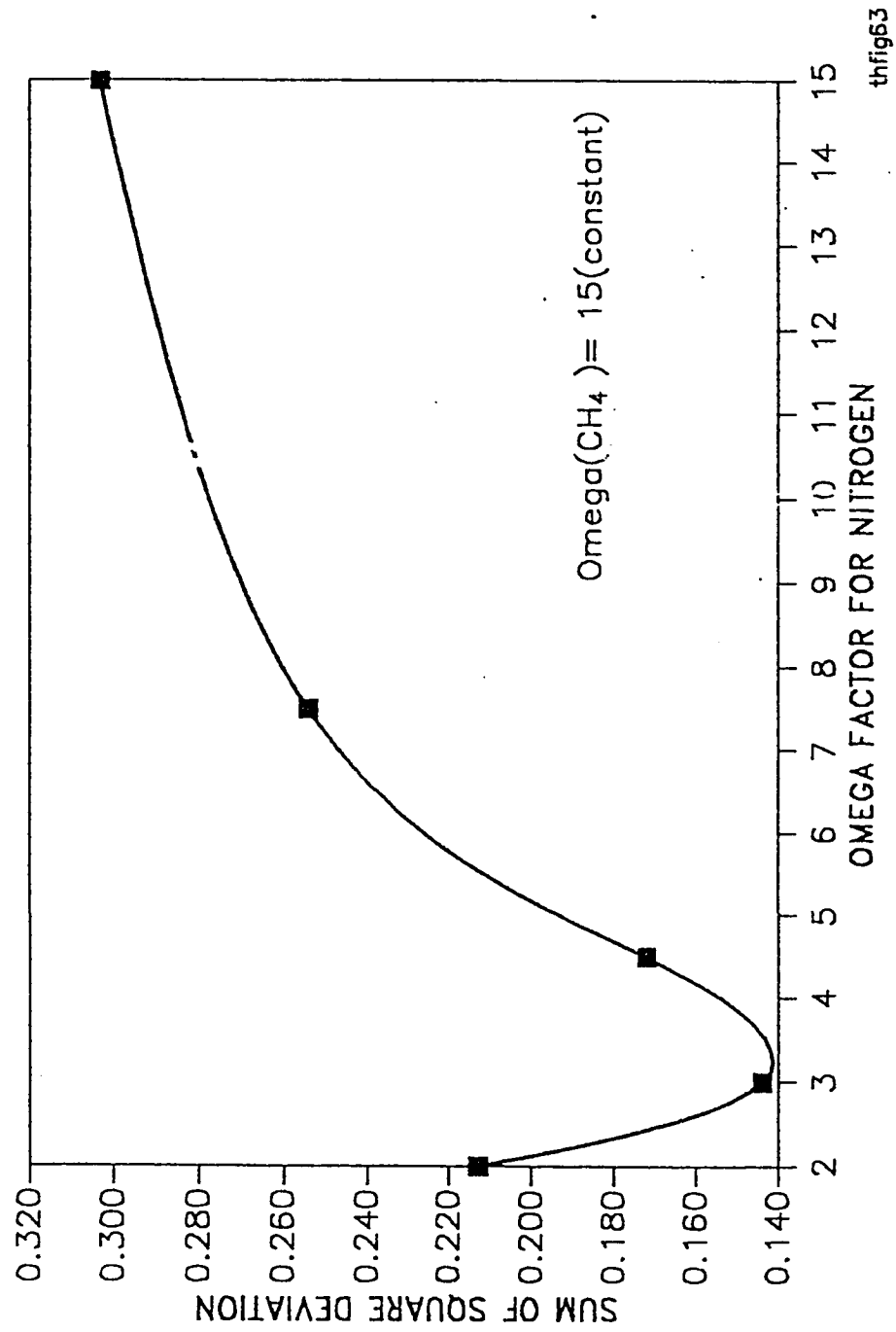


Fig. 6.3 Plot of deviation between experimental and simulated exit concentration vs. Ω factor for nitrogen.

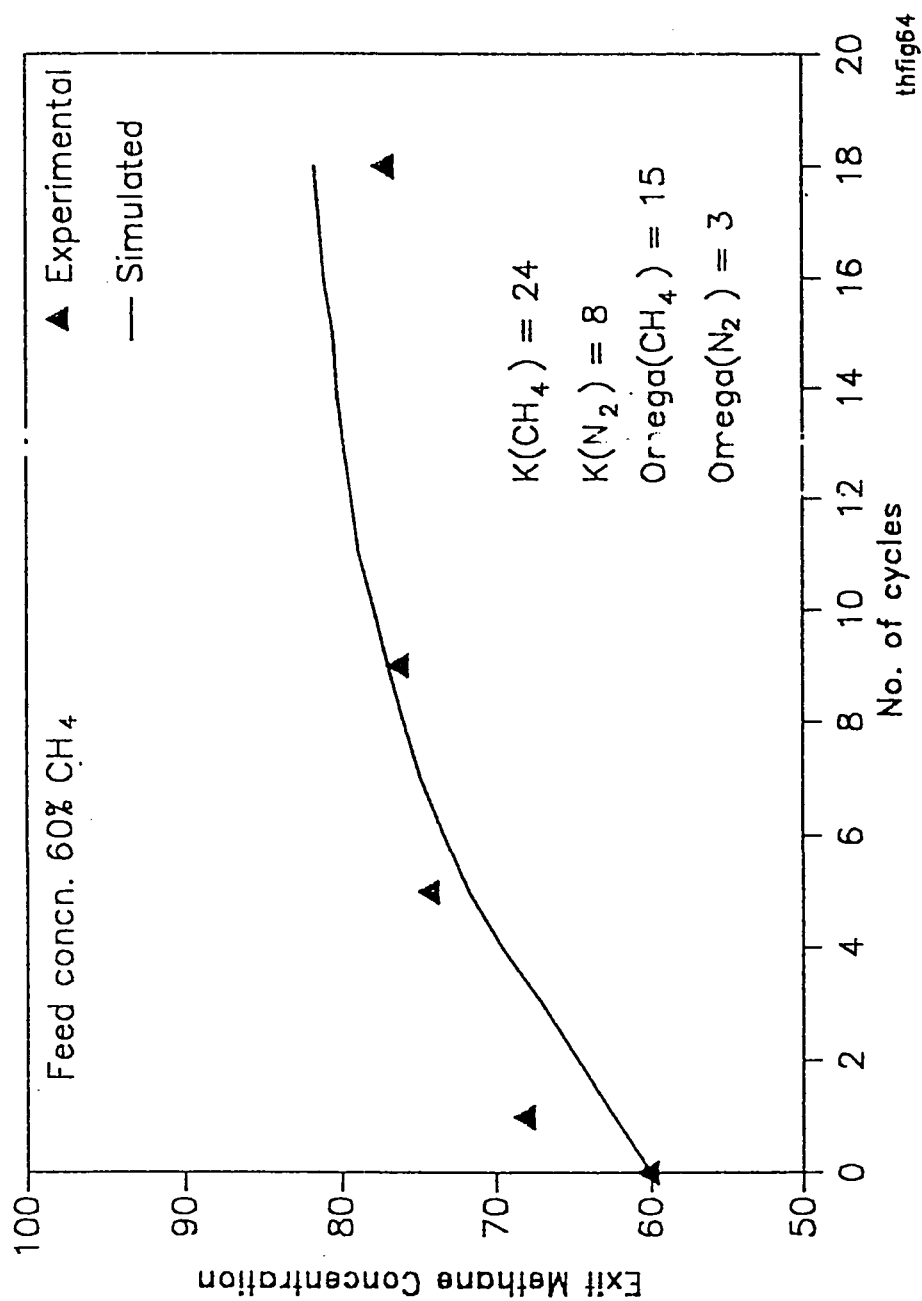


Fig. 6.4 Plot of experimental and simulated exit concentration vs. No. of Cycles on the single column (Run 4)

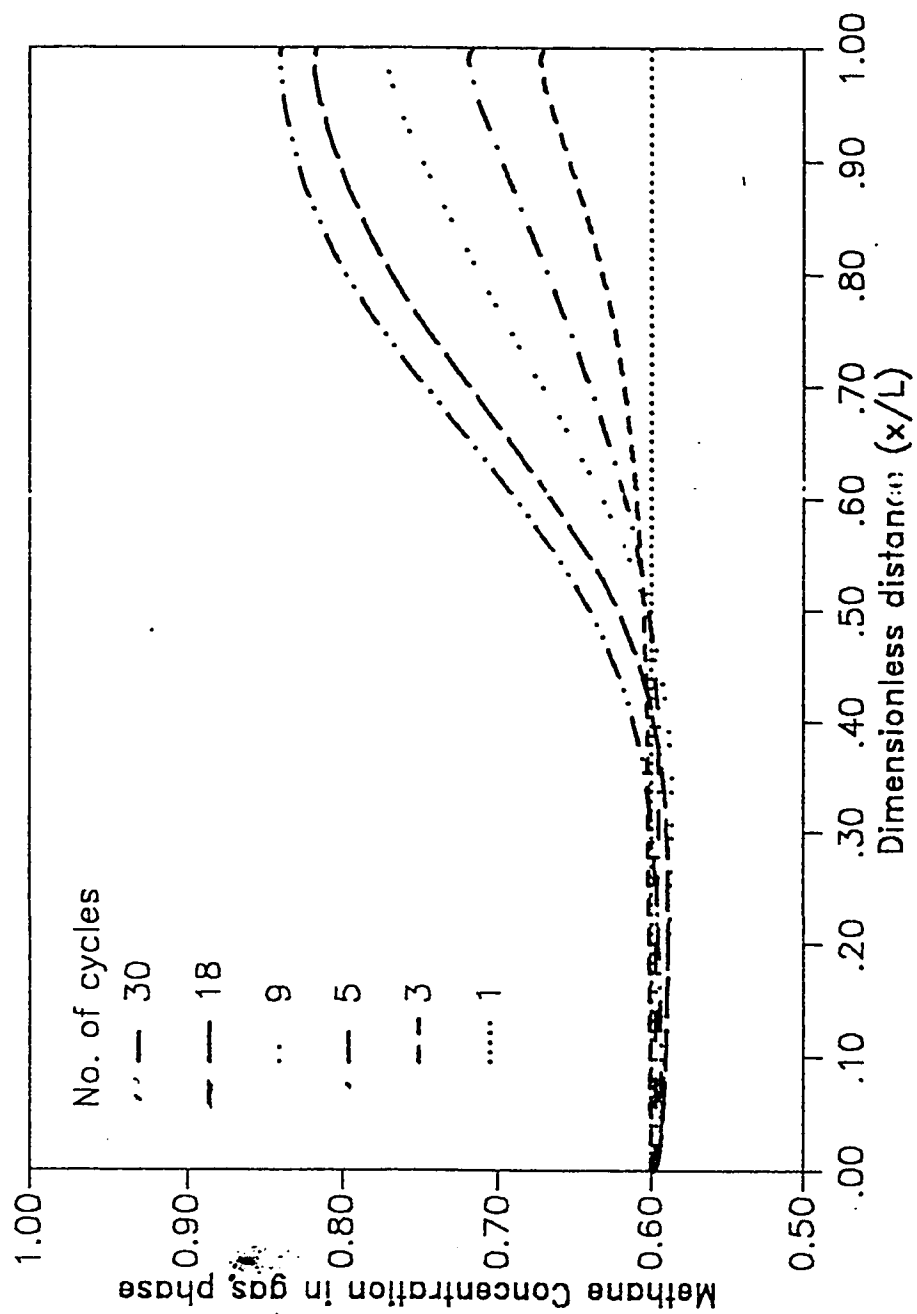


Fig. 6.5 Plot of Gas Phase methane Concentration Profile at the end of adsorption step vs. dimensionless distance in a single column (Run 4)

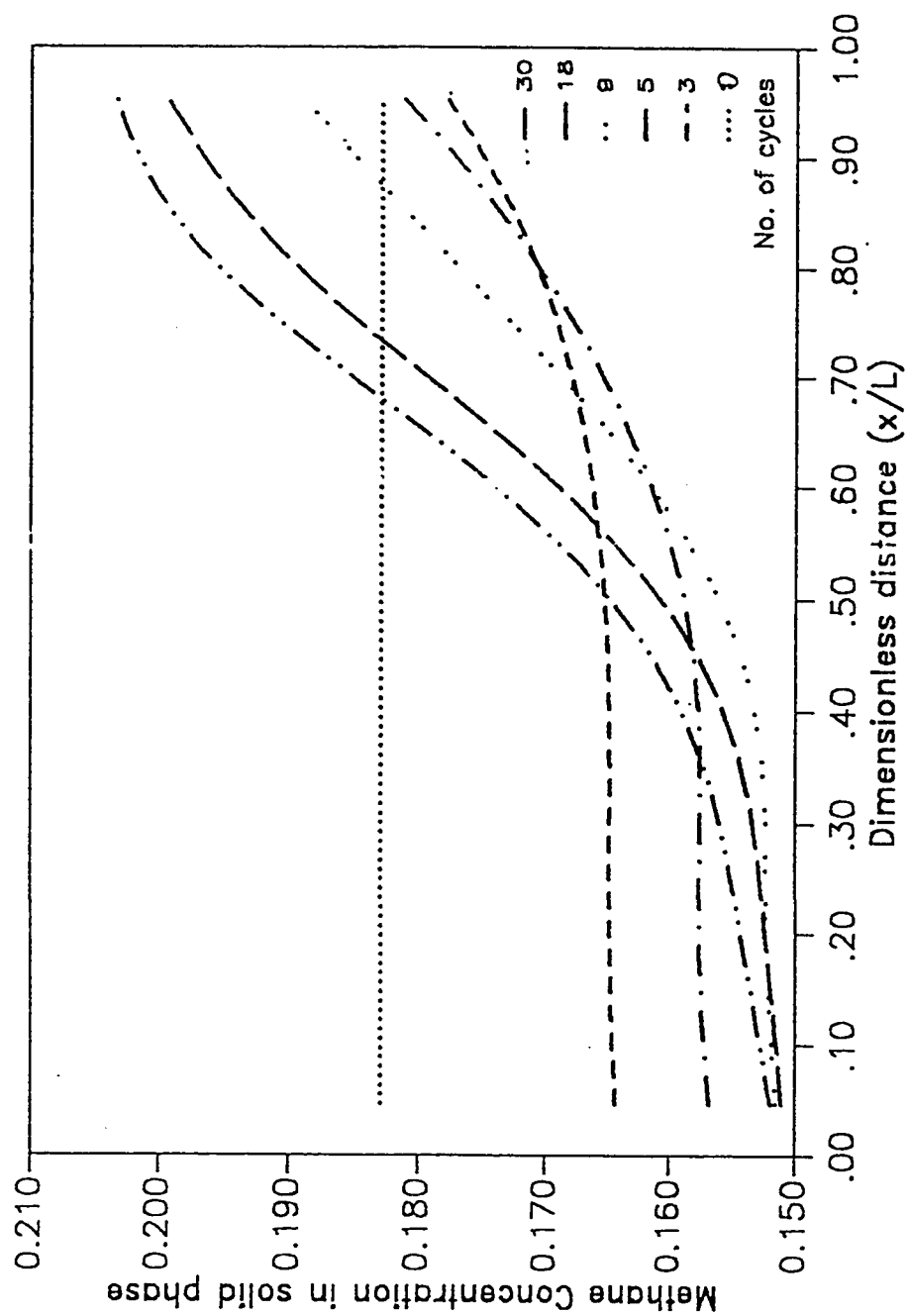


Fig. 6.6 Plot of Solid phase Methane Concentration profile at the end of adsorption step vs. dimensionless distance in a single column (Run 4)

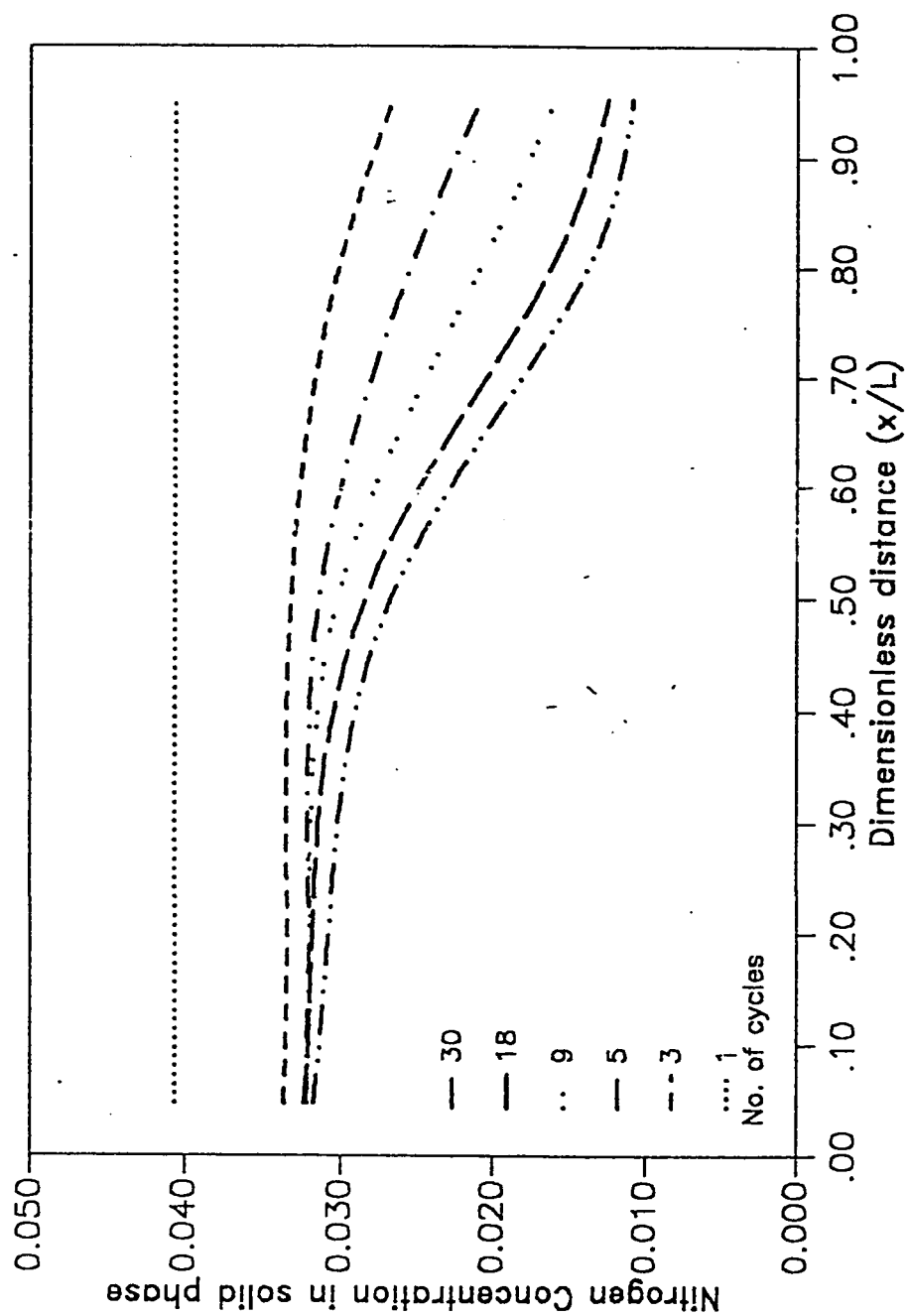


Fig. 6.7 Plot of Solid phase Nitrogen Concentration profile at the end of adsorption step vs. dimensionless distance in a single column (Run 4)

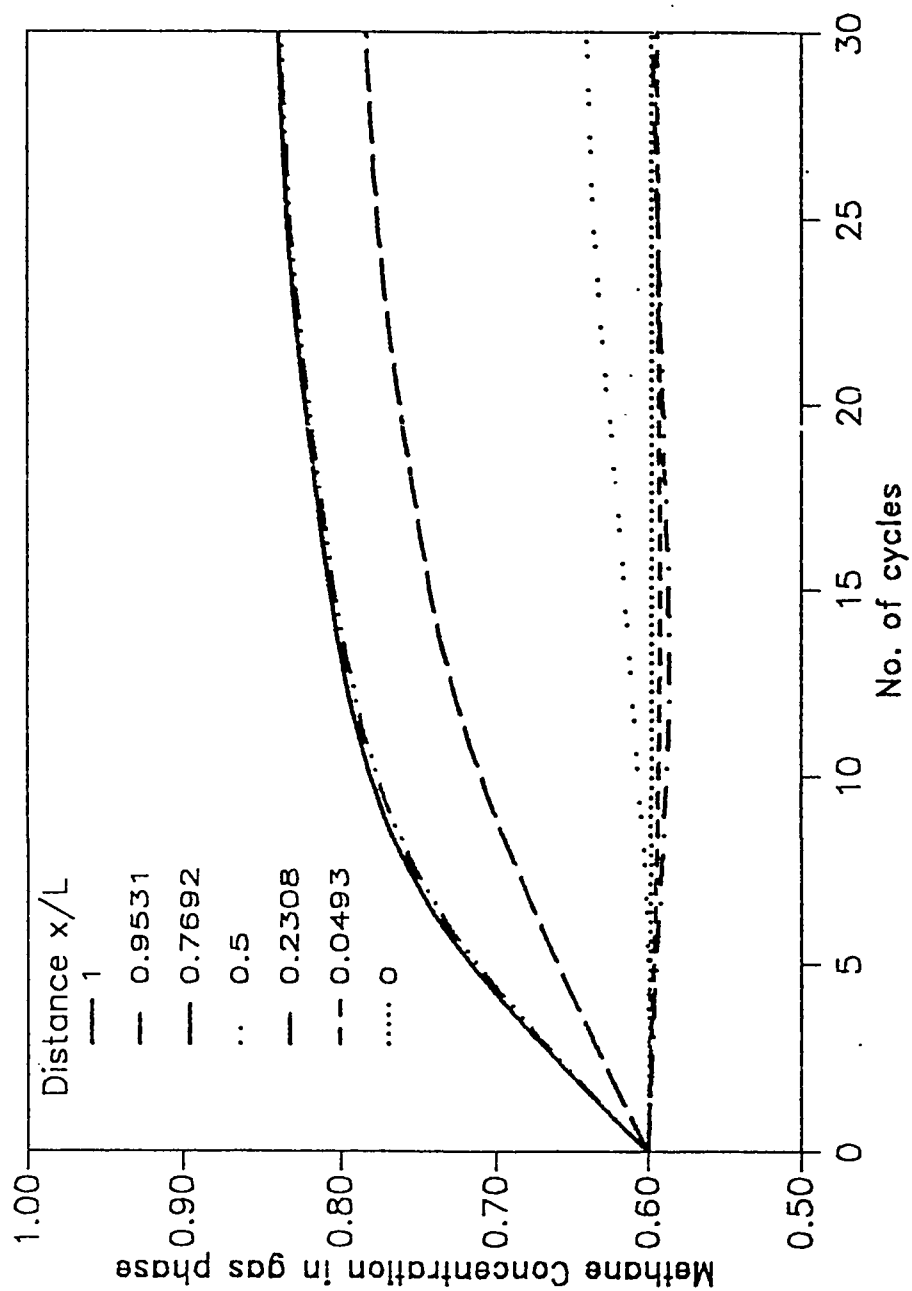


Fig 6.8 Plot of Gas phase Methane concentration profile at the end of adsorption step vs. No. of cycles in a single column (Run 4)

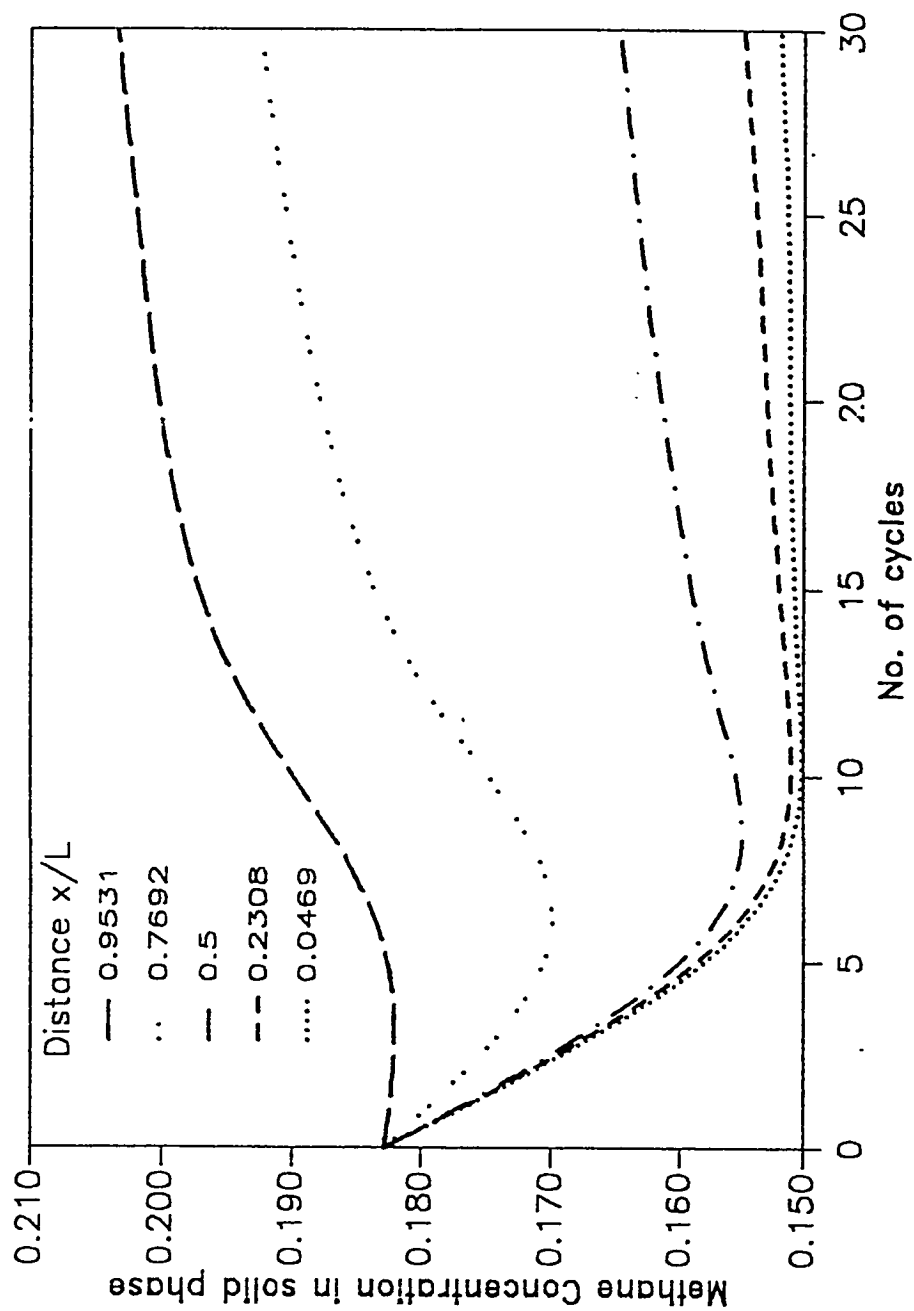


Fig 6.9 Plot of Solid phase Methane concentration profile at the end of adsorption step vs. No. of cycles in a single column (Run 4)

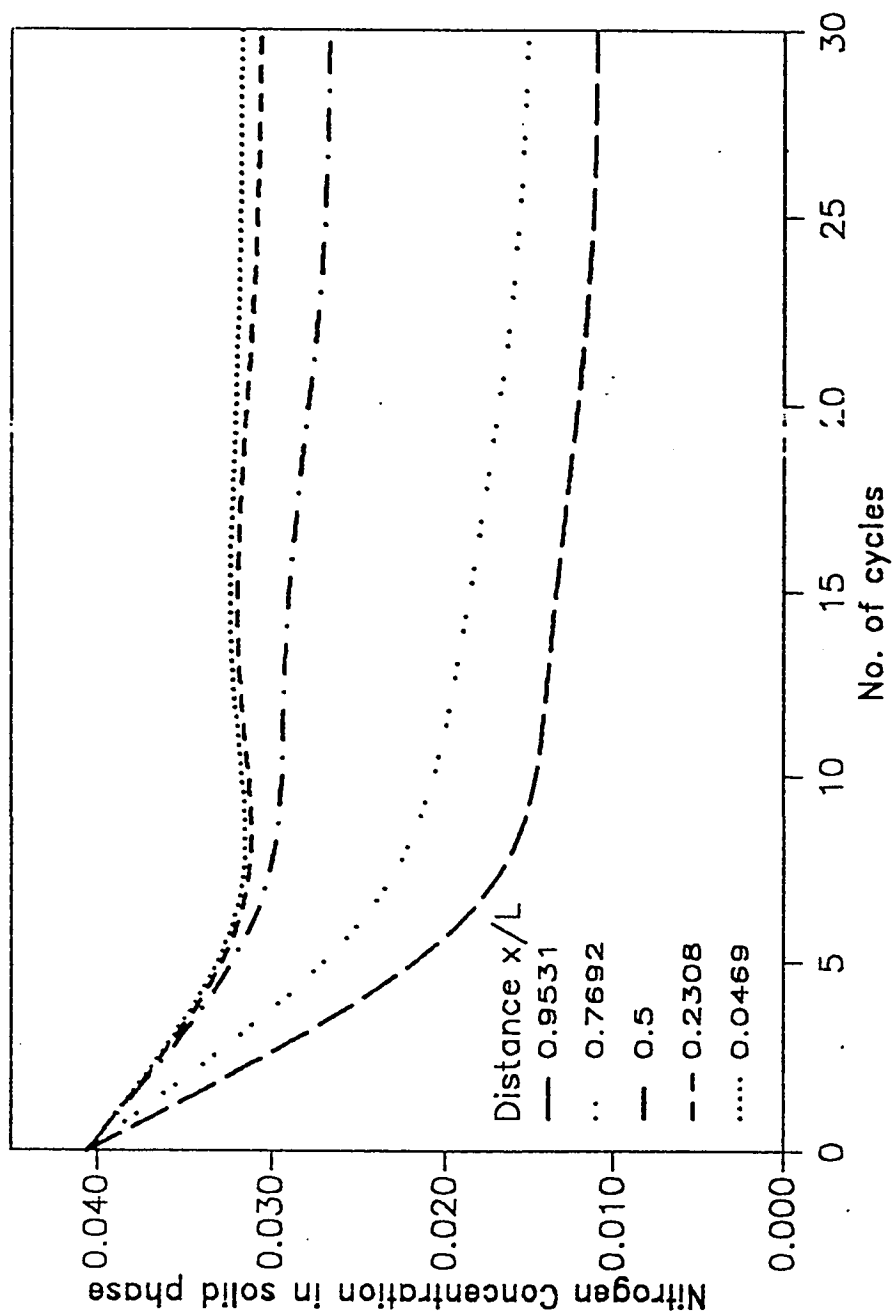


Fig. 6.10 Plot of Gas phase Methane concentration profile at the end of adsorption step vs. No. of cycles in a single column (Run 4)

CHAPTER 7

CONCLUSIONS AND RECOMMENDATIONS

7.1 CONCLUSIONS

The conclusions of the present study can be summarized as follows:

- 1.) For a microporous crystal adsorbing binary gas mixture under variety of conditions, the simulation studies with a generalised model, considering the various limiting conditions and parameters likely to affect the process, indicates that the initial normalized uptake ratio of the two gases decreases in case of significant mass transfer resistance. Also it is a function of diffusivity ratio in various adsorbents. It is independent of pressure, composition and non-linearity under conditions of fixed diffusivity, but is greatly dependent of pressure and composition, under conditions of concentration dependent diffusivity.
- 2.) The equivalent Peclet and cell numbers associated with a definitive mass transfer zone width $\tau_{0.99-0.01}$ for both equilibrium and non-equilibrium processes have been evaluated for packed bed adsorbers having non-linear isotherm. For both the equilibrium and non-equilibrium processes, the ratio of Peclet number to N changes from a value of 2 at low λ (linear isotherm) to unity when λ is high ($\lambda = 0.85$) during adsorption. However, this ratio can be taken as 2 for all values of λ during desorption. Hence we deduce that for liquids where $\lambda \approx 1.0$, the ratio of Peclet

number to N should be taken as 1.0 during adsorption, and 2.0 during desorption.

- 3.) Uptake measurements were performed using volumetric and gravimetric methods with the objective of determining the adsorption equilibrium and kinetic parameters in the carbon molecular sieve sample. The equilibrium data obtained compared well with the literature. For the kinetics, the uptake curves, obtained by the volumetric method, exhibited a behaviour other than the usual two resistance model, micropore - macropore, or the Fickian diffusion in finite volume. The behaviour of the uptake was similar to that exhibited by a particle with barrier resistance on the surface and a diffusion resistance within. The barrier resistance was dominant up to 90% of the uptake. Overall mass transfer rate constants were obtained.
- 4.) Experimental PSA studies were done with two model methane nitrogen feeds (8% and 40% nitrogen in methane) using a two column set up with carbon molecular sieves. A four step PSA cycle was used. Exit methane concentration spanned from 48% to 76% for the 60% feed and upto 96% for the 92% feed. An optimum cycle time as well as L/v_{II} ratio was observed for a set of operating conditions. Simulation studies to interpret the experimental results were done with an LDF dynamic model. The parameters for the simulation were experimentally determined. Correlation of data based on the micropore diffusion LDF

approximation, Ω , was not possible but with an equivalent factor, $15 \cdot \Phi$, the results were in fair agreement in lieu of the simplified model. This factor increased linearly for dimensionless half cycle time > 0.0045 . A hypothesis for such a behaviour was attributed to a barrier resistance for the mass transfer step. Correlation results were consistent with cycle time but not with L/v_{II} . A possible reason could have been that Φ was a coupled function of cycle time and L/v_{II} .

- 5.) Experimental PSA studies were done separately on single and two column units packed with zeolite 4A adsorbent. Two model methane nitrogen feeds (8% and 40% nitrogen in methane) were studied. In the two column experiments a four step PSA cycle was used with a portion of high pressure product as purge gas. Experiments were performed at ambient temperature with the exception of two runs at 90 ° C. No significant separation was achieved even with limiting values of L/v_{II} and purge to feed ratio. It was concluded that the desorption time was insufficient. Unequal sorption time was not possible with two column operations; hence single column experiments were performed in the usual 4 step cycle. Pure methane was used as the purge gas. An effective enrichment of 9% was obtained (with 60% methane feed). Experiments with unequal adsorption and desorption time with helium as well as vacuum purging were performed. Helium purge pushed concentration up to 85% while vacuum desorption was less effective and the concentration reached 74%. For the 92% feed the concentrations achieved

were 96.5% and 95.5% respectively. Simulation studies to interpret the selected experimental results were done with an LDF dynamic model. Experiments with vacuum desorption and helium purging were not considered due to non applicability of the model. The LDF approximation based on micropore diffusion time constant, obtained from literature, predicted a very high concentration ($> 94\%$). The effects of modifying the equilibrium and kinetic parameter was studied and the LDF factor for nitrogen, Ω_{N_2} , was found to be most sensitive. An optimised low value of 3 (instead of 15) correlated the diverse results in acceptable limits. The low value is attributed to a low diffusional time constant in the sample.

7.2 RECOMMENDATIONS FOR FURTHER STUDY:

- 1.) Simulation studies of the crystal and the pellet adsorbing a binary gas mixtures under cyclic boundary conditions using a generalised model, should be investigated. This study is useful for obtaining the linear driving force correlations.
- 2.) Application of the cell in series model in PSA simulation as an alternative to the widely used axial dispersion model.
- 3.) Analogous study to that of Nakao and Suzuki should be done for a barrier resistance particle to determine the variation of Φ with dimensionless half cycle time.

- 4.) Experimental study of the sorption characteristics of methane and nitrogen in the present zeolite 4A sample to determine the equilibrium and kinetic parameters.
- 5.) Experimental PSA study of methane nitrogen separation on CMS, on single column apparatus, similar to the present study done with 4A zeolite, with unequal step duration to enhance methane in the product. Vacuum purging option can also be studied. Similar study using multi column set up is a logical and useful extension.
- 6.) Modify the adsorbent, both CMS and zeolite 4A, to obtain a more effective separation.
- 7.) Study the PSA simulation on CMS to check for the dependency of the Φ factor on the L/v ratio.
- 8.) Model the pressurisation and blowdown steps in a PSA simulation; solve them and compare the results with the present model of a PSA simulation.

NOMENCLATURE

a	external surface of the catalyst particle
a_p	external surface area per unit volume of the particle
b	equilibrium constant
C_A	sorbate concentration in gas phase of component A
C_{Ai}, C_{Bi}	sorbate concentration in gas phase for component A and B in bed i
C_i, C_{is}	concentration of component i in the gas phase or cell i, on catalyst surface
C_i^k, C_{is}^k	concentration of component i in the gas phase in cell k, on catalyst surface in cell k.
d_t	particle diameter
D	micropore diffusivity
D_A, D_B	micropore diffusivity of component A,B
D_c	intracrystalline diffusivity
D_e	axial diffusivity
D_K	Knudsen diffusivity
$D_L (D_{L1}, D_{L2})$	axial dispersion coefficient (for flow in bed 1, bed 2)
D_m	molecular diffusivity
D_o	limiting intracrystalline diffusivity

D_p	pore diffusivity
k	rate constant
k_h	barrier rate constant
k_s	surface rate constant
$K(K_A, K_B)$	adsorption equilibrium constant (for A, B), ($= b q_s$)
l	axial coordinate for reactors
L	length of catalytic or adsorbent bed
$P(P_H, P_L)$	total column pressure (during adsorption, desorption)
P_A, P_B	partial pressure (of A, B)
Pc	Peclet Number
q_i, q_{Ai}	average solid phase concentration (of component A in bed 1)
q_0, q_r	solid phase concentration, initial and final
\bar{q}	average solid phase concentration in particles.
q^*	equilibrium solid phase concentration
q_A, q_i	adsorbed phase concentration
q_{Ai}^*, q_i^*	equilibrium adsorbed phase concentration
q_s, q_{As}	saturation adsorbed phase concentration
r	radius vector in crystal
R	radius vector in pellet
r_s	radius of the crystal

$R(c_i, T)$	surface reaction rate expressions
$R(c_i^*, T), R(c_{is}^*, T_{is}^*), R(c_{is}, T_{is})$	" "
R_p	radius of the pellet
S	bed cross sectional area
t	time
T_p	temperature of solid phase
T_0	temperature of gas phase
u, u_i	interstitial velocity, for bed i
v, v_H, v_L	interstitial velocity, high and low pressure
V	volume of cell
Y	mole fraction of trace component
z	axial distance coordinate

GREEK LETTERS

α	dimensionless group (ku/L)
α_{AB}	separation factor
β	capacity parameter
β	modified separation factor
β_A, β_B	parameter in equation(1) Appendix A.3
γ_{crit}	critical feed to purge ratio
Δt	time step
Δz	cell length

ε_p	porosity of the adsorbent particle
ε	bed voidage
λ	non linearity parameter
ζ	dimensionless distance
τ	dimensionless time
Φ	dimensionless gas phase concentration
Φ	dimensionless rate factor
Ψ	dimensionless solid phase concentration
Ω	Gluckauf's approximation factor

APPENDIX A.1

RAW DATA

APPENDIX A.1.1

RAW DATA FOR TWO COLUMN PSA EXPERIMENTS WITH CARBON MOLECULAR SIEVES

Run Nos. : 1-6
 Date : 10 Feb 90

The following process variable are held constant for the cycle time listed below:

Packing in the column	: CMS	
Feed flow rate	: 1.35	SLPM
Product flow rate	: 0.39	SLPM
Purge flow rate	: 0.91	SLPM
High pressure	: 44.1	psia
Low pressure	: 14.7	psia
Feed concentration	: 60	%CH ₄
Velocity	: 2.01	cm/sec
Purge gas	: Part of product	
Purge to Feed ratio	: 2.02	
Initial condition	: Saturated with feed	
Step duration	: 1:4:1:4	(press:adsorption:blowdown:purge)
Temperature	: 26	C

Concentrations are measured 2 sec before the end of adsorption step.

Cycle time : 60 sec

No. of cycles	Outlet product concentration (mole % methane)
---------------	---

0	61.19
1	61.53
4	60.98
7	60.60
10	60.42
16	60.26
20	60.23
24	60.01
31	60.15

Cycle time : 100 sec

No. of cycles	Outlet product concentration (mole % methane)
---------------	--

0	59.97
2	62.83
7	63.77
9	63.78
14	63.81
17	63.88
20	63.84
23	63.85

Cycle time : 120 sec

No. of cycles	Outlet product concentration (mole % methane)
---------------	--

0	60.24
2	63.39
4	64.16
6	64.42
9	64.42
11	64.40
13	64.43

Cycle time : 180 sec

No. of cycles	Outlet product concentration (mole % methane)
---------------	--

0	61.53
1	64.54
2	65.41
3	65.81
4	65.98
6	66.13
8	66.21

230

10
12

66.25
66.22

Cycle time : 240 sec

No. of cycles	Outlet product concentration (mole % methane)
---------------	---

0	60.12
2	64.90
3	65.23
5	65.51
6	65.53
8	65.58
10	65.77
11	65.59

Cycle time : 300 sec

No. of cycles	Outlet product concentration (mole % methane)
---------------	---

0	60.15
1	63.82
2	64.61
3	65.10
4	65.20
5	65.31
6	65.44
7	65.34
8	65.35

Run Nos. : 7-12
 Date : 12 Feb 90

The following process variable are held constant for the cycle times listed below:

Packing in the column : CMS
 Feed flow rate : 0.87 SLPM
 Product flow rate : 0.19 SLPM
 Purge flow rate : 0.66 SLPM
 High pressure : 44.1 psia
 Low pressure : 14.7 psia
 Feed concentration : 60 %CH₄
 Velocity : 1.29 cm/sec
 Purge gas : Part of product
 Purge to Feed ratio : 2.28
 Initial condition : Saturated with feed
 Step duration : 1:4:1:4
 Temperature : 26 C

Concentrations are measured 2 sec before the end of adsorption step.

Cycle time : 60 sec

No. of cycles Outlet product
 concentration
 (mole % methane)

0	59.85
3	56.03
6	53.44
9	50.05
13	48.85
16	52.62
20	48.59
25	47.28
29	47.31
33	46.96
43	46.26
53	46.32

Cycle time : 120 sec

No. of cycles	Outlet product concentration (mole % methane)
---------------	---

0	59.73
1	56.10
3	57.35
5	57.73
7	57.52
9	57.98
11	57.86
13	57.79

Cycle time : 180 sec

No. of cycles	Outlet product concentration (mole % methane)
---------------	---

0	59.92
1	64.24
2	65.77
3	66.35
4	66.54
6	66.57
8	66.62
10	66.70
14	66.80
15	67.38
16	67.10
18	67.42
21	66.98
24	66.76

Cycle time : 240 sec

No. of cycles	Outlet product concentration (mole % methane)
---------------	---

0	60.07
1	67.24
2	68.93
5	69.84
7	69.84
8	69.84
11	69.80
13	69.75
14	69.80

Cycle time : 300 sec

No. of cycles	Outlet product concentration (mole % methane)
---------------	---

0	60.07
1	66.77
2	67.95
3	68.33
4	68.46
6	68.68
11	68.67
13	68.67

Cycle time	: 360	sec
No. of cycles	Outlet product concentration (mole % methane)	
0	60.14	
1	66.30	
2	67.12	
4	67.61	
10	69.22	
12	67.84	
13	67.87	
14	67.85	
15	67.39	

Run Nos. : 13-24
 Date : 19 Feb 90

The following process variables are held constant for the cycle times listed below:

Packing in the column	: CMS	
Feed flow rate	: 0.50	SLPM
Product flow rate	: 0.05	SLPM
Purge flow rate	: 0.35	SLPM
High pressure	: 44.1	psia
Low pressure	: 14.7	psia
Feed concentration	: 60	%CH ₄
Velocity	: 0.74	cm/sec
Purge gas	: Part of product	
Purge to Feed ratio	: 2.1	
Initial condition	: Saturated with feed	
Step duration	: 1:4:1:4	
Temperature	: 26	C

Concentrations are measured 2 sec before the end of adsorption step.

Cycle time : 60 sec

No. of cycles	Outlet product concentration (mole % methane)
------------------	---

0	59.38
1	59.45
4	52.56
20	48.27
27	48.10
34	48.12

Cycle time : 120 sec

No. of cycles	Outlet product concentration (mole % methane)
---------------	---

0	59.80
1	62.58
3	57.53
5	57.87
7	57.37
9	58.46
11	57.91

Cycle time : 180 sec

No. of cycles	Outlet product concentration (mole % methane)
---------------	---

0	59.43
1	65.14
2	64.59
3	64.79
4	64.65
5	64.88
6	64.74
8	65.30
10	64.72

Cycle time : 240 sec

No. of cycles	Outlet product concentration (mole % methane)
---------------	---

0	60.03
1	61.39
2	63.08
3	63.90
5	64.38
6	64.35

7	64.39
8	64.47

Cycle time : 300 sec

No. of cycles	Outlet product concentration (mole % methane)
---------------	---

0	59.97
1	65.41
5	68.45
6	68.45
7	68.45

Cycle time : 360 sec

No. of cycles	Outlet product concentration (mole % methane)
---------------	---

0	60.11
1	69.17
2	71.09
3	71.52
4	71.66
4	69.49
5	71.95
6	71.71
10	71.71

Cycle time : 420 sec

No. of cycles	Outlet product concentration (mole % methane)
---------------	---

0	60.77
1	71.13
2	72.82
3	73.21
4	73.30
4	68.89
5	73.40
6	73.34
7	73.45
8	74.30
10	74.34
11	73.76
13	74.38
14	74.43
16	74.45
17	74.39

Cycle time : 480 sec

No. of cycles	Outlet product concentration (mole % methane)
---------------	---

0	60.04
1	72.81
2	74.74
3	75.16
4	75.29
5	75.36
6	75.33
7	75.33

Cycle time : 540 sec

No. of cycles	Outlet product concentration (mole % methane)
---------------	---

0	60.38
1	73.68
2	75.38
3	75.69
4	75.75
5	75.85
6	75.83
7	75.84

Cycle time : 600 sec

No. of cycles	Outlet product concentration (mole % methane)
---------------	---

0	59.66
1	73.08
2	74.00
3	75.18
3	73.94
4	75.24
6	75.35
6	73.95
7	75.30
8	75.36
8	74.03
9	75.34

Cycle time : 660 sec

No. of cycles	Outlet product concentration (mole % methane)
---------------	---

0	59.84
0	74.02

1	73.02
1	73.42
2	74.61
2	73.32
3	74.59
3	73.17
4	74.69
4	73.34
5	74.70
5	73.25
6	74.72
7	74.81
8	74.86
8	73.32
9	74.85
10	74.86
11	74.84
12	74.93
13	74.95

Cycle time : 720 sec

No. of cycles **Outlet product concentration (mole % methane)**

0	59.57
0	73.48
1	72.64
1	72.84
2	73.84
2	72.78
3	74.14
8	74.35
8	72.77
9	74.20
10	74.27

Run No. : 25
Date : 5 Mar 90

The following process variables are held constant for the cycle time listed below:

Packing in the column	: CMS	
Feed flow rate	: 0.42	SLPM
Product flow rate	: 0.03	SLPM
Purge flow rate	: 0.25	SLPM
High pressure	: 44.1	psia
Low pressure	: 14.7	psia
Feed concentration	: 60	%CH ₄
Velocity	: 0.62	cm/sec
Purge gas	: Part of product	
Purge to Feed ratio	: 1.79	
Initial condition	: Saturated with feed	
Step duration	: 1:4:1:4	
Temperature	: 26	C

Concentrations are measured 2 sec before the end of adsorption step.

Cycle time : 600 sec

No. of cycles	Outlet product concentration (mole % methane)	Outlet purge concentration (mole % methane)
0	59.52	59.91
1	70.22	61.35
1.5(*)	71.86	63.04
2	73.38	61.77
2.5(*)	73.36	63.81
3	74.40	62.18
4	74.75	62.31
5	74.90	62.41
7	75.01	62.84
9	75.15	63.16
10	75.21	62.12
12	75.21	63.21
(*) other bed		

Time during cycle sec	Product concentration (mole % methane)	Purge concentration (mole % methane)
0	75.40	61.52
60	73.93	52.85
120	72.06	45.86
180	74.85	52.57
240	76.83	56.93
298	76.69	59.81
300	76.63	60.35
360	75.41	52.84
420	72.46	47.77
480	74.29	54.14
540	76.07	58.54
598	75.40	61.28
600	75.40	61.52

Run Nos. : 26-30
Date : 14 Mar 90

The following process variables are held constant for the cycle times listed below:

Packing in the column : CMS
Feed flow rate : 0.42 SLPM
Product flow rate : 0.03 SLPM
Purge flow rate : 0.25 SLPM
High pressure : 44.1 psia
Low pressure : 14.7 psia
Feed concentration : 60 %CH₄
Velocity : 0.62 cm/sec
Purge gas : Part of product
Purge to Feed ratio : 2.02
Initial condition : Saturated with feed
Step duration : 1:4:1:4
Temperature : 26 C

Concentrations are measured 2 sec before the end of adsorption step.

Cycle time : 100 sec

No. of cycles	Outlet product concentration (mole % methane)	Outlet purge concentration (mole % methane)
0	92.36	92.36
1	92.15	93.76
3	90.03	92.55
5	89.33	92.03
8	89.23	90.52
13	88.23	91.10
17	87.94	90.97
19	87.78	91.17
21	87.76	90.85
24	87.70	90.88
26	88.15	90.52
29	87.68	90.87
31	87.55	90.86
33	87.63	90.84
36	87.70	90.96

Time during cycle sec	Product concentration (mole % methane)	Purge concentration (mole % methane)
0	87.70	90.96
10	87.69	93.29
20	87.29	93.17
30	87.43	92.64
40	87.77	91.71
50	87.70	90.96
60	86.96	93.41
70	86.66	93.16
80	86.82	92.63
90	87.58	91.44
100	87.70	90.96

Cycle time : 300 sec

No. of cycles	Outlet product concentration (mole % methane)	Outlet purge concentration (mole % methane)
0	92.40	92.85
1	93.24	90.72
2	93.75	90.19
3	94.04	89.90
5	94.22	89.77
7	94.29	89.77
11	93.90	89.77

Cycle time : 600 sec

No. of cycles	Outlet product concentration (mole % methane)	Outlet purge concentration (mole % methane)
0	91.71	91.54
0	95.39	89.27
1	94.76	91.03
1	95.56	91.15
2	95.53	91.04
2	95.68	91.90

3	95.80	91.22
4	96.00	91.28
19	96.16	92.18
20	96.15	92.20

Cycle time : 720 sec

No. of cycles	Outlet product concentration (mole % methane)	Outlet purge concentration (mole % methane)
0	91.97	92.02
0	95.51	91.09
1	95.31	91.95
1	95.77	92.63
2	95.96	92.13
2	95.90	93.09
3	96.09	92.28
4	96.18	92.40
6	96.23	92.51
7	96.02	93.38
9	96.25	92.65
10	96.25	92.70

Cycle time : 840 sec

No. of cycles	Outlet product concentration (mole % methane)	Outlet purge concentration (mole % methane)
0	91.95	92.95
0	95.33	91.27
1	95.03	92.62
1	95.36	92.15
2	95.57	92.97
2	95.39	92.25
3	95.66	93.08
3	95.42	92.37
4	95.70	93.16
5	95.76	92.46
11	95.45	93.59
12	95.79	92.95
13	95.79	92.92

APPENDIX A.1.2

RAW DATA FOR TWO COLUMN PSA EXPERIMENTS WITH 4A ZEOLITE

Run Nos. : 1-6
 Date : 28 Jul 90

The following process variables are held constant for the cycle times listed below:

Packing in the column : Zeolite 4A
 Feed flow rate : 0.42 SLPM
 Product flow rate : 0.06 SLPM
 Purge flow rate : 0.30 SLPM
 High pressure : 44.1 psia
 Low pressure : 14.7 psia
 Feed concentration : 60 %CH₄
 Velocity : 0.62 cm/sec
 Purge gas : Part of product
 Purge to Feed ratio : 2.14
 Initial condition : Saturated with feed
 Step duration : 1:4:1:4 (press.:adsorp.:blowdown:purge)
 Temperature : 26 C

Concentrations are measured 2 sec before the end of adsorption step.

Cycle time : 30 sec

No. of cycles	Outlet product concentration (mole % methane)	Outlet purge concentration (mole % methane)
0.0	60.52	60.56
1.0	60.37	60.96
8.0	59.36	60.95
15.0	56.49	60.88
22.0	55.39	60.93
29.0	54.95	60.88
40.0	54.75	60.87
48.0	54.62	60.82
57.0	54.63	60.86
64.5	54.59	60.80
71.5	54.68	61.06
90.0	54.56	60.85

Cycle time : 60 sec

No. of cycles	Outlet product concentration (mole % methane)	Outlet purge concentration (mole % methane)
0.0	59.97	60.23
1.0	59.90	61.10
5.0	57.56	61.05
10.0	54.55	60.90
15.0	53.52	60.89
19.0	53.25	60.82
24.0	53.52	60.89
28.0	53.06	60.82
32.0	53.05	60.89
38.0	53.02	60.80
47.0	53.05	60.85

Cycle time : 90 sec

No. of cycles	Outlet product concentration (mole % methane)	Outlet purge concentration (mole % methane)
0.0	60.21	60.31
1.0	60.23	61.09
4.0	57.46	60.90
7.0	55.15	60.72
10.0	54.40	60.15
13.0	54.07	60.69
16.0	53.92	60.66
19.0	53.84	60.23
23.0	53.27	60.65
26.0	53.75	60.65
29.0	53.78	60.65
30.5	54.89	59.38
34.0	53.72	60.66
80.0	53.79	60.73

Cycle time : 120 sec

No. of cycles	Outlet product concentration (mole % methane)	Outlet purge concentration (mole % methane)
0.0	59.87	60.24
1.0	59.57	61.16
3.0	57.14	60.96
5.0	55.78	60.78
7.0	55.24	60.51
10.0	55.08	60.64
12.0	54.96	60.64
14.0	54.94	60.53
17.0	55.01	60.65
19.0	55.00	60.66

Cycle time : 180 sec

No. of cycles	Outlet product concentration (mole % methane)	Outlet purge concentration (mole % methane)
0.0	60.53	60.59
1.0	59.64	61.01
3.0	58.52	60.62
5.0	58.40	60.60
7.0	58.29	60.59
9.0	58.27	60.58
11.0	58.31	60.63

Cycle time : 240 sec

No. of cycles	Outlet product concentration (mole % methane)	Outlet purge concentration (mole % methane)
0.0	60.54	60.96
1.0	60.05	59.07
2.0	60.35	59.02
4.0	60.51	59.06
5.0	60.57	59.16
6.0	60.58	59.78
7.5	59.01	58.63
16.0	60.56	59.16

Run Nos. : 7-9
Date : 7 Aug 90

The following process variables are held constant for the cycle times listed below:

Packing in the column : Zeolite 4A
Feed flow rate : 0.42 SLPM
Product flow rate : 0.05 SLPM
Purge flow rate : 0.24 SLPM
High pressure : 44.1 psia
Low pressure : 14.7 psia
Feed concentration : 60 %CH₄
Velocity : 0.62 cm/sec
Purge gas : Part of product
Purge to Feed ratio : 1.71
Initial condition : Saturated with feed
Step duration : 1:4:1:4
Temperature : 26 C

Concentrations are measured 2 sec before the end of adsorption step.

Cycle time : 60 sec

No. of cycles	Outlet product concentration (mole % methane)	Outlet purge concentration (mole % methane)
0.0	60.64	60.71
1.0	60.58	61.16
5.0	59.04	61.14
9.0	56.63	60.99
14.0	55.29	61.09
18.0	54.86	60.96
22.0	54.62	60.92
26.0	54.51	60.92
38.0	54.31	60.91
42.0	54.31	60.93
46.0	54.29	60.90
50.0	54.26	60.92
53.5	53.42	60.50
62.0	54.22	60.93
71.0	54.18	60.89
84.0	54.14	60.88

113.0	54.13	60.88
124.0	54.10	60.85
150.0	54.12	60.84

Cycle time : 90 sec

No. of cycles	Outlet product concentration (mole % methane)	Outlet purge concentration (mole % methane)
0.0	60.12	60.10
1.0	59.96	61.22
4.0	57.60	61.15
7.0	54.90	60.99
11.0	53.55	60.96
14.0	53.16	60.88
17.0	52.99	61.04
21.0	52.84	60.90
26.0	52.86	60.87
37.0	52.75	60.84
52.5	53.42	59.98

Cycle time : 120 sec

No. of cycles	Outlet product concentration (mole % methane)	Outlet purge concentration (mole % methane)
0.0	60.48	60.49
1.0	60.48	61.21
3.0	58.40	61.09
5.0	56.44	60.96
8.0	55.06	60.86
10.0	54.64	60.82
12.0	54.54	60.83
15.0	54.35	60.82
19.0	54.26	60.81
23.0	54.20	60.78
26.0	54.10	60.78
37.0	54.12	60.78
39.5	53.52	59.13
53.0	54.05	60.75

Run Nos. : 10-12
 Date : 18 Aug 90

The following process variables are held constant for the cycle times listed below:

Packing in the column : Zeolite 4A
 Feed flow rate : 0.36 SLPM
 Product flow rate : 0.03 SLPM
 Purge flow rate : 0.26 SLPM
 High pressure : 44.1 psia
 Low pressure : 14.7 psia
 Feed concentration : 92 %CH₄
 Velocity : 0.53 cm/sec
 Purge gas : Part of product
 Purge to Feed ratio : 2.17
 Initial condition : Saturated with feed
 Step duration : 1:4:1:4
 Temperature : 26 C

Concentrations are measured 2 sec before the end of adsorption step.

Cycle time : 60 sec

No. of cycles	Outlet product concentration (mole % methane)	Outlet purge concentration (mole % methane)
0.0	92.43	92.50
1.0	92.36	92.66
5.0	91.37	92.69
9.0	90.65	92.66
13.0	90.39	92.66
17.0	90.27	92.66
21.0	90.23	92.74
27.0	90.24	92.64
33.0	90.23	92.67
37.0	90.22	92.65
44.5	90.53	92.58
77.0	90.21	92.68

Cycle time : 90 sec

No. of cycles	Outlet product concentration (mole % methane)	Outlet purge concentration (mole % methane)
0.0	92.36	92.44
1.0	92.34	92.81
4.0	91.39	92.69
7.0	90.57	92.65
10.0	90.29	92.63
13.0	90.17	92.64
16.0	90.12	92.63
26.0	90.12	92.64
29.0	90.07	93.65
35.0	90.08	92.64
127.0	90.12	92.62
148.5	90.53	92.49

Cycle time : 120 sec

No. of cycles	Outlet product concentration (mole % methane)	Outlet purge concentration (mole % methane)
0.0	92.38	92.45
1.0	92.41	92.73
3.0	91.85	92.67
5.0	91.39	92.66
8.0	91.08	92.61
11.0	91.01	92.61
70.0	90.96	92.61
72.0	90.91	92.58
75.5	90.57	92.04

Run Nos. : 13-14
 Date : 20 Aug 90

The following process variables are held constant for the cycle times listed below:

Packing in the column : Zcolite 4A
 Feed flow rate : 0.80 SLPM
 Product flow rate : 0.13 SLPM
 Purge flow rate : 0.58 SLPM
 High pressure : 44.1 psia
 Low pressure : 14.7 psia
 Feed concentration : 92 %CH₄
 Velocity : 1.19 cm/sec
 Purge gas : Part of product
 Purge to Feed ratio : 2.17
 Initial condition : Saturated with feed
 Step duration : 1:4:1:4
 Temperature : 26 C

Concentrations are measured 2 sec before the end of adsorption step.

Cycle time : 30 sec

No. of cycles	Outlet product concentration (mole % methane)	Outlet purge concentration (mole % methane)
0	92.48	92.55
1	92.51	92.74
8	91.18	92.65
15	90.88	92.67
32	90.85	92.68

Cycle time : 60 sec

No. of cycles	Outlet product concentration (mole % methane)	Outlet purge concentration (mole % methane)
0	92.56	92.64
1	92.49	92.76
5	91.31	92.66
12	90.93	92.69
34	90.94	92.69

Run No. : 15
Date : 18 Sep 90

The following process variables are held constant for the cycle time listed below:

Packing in the column : Zeolite 4A
Feed flow rate : 0.67 SLPM
Product flow rate : 0.10 SLPM
Purge flow rate : 0.49 SLPM
High pressure : 58.8 psia
Low pressure : 14.7 psia
Feed concentration : 60 %CH₄
Velocity : 0.75 cm/sec
Purge gas : Part of product
Purge to Feed ratio : 2.92
Initial condition : Saturated with feed
Step duration : 1:4:1:4
Temperature : 26 C

Concentrations are measured 2 sec before the end of adsorption step.

Cycle time : 30 sec

No. of cycles	Outlet product concentration (mole % methane)	Outlet purge concentration (mole % methane)
1	60.64	61.31
5	56.44	61.04
11	54.85	60.93
15	54.67	60.91
19	54.66	60.91
24	54.60	61.05
33	54.59	61.12
43	54.59	60.93
Time during the cycle sec	Product Concentration (mole % methane)	Purge Concentration (mole % methane)
5	54.42	60.99
10	54.42	61.08
20	54.53	61.03

Run Nos. : 16-18
 Date : 24 Sep 90

The following process variables are held constant for the cycle times listed below:

Packing in the column : Zeolite 4A
 Feed flow rate : 0.42 SLPM
 Product flow rate : 0.10 SLPM
 Purge flow rate : 0.26 SLPM
 High pressure : 29.4 psia
 Low pressure : 14.7 psia
 Feed concentration : 60 %CH₄
 Velocity : 0.94 cm/sec
 Purge gas : Part of product
 Purge to Feed ratio : 1.24
 Initial condition : Saturated with feed
 Step duration : 1:4:1:4
 Temperature : 26 C

Concentrations are measured 2 sec before the end of adsorption step.

Cycle time : 60 sec

No. of cycles	Outlet product concentration (mole % methane)	Outlet purge concentration (mole % methane)
0	60.61	60.72
1	60.12	61.19
5	57.28	61.20
12	56.20	61.20
17	56.09	61.21
22	56.17	61.33
27	56.09	61.17
32	56.11	61.19
Time during the cycle sec	Product Concentration (mole % methane)	Purge Concentration (mole % methane)
5	56.12	60.99
10	56.74	61.12
20	56.21	61.17

Cycle time : 90 sec

No. of cycles	Outlet product concentration (mole % methane)	Outlet purge concentration (mole % methane)
0	60.67	60.79
1	59.97	61.26
4	58.57	61.30
8	57.95	61.27
11	57.92	61.28
16	57.88	61.22
19	58.02	61.27
38	57.85	61.26
Time during the cycle sec	Product concentration (mole % methane)	Purge concentration (mole % methane)
5	57.24	61.17
10	56.77	61.17
20	56.28	61.30
30	56.98	61.34
40	57.37	61.32

Cycle time : 40 sec

No. of cycles	Outlet product concentration (mole % methane)	Outlet purge concentration (mole % methane)
0	60.65	60.78
1	59.75	61.08
6	58.10	61.04
15	56.71	61.05
24	56.53	61.15
36	56.53	61.07
Time during the cycle sec	Product concentration (mole % methane)	Purge concentration (mole % methane)
5	56.87	60.92
10	56.78	61.10
15	-	61.02

Run No. : 19
Date : 25 Sep 90

The following process variables are held constant for the cycle time listed below:

Packing in the column : Zeolite 4A
Feed flow rate : 0.59 SLPM
Product flow rate : 0.10 SLPM
Purge flow rate : 0.26 SLPM
High pressure : 29.4 psia
Low pressure : 14.7 psia
Feed concentration : 60 %CH₄
Velocity : 1.31 cm/sec
Purge gas : Part of product
Purge to Feed ratio : 0.88
Initial condition : Saturated with feed
Step duration : 1:4:1:4
Temperature : 26 C

Concentrations are measured 2 sec before the end of adsorption step.

Cycle time : 60 sec

No. of cycles	Outlet product concentration (mole % methane)	Outlet purge concentration (mole % methane)
0	60.69	60.77
1	60.57	61.41
5	57.10	61.25
9	56.43	61.24
14	56.32	61.26
20	56.25	61.56
26	56.25	61.21

Run Nos. : 20-21
Date : 25 Sep 90

The following process variables are held constant for the cycle times listed below:

Packing in the column : Zeolite 4A
Feed flow rate : 0.34 SLPM
Product flow rate : 0.05 SLPM
Purge flow rate : 0.21 SLPM
High pressure : 29.4 psia
Low pressure : 14.7 psia
Feed concentration : 60 %CH₄
Velocity : 0.76 cm/sec
Purge gas : Part of product
Purge to Feed ratio : 1.24
Initial condition : Saturated with feed
Step duration : 1:4:1:4
Temperature : 26 C

Concentrations are measured 2 sec before the end of adsorption step.

Cycle time : 60 sec

No. of cycles	Outlet product concentration (mole % methane)	Outlet purge concentration (mole % methane)
0	60.65	60.72
1	60.66	61.07
5	59.64	61.07
9	57.48	61.06
13	55.94	61.05
21	54.46	61.00
28	53.85	60.97
36	53.52	61.03
45	53.34	61.00
Time during the cycle sec	Product concentration (mole % methane)	Purge concentration (mole % methane)
5	53.72	60.91
10	53.64	60.98
20	53.28	61.03

Cycle time : 90 sec

No. of cycles	Outlet product concentration (mole % methane)	Outlet purge concentration (mole % methane)
0	60.47	60.60
1	60.46	61.19
4	59.61	61.19
7	57.48	61.18
11	55.74	61.17
14	55.08	61.13
26	53.92	61.12
49	53.51	61.10
66	53.31	61.08

Time during the cycle sec	Product concentration (mole % methane)	Purge concentration (mole % methane)
5	53.53	60.85
10	53.70	61.07
20	53.95	61.19
30	53.86	61.14
40	53.47	61.13

Run No. : 22
Date : 26 Sep 90

The following process variables are held constant for the cycle time listed below:

Packing in the column : Zeolite 4A
Feed flow rate : 0.34 SLPM
Product flow rate : 0.05 SLPM
Purge flow rate : 0.21 SLPM
High pressure : 44.1 psia
Low pressure : 14.7 psia
Feed concentration : 60 %CH₄
Velocity : 0.51 cm/sec
Purge gas : Part of product
Purge to Feed ratio : 1.85
Initial condition : Saturated with feed
Step duration : 1:4:1:4
Temperature : 26 C

Concentrations are measured 2 sec before the end of adsorption step.

Cycle time : 90 sec

No. of cycles	Outlet product concentration (mole % methane)	Outlet purge concentration (mole % methane)
0	60.38	60.51
2	60.49	61.24
5	59.79	61.08
8	57.51	60.98
20	53.44	60.88
27	52.99	60.81
33	52.87	60.83
39	52.80	60.81
55	52.66	60.81
Time during the cycle sec	Product concentration (mole % methane)	Purge concentration (mole % methane)
10	52.69	61.02
20	52.80	61.01
30	52.70	60.94
40	52.69	60.88

Run No. : 23
Date : 29 Sep 90

The following process variables are held constant for the cycle time listed below:

Packing in the column : Zeolite 4A
Feed flow rate : 0.30 SLPM
Product flow rate : 0.05 SLPM
Purge flow rate : 0.14 SLPM
High pressure : 29.4 psia
Low pressure : 14.7 psia
Feed concentration : 60 %CH₄
Purge to Feed ratio : 0.93
Velocity : 0.67 cm/sec
Purge gas : Part of product
Initial condition : Saturated with feed
Step duration : 1:4:1:4
Temperature : 26 C

Concentrations are measured 2 sec before the end of adsorption step.

Cycle time : 60 sec

No. of cycles	Outlet product concentration (mole % methane)	Outlet purge concentration (mole % methane)
0	60.76	60.74
1	60.62	60.96
6	60.35	61.03
19	55.86	61.08
34	54.39	60.99
62	53.75	60.91
80	53.60	60.96

Run No. : 24
Date : 7 Oct 90

The following process variables are held constant for the cycle time listed below:

Packing in the column : Zeolite 4A
Feed flow rate : 0.42 SLPM
Product flow rate : 0.06 SLPM
Purge flow rate : 0.21 SLPM
High pressure : 29.4 psia
Low pressure : 14.7 psia
Feed concentration : 60 %CH₄
Velocity : 0.94 cm/sec
Purge gas : Part of product
Purge to Feed ratio : 1.00
Initial condition : Saturated with methane
Step duration : 1:4:1:4
Temperature : 26 C

Concentrations are measured 2 sec before the end of adsorption step.

Cycle time : 60 sec

No. of cycles	Outlet product concentration (mole % methane)	Outlet purge concentration (mole % methane)
4	99.01	99.73
8	89.33	62.77
12	79.95	62.17
16	73.22	61.93
21	67.47	61.80
25	64.40	61.87
29	62.17	61.58
36	59.70	61.50
45	57.86	61.64
52	56.92	61.44
65	55.81	61.34
73	55.35	61.33
87	54.76	61.30
128	53.80	61.31
134	53.72	61.25
138	53.65	61.23

Run Nos. : 25-26
Date : 8 Oct 90

The following process variables are held constant for the cycle times listed below:

Packing in the column : Zeolite 4A
Feed flow rate : 0.42 SLPM
Product flow rate : 0.06 SLPM
Purge flow rate : 0.24 SLPM
High pressure : 29.4 psia
Low pressure : 14.7 psia
Feed concentration : 60 %CH₄
Velocity : 0.94 cm/sec
Purge gas : Part of product
Purge to Feed ratio : 1.14
Initial condition : Saturated with methane
Step duration : 1:4:1:4
Temperature : 90 C

Concentrations are measured 2 sec before the end of adsorption step.

Cycle time : 30 sec

No. of cycles	Outlet product concentration (mole % methane)	Outlet purge concentration (mole % methane)
1	99.99	63.96
8	92.10	61.97
16	74.76	61.67
24	65.48	61.40
37	59.38	61.31
58	56.46	61.20
81	55.48	61.15
231	54.53	61.12
259	54.43	61.12
270	54.45	61.10
279	54.42	61.13

Cycle time : 60 sec

No. of cycles	Outlet product concentration (mole % methane)	Outlet purge concentration (mole % methane)
1	91.33	67.15
5	90.22	63.58
9	74.78	62.73
13	66.71	62.29
17	62.74	62.04
21	60.31	61.92
28	58.74	61.70
35	57.89	61.67
43	57.39	61.66

APPENDIX A.1.3

RAW DATA FOR SINGLE COLUMN PSA EXPERIMENTS WITH 4A ZEOLITE

Run No. : 1
Date : 15 Oct 90

The following process variables are held constant for the cycle time listed below:

Single column
Packing in the column : Zeolite 4A
Feed flow rate : 0.5659 SLPM
Purge flow rate : 0.262 SLPM
High pressure : 29.4 psia
Low pressure : 14.7 psia
Feed concentration : 60 %CH₄
Velocity : 1.26 cm/sec
Purge gas : Pure methane
Purge to Feed ratio : 0.926
Initial condition : Saturated with feed
Step duration : 1:4:1:4 (press:adsorp:blowdown:purge)
Temperature : 26 C

Concentrations are measured 2 sec before the end of adsorption step.

Cycle time : 60 sec

No. of cycles	Outlet product concentration (mole % methane)
0	60.87
1	71.38
5	78.33
8	79.08
13	81.61
16	81.81
23	82.54
38	82.73
43	82.57
71	81.64

Time during the cycle sec	Outlet product concentration (mole % methane)	Time during the cycle sec	Outlet purge concentration (mole % methane)
8	77.14	5	59.95
12	94.42	11	60.05
15	91.92	14	59.83
18	89.11	37	59.93
23	84.92	40	60.39
		45	61.15
		50	61.51
		53	59.97
		60	60.91

Run No. : 2
Date : 15 Oct 90

The following process variables are held constant for the cycle time listed below:

Single column
Packing in the column : Zeolite 4A
Feed flow rate : 0.2579 SLPM
Purge flow rate : 0.262 SLPM
High pressure : 29.4 psia
Low pressure : 14.7 psia
Feed concentration : 60 %CH₄
Velocity : 0.58 cm/sec
Purge gas : Pure methane
Purge to Feed ratio : 2.032
Initial condition : Saturated with feed
Step duration : 1:4:1:4
Temperature : 26 C

Concentrations are measured 2 sec before the end of adsorption step.

Cycle time : 60 sec

No. of cycles	Outlet product concentration (mole % methane)	No of cycles	Outlet purge concentration (mole % methane)
1	94.52	40	64.21
7	97.35	74	66.45
12	97.92	87	64.33
17	98.23	94	62.11
28	98.44		
99	98.82		

Time during the cycle sec	Outlet product concentration (mole % methane)	Time during the cycle sec	Outlet purge concentration (mole % methane)
8	98.76	40	69.92
10	98.82	42	68.04
18	98.71	45	63.57
23	98.62	47	67.27
		50	66.60
		60	66.85

Run No. : 3
Date : 16 Oct 90

The following process variables are held constant for the cycle time listed below:

Single column
Packing in the column : Zeolite 4A
Feed flow rate : 0.7059 SLPM
Purge flow rate : 0.158 SLPM
High pressure : 29.4 psia
Low pressure : 14.7 psia
Feed concentration : 60 %CH₄
Velocity : 1.57 cm/sec
Purge gas : Pure methane
Purge to Feed ratio : 0.448
Initial condition : Saturated with feed
Step duration : 1:4:1:4
Temperature : 26 C

Concentrations are measured 2 sec before the end of adsorption step.

Cycle time : 60 sec

No. of cycles	Outlet product concentration (mole % methane)	No of cycles	Outlet purge concentration (mole % methane)
0	59.69	74	60.43
6	71.06	86	60.59
10	76.83	98	60.45
14	76.91		
19	77.41		
24	77.15		
33	73.91		
37	76.69		
41	77.32		
60	72.57		
64	77.05		
102	76.30		
117	77.32		

Time during the cycle sec	Outlet product concentration (mole % methane)	Time during the cycle sec	Outlet purge concentration (mole % methane)
13	68.50	40	62.03
18	64.63	45	61.75
23	71.14	53	60.97
30	75.36		

Run No. : 4
Date : 20 Oct 90

The following process variables are held constant for the cycle time listed below:

Single column
Packing in the column : Zeolite 4A
Feed flow rate : 0.4259 SLPM
Purge flow rate : 0.158 SLPM
High pressure : 29.4 psia
Low pressure : 14.7 psia
Feed concentration : 60 %CH₄
Velocity : 0.95 cm/sec
Purge gas : Pure methane
Purge to Feed ratio : 0.7419
Initial condition : Saturated with feed
Step duration : 1:4:1:4
Temperature : 26 C

Concentrations are measured 2 sec before the end of adsorption step.

Cycle time : 60 sec

No. of cycles	Outlet product concentration (mole % methane)	No of cycles	Outlet purge concentration (mole % methane)
0	60.87	1	59.23
1	67.98	9	60.36
5	74.16		
9	76.09		
58	77.48		

Time during the cycle sec	Outlet purge concentration (mole % methane)
31	60.61
33	62.24
35	60.39
40	62.97
41	60.75
45	63.09
53	63.11

Run No. : 5
Date : 20 Oct 90

The following process variables are held constant for the cycle time listed below:

Single column
Packing in the column : Zeolite 4A
Feed flow rate : 0.4259 SLPM
Purge flow rate : 0.230 SLPM
High pressure : 29.4 psia
Low pressure : 14.7 psia
Feed concentration : 60 %CH₄
Velocity : 0.95 cm/sec
Purge gas : Pure helium
Purge to Feed ratio : 1.08
Initial condition : Saturated with feed
Step duration : 1:4:1:4
Temperature : 26 C

Concentrations are measured 2 sec before the end of adsorption step.

Cycle time : 60 sec

No. of cycles	Outlet product concentration (mole % methane)	No of cycles	Outlet purge concentration (mole % methane)
1	58.43	3	61.26
9	62.07	11	62.43
19	60.36	19	62.41
26	58.59	26	62.29
32	57.42	33	62.23
39	55.76	39	63.25
43	55.71	43	62.04

Run No. : 6
 Date : 21 Oct 90

The following process variables are held constant for the cycle time listed below:

Single column
 Packing in the column : Zeolite 4A
 Feed flow rate : 0.4259 SLPM
 Purge flow rate : 0.230 SLPM
 High pressure : 29.4 psia
 Low pressure : 14.7 psia
 Feed concentration : 60 %CH₄
 Velocity : 0.95 cm/sec
 Purge gas : Pure helium
 Purge to Feed ratio : 1.08
 Initial condition : Saturated with feed
 Step duration : 1:2:1:6
 Temperature : 26 C

Concentrations are measured 2 sec before the end of adsorption step.

Cycle time : 120 sec

No. of cycles	Outlet product concentration (mole % methane)	No of cycles	Outlet purge concentration (mole % methane)
5	47.37	1	52.82
7	48.82	3	51.52
9	50.53	5	51.88
13	53.19	7	52.61
27	58.04	9	53.12
31	58.84	13	54.19
35	59.45	27	55.77
39	59.41	31	57.83
70	60.07	35	55.98
72	60.32	39	56.14
112	60.18	72	56.24
125	59.94	113	56.53

Time during the cycle sec	Outlet product concentration (mole % methane)	Time during the cycle sec	Outlet purge concentration (mole % methane)
20	62.26	50	63.45
24	48.93	55	63.99
25	50.67	60	63.68
30	56.84	65	71.91
		72	63.96
		80	61.58
		90	59.90
		100	58.34
		110	56.88

Run Nos. : 7-13
 Date : 24 Oct 90

The following process variables are held constant for the cycle times listed below:

Single column
 Packing in the column : Zeolite 4A
 Feed flow rate : 0.5659 SLPM
 Purge flow rate : 0.230 SLPM
 High pressure : 29.4 psia
 Low pressure : 14.7 psia
 Feed concentration : 60 %CH₄
 Velocity : 1.26 cm/sec
 Purge gas : Pure helium
 Purge to Feed ratio : 0.813
 Initial condition : Saturated with feed
 Step duration : 3:1:6 (adsorp:blowdown:purge)
 Temperature : 26 C

Concentrations are measured 2 sec before the end of adsorption step.

Cycle time : 120 sec

No. of cycles	Outlet product concentration (mole % methane)	No of cycles	Outlet purge concentration (mole % methane)
4	51.73	1	57.66
12	53.77	4	53.58
18	56.14	12	53.87
32	59.76	18	54.74
88	63.19	32	56.09
110	63.97	90	57.38
262	64.08	110	57.55
		262	57.84

Time during the cycle sec	Outlet product concentration (mole % methane)	Time during the cycle sec	Outlet purge concentration (mole % methane)
15	52.40	55	62.82
20	56.24	60	63.41
25	59.77	65	63.30
30	62.51	75	63.29

80	62.18
90	60.80
100	59.65
110	58.44

Cycle time : 150 sec

No. of cycles	Outlet product concentration (mole % methane)	No of cycles	Outlet purge concentration (mole % methane)
1	63.37	1	52.03
3	62.15	3	52.23
6	63.82	7	53.84
23	69.00	23	57.07
47	70.05	47	57.14
64	70.02		

Time during the cycle sec	Outlet product concentration (mole % methane)	Time during the cycle sec	Outlet purge concentration (mole % methane)
25	64.44	60	62.06
30	66.15	70	62.44
35	67.71	80	62.73
41	69.37	90	61.66
43	70.63	100	60.66
		110	60.28
		130	58.71
		140	57.39

Cycle time : 180 sec

No. of cycles	Outlet product concentration (mole % methane)	No of cycles	Outlet purge concentration (mole % methane)
20	73.54	20	56.54
22	73.37	22	56.44
26	73.80	26	56.41
29	73.66	29	56.65
53	73.87	53	56.70

Cycle time : 210 sec

No. of cycles	Outlet product concentration (mole % methane)	No of cycles	Outlet purge concentration (mole % methane)
20	72.61	20	56.70
22	75.94	22	55.52
24	76.48	24	57.01
26	76.73	26	56.69
28	76.68	28	57.00
30	76.59	30	56.71
34	76.61	34	56.64
36	76.52	36	56.59
38	76.62	38	56.55

Cycle time : 240 sec

No. of cycles	Outlet product concentration (mole % methane)	No of cycles	Outlet purge concentration (mole % methane)
1	84.33	1	46.83
2	76.64	2	48.76
3	75.32	3	50.25
4	75.53	4	51.82
6	75.82	6	53.11
8	76.67	8	54.18
17	77.35	17	56.03
24	77.55	24	56.36
27	77.81	27	56.43
34	77.52	34	57.08

Cycle time : 270 sec

No. of cycles	Outlet product concentration (mole % methane)	No of cycles	Outlet purge concentration (mole % methane)
11	76.53	11	56.80
13	76.88	13	56.25
25	76.86	25	56.38
28	76.89	28	56.68
36	76.95		

Time during the cycle sec	Outlet product concentration (mole % methane)
---------------------------------	---

65	77.32
70	77.60
75	77.33

Cycle time : 300 sec

No. of cycles	Outlet product concentration (mole % methane)	No of cycles	Outlet purge concentration (mole % methane)
1	75.65	1	56.60
2	75.61	2	56.50
25	75.60	25	56.32
27	75.62	27	56.21

Run Nos. : 14-16
 Date : 29 Oct 90

The following process variables are held constant for the cycle times listed below:

Single column
 Packing in the column : Zcolite 4A
 Feed flow rate : 0.8459 SLPM
 Purge flow rate : 0.230 SLPM
 High pressure : 44.1 psia
 Low pressure : 14.7 psia
 Feed concentration : 60 %CH₄
 Velocity : 1.26 cm/sec
 Purge gas : Pure helium
 Purge to Feed ratio : 0.816
 Initial condition : Saturated with feed
 Step duration : 3:1:6
 Temperature : 26 C

Concentrations are measured 2 sec before the end of adsorption step.

Cycle time : 240 sec

No. of cycles	Outlet product concentration (mole % methane)	No of cycles	Outlet purge concentration (mole % methane)
1	74.04	1	53.89
3	73.32	3	54.85
5	73.44	5	55.08
7	73.68	6	55.31
11	73.69	7	55.36
30	73.77	10	55.88
		12	55.91
		13	55.97
		15	56.02

Time during the cycle
sec Outlet product
 concentration
 (mole % methane)

50	74.16
55	74.54
60	74.44
65	73.96

Cycle time : 180 sec

No. of cycles	Outlet product concentration (mole % methane)	No of cycles	Outlet purge concentration (mole % methane)
------------------	---	-----------------	---

1	79.58	1	51.72
2	74.08	2	50.32
3	72.41	3	50.67
4	72.11	4	51.29
8	72.52	8	53.56
12	73.02	12	54.86
15	73.25	15	55.07

Time during the cycle	Outlet product concentration	Time during the cycle	Outlet purge concentration
47	71.72	173	54.94

Cycle time : 210 sec

No. of cycles	Outlet product concentration (mole % methane)	No of cycles	Outlet purge concentration (mole % methane)
------------------	---	-----------------	---

1	79.65	1	47.83
2	74.09	2	48.95
3	72.86	3	49.26
6	72.98	6	52.47
9	73.50	9	53.96
31	74.03	31	55.86

Run Nos. : 17-20
 Date : 31 Oct 90

The following process variables are held constant for the cycle times listed below:

Single column
 Packing in the column : Zeolite 4A
 Feed flow rate : 0.5939 SLPM
 Purge flow rate : 0.230 SLPM
 High pressure : 44.1 psia
 Low pressure : 14.7 psia
 Feed concentration : 60 %CH₄
 Velocity : 0.88 cm/sec
 Purge gas : Pure helium
 Purge to Feed ratio : 1.162
 Initial condition : Saturated with feed
 Step duration : 3:1:6
 Temperature : 26 C

Concentrations are measured 2 sec before the end of adsorption step.

Cycle time : 210 sec

No. of cycles	Outlet product concentration (mole % methane)	No of cycles	Outlet purge concentration (mole % methane)
1	72.77	1	56.70
2	73.40	2	56.79
3	73.65	3	57.01
4	73.69	31	56.56
31	73.94	32	56.89
32	74.10		
36	74.08		

Time during the cycle sec	Outlet product concentration (mole % methane)
63	74.45

Cycle time : 240 sec

No. of cycles	Outlet product concentration (mole % methane)	No of cycles	Outlet purge concentration (mole % methane)
1	76.26	1	56.27
3	76.32	2	56.32
6	76.40	3	56.26
		6	56.49
		10	57.00

Time during the cycle sec	Outlet product concentration (mole % methane)
72	76.55

Cycle time : 270 sec

No. of cycles	Outlet product concentration (mole % methane)	No of cycles	Outlet purge concentration (mole % methane)
1	77.05	1	56.93
9	77.49	9	57.10
		10	57.30

Time during the cycle sec	Outlet product concentration (mole % methane)	Time during the cycle sec	Outlet purge concentration (mole % methane)
75	77.26		

Cycle time : 300 sec

No. of cycles	Outlet product concentration (mole % methane)	No of cycles	Outlet purge concentration (mole % methane)
1	77.88	1	57.68
5	77.83	2	57.34
		4	57.25
		5	57.15

Time during the cycle sec	Outlet product concentration (mole % methane)
80	77.90
85	77.91
90	77.74

Run Nos. : 21-24
 Date : 3 Nov 90

The following process variables are held constant for the cycle times listed below:

Single column
 Packing in the column : Zcolite 4A
 Feed flow rate : 0.3979 SLPM
 Purge flow rate : 0.230 SLPM
 High pressure : 29.4 psia
 Low pressure : 14.7 psia
 Feed concentration : 60 %CH₄
 Velocity : 0.88 cm/sec
 Purge gas : Pure helium
 Purge to Feed ratio : 1.156
 Initial condition : Saturated with feed
 Step duration : 3:1:6
 Temperature : 26 C

Concentrations are measured 2 sec before the end of adsorption step.

Cycle time : 300 sec

No. of cycles	Outlet product concentration (mole % methane)	No of cycles	Outlet purge concentration (mole % methane)
1	63.11	1	45.28
2	70.29	2	48.70
3	65.76	3	50.80
		4	52.20

Time during the cycle sec	Outlet product concentration (mole % methane)
91	75.06

Cycle time : 360 sec

No. of cycles	Outlet product concentration (mole % methane)	No of cycles	Outlet purge concentration (mole % methane)
1	79.47	1	53.24
2	79.50	2	54.10
3	79.93	3	54.97
4	80.72	4	55.50

Cycle time : 420 sec

No. of cycles	Outlet product concentration (mole % methane)	No of cycles	Outlet purge concentration (mole % methane)
1	85.99	1	45.09
2	80.34	4	53.40
4	80.84	5	54.54
26	82.37	27	58.25
27	82.47	39	57.74
39	82.28		

Time during the cycle sec Outlet product concentration (mole % methane)

110	82.54
115	82.63
120	82.51

Cycle time : 390 sec

No. of cycles	Outlet product concentration (mole % methane)	No of cycles	Outlet purge concentration (mole % methane)
1	81.78	1	57.47
10	82.44	10	57.80
17	82.36	17	58.04
23	82.67		
Time during the cycle sec	Outlet product concentration (mole % methane)	Time during the cycle sec	Outlet purge concentration (mole % methane)
110	82.36		

Run Nos. : 25-29
 Date : 6 Nov 90

The following process variables are held constant for the cycle times listed below:

Single column	
Packing in the column	: Zeolite 4A
Feed flow rate	: 0.3979 SLPM
Purge flow rate	: - SLPM
High pressure	: 29.4 psia
Low pressure	: 0.1 psia
Feed concentration	: 60 %CH ₄
Velocity	: 0.88 cm/sec
Purge gas	: - (Vacuum to < 10 mm Hg)
Purge to Feed ratio	: -
Initial condition	: Saturated with feed
Step duration	: 3:1:6
Temperature	: 26 C

Concentrations are measured 2 sec before the end of adsorption step.

Cycle time : 240 sec

No. of cycles	Outlet product concentration (mole % methane)
1	72.41
2	72.17
4	72.50
5	72.64
8	72.83

Time during the cycle sec	Outlet product concentration (mole % methane)
55	70.17
60	70.93
71	72.88

Cycle time : 300 sec

No. of cycles	Outlet product concentration (mole % methane)
---------------	---

1	72.91
2	73.85
12	74.17
14	74.18

Time during the cycle sec	Outlet product concentration (mole % methane)
---------------------------	---

79	73.98
80	73.97
82	74.02
83	74.16

Cycle time : 330 sec

No. of cycles	Outlet product concentration (mole % methane)
---------------	---

1	74.20
2	74.22

Time during the cycle sec	Outlet product concentration (mole % methane)
---------------------------	---

80	74.13
85	74.30
90	74.32
97	74.25

Cycle time : 330 sec (repeat run)

No. of cycles	Outlet product concentration (mole % methane)
---------------	---

1	73.27
2	73.62
3	73.86
8	74.35
9	74.28

Cycle time : 360 sec

No. of cycles	Outlet product concentration (mole % methane)
---------------	---

1	74.31
2	74.38
3	74.29
4	74.43
6	74.56
9	74.55

Time during the cycle sec	Outlet product concentration (mole % methane)
---------------------------	---

101	74.54
-----	-------

Cycle time : 390 sec

No. of cycles	Outlet product concentration (mole % methane)
---------------	---

1	74.23
3	74.19
4	74.21
8	74.21

Time during the cycle sec	Outlet product concentration (mole % methane)
---------------------------	---

100	74.56
110	74.38

Run Nos. : 30-33
 Date : 7 Nov 90

The following process variables are held constant for the cycle times listed below:

Single column
 Packing in the column : Zcolite 4A
 Feed flow rate : 0.5939 SLPM
 Purge flow rate : - SLPM
 High pressure : 44.1 psia
 Low pressure : 0.1 psia
 Feed concentration : 60 %CH₄
 Velocity : 0.88 cm/sec
 Purge gas : - (Vacuum to < 10 mm Hg)
 Purge to Feed ratio : -
 Initial condition : Saturated with feed
 Step duration : 3:1:6
 Temperature : 26 C

Concentrations are measured 2 sec before the end of adsorption step.

Cycle time : 300 sec

No. of cycles	Outlet product concentration (mole % methane)
---------------	---

1	56.26
2	69.29
3	73.05
6	73.90
7	73.85

Time during the cycle sec	Outlet product concentration (mole % methane)
---------------------------	---

70	73.19
75	73.54
80	73.67
83	73.77
90	73.74

Cycle time : 330 sec

No. of cycles	Outlet product concentration (mole % methane)
---------------	---

1	73.48
5	73.66

Time during the cycle sec	Outlet product concentration (mole % methane)
---------------------------	---

82	73.81
87	73.86
92	73.81

Cycle time : 270 sec

No. of cycles	Outlet product concentration (mole % methane)
---------------	---

1	71.59
2	72.70
3	72.12
6	72.22
11	73.81
13	73.26
23	73.44

Time during the cycle sec	Outlet product concentration (mole % methane)
---------------------------	---

55	71.19
60	73.42
68	72.87
73	72.26

Cycle time : 420 sec

No. of cycles	Outlet product concentration (mole % methane)
---------------	---

10	72.10
----	-------

Run Nos. : 34-36
 Date : 10 Nov 90

The following process variables are held constant for the cycle times listed below:

Single column	
Packing in the column	: Zeolite 4A
Feed flow rate	: 0.8459 SLPM
Purge flow rate	: - SLPM
High pressure	: 44.1 psia
Low pressure	: 0.1 psia
Feed concentration	: 60 %CH ₄
Velocity	: 1.26 cm/sec
Purge gas	: - (Vacuum to < 10 mm Hg)
Purge to Feed ratio	: -
Initial condition	: Saturated with feed
Step duration	: 3:1:6
Temperature	: 26 C

Concentrations are measured 2 sec before the end of adsorption step.

Cycle time : 360 sec

No. of cycles	Outlet product concentration (mole % methane)
---------------	---

2	68.59
20	68.69

Time during the cycle sec	Outlet product concentration (mole % methane)
---------------------------	---

50	72.59
55	72.30
60	72.64
70	72.30
80	71.46
104	68.62
110	67.45

Cycle time : 240 sec

No. of cycles	Outlet product concentration (mole % methane)
---------------	---

2	70.45
---	-------

5	71.74
---	-------

10	72.00
----	-------

11	72.00
----	-------

Time during the cycle sec	Outlet product concentration (mole % methane)
---------------------------	---

50	71.84
----	-------

55	72.17
----	-------

60	72.07
----	-------

Cycle time : 210 sec

No. of cycles	Outlet product concentration (mole % methane)
---------------	---

1	72.06
---	-------

6	72.13
---	-------

7	72.06
---	-------

Time during the cycle sec	Outlet product concentration (mole % methane)
---------------------------	---

40	72.40
----	-------

50	71.76
----	-------

55	71.99
----	-------

Run Nos. : 37-40
 Date : 10 Nov 90

The following process variables are held constant for the cycle times listed below:

Single column
 Packing in the column : Zeolite 4A
 Feed flow rate : 0.5659 SLPM
 Purge flow rate : - SLPM
 High pressure : 29.4 psia
 Low pressure : 0.1 psia
 Feed concentration : 60 %CH₄
 Velocity : 1.26 cm/sec
 Purge gas : - (Vacuum to < 10 mm Hg)
 Purge to Feed ratio : -
 Initial condition : Saturated with feed
 Step duration : 3:1:6
 Temperature : 26 C

Concentrations are measured 2 sec before the end of adsorption step.

Cycle time : 210 sec

No. of cycles	Outlet product concentration (mole % methane)
---------------	---

1	71.34
3	71.51
5	69.90
6	72.30
32	72.13

Time during the cycle sec	Outlet product concentration (mole % methane)
---------------------------	---

55	71.23
63	72.29

Cycle time : 240 sec

No. of cycles	Outlet product concentration (mole % methane)
---------------	---

1	72.26
2	73.03
4	73.10
8	73.19

Time during the cycle sec	Outlet product concentration (mole % methane)
---------------------------	---

50	72.89
65	72.81
72	73.24

Cycle time : 270 sec

No. of cycles	Outlet product concentration (mole % methane)
---------------	---

1	73.46
2	73.59
5	73.69

Time during the cycle sec	Outlet product concentration (mole % methane)
---------------------------	---

74	73.54
81	73.81

Cycle time : 300 sec

No. of cycles	Outlet product concentration (mole % methane)
---------------	---

1	71.62
---	-------

5	73.41
---	-------

6	73.45
---	-------

9	73.68
---	-------

28	73.86
----	-------

Time during the cycle sec	Outlet product concentration (mole % methane)
---------------------------	---

83	73.57
----	-------

90	73.64
----	-------

Run Nos. : 41-42
 Date : 11 Nov 90

The following process variables are held constant for the cycle times listed below:

Single column	
Packing in the column	: Zeolite 4A
Feed flow rate	: 0.548 SLPM
Purge flow rate	: - SLPM
High pressure	: 29.4 psia
Low pressure	: 0.1 psia
Feed concentration	: 92 %CH ₄
Velocity	: 1.22 cm/sec
Purge gas	: - (Vacuum to < 10 mm Hg)
Purge to Feed ratio	: -
Initial condition	: Saturated with feed
Step duration	: 3:1:6
Temperature	: 26 C

Concentrations are measured 2 sec before the end of adsorption step.

Cycle time : 300 sec

No. of cycles	Outlet product concentration (mole % methane)
1	94.48
6	95.46
12	95.50

Time during the cycle sec	Outlet product concentration (mole % methane)
30	93.55
50	95.04
60	95.29
60	95.36
70	95.30
70	95.38
70	95.42
70	95.47
80	95.55

Cycle time : 270 sec

No. of cycles	Outlet product concentration (mole % methane)
---------------	---

3	95.42
---	-------

5	95.44
---	-------

8	95.57
---	-------

9	95.47
---	-------

Time during the cycle sec	Outlet product concentration (mole % methane)
---------------------------	---

70	95.47
----	-------

74	95.45
----	-------

77	95.55
----	-------

Run No. : 43-45
 Date : 12 Nov 90

The following process variables are held constant for the cycle time listed below:

Single column
 Packing in the column : Zeolite 4A
 Feed flow rate : 0.548 SLPM
 Purge flow rate : 0.230 SLPM
 High pressure : 29.4 psia
 Low pressure : 14.7 psia
 Feed concentration : 92 %CH₄
 Velocity : 1.22 cm/sec
 Purge gas : Pure helium
 Purge to Feed ratio : 0.839
 Initial condition : Saturated with feed
 Step duration : 3:1:6
 Temperature : 26 C

Concentrations are measured 2 sec before the end of adsorption step.

Cycle time : 270 sec

No. of cycles	Outlet product concentration (mole % methane)	No of cycles	Outlet purge concentration (mole % methane)
3	96.04	1	90.53
22	96.35	3	91.15
		22	92.07

Time during the cycle sec	Outlet product concentration (mole % methane)
70	96.04
83	96.43

Cycle time : 330 sec

No. of cycles	Outlet product concentration (mole % methane)	No of cycles	Outlet purge concentration (mole % methane)
1	96.35	1	92.20
3	96.32	3	91.35
Time during the cycle sec	Outlet product concentration (mole % methane)	Time during the cycle sec	Outlet purge concentration (mole % methane)
87	96.47		
92	96.46	268	92.18

Cycle time : 300 sec

No. of cycles	Outlet product concentration (mole % methane)	No of cycles	Outlet purge concentration (mole % methane)
1	96.43	1	92.08
3	96.42	3	92.13
5	96.50	5	92.12
		9	92.23
Time during the cycle sec	Outlet product concentration (mole % methane)	Time during the cycle sec	Outlet purge concentration (mole % methane)
83	96.39	240	91.38
88	96.43		

APPENDIX A.1.4

RAW DATA FOR SORPTION EXPERIMENTS WITH CARBON MOLECULAR SIEVES

Run no. : 1
 Date : 21st August 1991
 Adsorbent : carbon molecular sieve
 Adsorbate : nitrogen
 Method : volumetric
 Temperature : 79.0 c
 Weight cms : 47.4 grams
 Initial cell pressure : 0.00 psia
 Step to pressure : 4.18 psia
 Final cell pressure : 3.345 psia
 q : 0.0277 moles/kg cms @ 3.345 psia
 Volume cell E : 668.21 ccms.

Cell E isolated for experiment.

P(psia)	Time(secs)
0.00	0-
4.18	0 +
4.00	18.5
3.97	22
3.86	40
3.75	64
3.636	100
3.58	136
3.508	172
3.47	208
3.456	226
3.38	496
3.372	656
3.345	infinity

Run no. : 2
 Date : 21st August 1991
 Adsorbent : carbon molecular sieve
 Adsorbate : nitrogen
 Method : volumetric
 Temperature : 79.0 c
 Weight cms : 47.4 grams
 Initial cell pressure : 3.345 psia
 Step to pressure : 2.00 psia
 Final cell pressure : 2.26 psia
 q : 0.0191 moles/kg cms @ 2.26 psia
 Volume cell E : 668.21 ccms.

Cell E isolated for experiment.

P(psia)	Time(secs)
3.345	0-
2.0	0+
2.036	12
2.074	30
2.102	48
2.134	84
2.174	120
2.191	150
2.205	186
2.246	546
2.256	906
2.26	infinity

Run no. : 3
 Date : 21st August 1991
 Adsorbent : carbon molecular sieve
 Adsorbate : nitrogen
 Method : volumetric
 Temperature : 79.0 c
 Weight cms : 47.4 grams
 Initial cell pressure : 2.26 psia
 Step to pressure : 1.356 psia
 Final cell pressure : 1.527 psia
 q : 0.0134 moles/kg cms @ 1.527 psia
 Volume cell E : 668.21 ccms.

Cell E isolated for experiment.

P(psia)	Time(secs)
2.26	0-
1.356	0+
1.369	10
1.404	28
1.419	46
1.446	76
1.469	112
1.484	148
1.502	220
1.506	244
1.523	604
1.528	infinity

Run no. : 4
 Date : 24th August 1991
 Adsorbent : carbon molecular sieve
 Adsorbate : nitrogen
 Method : volumetric
 Temperature : 50.0 c
 Weight cms : 47.4 grams
 Initial cell pressure : 0.00 psia
 Step to pressure : 2.45 psia
 Final cell pressure : 1.76 psia
 q : 0.025 moles/kg cms @ 1.76 psia
 Volume cell E : 668.21 ccms.

Cell E isolated for experiment.

P(psia)	Time(secs)
0.0	0-
2.45	0+
2.40	12
2.34	36
2.28	63
2.22	95
2.193	111
2.094	183
2.019	255
1.962	327
1.92	399
1.82	759
1.782	1119
1.769	1479
1.763	1839
1.7588	infinity

Run no. : 5
 Date : 24th August 1991
 Adsorbent : carbon molecular sieve
 Adsorbate : nitrogen
 Method : volumetric
 Temperature : 50.0 c
 Weight cms : 47.4 grams
 Initial cell pressure : 1.76 psia
 Step to pressure : 1.093 psia
 Final cell pressure : 1.276 psia
 q : 0.0184 moles/kg cms @ 1.276 psia
 Volume cell E : 668.21 ccms.

Cell E isolated for experiment.

P(psia)	Time(secs)
1.76	0-
1.093	0 +
1.114	31
1.126	49
1.1404	73
1.157	109
1.1704	145
1.1932	214
1.213	290
1.24	470
1.264	990
1.2748	1350
1.2778	infinity

Run no. : 6
 Date : 25th August 1991
 Adsorbent : carbon molecular sieve
 Adsorbate : methane
 Method : volumetric
 Temperature : 78.2 c
 Weight cms : 47.4 grams
 Initial cell pressure : 0.0 psia
 Step to pressure : 4.206 psia
 Final cell pressure : 2.17 psia
 q : 0.068 moles/kg cms @ 2.17 psia
 Volume cell E : 668.21 ccms.

Cell E isolated for experiment.

P(psia)	Time(secs)
0.0	0-
4.206	0 +
4.168	14
4.12	74
4.078	170
4.0	350
3.928	530
3.797	890
3.683	1250
3.488	1970
3.314	2690
3.188	3370
3.177	3410
3.052	4130
2.948	4850
2.81	5930
2.696	7010
2.54	9170
2.432	11330
2.376	13490
2.273	17810
2.228	22130
2.1884	26450
2.186	30770
2.17	infinity

Run no. : 7
 Date : 27th-30th August 1991
 Adsorbent : carbon molecular sieve
 Adsorbate : methane
 Method : volumetric
 Temperature : 50 c
 Weight CMS : 47.4 grams
 Initial cell pressure : 0.0 psia
 Step to pressure : 3.969 psia
 Final cell pressure : 1.486 psia
 q : 0.0898 moles/kg cms @ 1.486 psia
 Volume cell E : 668.21 ccms.

Cell E isolated for experiment.

P(psia)	Time(secs)
0.0	0-
3.96	0 +
3.9	270
3.74	1350
3.61	1710
3.37	3510
3.16	5310
2.97	7110
2.814	8910
2.68	10710
2.52	12510
2.45	14310
2.356	16110
2.144	20790
1.90	29790
1.71	42390
1.596	60390
1.55	78390
1.526	96390
1.51	114390
1.486	infinity

Run no. : 8
 Date : 2nd September 1991
 Adsorbent : carbon molecular sieve
 Adsorbate : methane
 Method : volumetric
 Temperature : 127 c
 Weight CMS : 47.4 grams
 Initial cell pressure : 0.0 psia
 Step to pressure : 5.701 psia
 Final cell pressure : 4.513 psia
 Q q : 0.0347 moles/kg cms @ 4.513 psia
 Volume cell E : 668.21 ccms.

Cell E isolated for experiment.

P(psia)	Time(secs)
0.0	0-
5.701	0 +
5.602	33
5.38	93
5.217	153
5.090	213
4.908	333
4.792	453
4.715	573
4.666	693
4.63	813
4.604	933
4.572	1173
4.551	1473
4.539	1773
4.520	3573
4.513	infinity

Run no. : 9
 Date : 4th September 1991
 Adsorbent : carbon molecular sieve
 Adsorbate : nitrogen
 Method : volumetric
 Temperature : 147 c
 Weight CMS : 47.4 grams
 Initial cell pressure : 4.606 psia
 Step to pressure : 2.548 psia
 Final cell pressure : 2.636 psia
 q : 0.0016 moles/kg cms @ 2.636 psia
 Volume cell E : 668.21 ccms.

Cell E isolated for experiment.

P(psia)	Time(secs)
4.606	0-
2.548	0+
2.562	2
2.582	5
2.6	8
2.608	11
2.615	14
2.622	20
2.625	26
2.627	41
2.632	101
2.636	infinity

Run no. : 10
 Date : 3rd September 1991
 Adsorbent : carbon molecular sieve
 Adsorbate : methane
 Method : volumetric
 Temperature : 147 c
 Weight CMS : 47.4 grams
 Initial cell pressure : 0.0 psia
 Step to pressure : 6.34 psia
 Final cell pressure : 5.315 psia
 q : 0.0285 moles/kg cms @ 5.315 psia
 Volume cell E : 668.21 ccms.

Cell E isolated for experiment.

P(psia)	Time(secs)
0.0	0-
6.34	0 +
6.14	35
5.97	65
5.84	95
5.743	125
5.67	155
5.56	215
5.49	265
5.44	325
5.4	400
5.375	475
5.345	655
5.315	infinity

Run no. : 11
 Date : 27th August 1991
 Adsorbent : carbon molecular sieve
 Adsorbate : nitrogen
 Method : gravimetric
 Temperature : 80 c
 Initial cell pressure : 0.0 mba
 Final cell pressure : 171. mba
 q : 0.0178 moles/kg cms @ 171. mba
 Range scale : 1 mg
 Base weight CMS : 390.1 mgs

Wt(mgs)	Time(secs)
0.075	0-
0.137	112
0.17	188
0.20	292
0.21	344
0.228	464
0.24	584
0.255	824
0.262	1064
0.27	infinity

Run no. : 12
Date : 27th August 1991
Adsorbent : carbon molecular sieve
Adsorbate : nitrogen
Method : gravimetric
Temperature : 80 c
Initial cell pressure : 171 mba
Final cell pressure : 271. mba
q : 0.027 moles/kg cms @ 255. mba
Range scale : 1 mg
Base weight CMS : 390.1 mgs

Wt(mgs)	Time(secs)
0.27	0-
0.294	132
0.31	204
0.328	324
0.34	444
0.355	684
0.363	924
0.37	infinity

Run no. : 13
 Date : 28th August 1991
 Adsorbent : carbon molecular sieve
 Adsorbate : nitrogen
 Method : gravimetric
 Temperature : 80 c
 Initial cell pressure : 271 mba
 Final cell pressure : 0. mba
 q : 0.0 moles/kg cms @ 0. mba
 Range scale : 1 mg
 Base weight CMS : 390.1 mgs

Wt(mgs)	Time(secs)
0.36	0-
0.345	27
0.32	51
0.295	75
0.255	99
0.238	123
0.226	147
0.17	267
0.138	387
0.1	627
0.085	867
0.058	infinity

Run no. : 14
 Date : 28th August 1991
 Adsorbent : carbon molecular sieve
 Adsorbate : nitrogen
 Method : gravimetric
 Temperature : 50 c
 Initial cell pressure : 0. mba
 Final cell pressure : 145. mba
 q : 0.0286 moles/kg cms @ 145. mba
 Range scale : 1 mg
 Base weight CMS : 390.1 mgs

Wt(mgs)	Time(secs)
0.08	0-
0.10	86
0.124	158
0.145	230
0.2	470
0.24	710
0.275	950
0.298	1190
0.32	1430
0.335	1670
0.355	2150
0.37	2630
0.383	3590
0.390	infinity

Run no. : 15
 Date : 31st August 1991
 Adsorbent : carbon molecular sieve
 Adsorbate : nitrogen
 Method : gravimetric
 Temperature : 50 c
 Initial cell pressure : 145. mba
 Final cell pressure : 329. mba
 q : 0.0537 moles/kg cms @ 329. mba
 Range scale : 1 mg
 Base weight CMS : 390.1 mgs

Wt(mgs)	Time(secs)
0.328	0-
0.392	395
0.445	635
0.486	875
0.520	1115
0.548	1355
0.569	1595
0.585	1835
0.597	2075
0.61	2555
0.625	3035
0.642	3755
0.667	infinity

Run no. : 16
 Date : 31st August 1991
 Adsorbent : carbon molecular sieve
 Adsorbate : nitrogen
 Method : gravimetric
 Temperature : 50 c
 Initial cell pressure : 329. mba
 Final cell pressure : 183. mba
 q : 0.0304 moles/kg cms @ 183. mba
 Range scale : 1 mg
 Base weight CMS : 390.1 mgs

Wt(mgs)	Time(secs)
0.67	0-
0.642	240
0.595	480
0.558	720
0.528	960
0.502	1200
0.472	1680
0.45	2160
0.422	2880
0.42	3600
0.412	infinity

Run no. : 17
 Date : 31st August 1991
 Adsorbent : carbon molecular sieve
 Adsorbate : nitrogen
 Method : gravimetric
 Temperature : 50 c
 Initial cell pressure : 183 mba
 Final cell pressure : 0. mba
 q : 0.0 moles/kg cms @ 0. mba
 Range scale : 1 mg
 Base weight CMS : 390.1 mgs

Wt(mgs)	Time(secs)
0.41	0-
0.38	150
0.315	390
0.268	630
0.225	870
0.167	1350
0.128	1830
0.103	2310
0.080	3030
0.065	3750
0.048	infinity

Run no. : 18
 Date : 1st September 1991
 Adsorbent : carbon molecular sieve
 Adsorbate : nitrogen
 Method : gravimetric
 Temperature : 25 c
 Initial cell pressure : 0. mba
 Final cell pressure : 217. mba
 q : 0.0742 moles/kg cms @ 217. mba
 Range scale : 1 mg
 Base weight CMS : 390.1 mgs

Wt(mgs)	Time(secs)
0.08	0-
0.105	250
0.157	490
0.20	730
0.24	970
0.275	1210
0.343	1690
0.403	2170
0.453	2650
0.500	3130
0.538	3610
0.592	4330
0.633	5050
0.675	5770
0.703	6490
0.742	7690
0.775	8890
0.795	9610
0.818	11050
0.838	12490
0.862	15370
0.890	infinity

Run no. : 19
 Date : 1st September 1991
 Adsorbent : carbon molecular sieve
 Adsorbate : nitrogen
 Method : gravimetric
 Temperature : 25 c
 Initial cell pressure : 237. mba
 Final cell pressure : 0. mba
 q : 0.0 moles/kg cms @ 0. mba
 Range scale : 1 mg
 Base weight CMS : 390.1 mgs

Wt(mgs)	Time(secs)
0.89	0-
0.867	320
0.833	560
0.783	800
0.713	1280
0.622	2000
0.570	2480
0.467	3680
0.386	4880
0.328	6080
0.280	7280
0.245	8480
0.215	9680
0.195	10880
0.177	12080
0.162	13280
0.138	14480
0.1	infinity

Run no. : 20
 Date : 2nd September 1991
 Adsorbent : carbon molecular sieve
 Adsorbate : nitrogen
 Method : gravimetric
 Temperature : 10 c
 Initial cell pressure : 0. mba
 Final cell pressure : 120. mba
 q : 0.0675 moles/kg cms @ 120. mba
 Range scale : 1 mg
 Base weight CMS : 390.1 mgs

Wt(mgs)	Time(secs)
0.108	0-
0.144	540
0.190	1260
0.228	1980
0.263	2700
0.293	3420
0.328	4140
0.373	5220
0.425	6660
0.47	8100
0.51	9540
0.55	11340
0.59	13140
0.64	15300
0.683	18900
0.722	22500
0.732	23700
0.775	31380
0.803	38580
0.822	45780
0.845	infinity

Run no. : 21
 Date : 3rd September 1991
 Adsorbent : carbon molecular sieve
 Adsorbate : nitrogen
 Method : gravimetric
 Temperature : 10 c
 Initial cell pressure : 120. mba
 Final cell pressure : 0. mba
 q : 0.0 moles/kg cms @ 0. mba
 Range scale : 1 mg
 Base weight CMS : 390.1 mgs

Wt(mgs)	Time(secs)
0.765	0-
0.71	600
0.65	1320
0.60	2040
0.557	2760
0.520	3480
0.435	4920
0.4	6360
0.356	7800
0.298	9960
0.255	12120
0.22	14280
0.19	16460
0.17	18620
0.153	20780
0.13	22940
0.11	infinity

Run no. : 22
 Date : 20th September 1991
 Adsorbent : carbon molecular sieve
 Adsorbate : nitrogen
 Method : gravimetric
 Temperature : 75 c
 Initial cell pressure : 0.0 mba
 Final cell pressure : 225.9 mba
 q : 0.0 moles/kg cms @ 0. mba
 Range scale : 1 mg
 Base weight CMS = 354.2 mgs

Wt(mgs)	Time(secs)
0.115	0
0.125	415
0.185	895
0.223	1375
0.253	1855
0.274	2355
0.290	2815
0.312	3775
0.327	4735
0.345	infinity

Run no. : 23
 Date : 20th September 1991
 Adsorbent : carbon molecular sieve
 Adsorbate : nitrogen
 Method : gravimetric
 Temperature : 75 c
 Initial cell pressure : 225.9 mba
 Final cell pressure : 0.0 mba
 q : 0.0 moles/kg cms @ 0. mba
 Range scale : 1 mg
 Base weight CMS : 354. mgs

Wt(mgs)	Time(secs)
0.545	0
0.500	490
0.450	970
0.412	1450
0.385	1930
0.360	2410
0.344	3130
0.325	4090
0.315	5050
0.295	infinity

Run no. : 24
 Date : 21st September 1991
 Adsorbent : carbon molecular sieve
 Adsorbate : nitrogen
 Method : gravimetric
 Temperature : 60 c
 Initial cell pressure : 0. mba
 Final cell pressure : 205.3 mba
 q : 0.0 moles/kg cms @ 0. mba
 Range scale : 1 mg
 Base weight CMS : 354.2 mgs

Wt(mgs)	Time(secs)
0.110	0
0.143	560
0.185	1040
0.220	1520
0.250	2000
0.285	2720
0.310	3440
0.338	4400
0.365	5600
0.381	6800
0.393	8000
0.423	infinity

Run no. : 25
 Date : 21st September 1991
 Adsorbent : carbon molecular sieve
 Adsorbate : nitrogen
 Method : gravimetric
 Temperature : 60 c
 Initial cell pressure : 205.3 mba
 Final cell pressure : 0.0 mba
 q : 0.0 moles/kg cms @ 0. mba
 Range scale : 1 mg
 Base weight CMS : 354. mgs

Wt(mgs)	Time(secs)
0.623	0-
0.570	950
0.518	1670
0.480	2390
0.442	3350
0.410	4550
0.385	5750
0.368	6950
0.355	8150
0.338	10550
0.328	12950
0.313	infinity

Run no. : 26
 Date : 22nd September 1991
 Adsorbent : carbon molecular sieve
 Adsorbate : nitrogen
 Method : gravimetric
 Temperature : 40 c
 Initial cell pressure : 0. mba
 Final cell pressure : 217.4 mba
 q : 0.0 moles/kg cms @ 0. mba
 Range scale : 1 mg
 Base weight CMS : 354.2 mgs

Wt(mgs)	Time(secs)
0.108	0-
0.135	300
0.175	780
0.222	1500
0.280	2700
0.330	3900
0.368	5100
0.403	6300
0.430	7740
0.493	10620
0.531	13500
0.595	20700
0.625	27900
0.640	infinity

Run no. : 27
 Date : 21st September 1991
 Adsorbent : carbon molecular sieve
 Adsorbate : nitrogen
 Method : gravimetric
 Temperature : 40 c
 Initial cell pressure : 217.4 mba
 Final cell pressure : 0. mba
 q : 0.0 moles/kg cms @ 0. mba
 Range scale : 1 mg
 Base weight CMS : 354.0 mgs

Wt(mgs)	Time(secs)
0.840	0-
0.805	920
0.766	1640
0.735	2360
0.688	3560
0.648	4760
0.584	7160
0.530	9560
0.490	11960
0.470	13440
0.415	19000
0.380	26200
0.345	infinity

Run no. : 28
 Date : 23rd September 1991
 Adsorbent : carbon molecular sieve
 Adsorbate : nitrogen
 Method : gravimetric
 Temperature : 20 c
 Initial cell pressure : 0.0 mba
 Final cell pressure : 203.0 mba
 q : 0.0 moles/kg cms @ 0. mba
 Range scale : 1 mg
 Base weight CMS : 354.0 mgs

Wt(mgs)	Time(secs)
0.080	0
0.105	365
0.130	845
0.172	2045
0.205	3245
0.260	5645
0.310	9805
0.410	13645
0.510	20845
0.587	28045
0.645	35245
0.692	42445
0.753	56845
0.800	71245
0.835	85645
0.857	100045
0.945	infinity

APPENDIX A.2

SPECIFICATION OF APPARATUS INSTRUMENTATION

1. Universal Programmable Timer (UPT):

Model No. : M78-100

Make : Electroid Company, Xanadu Division

Details

Output Channels : 10

Cycle Duration : 10 msec to 99.9 Hours

Relays : Teledyne P/N 601-1402, Control : 3-28 VDC,
Load : 140 VAC, 10 AMP 50/60 Hz

2. Solenoid Valves (2- Way and 3- Way):

Model No.(3 way) : 8320 A171

Model No.(2 way) : 8223 A22

Make : ASCO, Netherlands

Details :Compatible with the UPT Relay
Internal Pilot Operated
Piston Type 1/4" and 3/8 NPT

Rating : 140 VAC, 10 AMP 50/60 Hz

3. Gas Chromatographs: 2 Nos.

Model No. : Series 150 with Thermal Conductivity Detector

Model No. : Series 350 with Thermal Conductivity Detector

Make : GOW-MAC

Details :

Column used : 20% Chromosorb

Sample injection : Sampling valve.

4. Integrators: 2 Nos.

Model No. : HP 3396 A

Make : Hewlett-Packard, USA

5. Strip Chart Recorders: 2 Nos.

Make : LINSIES, Germany

6. Data Logger:

Model No. : OM205

Make : OMEGA Engineering, USA

7. Electronic Manometer and Barocel Pressure Server:

Model No. : 1018C (Manometer)
Model No. : 570D-200P-3T1-H4X (Barocel)
Make : Datametrics, Edwards, USA
Details :
Range : 0 - 200 psi

8. Flow Meters, Controllers and Solenoid Valves:

Model No. : 8143A Series Mass Flow meters (Read outs).
Model No. : 8200 Series Mass Flow controllers.
Model No. : 8102-141-FC (Control sensor)
Model No. : 8202-1414 (Solenoid valve)
Model No. : 8102-1423-FM (Flow sensor)
Make : Matheson, USA
Details
Range : 0 - 3 SLPM, 0-10 SLPM.
Gas : Methane + Nitrogen Mixture.

APPENDIX A.3

DIMENSIONLESS FORM OF THE COLLOCATION EQUATIONS

For the high pressure flow in bed 2 and the low pressure flow in bed 1 during the adsorption step in bed 2 and purge step in bed 1 respectively, equations 5.1, 5.2, in the dimensionless form as follows:

Mass balance of fluid phase in bed 2:

$$\begin{aligned} \frac{\partial X_{A2}}{\partial \tau} = & \frac{1}{Pe_H} \cdot \frac{\partial^2 X_{A2}}{\partial x^2} - \bar{v}_2 \cdot \frac{\partial X_{A2}}{\partial x} \\ & + \psi_2 \cdot (X_{A2} - 1) \cdot \alpha_{A2} \cdot \left\{ \frac{\beta_{A2} X_{A2}}{1 + \beta_{A2} X_{A2} + \beta_{n2} (1 - X_{A2})} - Y_{A2} \right\} \\ & + \psi_2 \cdot Y \cdot X_{A2} \cdot \alpha_{n2} \cdot \left\{ \frac{\beta_{n2} (1 - X_{A2})}{1 + \beta_{A2} X_{A2} + \beta_{n2} (1 - X_{A2})} - Y_{n2} \right\} \end{aligned} \quad (1)$$

Mass balance of solid phase in bed 2:

$$\frac{\partial Y_{A2}}{\partial \tau} = \alpha_{A2} \cdot \left\{ \frac{\beta_{A2} X_{A2}}{1 + \beta_{A2} X_{A2} + \beta_{n2} (1 - X_{A2})} - Y_{A2} \right\} \quad (2)$$

$$\frac{\partial Y_{n2}}{\partial \tau} = \alpha_{n2} \cdot \left\{ \frac{\beta_{n2} (1 - X_{A2})}{1 + \beta_{A2} X_{A2} + \beta_{n2} (1 - X_{A2})} - Y_{n2} \right\} \quad (3)$$

Boundary conditions of bed 2:

$$\frac{\partial X_{A2}}{\partial x} \Big|_{x=0} = -Pe_H \bar{v}_2 (X_{A2} \Big|_{x=0} - X_{A2} \Big|_{x=1}) \quad (4)$$

$$\frac{\partial X_{A2}}{\partial x} \Big|_{x=1} = 0 \quad (5)$$

Velocity expression is given by

$$\begin{aligned} \frac{\partial \bar{v}_2}{\partial x} = & -\psi_2 \cdot \alpha_{A2} \cdot \left\{ \frac{\beta_{A2} X_{A2}}{1 + \beta_{A2} X_{A2} + \beta_{B2}(1 - X_{A2})} - Y_{A2} \right\} \\ & + \psi_2 \cdot \gamma \cdot \alpha_{B2} \cdot \left\{ \frac{\beta_{B2}(1 - X_{A2})}{1 + \beta_{A2} X_{A2} + \beta_{B2}(1 - X_{A2})} - Y_{B2} \right\} \end{aligned} \quad (6)$$

Mass balance of fluid phase in bed 1:

$$\begin{aligned} \frac{\partial X_{A1}}{\partial \tau} = & \frac{1}{Pc_L} \cdot \frac{\partial^2 X_{A1}}{\partial x^2} - \bar{v}_1 \cdot \frac{\partial X_{A1}}{\partial x} \\ & + \psi_1 \cdot (X_{A1} - 1) \cdot \alpha_{A1} \cdot \left\{ \frac{\beta_{A1} X_{A1}}{1 + \beta_{A1} X_{A1} + \beta_{B1}(1 - X_{A1})} - Y_{A1} \right\} \\ & + \psi_1 \cdot \gamma \cdot X_{A1} \cdot \alpha_{B1} \cdot \left\{ \frac{\beta_{B1}(1 - X_{A1})}{1 + \beta_{A1} X_{A1} + \beta_{B1}(1 - X_{A1})} - Y_{B1} \right\} \end{aligned} \quad (7)$$

Mass balance of solid phase in bed 1:

$$\frac{\partial Y_{A1}}{\partial \tau} = \alpha_{A1} \cdot \left\{ \frac{\beta_{A1} X_{A1}}{1 + \beta_{A1} X_{A1} + \beta_{B1}(1 - X_{A1})} - Y_{A1} \right\} \quad (8)$$

$$\frac{\partial Y_{B1}}{\partial \tau} = \alpha_{B1} \cdot \left\{ \frac{\beta_{B1}(1 - X_{A1})}{1 + \beta_{A1} X_{A1} + \beta_{B1}(1 - X_{A1})} - Y_{B1} \right\} \quad (9)$$

Boundary conditions of bed 1:

$$\frac{\partial X_{A1}}{\partial x} \Big|_{x=0} = -Pc_L \cdot \bar{v}_1 \cdot (X_{A1} \Big|_{x=0} - X_{A1} \Big|_{x=L}) \quad (10)$$

$$\frac{\partial X_{A1}}{\partial x} \Big|_{x=L} = 0 \quad (11)$$

Velocity expression is given by

$$\begin{aligned} \frac{\partial \bar{v}_1}{\partial x} = & -\psi_1 \cdot \alpha_{A1} \cdot \left\{ \frac{\beta_{A1} X_{A1}}{1 + \beta_{A1} X_{A1} + \beta_{B1} (1 - X_{A1})} - Y_{A1} \right\} \\ & + \psi_2 \cdot \gamma \cdot \alpha_{B1} \cdot \left\{ \frac{\beta_{B1} (1 - X_{A1})}{1 + \beta_{A1} X_{A1} + \beta_{B1} (1 - X_{A1})} - Y_{B1} \right\} \end{aligned} \quad (12)$$

Initial conditions for clean beds:

$$X_{A2}(x, \tau = 0) = 0, \quad X_{B2}(x, \tau = 0) = 0, \quad Y_{A2}(x, \tau = 0) = 0, \quad Y_{B2}(x, \tau = 0) = 0, \quad (13)$$

$$X_{A1}(x, \tau = 0) = 0, \quad X_{B1}(x, \tau = 0) = 0, \quad Y_{A1}(x, \tau = 0) = 0, \quad Y_{B1}(x, \tau = 0) = 0, \quad (14)$$

Equations 1, 4 and 5 are combined and written in collocation form based on a Legendre type polynomial to represent the trial function, the following set of ordinary differential equation results for the high pressure flow step in bed 2 (step 1):

$$\frac{\partial X_{A_2}(j)}{\partial \tau} = \left\{ \sum_{i=2}^{M+1} (P \cdot Bx(j, i) - \bar{V}_2(j) \cdot Ax(j, i)) - (A_4 \cdot (P \cdot Bx(j, 1) - \bar{V}_2(j) \cdot Ax(j, 1))) \cdot \sum_{i=2}^{M+1} Ax(M+2, i) \right\} -$$

$$(A_5 \cdot (P \cdot Bx(j, 1) - \bar{V}_2(j) \cdot Ax(j, 1))) \cdot \sum_{i=2}^{M+1} (A_3 \cdot Ax(M+2, i) - Ax(1, i))) +$$

$$(A_1 \cdot (P \cdot Bx(j, M+2) - \bar{V}_2(j) \cdot Ax(j, M+2))) \cdot \sum_{i=2}^{M+1} (A_3 \cdot Ax(M+2, i) - Ax(1, i))) \cdot X_{A_2}(i) +$$

$$A_5 \cdot Pe_H \cdot X_{A_2} \Big|_{x=0} \cdot (P \cdot Bx(j, 1) - \bar{V}_2(j) \cdot Ax(j, 1)) -$$

$$A_1 \cdot Pe_H \cdot X_{A_2} \Big|_{x=0} \cdot (P \cdot Bx(j, M+2) - \bar{V}_2(j) \cdot Ax(j, M+2)) + F_2(j) \quad (15)$$

where,

$$F_2(j) = \psi_2 [(X_{A_2}(j) - 1)^{\alpha_{A_2}} \left\{ \frac{\beta_{A_2} \cdot X_{A_2}(j)}{1 + \beta_{A_2} \cdot X_{A_2}(j) + \beta_{B_2} \cdot (1 - X_{A_2}(j))} - Y_{A_2}(j) \right\} + Y_{A_2}(j) \cdot \alpha_{B_2} \left\{ \frac{\beta_{B_2} \cdot (1 - X_{A_2}(j))}{1 + \beta_{A_2} \cdot X_{A_2}(j) + \beta_{B_2} \cdot (1 - X_{A_2}(j))} - Y_{B_2}(j) \right\}]$$

Equations 2 and 3 now become:

$$\frac{\partial Y_{A_2}(j)}{\partial \tau} = \alpha_{A_2} \left\{ \frac{\beta_{A_2} \cdot X_{A_2}(j)}{1 + \beta_{A_2} \cdot X_{A_2}(j) + \beta_{B_2} \cdot (1 - X_{A_2}(j))} - Y_{A_2}(j) \right\} \quad (16)$$

$$\frac{\partial Y_{B_2}(j)}{\partial \tau} = \alpha_{B_2} \left\{ \frac{\beta_{B_2} \cdot (1 - X_{A_2}(j))}{1 + \beta_{A_2} \cdot X_{A_2}(j) + \beta_{B_2} \cdot (1 - X_{A_2}(j))} - Y_{B_2}(j) \right\} \quad (17)$$

The expression for velocity is given by a set of algebraic equation as follows:

$$\sum_{i=2}^{M+1} [\Lambda x(j, i) - \frac{\Lambda x(M+2, i) \cdot \Lambda x(j, M+2)}{\Lambda x(M+2, M+2)}] \bar{V}_2(i) = F_2(j) - \frac{\Lambda x(M+2, 1) \cdot \Lambda x(j, M+2)}{\Lambda x(M+2, M+2)} \bar{V}_2(1) \quad (18)$$

Note: $\bar{V}_2(1)=1.0$ and $\frac{d\bar{V}_2}{dx}(M+2) = 0$ $j=2, M+1$

In equation 15 ,

$$\Lambda_1 = 1 / (\Lambda x(1, M+2) - (\Lambda_3 \cdot \Lambda x(M+2, M+2)))$$

$$\Lambda_2 = \Lambda x(M+2, M+2) / (\Lambda x(1, M+2) - (\Lambda_3 \cdot \Lambda x(M+2, M+2)))$$

$$\Lambda_3 = (\Lambda x(1, 1) - Pe_{||}) / \Lambda x(M+2, 1)$$

$$\Lambda_4 = 1 / \Lambda x(M+2, 1)$$

$$\Lambda_5 = \Lambda_2 \cdot \Lambda_4$$

$$P = 1 / Pe_{||}$$

M = Number of collocation points

where,

$$F_3(j) = \psi_2 \left(\frac{\partial y_{A2}(j)}{\partial \tau} + \gamma \frac{\partial y_{B2}(j)}{\partial \tau} \right)$$

Equations 7, 10 and 11, combined and transformed into ODEs by the collocation method lead to:

$$\begin{aligned}
 \frac{\partial X_{A1}(j)}{\partial \tau} &= \left\{ \sum_{i=2}^{M+1} (Q \cdot Bx(j, i) - \bar{V}_1(j) \cdot Ax(j, i)) - (B_4 \cdot (Q \cdot Bx(j, 1) - \bar{V}_2(j) \cdot Ax(j, 1)) \cdot \sum_{i=2}^{M+1} Ax(M+2, i)) - \right. \\
 &\quad (B_5 \cdot (Q \cdot Bx(j, 1) - \bar{V}_1(j) \cdot Ax(j, 1)) \cdot \sum_{i=2}^{M+1} (B_3 \cdot Ax(M+2, i) - Ax(1, i))) - Ax(1, i)) + \\
 &\quad (B_1 \cdot (Q \cdot Bx(j, M+2) - \bar{V}_1(j) \cdot Ax(j, M+2)) \cdot \sum_{i=2}^{M+1} (B_3 \cdot Ax(M+2, i) - Ax(1, i))) \cdot X_{A1}(i) + \\
 &\quad B_5 \cdot Pe_L \cdot G \cdot X_{A2} \Big|_{j=M+2} (Q \cdot Bx(j, 1) - \bar{V}_1(j) \cdot Ax(j, 1)) - \\
 &\quad B_1 \cdot Pe_L \cdot G \cdot X_{A2} \Big|_{j=M+2} (Q \cdot Bx(j, M+2) - \bar{V}_1(j) \cdot Ax(j, M+2)) + F_1(j) \Big\}
 \end{aligned} \quad (19)$$

where,

$$\begin{aligned}
 F_1(j) &= \psi_1 \left\{ (X_{A1}(j) - 1) \cdot \left(\frac{\beta_{A1} \cdot X_{A1}(j)}{1 + \beta_{A1} \cdot X_{A1}(j) + \beta_{B1} \cdot (1 - X_{A1}(j))} - Y_{A1}(j) \right) \right. \\
 &\quad \left. + Y \cdot X_{A1}(j) \cdot \alpha_{B1} \left(\frac{\beta_{B1} \cdot (1 - X_{A1}(j))}{1 + \beta_{A1} \cdot X_{A1}(j) + \beta_{B1} \cdot (1 - X_{A1}(j))} - Y_{B1}(j) \right) \right\}
 \end{aligned}$$

Equations 8 and 9 can be written as:

$$\frac{\partial Y_{A1}(j)}{\partial \tau} = \alpha_{A1} \left(\frac{\beta_{A1} \cdot X_{A1}(j)}{1 + \beta_{A1} \cdot X_{A1}(j) + \beta_{B1} \cdot (1 - X_{A1}(j))} - Y_{A1}(j) \right) \quad (20)$$

$$\frac{\partial Y_{B1}(j)}{\partial \tau} = \alpha_{B1} \left(\frac{\beta_{B1} \cdot X_{A1}(j)}{1 + \beta_{A1} \cdot X_{A1}(j) + \beta_{B1} \cdot (1 - X_{A1}(j))} - Y_{B1}(j) \right) \quad (21)$$

The expression for velocity is given by a set of algebraic equations which is:

$$\sum_{i=2}^{M+1} [\Lambda x(j, i) - \frac{\Lambda x(M+2, i) \cdot \Lambda x(j, M+2)}{\Lambda x(M+2, M+2)}] \bar{V}_1(i) = F_4(j) - \frac{\Lambda x(M+2, 1) \Lambda x(j, M+2)}{\Lambda x(M+2, M+2)} \bar{V}_1(1) \quad J=2, M+1 \quad (22)$$

Note: $\bar{V}_1(1) = G$ and $\frac{d\bar{V}_1(M+2)}{dx} = 0$

In equation 19:

$$B_1 = 1 / (\Lambda x(1, M+2) - (B_3 \cdot \Lambda x(M+2, M+2)))$$

$$B_2 = \Lambda x(M+2, M+2) / (\Lambda x(1, M+2) - (B_3 \cdot \Lambda x(M+2, M+2)))$$

$$B_3 = (\Lambda x(1, 1) - Pe_L) / \Lambda x(M+2, 1)$$

$$B_4 = 1 / \Lambda x(M+2, 1)$$

$$B_5 = B_2 \cdot B_4$$

$$Q = 1 / Pe_L$$

where,

$$F_4(j) = -\psi_1 \left(\frac{\partial Y_{A1}(j)}{\partial \tau} + \gamma \frac{\partial Y_{B1}(j)}{\partial \tau} \right)$$

VITA

ASHRAFHUSEIN ISMAIL FATEHI

Permanent Address 81, Mohamadali Road, 1st Floor,
Bombay 400 003, India.

Personal Data Born on April 9, 1957; Indian; Married; one child

Education

8/80 to 9/82 M. Tech in Chemical Engineering, 1983,
Indian Institute of Technology, Bombay, India.

8/75 to 5/80 B. Tech in Chemical Engineering, 1980
Indian Institute of Technology, Bombay, India

Publications

- 1) Hassan, M. M., Fatehi, A. I. and Loughlin, K. F., "Non - linear isothermal packed bed adsorbers; Comparison of Peclet and Cell Numbers", Gas Separation & Purification, pgs. 50-57, Vol. 4, March, 1990.
- 2) Fatehi, A. I., Loughlin, K. F. and Hassan M. M., "Nonlinear Nonisothermal Adsorptive Diffusion of Binary Mixtures in Microporous Crystals", Paper presented at International Symposium on Gas Separation Technology, Antwerp, Belgium, Sep 10-15, 1989.
- 3) Hassan, M. M., Fatehi, A. I. and Loughlin, K. F., "Comparison of Axial Dispersion and Cell Model Predictions for a Packed Bed Adsorber with a Non - linear Isotherm", Paper presented at 80th Anniversary Meeting of AIChE in Washington, D. C., Nov 27-Dec 2, 1988.
- 4) Fatehi, A. I. and Dwivedi, M. C., "Synlubes", Paper presented at 2nd LAWSPS (Lubricant - Additives - Waxes - Petroleum Speciality Products) Symposium at Indian Institute of Technology, Bombay and published in 2nd LAWSPS Publications, Vol. 3, No. 3, 3-33 to 3-44, 1982.
- 5) Fatehi, A. I., "Synthetic Lubricants", M. S. Thesis, Indian Institute of Technology, Bombay, 1982.

Papers accepted for Presentation

- 1) Loughlin, K. F., Fatehi, A. I., Hassan, M. M. and Zahur, M., "Measurement of Barrier Resistance and Micropore Diffusion in Carbon Molecular Sieve", to be presented at the AIChE Annual Meeting in Miami, Florida on Nov. 1-6, 1992.

- 2) Fatehi, A. I., Loughlin, K. F. and Hassan M. M., "Theoretical and Experimental Study of PSA Separation of methane nitrogen mixtures using Carbon Molecular Sieve", to be presented at the AIChE Annual Meeting in Miami, Florida on Nov. 1-6, 1992.
- 3) Loughlin, K. F., Hassan, M. M., Fatehi, A. I. and Zahur, M., "Physical Adsorption of Methane and Nitrogen on Carbon Molecular Sieve", to be presented at the 1st International Conference on Chemistry in Industry in Manama, Bahrain on Nov. 14 -16, 1992.